STUDY OF THE INDUCTION OF SMECTIC A_d AND RE-ENTRANT NEMATIC PHASES IN BINARY MIXTURES OF LIQUID CRYSTALS

A thesis submitted to the University of North Bengal

for the award of

Doctor of Philosophy

in

Physics

By

Akhileshwar Prasad

Guide

Dr. Malay Kumar Das

Department of Physics
University of North Bengal
Rajarammohunpur, Dist. Darjeeling
West Bengal, India 734013

July 2013

I would like to dedicate this thesis to my loving parents
whose sacrifices have helped me to reach this far.

Declaration

I declare that the thesis entitled "*Study of the induction of smectic A_d and re-entrant nematic phases in binary mixtures of liquid crystals*" has been prepared by me under the guidance of Dr. Malay Kumar Das, Associate Professor, Department of Physics, University of North Bengal. No part of this thesis has formed the basis for the award of any degree or fellowship previously.

Akhileshwar Prasad
Department of Physics,
University of North Bengal,
Raja Rammohunpur.

Date:

Certificate

Replace this page with the certificate

Abstract

In this work, an in-depth study of the phenomenon of the induction of smectic A_d and re-entrant nematic phases through investigations into the physical properties of two polar - polar binary mixtures of liquid crystalline molecules from different experimental techniques has been undertaken. Two series of mixtures with 4-cyanophenyl 4-nonylbenzoate, 9.CN as one component and 4-cyanobiphenyl-4′ 4-heptylbenzoate, 7BCB and 4-cyanophenyl [4′ (4″-n- heptylphenyl)] benzoate, 7CPB as the second component has been studied. The following are the conclusions summarizing the work done in this thesis:

System 1: Binary mixture of 7CPB and 9.CN:

1. The phase diagram shows the presence of induced smectic and re-entrant nematic phases in the concentration range $0.4 < x_{9.\,CN} < 0.87$. From textures studies it is observed that both the normal and re-entrant nematic phases in this system are similar.

2. The order of the induced smectic A_d to nematic as well as the induced smectic A_d to re-entrant nematic phase transition is continuous for all the mixtures. This observation has been supported from DSC, density and orientational order parameter values determined from X-ray diffraction measurements.

3. Using a simple extension of the McMillan's treatment of the smectic A phase, the theoretically estimated $\langle P_2 \rangle$ and $\langle P_4 \rangle$ values have been found to fit quite well with those determined from X-ray diffraction studies.

4. Further analysis of the X-ray data has revealed a maximum in the smectic layer spacing near $x_{9.\,CN} = 0.5$. The variation of layer thickness with molar concentration of 9.CN has been explained fairly well by assuming the presence of both homo and hetero dimers.

5. Optical transmission studies made on this system revealed no discontinuity in the Δn values at the N_{re}–Sm A_d as well as Sm A_d–N transition temperatures indicating second order phase transition. The critical exponent associated with the N–Sm A_d and Sm A_d–re-entrant nematic transitions is found to be 0.275 and 0.21 from optical birefringence data. These values lie between the 3D-XY and tricritical values.

6. The agreement between the experimental $\langle P_2 \rangle$ values from birefringence measurements with those calculated from McMillan's theory have been found to be poor in the smectic A_d phase. This discrepancy has been removed by using the Luckhurst and Timimi model. Both N–Sm A_d and Sm A_d–N_{re} phase transitions which are predicted to be of second order by this model, are also found to be in agreement with our birefringence as well as DSC measurement. The measurement of density and refractive indices in the solid phase enabled me to verify the validity of Haller's extrapolation technique. For all the mixtures the value of the critical exponent β obtained from Haller's extrapolation is less than 0.2. The temperature dependence of polarisibility anisotropy has also been fitted by a four parameter fitting procedure which yields an average value of β as 0.223 ± 0.07 which is close to the tricritical hypothesis predicting $\beta = 0.25$.

7. The temperature variation of the dielectric permittivity at the nematic – smectic A_d and smectic A_d – re-entrant nematic transition for all the mixtures has been found to be continuous.

8. The parallel component of the dielectric permittivity shows a pronounced decrease in the Sm A_d phase due to dipole-dipole correlation. The maximum decrease is found for mixtures situated near the middle of the Sm A_d island.

9. The effective values of the dipole moments in the mixtures are found to be less than the values observed in the pure compounds. Moreover, μ_{eff} in the smectic phase A_d phase is found to be slightly smaller than those obtained by extrapolation from either the nematic or re-entrant nematic phases. The lower effective dipole moment in the smectic A_d phase implies the development of additional anti-parallel ordering of the molecular dipoles in the induced smectic phase.

10. For the average value of the nematic permittivity, ϵ_{av}, as well as the isotropic permittivity ϵ_{iso}, the value of the critical exponent α is nearly the same (≈ 0.5) which corresponds to the tricritical behaviour of the I–N transition.

11. A simple electro-optical method was used to determine the relaxation time and hence the rotational viscosity (γ_1) of this binary system. Upon cooling, the γ_1 values not only increase in the normal N phase but also in the N_{re} phase and have same order of magnitudes about 0.5 to a few Pa s. Rotational viscosity values are about two to three order of magnitude higher in the Sm A_d phase than those measured in the N phase.

12. The magnitude of splay elastic constant in the induced smectic A_d phase is about two to three order of magnitude higher in the normal nematic and re-entrant nematic phases. The bend elastic constant shows a strong pretransitional effect near the nematic–smectic and smectic–re-entrant nematic transitions.

13. The activation energies for the N_{re} phase are smaller than those for the normal nematic phase. The difference $[(E_a)_N - (E_a)_{N_{re}}]$ is maximum near the centre of the phase diagram.

System 2: Binary mixture of 7BCB and 9.CN:

1. The only difference between the previous system (system 1) and the present system (system 2) is the replacement of 7CPB by 7BCB, which translates to a shift in the position of the ester group (–COO). It is observed that a change in the position of the ester group leads to a stronger induction of the smectic A_d phase.

2. The order of the induced smectic A_d to nematic as well as the induced smectic A_d to re-entrant nematic phase transition is continuous for all the mixtures which have been supported from DSC, birefringence, orientational order parameter values determined from X-ray diffraction measurements.

3. The transverse correlation lengths are found to diverge at the Sm A_d–N as well as Sm A_d–N_{re} phase region is approached from either side, again indicating a second-order phase transition.

4. The McMillan's theory of the smectic A phase was modified in conformity with the Luckhurst-Timimi model, by considering a temperature dependent term α parameter to yield theoretical values of the OOP's $\langle P_2 \rangle$ and $\langle P_4 \rangle$ which were found to fit quite well with those determined from X-ray diffraction studies.

5. It is observed that the value of $\epsilon_{\parallel}$ falls with the decrease in temperature in the re-entrant nematic and low temperature region of the smectic A_d phase. This decrease in $\epsilon_{\parallel}$ value with decrease in temperature has been explained from the results of low frequency dielectric spectroscopy measurements. In the dielectric loss graph two well separated dispersion region has been obtained. It is seen that the activation energy is higher in the re-entrant nematic phase as compared to the Sm A_d phase.

Preface

My journey toward this thesis began in mid 2007 after I joined the department of Physics, University of North Bengal as a junior research fellow in a Department of Science and Technology funded research project, under the supervision of Dr. Malay Kumar Das. These six years have been a challenging as well as an enjoyable learning experience as I was fortunate to have got an opportunity to participate in the establishment of a new section of our laboratory from scratch. Apart from liquid crystals, during this period I could learn about hardware interfacing and laboratory automation. I got the opportunity to design, automate and/or assemble several experimental setups like, refractive index from thin prism method, birefringence from optical transmission method, rotational viscosity from optical and capacitance decay method, dielectric measurements and elastic constant measurements.

The results of the work performed during these six years (three years as a research fellow and three years spent as an Assistant Professor at Malda College) has been presented in this thesis.

The first chapter contains a brief introduction and a review about liquid crystals. I have only touched those parts that are related to the topic of this thesis or are required for a general awareness about liquid crystals. Chapter 2 contains a brief description about the experimental techniques and the theories used in this work.

Chapter 3 – 8 contains the results obtained and their discussions. They are basically based on published works, except for chapter 8 and parts of chapter 7, which are under preparation for publication. A complete list of publications has been given at the end of this thesis.

I would like to avail this opportunity to thank all the people who have helped me in doing this work at the Department of Physics, University of North Bengal. I would specially like to thank Dr. Banani Adhikari (Das), Prof. Ranjit Paul, Dr. Sukla Paul and my co-workers Dr. Prithwi Dev Roy, Mr. Gautam Sarkar,

Ms. Somedatta Basak, Ms. Prajnamita Dasgupta, Mr. Anish Chakraborty , Mr. Sudipta Kumar Sarkar and Ms. Anamika Pramanik for their help and support.

I am sincerely thankful to all the members of the Department of Physics, University of North Bengal, especially Prof. B. Bhattacharjee and Prof. D. Dasgupta whose constant encouragement and support has helped me in carrying out this work successfully. I am also grateful to all the staff of U.S.I.C. who have eagerly helped me in fabrication of various items. I would also like to express my thanks to all my colleagues at Malda College especially Dr. Achintya Kumar Chatterjee, without their cooperation it would not have been possible to complete this work.

I wish to convey my sincere thanks to the Department of Science and Technology, New Delhi, for the award of research fellowship.

I would like to acknowledge my indebtedness to my family members for their unfailing encouragement, support and sacrifices especially my wife Rina because some of the time spent in the laboratory was rightfully theirs.

No words will be sufficient to thank Dr. Malay Kumar Das and any attempt to do so will only demean what he has done for me. I am fortunate to have benefited from his guidance and advice.

Akhileshwar Prasad

Date:
Place: Raja Rammohunpur

Contents

List of Figures

List of Tables

Chapter 1

Introduction

1.1 Liquid crystals

Liquid crystals are partially ordered anisotropic fluids, thermodynamically located between the three dimensionally ordered solid state crystal and the isotropic liquid [1]. Their discovery is dated back to the year 1888, when the Austrian Botanist Friedrich Reinitzer reported on the observation of cholesteryl benzoate with apparently two melting points [2]. At the first melting temperature, the substance goes into a state where it possesses the flow properties of liquid while retaining some of the anisotropic properties of solids. Then, finally at the second melting point, it turns into an isotropic liquid. These intermediate state of matter, between the crystalline solid and isotropic liquid, also known as mesophases, retain a certain degree of order. If the molecules do not exhibit pronounced anisotropy, there is a possibility that on heating they will lose long range orientational order while the translational order is still retained. Such mesophases are known as disordered crystalline mesophases or plastic crystals. The opposite can also happen, i.e. if the molecules are highly anisotropic, they can lose their long range translational order while still possessing a certain degree of orientational order. Such a mesophase is known as ordered fluid mesophase or liquid crystal. Liquid crystals find their greatest technological application in the field of displays. At the same time they are extensively used in a multitude of other areas like temperature sensors, light modulators, high-strength fibers, optical imaging and recording, nondestructive mechanical testing of materials under stress, medical applications, switchable

windows etc. Further more these materials are important because they provide thermodynamically stable phases for the study of phase transitions and critical phenomena. A number of books and review articles on liquid crystals are available that describe the basics, as well as the recent development in the field of liquid crystals [3–29].

1.2 Classification of liquid crystals

Depending upon the way in which the transition to the mesophase is brought about, liquid crystals can be divided into two broad groups: **Thermotropic** and **Lyotropic Liquid Crystals**. In thermotropic liquid crystals transformation from one phase to another can be obtained by changing the temperature. However, there exists another class of compounds where such changes are brought about by the influence of solvents. These compounds are known as lyotropic liquid crystals. Lyotropic liquid crystals are biologically important while thermotropic class of liquid crystals are mainly of technological importance. Both thermotropic and lyotropic liquid crystals can be further classified according to the degree of order/symmetry retained.

1.2.1 Lyotropic liquid crystals

Lyotropic liquid crystals are the most commonly encountered liquid crystals in nature and are generally made up of two or more components of which at least one is an isotropic solvent. The transition to its different mesophases is controlled by changing the amount of solvent present. The most common example of lyotropic liquid crystals is cell membrane which is formed by the dissolution of phospholipids in water. Another commonly found lyotropic liquid crystalline compounds are the amphiphiles, which are single molecules possessing both polar and non- polar parts. Lyotropic liquid crystals play a very important role in living systems and are of interest for biological studies. Since, this dissertation is not concerned with lyotropic liquid crystals; further details on lyotropic systems are not being discussed here.

1.2.2 Thermotropic liquid crystals

If the transition to the different mesophases takes place by changing the temperature, then the liquid crystal is said to be thermotropic. If there is a reversibility of phase transition, i.e. the same phases appear both during heating and cooling then the thermotropic liquid crystal is said to be enantiotropic. However, if some phases are exhibited only during cooling then the liquid crystalline phase is said to be monotropic. Depending on the degree of ordering, thermotropic liquid crystals are classified as nematic, cholesteric and smectic. The nematic liquid crystal is by far the most important phase for applications. The most commonly observed thermotropic mesophases are nematic and smectic A phases.

1.2.2.1 Nematic phase

Nematic (N) liquid crystals are the simplest of all the mesophases and is characterised by the fact that the molecules do not have long range positional ordering of the centre of mass of the molecules. However, they have a long range orientational order, i.e. the molecular long axis tends to align along a preferred direction known as the director ($\hat{n}$). The director is the local average of the molecular long axis. This preferred direction can have a spatial dependence and hence vary from point to point in the medium. However, a uniformly aligned monodomain sample of an ordinary nematic is optically uniaxial, positive and birefrigent. Biaxial nematics are known to exist [30] but their number is very small. Though the constituent molecules may be polar, the nematic phase has no polarity, i.e. ($\hat{n}$) and ($-\hat{n}$) are equivalent. The molecules in the nematic phase can form clusters and such nematics are known as "cybotactic nematics". These were first observed and classified by Adrian de Vries [27]. Nematic phases only occur in materials that are either achiral or racemic mixtures.

Assuming the molecules to be cylindrically symmetric, the ordering in the nematic phase can be described by the distribution function $f(\theta)$ where θ is the angle between the director ($\hat{n}$) and the molecular long axis. $f(\theta)$ can be expanded in Legendre polynomials as

$$f(\theta) = \frac{1}{2} + \sum_{n=1}^{\infty} \frac{1}{2}(4n+1)\langle P_{2n}\rangle P_{2n}(\cos\theta) \tag{1.1}$$

where

$$\langle P_{2n} \rangle = \int_{-1}^{1} P_{2n}(\cos\theta) f(\theta) d(\cos\theta)$$

Due to the equivalence of $\hat{n}$ and $-\hat{n}$ only the even powers of $\cos(\theta)$ appears in the above expansion. The dominant parameter $\langle P_2 \rangle = \frac{1}{2}\langle 3\cos^2\theta - 1 \rangle$ can be easily measured and is referred to as order parameter of the nematic phase. The typical value of $\langle P_2 \rangle$ lies in between 0.3 to 0.9.

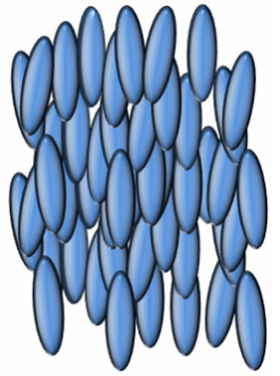

Figure 1.1: Nematic liquid crystal.

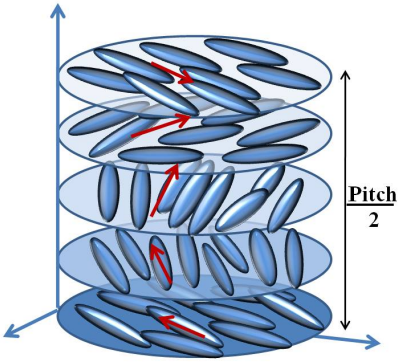

Figure 1.2: Cholesteric liquid crystal.

1.2.2.2 Cholesteric or chiral nematic (N*) phase

If a molecule does not have mirror symmetry then it is said to be chiral and the two resulting molecular structures, which are mirror image of one another, are said to be enantiomers. Cholesteric liquid crystals are made up of chiral molecules. This phase is known as **cholesteric** phase since it was first discovered in derivatives of cholesterols. However, not all cholesteric liquid crystals are derived from cholesterol and a more general term is chiral nematic phase. If the chirality is removed, a cholesteric phase becomes a nematic phase. However, due to the presence of the chiral center in the molecules the nematic phase is modified so that the molecules gradually twist with respect to one another to form a macroscopic helix, the handedness of which depends upon the conformation of the molecules. Locally, the nematic and the cholesteric phases are almost identical. However, in the cholesteric phase, the director precesses along the helix's axis and the distance required for 360° turn is known as the pitch. The director

may be described by

$$n_x = \cos\left(\frac{2\pi}{p}z + \phi_0\right) \tag{1.2a}$$

$$n_y = \sin\left(\frac{2\pi}{p}z + \phi_0\right) \tag{1.2b}$$

$$n_z = 0 \tag{1.2c}$$

where it has been assumed that the helix is along the z direction, p is the pitch of the helix and ϕ_0 is a constant which depends on the boundary condition.

Cholesteric liquid crystals are optically active and they rotate the plane of a plane polarised light if the pitch is much larger than the wavelength (λ) of light used. They have very high specific rotation. The cholesteric phase exhibits circular dichroism and selective reflection of white light when $\lambda = p$.

1.2.2.3 Smectic phase

The term smectic was first used by Friedel and has been derived from the Greek word soap($\sigma\mu\eta\gamma\mu\alpha$). He used this term for the liquid crystals which had properties similar to that of soap. In this mesophase, the molecules are stacked in layers with a well-defined interlayer spacing. Thus the translational symmetry is broken in at least one direction. The smectic mesophase can be further classified depending on the tilt of the molecular long axis with respect to the layer plane and also on the presence of the partial ordering of the molecules within the layers. A large number of smectic mesophases have been identified. They may be written in order of decreasing symmetry as $SmA, SmC, SmB, \cdots$

However, only Smectic A phase is relevant to the present work and the discussion about the other smectic phases will be very limited.

Smectic A

Smectic A (SmA) is the simples of all the smectic phases. In this phase, the molecules are arranged in layers with the molecular long axis parallel to the layer normal. However within the layers, the molecules have no correlation between their center of mass, and have a short range order typical of liquids. Thus, each layer behaves like a two dimensional fluid where the molecules are free to move about. The molecules can also rotate freely along their long axis and

thus have an infinite fold rotational symmetry along this axis. Therefore, the smectic A liquid crystals in thermal equilibrium are uniaxial systems with the optic axis along the director. The smectic A phase has a well defined inter layer spacing which may not be always equal to the molecular length. On the basis of the relation between the molecular length and the layer spacing smectic A phase has been subdivided into several distinct phases, namely: Smectic A_1, A_2, A_d and Smectic $\tilde{A}$. Smectic A_1, A_2, and A_d have the same point group symmetry but differ by translational symmetry due to specific packing of the molecules.

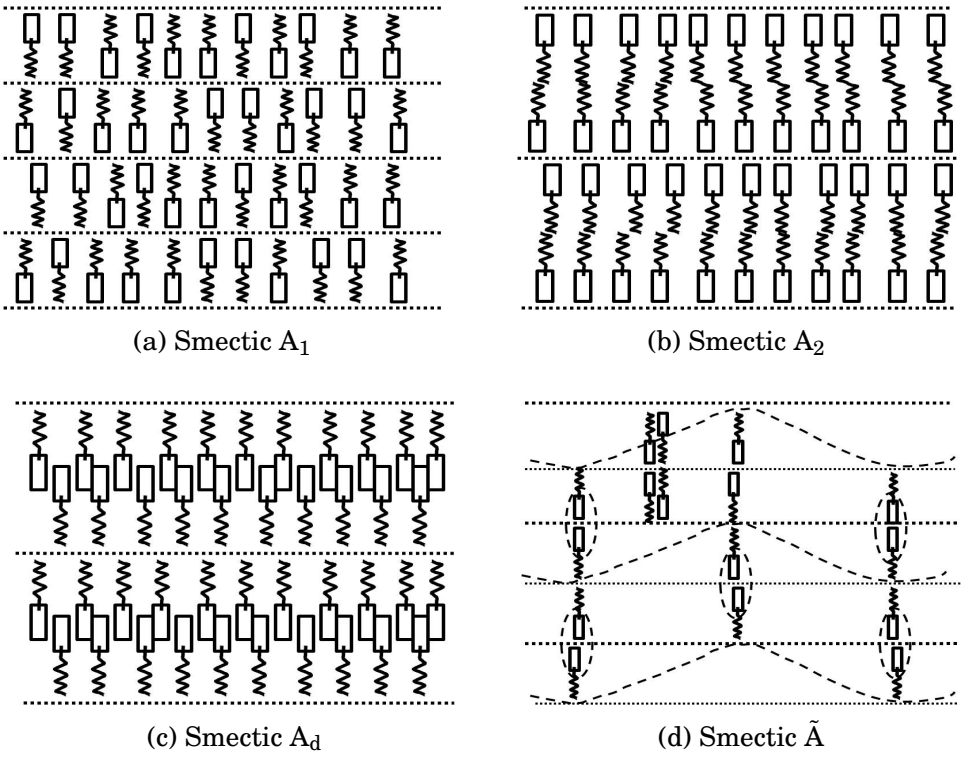

(a) Smectic A_1 (b) Smectic A_2

(c) Smectic A_d (d) Smectic $\tilde{A}$

Figure 1.3: Different types of smectic A phases.

Monolayer Smectic A_1: In smectic A_1 the layer thickness is equal to the molecular length (figure 1.3a).

Bilayer Smectic A_2: In smectic A_2 the layer thickness is equal to twice the molecular length (figure 1.3b).

Partially Bilayer Smectic A_d: Smectic A_d phase has an intermediate structure between smectic A_1 and smectic A_2. The layer thickness (l) lies in

between the molecular length (d) and twice the molecular length (2d) (figure 1.3c).

Smectic Antiphase Ã: In an effort to relive frustration some highly polar calamatic liquid crystals having an aliphatic chain form the smectic antiphase (Ã). The local structure is that of a bilayer smectic but, the polar heads of the molecules jump periodically from one layer to the next perpendicularly (figure 1.3d), i.e. alternately there are regions where the molecules between two layers meet head-head and tail-tail. Thus, there is a two-dimensional array, while the in-plane ordering stays liquid-like. The head-head and tail-tail regions may have different widths, in such a case the structure is said to be crenellated and denoted by the symbol SmÃ. A tilted version of antiphase SmÃ is the SmC antiphase and it differs from the SmÃ in that the lattice built by the polar head is tilted with respect to that of the smectic layers. Crenellated versions of antiphase SmC have also been reported [3, 18, 31].

Other smectic phases:

As the symmetry of the phase decreases a number of higher order smectic phases are formed some of which are almost crystal like and sometimes it becomes very difficult to differentiate between such mesophase and the crystalline phase. Some of the commonly found smectic phases have been discussed below in brief.

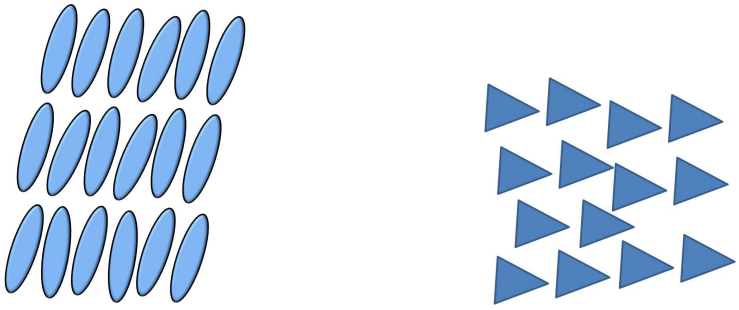

Figure 1.4: Smectic C phase.

Smectic C: Smectic C phase is similar to smectic A phase except that the molecular long axis is not orthogonal to the layer plane (figure 1.4). Due

to the presence of the molecular tilt the infinite fold rotational symmetry along the molecular long axis, which is present in smectic A , is broken and hence the smectic C phase is optically biaxial and also more viscous that smectic A phase.

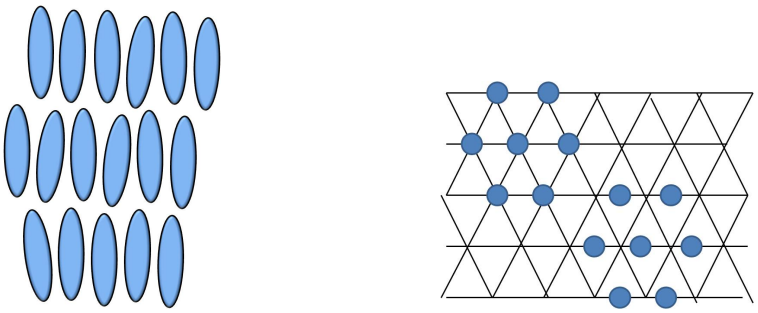

Figure 1.5: Smectic B phase.

Smectic B: Smectic B phase has a layered orthogonal structure where in each plane the molecules are arranged in a hexagonal pattern (figure 1.5). Thus an additional order parameter, i.e. bond order parameter is needed to describe this phase. The smectic B phase can be further classified into smectic B_{hex} and crystal B phase depending upon the presence of short range or long range order within the layers. Smectic B_{hex} phase has short range in plane positional order and long range bond orientational order. However, the crystal B phase has long range inter and intra layered translational order and long range bond orientational order. The crystal B phase is not considered to be a crystalline phase because they exhibit shear flow under stress. This is due to the fact that the coupling between the smectic layers is weak.

1.2.2.4 Other liquid crystalline phases

Blue Phases (BP)

The blue phases are thermodynamically distinct mesophases that appear in a very small temperature range of about one degree centigrade just below the isotropic phase. This phase is usually exhibited by highly chiral mesogens having pitch less than 700 nm. Certain wavelengths in the visible part of the spectrum are selectively reflected by these phases. Three distinct and stable blue phases have been reported, namely BP1*, BPII* and BPIII* [32]. However, the three phases may or may not be exhibited by a single compound. The structure of

BPIII* is not clearly understood. However, it is known to have an amorphous structure possessing a helical superstructure due to which it selectively reflects polarized light. BPI* and BPII* structures have been well understood and have a cubic symmetry. The NMR structures of blue phases are known to be different from those of chiral nematic phase [28, 33, 34].

Twist grain boundary smectic A (TGBA) Phase

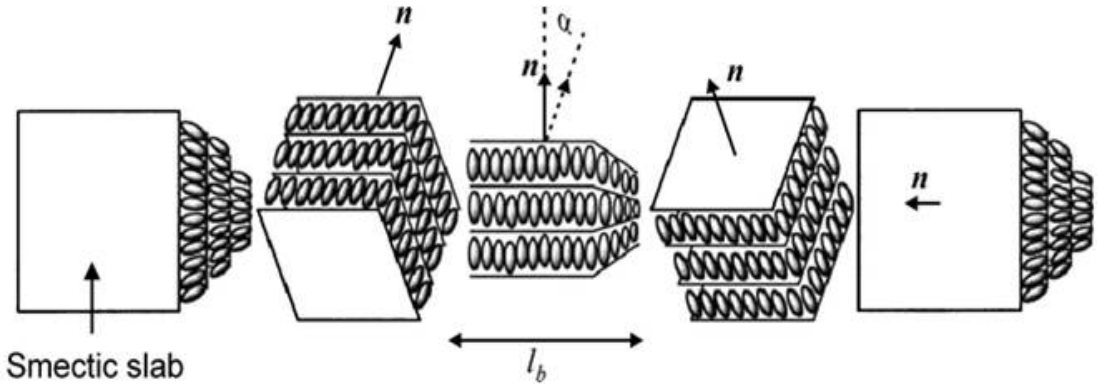

Figure 1.6: Twist grain boundary smectic A phase.

The TGBA phase consist of smectic slabs separated by the defect walls, the neighbouring slabs being tilted with respect to each other leading to a helical structure (figure 1.6). The order within each slab is equivalent to the S_A phase. The molecules are uniaxially aligned along the local director $\hat{n}$ and arranged in layers. The slabs have a typical thickness of about 10nm. The grain boundaries between the slabs are defect walls consisting of parallel defect lines. The distance between the defect lines is similar to the slab thickness. The director forms a helical structure due to the tilt between the neighbouring slabs. The helix axis is perpendicular to the director and the pitch is in the range from few hundred nm to a few μm. The director field of TGBA is similar to the director field of N* phase. However, the TGBA structure behaves optically like a stack of discrete birefringent blocks of finite thickness having a uniform orientation of the optic axis. The reason for the appearance of the TGBA phase is that a direct cholesteric – smectic transition cannot occur in a continuous way since the cholesteric twist of the director is not compatible with the smectic layering. Thus at the TGBA–SmA transition the blocks of layered SmA appear, the blocks having a relative

twist with each other. As the temperature is lowered the helix gradually unwinds and at the TGBA–SmA phase transition the unwinding completes and the SmA phase appears [36–40].

Ferroelectric Liquid crystal

An isotropic liquid cannot have macroscopic polarisation in any direction because of the spherical symmetry of the phase. Spontaneous polarisation is generally not observed in nematic and smectic A phases because it would be energetically unfavourable and the phase would decrease its electrostatic energy by adjusting the director. Finally a minimum energy configuration would result in total cancellation of the polarisation. However in chiral smectic C (smectic C*) phase the symmetry of the phase permits spontaneous polarisation. In 1969 Saupe predicted [35] that smectic C* would be ferroelectric. In 1975 Meyer, along with Liebert, Strzelecki, and Keller experimentally showed observable polarization in liquid crystals [41] thereby starting a new branch of ferroelectric liquid crystals.

Non calamatic liquid crystals

Discotic liquid crystals: Chandrasekhar *et. al.* reported for the first time thermotropic mesomorphism in pure compounds consisting of simple disc like molecules [42]. The disc like molecules can either arrange themselves in stacks one on top of the other like a pile of disordered plate forming the nematic phase or they may arrange themselves in columns one on top of the other thereby forming the columnar phases. Depending upon the orientation of the different columns the columnar phase can be further subdivided in several groups such as hexagonal and rectangular columnar phases.

Bent core liquid crystals: As the name suggests, in bent core liquid crystals the molecular core is not straight. These phases are also known as banana or hockey liquid crystals. During the formative years of liquid crystal research, bent core molecules were not considered as suitable for liquid crystalline research. In calamatic liquid crystals, the rotation about the molecular long axis does not affect the order parameter. The liquid crystal molecules can rotate freely along this symmetry axis. In bent core molecules such free rotation

about the molecular long axes would result in a large excluded volume and the phase would be unstable [43]. Due to this reason not much attention was paid to bent-core molecules and only a few were synthesized before the discovery of their polar switching [44, 45]. Volarander [46, 47] synthesized several bent-core liquid crystals and reported about their mesogenic properties in 1929, mentioning that the thermal stability of the mesophase is low compared with that of the calamatic liquid crystals. After a gap of almost six decades Matsunaga *et. al.* revived the interest in this field [48–51]. Since then, interest in bent core liquid crystals have grown considerably. Bent core liquid crystals have been synthesised which exhibit nematic phase and given the fact that polar switching is possible in these compounds, there is a possibility that such phase may have practical application.

Bent-core LCs are generally composed of five or more aromatic rings with a meta-substituted central ring, linking groups, and terminal chains. The type and position of the linkage groups and nature of the terminal chain determines the molecular properties such as the bend angle, transition temperatures and the mesogenic behaviour. The sterically induced packing leads to unconventional mesophases, some of which have no analogue in calamatic or discotic liquid crystals. The bent core liquid crystals may exhibit uniaxial neamtic, biaxial nematic, smectic C and several banana phases from B_1 to B_7 [43, 52]. Several reviews on bent-core liquid crystals are available [43, 52–55].

1.3 Liquid crystalline mixtures

More than 100,000 liquid crystalline compounds have been synthesized so far [56]. However no single compound has all the desired properties required for the electro-optic display devices. Hence, mixtures of pure compounds are used, where the compositions of the individual components are adjusted so as to obtain the desired properties needed for display applications. The physical properties of such mixtures cannot be always interpolated from the properties of the pure components, notable examples being formation of an induced smectic phase in a mixture of pure nematogens [57–67] and exhibition of re-entrant nematic (N_{re}) phase in mixtures of liquid crystal compounds [68–71] which do not show such phase in their pure form. Such mixtures are of interest, not only from the application point of view but are also of fundamental importance because they present

some unique opportunity to study the phase transition behaviour and molecular interaction within these soft condensed matter systems.

1.3.1 Induced phases

While preparing a binary or a multi component mixture of liquid crystals, the deviation from the linear behaviour may be of two types. The thermal stability may be enhanced and a new phase of higher order may emerge. This new phase is known as the induced phase. The reverse may also happen and the thermal stability of liquid crystalline phase may decrease and a phase of lower order may appear [11].

Induced smectic phases are mostly formed in binary mixtures of nematogenic compounds, one having terminal polar group and other being terminal nonpolar one [71–74]. The smectic phase can also be induced in mixtures of two polar compounds [74, 75] as well as in two non polar mesogenic mixtures [58, 76, 77].

The induction or suppression of a phase in mesogenic mixtures depends upon the delicate balance of the different intermolecular forces such as Van der waals force, hydrogen bonds, electron donor interactions and steric forces. Hence it is difficult to obtain a successful general theory which can explain such non linear behaviours. A number of attempts have been made [59, 74, 75, 78–85] to explain the induced phases. de Jeu *et. al.* [81] proposed a molecular model using mean field approximation for the induced smectic phase in cyano compounds. According to this model, the dispersion interactions as well as the charge transfer complex formation in which the cyano compounds acts as electron acceptor are responsible for the occurrence of the induced smectic phase. Kyu *et. al.* [84] have demonstrated that the strong nematic interaction between the dissimilar mesogens can give rise to a more stable nematic in the nematic mixtures relative to that in the constituent compounds having the same mesogenic moiety. To account for an induced smectic phase boundary in mixtures of pure nematogens, they have developed a theoretical model [85] by combining Flory-Huggins theory for isotropic mixing [86] and Maier-Saupe-McMillan theory for ordering of smectic-A phase [87, 88] in nematic mixture. They conjectured that a strong mesogenic interaction could induce a smectic phase although smectic ordering was absent in the constituent pure compound. In spite of a number of attempts

being made to develop a theory for the induced smectic phase our knowledge is far from being complete.

1.3.2 Re-entrant nematic phase

In any material, it is expected that on increasing the temperature the entropy will increase and hence the degree of molecular ordering will decrease. Hence, if a liquid crystalline material is cooled from its isotropic phase then the liquid crystalline phases should occur in order of decreasing symmetry. That is if all the phase are assumed to be present then the following phase sequence is expected.

$$\textbf{Isotropic Liquid} \rightarrow \textbf{blue} \rightarrow \textbf{N} \rightarrow \textbf{SmA} \rightarrow \textbf{SmC} \rightarrow \textbf{SmB}_{\textbf{hex}} \rightarrow \textbf{SmI} \rightarrow \textbf{SmB}_{\textbf{cry}} \rightarrow \textbf{SmJ} \rightarrow \textbf{SmG} \rightarrow \textbf{SmE} \rightarrow \textbf{SmK} \rightarrow \textbf{SmH} \rightarrow \textbf{Crystal/Solid}$$

An exception to this phase sequence was observed by Cladis in binary mixture of strongly polar compounds HBAB and CBOOA at atmospheric pressure [58]. Over a certain composition range it was found that on cooling, a nematic phase was found below a smectic A_d phase. Since then re-entrance has been observed in mixtures [89, 90] as well as in pure compounds at high [91] and normal pressure [92, 93]. Multiple re-entrance has also been reported [94–98] and the most interesting phase sequence is probably exhibited by 4-nonyloxyphenyl-4'-nitrobenzoyloxybenzozte (DB90NO2) where the following phase sequence is observed [96–99].

$$\textbf{Isotropic Liquid} \rightarrow \textbf{N} \rightarrow \textbf{SmA}_{\textbf{d}} \rightarrow \textbf{N}_{\textbf{re}} \rightarrow \textbf{SmA}_{\textbf{1}} \rightarrow \textbf{SmC} \rightarrow \textbf{SmA}_{\textbf{2}} \rightarrow \textbf{SmC}_{\textbf{2}} \rightarrow \textbf{Crystal/Solid}$$

This type of phase transition, where a phase of higher symmetry appears below a phase of lower symmetry is not unique to liquid crystalline materials and is has been observed in diverse systems such as binary gases [100–102], liquid mixtures [103–107], ferroelectricity [108], organometallic compounds [109], granular superconductor [110], gels [111], aqueous electrolyte [112], antiferromagnets [113] etc.

Apart from strongly polar systems re-entrance is also possible in mixtures of compounds having high and low polarity [114–117], low polar calamatic [118] as well as low polar discotic [119, 120] systems.

A number of systems [66, 67, 121–126] have been reported where the induced smectic and the re-entrant nematic phase occur simultaneously in a mixture.

As in the case of induced phase, the appearance of the re-entrant phase also depends on the delicate balance between the different intermolecular forces, making a general quantitative theory difficult. The situation is further complicated by the fact that the re-entrance in different compounds results from different mechanisms [127]. Thus, from the molecular point of view only an approximate qualitative explanation of the re-entrant behaviour has been possible.

The first model for the nematic re-entrance was proposed by Cladis [128]. Since then, a number of theories have been given [128–145]. Cladis [116, 145] proposed a mechanism for the formation of the re-entrant nematic phase. This model assumes that the re-entrance appears only in compounds exhibiting layered phases of amphiphilic molecules having both a polar and a non polar part, the two part of the molecule being immiscible. In the smectic A phase the molecules move freely within each layer and with difficulty between the layers. There exists no correlation between molecules in different layers. Usually, in most of the liquid crystals, the polar segments of the molecules occupy a middle position with the hydrocarbon chains extending outwards. These kind of configurations prefer to form a monolayer smectic A phase. In case of re-entrance, owing to antiparallel correlation, the molecules form dimers which are assumed to be somewhat bulgy in the middle. As a result, the occurrence of incommensurate smectic A_d phases are probable. Once the smectic A_d phase is formed, the bulgy parts are lined up in a plane, whereas the alkyl chain cannot fill the rest of the space. With decreasing temperature and also possibly with the stiffening of the end chains, the packing becomes so unfavourable that the smectic A_d phase becomes unstable and nematic re-entrance appears.

A more complete theoretical discussion was proposed by Longa and de Jeu [129], who showed that re-entrant behaviour in nematic liquid crystal can be described by treating the system as a mixture of monomers and dimers interacting through induced soft interactions as well as hard-core repulsions. They showed

that the induced forces between dimers, monomers, and between monomers and dimers, respectively, under suitable conditions of temperature and density lead to a smectic layer structure with a period equal to the length of the dimer. However, with decreasing temperature or increasing density, repulsive steric forces, due to the unfavourable packing of the dimers in the smectic planes, may take over and thus favours the nematic phase again. It is predicted that the best condition to get re-entrant nematic phase are for the ratio of length of dimer to that of the monomer between 1.3 and 1.4.

Luckhurst and Timimi [130] developed a molecular theory for the re-entrant nematic and smectic A mesophases by extending McMillan's treatment of the smectic A phase [87, 88]. According to McMillan's theory, the single particle potential is given by

$$V_M(\cos\theta, z) = -v\left[\delta\alpha\tau\cos\left(\frac{2\pi z}{d}\right) + \left\{\eta + \alpha\sigma\cos\left(\frac{2\pi z}{d}\right)\right\}P_2(\cos\theta)\right] \tag{1.3}$$

where α and δ are two adjustable parameters, z is the displacement along the layer normal, d is the layer thickness, $\eta = \langle P_2(\cos\theta)\rangle$, the orientational order parameter, while $\tau = \langle\cos(2\pi z/d\rangle$, is the translational order parameter and $\sigma = \langle P_2(\cos\theta)\cos(2\pi z/d\rangle$, is the mixed translational and orientational order parameter. The parameter v is obtained from the nematic/isotropic transition temperature, assuming the simple mean field theory result ($kT_{NI}/v = 0.22019$). The values of η, τ and σ are calculated using the self-consistent relationships [87, 88] as a function of temperature for various values of the parameters α and δ. The stability of the smectic A_d phase is controlled by the two adjustable parameters α and δ, with α being the primary variable. In the McMillan's theory the molecules are assumed to be rigid and the parameters α and δ are taken to be independent of temperature. However Luckhurst and Timimi argued that the parameter α depends on the molecular length, which varies with the chain length of the mesogenic molecules. Thus, α cannot be independent of temperature. Further, in polar systems partial dimers are formed whose structure may change with temperature. Based on these arguments Luckhurst and Timimi identified the particles in McMillan's theory as the dimers and suggested that α should have a weak temperature dependence. The parameter δ , being the ratio of the translational to the orientational part of the potential, was assumed to be independent of composition and temperature. According to Luckhurst and Timimi

[130], the orientational order parameter increases with decreasing temperature in a manner almost independent of the SmA–N transition. If α decreases with temperature then the SmA–N transition temperature will be reduced. An appropriate choice of the temperature dependence of the parameter α gives rise to a situation where lowering the temperature still produces the usual SmA–N transition. Further decrease in temperature reduces α to such an extent that the SmA phase becomes and reverts to the nematic phase; in other words a re-entrant nematic phase is formed.

Bose *et. al.* [146] proposed a mean field model by extending the McMillan's potential, which could reproduce the $N-SmA-N_{re}-S_{re}$ phase sequence in strongly polar pure compounds. They showed that dimers in the presence of space filling monomers can account for the high temperature SmA phase. As the temperature is lowered, more and more monomers form dimers leaving empty spaces and this initiates an intercalation of dimers belonging to the neighbouring layers. This intercalation is responsible for the lowering of the strength of layer interaction in a McMillan type potential and thus a re-entrant nematic phase occurs. This model could account for the thickness of the low temperature smectic phase. Bose *et. al.* [147] also proposed an alternative mechanism for space filling which could account for SmA_d-N_{re} transition with an accompanying increase of layer thickness. They showed that their proposed mechanism of space filling coupled with intercalation could lead to SmA_d-N_{re} transition at constant layer thickness.

Berker *et. al.* [134, 135] have formulated a spin gas model which can explain multiple re-entrance in polar liquid crystals. They considered the molecules to have an aliphatic chain and a polar head along the molecular axis. The molecules are assumed to be closely packed in a two dimensional array and have a perfect orientational order in a direction perpendicular to the lattice plane. The molecules are free to move along the axis but this movement is restricted by the presence of notches in the molecules. These notches are assumed to be related to the number of carbon atoms in the alkyl chain. The close packing arrangement in two dimensions being triangular they considered triplet of molecules. However, each triplet of the array is frustrated and hence a long range antiferroelectric order cannot be supported. If the local distribution is like figure 1.7d

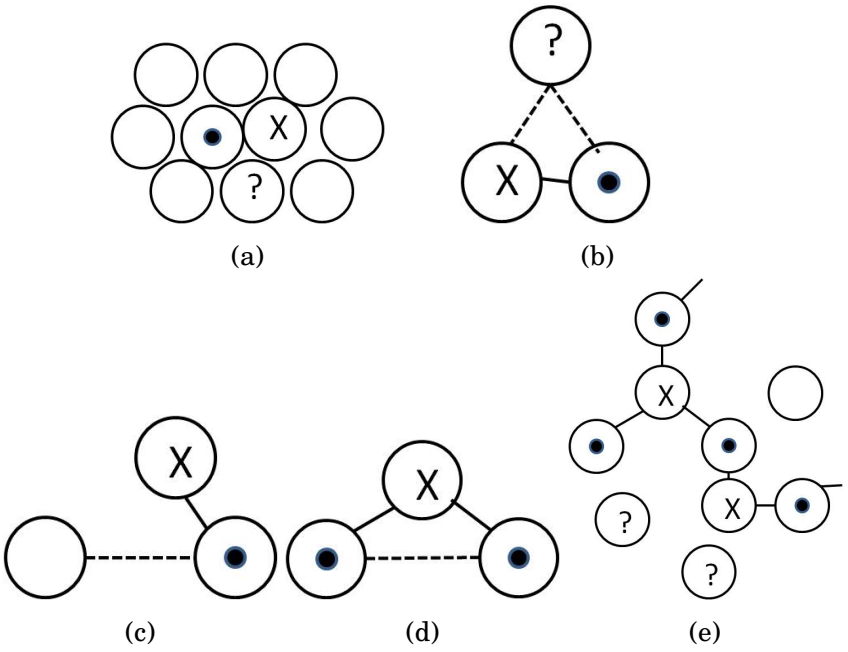

Figure 1.7: Positional configuration of a layer normal to the molecule axis. Molecular dipoles which are pointing into or out of the figure, or which are frustrated, are respectively indicated by crosses, closed circles, or question marks. Strong (weak) bonds are shown with full (dotted) lines.

with one weak and two strong bonds, frustration will be lifted, and two dimensional antiferroelectric order can propagate across the unit. On the other hand if the elementary triangle is like figure 1.7b with one strong and two weak bonds, it will still be frustrated and at most a one dimensional antiferroelectric correlation can propagate across, which is not sufficient for antiferroelectric ordering. In any given snapshot of the layer, each elementary triangle is between these two cases, with one strong, one weak and one intermediate bond (figure 1.7c). Whether the intermediate bond is closer to the stronger one or to the weaker one determines the ordering characteristics of the unit. If there is enough of the former type of units, they will percolate across the system and form an infinite network of positionally disordered, but antiferroelectrically ordered molecules (figure 1.7e). Each layer, consecutively along the z direction (along the layer normal), will have its own network. These networks will not pass through each other because this would involve disrupting infinitely many strong bonds. The result is the density modulation along z axis, namely the smectic phase. Even in the presence of the networks, many antiferroelectrically ordered but finite clusters slide up

and down the z axis giving a constant background to the smectic modulation. Although the percolating network must be sustained for the smectic modulation, individual molecules join it and leave it as time progresses. As the system is further cooled local positioning order sets in, turning on frustration, eventually destroying the network and re-entering the nematic phase.

Several reviews are available which discuss these theories and the re-entrant phenomenon in details [11, 23–25, 97, 127, 128].

References

[1] F. Reinitzer, *Monatsh. Chem.*, **9**, 421 (1888).

[2] F. Reinitzer, *Liq. Cryst.*, **5**, 7 (1989) (translation of reference (1)).

[3] P. G. de Gennes, *The Physics of Liquid Crystal*, 2nd Ed, Clarendon Press, Oxford (1993).

[4] L. M. Blinov, *Usp. Fiz. Nauk.*, **114**, 67 (1974) (Sov. Phys. Usp.), 17, 658 (1975).

[5] S. Chandrasikhar, *Liquid Crystals*, Cambridge University Press, Cambridge (1977).

[6] E. B. Priestley, P. J. Wojtowicz and P. Sheng, Eds., *Introduction to Liquid Crystals*, Plenum, N. Y. (1974).

[7] G. W. Gray, *Molecular structure and the properties of Liquid Crystals*, Academic Press (1962).

[8] G. Vertogen and W. H. de Jeu, *Thermotropic Liquid Crystals, Fundamentals*, Springer-Verlag (1988).

[9] G. W. Gray and P. A. Winsor (Ed.), *Liquid Crystals*, **1 & 2**, Ellis Horwood Ltd. (1974).

[10] G. W. Brown (Ed.), *Advances in Liquid Crystals,* ***1-6***, Academic Press (1975-1983).

[11] A. Buka, (Ed.), *Modern Topics in Liquid Crystals*, World Scientific (1993).

[12] S. J. Elston and J. R. Sambles (Edn.), *The Optics Of Thermotropic Liquid Crystals*, Taylor & Francis (1998).

[13] D. Demus, *Liquid Crystals Applications and Uses*, Ed. B. Bahadur (Utopia Press, Singapore, New Jersey, London, Hong Kong, 1990), **Vol.I**.

[14] B. Bahadur, *Liquid Crystals, Applications and Uses*, Ed., World Scientific, **Vol. 1,2,3** (1991).

[15] G. R. Luckhurst and G. W. Gray (Eds.), *The molecular physics of liquid crystals*, Academic Press, London (1979).

[16] S. Chandrasekhar (Ed.), *Liquid Crystals*, Heyden, London (1980).

[17] D. Demus, J. Goodby, G. W. Gray, H. W. Spiess, V. Vill, (Eds.), *Handbook of Liquid Crystals: Low Molecular Weight Liquid Crystals I,* ***2A***, Wiley-VCH (1998).

[18] S. Singh, *Liquid Crystals: Fundamentals*, World Scientific (2002).

[19] I. C. Khoo. *Liquid crystals (2^{nd} ed.)* John Wiley & Sons, Inc., New Jersey (2007).

[20] P. Oswald, P. Pieranski, *Nematic and Cholesteric Liquid Crystals*. Taylor & Francis (2005).

[21] S. V. Pasechnik, V. G. Chigrinov, D. V. Shmeliova, *Liquid Crystals: Viscous and Elastic Properties* Wiley-VCH Verlag GmbH & Co. KGaA (2009).

[22] S. Singh, *Physics Reports*, **277**, 283 (1996).

[23] S. Singh, *Phase transitions*, **72**, 183 (2000).

[24] S. Singh, *Physics Reports*, **324**, 107 (2000).

[25] P. E. Cladis, *Mol. Cryst. Liq. Cryst*, **165**, 85 (1988).

[26] G. Friedel, *Ann. Physique*, **18**, 273 (1922).

[27] A. de Vries, *Mol. Cryst. Liq. Cryst*. **10**, 31 (1970); *ibid* **10**, 219 (1970); *ibid* **11**, 36 (1970).

[28] L. M. Blinov, *Structure and Properties of Liquid Crystals*, Springer, (2011).

[29] P. Oswald, P. Pieranski, *Smectic and Columnar Liquid Crystals*, Taylor & Francis (2006).

[30] L. A. Madsen, T. J. Dingemans, M. Nakata, E. T. Samulski, *Phys. Rev. Lett.*, **92**, 14 (2004).

[31] G. Sigaud, F. Hardouin, M. F. Achard, and A. M. Levelut, *J. Phys. (Paris)* **42**, 107 (1981).

[32] V. A. Belyakov, V. E. Dmitrienko, *Blue phase of liquid crystals*, Uspekhi Fis. Nauk., **146**, 369 (1985).

[33] N. C. Shivaprakash and J. S. Prasad, *J. Chem. Phys.*, **76**, 1209 (1982).

[34] B. Das, A. Pramanik, M. K. Das, A. Bubnov, V. Hamplova, M. Kaspar, *J. Mol. Struct.*, **1013**, 119 (2012).

[35] A. Saupe, *Mol. Cryst. Liq. Cryst.*, **7**, 59 (1969).

[36] J. W. Goodby, *Structure and Bonding: Liquid Crystal II*, **95**, 83-147, (1999).

[37] J. W. Goodby, M. A. Waugh, S. M. Stein, E. Chin, R. Pindak and J. S. Patel, *Nature*, London, **337**, 449 (1989).

[38] J. W. Goodby, M. A. Waugh, S. M. Stein, E. Chin, R. Pindak and J. S. Patel, *J. Am. Chem. Soc.*, **111**, 8119 (1989).

[39] S. R. Renn and T. C. Lubensky, *Phys. Rev. A*, **38**, 2132 (1988).

[40] S. R. Renn and T. C. Lubensky, *Mol. Cryst. Liq. Cryst.*, **209**, 349 (1991).

[41] R. B. Meyer, L. Liebert, L. Strzelecki, P. J. Keller, *Phys. Lett. (Orsay, Fr.)*, **36**, L-69 (1975).

[42] S. Chandrasekhar, B. K. Sadashiva and K. A. Suresh, *Pramana*, **9** (5), 471 (1977).

[43] H. Takezoe and Y. Takanishi, *Jpn. J. Appl. Phys.*, **45**, **2A**, 597 (2006).

[44] H. R. Brand, P. E. Cladis, H. Pleiner, *Macromolecules*, **25**, 7223 (1992).

[45] T. Niori, T. Sekine, J. Watanabe, T. Furukawab and H. Takezoeb, *J. Mater. Chem.*, **6**, 1231 (1996).

[46] D. Vorlander, *Ber. Dtsch. Chem. Ges.*, **62**, 2831 (1929).

[47] D. Vorlander and A. Apel, *Ber. Dtsch. Chem. Ges.*, **65**, 1101 (1932).

[48] M. Kuboshita, Y. Matsunaga and H. Matsuzaki, *Mol. Cryst. Liq. Cryst.*, **199**, 319 (1991).

[49] T. Matsuda and Y. Matsunaga, *Bull. Chem. Soc. Jpn.*, **64**, 2192 (1991).

[50] H. Matsuzaki and Y. Matsunaga, *Liq. Cryst.*, **14**, 105 (1993).

[51] T. Akutagawa, Y. Matsunaga and K. Yasuhara, *Liq. Cryst.*, **17**, 659 (1994).

[52] G. Pelzl, S. Diele and W. Weissflog, *Adv. Mater.*, **11** (9), 707 (1999).

[53] C. Tschierske and G. Dantlgraber, *Pramana*, **61**, 455 (2003).

[54] M. B. Ros, J. L. Serrano, M. R. de la Fuente and C. L. Folcia, *J. Mater. Chem.*, *15*, 5093 (2005).

[55] R. A. Reddy and C. Tschierske, *J. Mater. Chem.*, **16**, 907 (2006).

[56] X. H. Cheng, M. Prehm, M. K. Das, J. Kain, S. Diele, D. Leine, A. Blume and C. Tschierske. *J. Am. Chem. Soc.*, **125** (36), 10977 (2003).

[57] J. W. Park, C. S. Bak and M. M. Labes, *J. Am. Chem. Soc.*, **97**, 4398 (1975).

[58] C. S. Oh, *Mol. Cryst. Liq. Cryst.*, **42**, 1 (1977).

[59] B. Engelen and F. Schneider, *Z. Naturforsch*, **33A**, 1077 (1978).

[60] M. Domon and J. Billard, *J. Phys. (Paris)*, **40**, C3-413 (1979).

[61] F. Schneider and N. K. Sharma, *Z. Naturforsch.*, **36A**, 62 (1981).

[62] D. Demus, *Mol. Cryst. Liq. Cryst.*, **364**, 25 (2001).

[63] M. K. Das and R. Paul, *Phase Transitions*, **48**, 255(1994), ibid. **46**, 185 (1994).

[64] M. K. Das, R. Paul and D. A. Dunmur, *Mol. Cryst. Liq. Cryst.*, **285**, 239 (1995).

[65] D. A. Dunmur, R. G. Walker and P. Palffy-Muhoray, *Mol. Cryst. Liq. Cryst.*, **122**, 321 (1985).

[66] M. Brodzik and R. Dabrowski, *Liq. Cryst.*, **18**, 61 (1995).

[67] M. Tykarska, B. Wazynska, I. Ulbin, *Proceeding of SPIE.*, **4147**, 55 (2000).

[68] P. E. Cladis, *Phys. Rev. Lett.*, **35**, 48 (1975).

[69] D. Guillon, P. E. Cladis and J. Stamatoff, *Phys. Rev. Lett.*, **41**, 1598 (1978).

[70] P. E. Cladis, *Mol. Cryst. Liq. Cryst.*, **67**, 177 (1981).

[71] S. Diele, G. Pelzl, I. Latif and D. Demus, *Mol. Cryst. Liq. Cryst.*, **92**, 27 (1983).

[72] L. K. M. Chen, G. W. Gray, D. Lacey, S. Srilhauratana, K. L. Toyne, *Mol. Cryst. Liq. Cryst.*, **150B**, 335 (1985).

[73] G. Pelzl, I. Latif, S. Diele, M. Novak, D. Demus, H. Sackmann, *Mol. Cryst. Liq. Cryst.*, **139**, 333 (1986).

[74] N. K. Sharma, G. Pelzl, D. Demus and W. Weissflog, *Z. Phys. Chem.*, **261** (1980).

[75] K. Araya and Y. Matsunaga, *Bull. Chem.. Soc. Jap.*, **53**, 3079 (1980).

[76] G. P. Montgomery, *large-Area Chromogenics: Materials and devices for Transmittance Control*, C. M. Lampert and G. G. Granqvist (Ed. SPIE)

[77] P. S. Drzaic, *J. Appl. Phys.*, **60**, 2142 (1986).

[78] F. Schneider, N. K. Sharma, Z. Naturforsch., **36A**, 1086 (1981).

[79] K. Arya, Y. Mastunga , *Mol. Cryst. Liq. Cryst.*, **84**, 225 (1982).

[80] Y. Iida, *Bull. Chem. Bull. Chem. Soc. Jap.*, **55**, 2661 (1982).

[81] W. H. de Jue, L. Longa, *J. Chem. Phys.*, **84**, 6410 (1986).

[82] W. Wagner, *Cryst. Res. Tech.*, **17**, K67 (1982).

[83] P. Palffy-Muhoray, D. A. Dunmur, W. H. Miller and D. A. Balzarini, *Liquid Crystal and Ordered Fluid*, **Vol 4**, Eds. A. C. Griggin and J. F. Johonson Plenum, N.Y., p. 615 (1984).

[84] H. W. Chiu and T. Kyu, *J. Chem. Phys.* **103**, 7471 (1995).

[85] T. Kyu, H. W. Chiu and T. kajiyama, *Phys. Rev. E*, **55**, 7105 (1997).

[86] P. J. Flory, *Principles of Polymer Chemistry*, Cornell University press, Ithaca (1953).

[87] W. Maier and A. Saupe, *Z. Naturforsch*, **15A**, 287 (1960).

[88] W. L. McMillan, *Phys. Rev. A*, **4**, 1238 (1971).

[89] R. Dabrowski and K. Czuprynski, *Mol. Cryst. Liq. Cryst.*, **146**, 341 (1987).

[90] K. Czuprynski and R. Dabrowski, *Mol. Cryst. Liq. Cryst. Lett.*, **4**, 153 (1987).

[91] R. Dabrowski and K. Czuprynski, J. Przedmojski, B. Wazynska, *Liq. Cryst.*, **14**, 1359 (1993).

[92] B. Wazynska, *Liq. Cryst.*, **4**, 399 (1989).

[93] H. T. Nguyen, *J. Chem. Phys.*, **80**, 83 (1983).

[94] F. Hardouin, G. Sigaud, M. F. Achard, H. Gasparoux, *Phys. Lett.* **71**, 347 (1979).

[95] K. W. Evans-Lutterodt, J. W. Chung, B. M. Ocko, R. J. Birgeneau, C. Chiang, C. W. Garland, E. Chin, J. Goodby, N. H. Tinh, *Phys. Rev. A*, **36**, 1387 (1987).

[96] F. Hardouin, A. M. Levelut, M. F. Achard, G. Sigaud, *J. Chim. Phys.*, **80**, 53 (1983).

[97] N. H. Tinh, *J. Chim. Phys.* 80, **83** (1983).

[98] R. Shashidhar, B. R. Ratna, V. Surendranath, V. N. Raja, K. S. Prasad, C. Nagabhushana, *J. Phys. Lett. (Paris)*, **46**, L445 (1985).

[99] N. H. Tinh, F. Hardouin, C. Destrade, A. M. Levelut, *J. Phys. Lett. (Paris)*, **43**, L33 (1982).

[100] A. Deerenberg, J. A. Schoutem, N. J. Trappeniers, *Physica*, **103A**, 183 (1980).

[101] J. A. Schouton, *Phys. Rep.*, **172**, 33 (1989).

[102] R. J. Tufeu, P. H. Keyes, W. B. Daniels, *Phys. Rev. Lett.*, **35**, 1004 (1975).

[103] J. D. Cox, *J. Chem. Soc.*, **4**, 606 (1952).

[104] T. Narayanan, A. Kumar, E. S. R. Gopal, *Phys. Lett. A*, **155**, 276 (1991).

[105] R. G. Johnston, N. A. Clark, P. Wiltzins, D. S. Cannel, *Phys. Rev. Lett.*, **54**, 49 (1985).

[106] V. P. Zaitsev, S. V. Krivokhizha, I. L. Fabelinskii, A. Tsitrovskii, L. L. Chaikov, E. V. Shvelts, P. Yani, *Sov. Phys. JETP Lett.*, **43**, 112 (1986).

[107] S. V. Krivokhizha, O. A. Dugovaya, I. L. Fabelinskii, L. L. Chaikov, A. Tsitrovskii, P. Yani, *Sov. Phys. JETP* **76**, 62 (1993).

[108] G. B. Kozlov, E. B. Kryukova, S. P. Lobedev, A. A. Sobyanin, *Sov. Phys. JETP*, **67**, 1689 (1988).

[109] M. J. Naughton, R. V. Chamberlin, X. Yan, S. Y. Ysu, L. Y. Chiang, M. Y. Azbel, P. M. Chaikin, *Phys. Rev. Lett.*, **61**, 621 (1988).

[110] T. H. Lin, X. Y. Shao, M. K. Wu. P. H. Hoy, X.C. Jin, C.W. Chu, N. Evans, R. Bayuzick, *Phys. Rev. B*, **29**, 1493 (1984).

[111] S. Katayama, Y. Hirokawa, T. Kanaka, *Macromolecules*, **17**, 2649 (1984).

[112] H. Glusbrenner, H. Weingartner, *J. Phys. Chem.*, **93**, 3378 (1989).

[113] R. B. Griffiths, *Critical Phenomena in Alloys, magnets and superconductors*, Eds., R.E. Mills, E. Ascher, R.I. Jaffee, McGraw-Hill, New York, p.377, (1971).

[114] G. Pelzl, U. Bottger, D. Demus, *Cryst. Res. Technol.*, **16**, K67 (1981).

[115] B. Engelen, G. Heppke, R. Hopf and F. Schneider, *Mol. Cryst. Liq. Cryst. Lett.*, **49**, 193 (1979).

[116] W. Weissflog, N. K. Sharma, G. Pelzl and D. Demus, *Krist. and Techn.*, **15**, K35 (1980).

[117] S. Takenaka, H. Nakai and S. Kusabayashi, *Cryst. Liq. Cryst.*, **100**, 299 (1983).

[118] G. Pelzl, J. Latif, S. Diele, M. Novak, D. Demus and H. Sackmann, *Mol. Cryst. Liq. Cryst.*, **139**, 333 (1986).

[119] N. H. Tinh, J. Malthete and C. Destrade, *Mol. Cryst. Liq. Cryst.*, **64**, 291 (1981).

[120] N. H. Tinh, P foucher, C Destrade, A M Levelut and J Malthete, *Mol. Cryst. Liq. Cryst.*, **111**, 277 (1984).

[121] M. Brodzik and R. Dabrowski, *Mol. Cryst. Liq. Cryst.*, **260**, 361 (1995).

[122] R. Dabrowski and K. Czuprynski, *Modern topics in Liquid Crystals – from Neutron Scattering to Ferroelectricity*, (Ed.) A. Buka, World Scientific (London), (1993).

[123] M. Brodzik and R. Dabrowski, *Proceeding of SPIE*, **2372**, 280 (1995).

[124] M. Brodzik, Ph. D. Thesis, Wojskowa Akademia Techniczna (1995).

[125] M. Brodzik and R. Dabrowski, *Liquid Crystals*, **20**, 99 (1996).

[126] M. Brodzik, R. Dabrowski and J. Przedmojski, *J. Phys. II France*, **5**, 1805 (1995).

[127] P. E. Cladis, *Hand Book of Liquid Crystals*, **Vol 1**, Eds. D. Demus, J. Goodby, G. W. Gray, H. -W. Spiess, V. Vill, 391-405 (1998).

[128] P. E. Cladis, R. K. Begardus, W. B. Daniels, G. N. Taylor, *Phys. Rev. Lett.*, **39**, 720 (1977).

[129] L. Longa, W. H. de Jeu, *Phys. Rev. A*, **26**, 1632 (1982).

[130] G. R. Luckhurst, B. A. Timimi, *Mol. Cryst. Liq. Cryst. (Lett.)*, **64**, 253, (1981).

[131] W. H. de Jeu, *Solid State Comm.*, **41**, 529 (1982).

[132] T. R. Bose, D. Ghosh, C. D. Mukherjee, J. Saha, M. K. Roy, M. Saha, *Phys. Rev. A*, **43**, 4372 (1991).

[133] L. V. Miramtser, *Mol. Cryst. Liq. Cryst.*, **133**, 151 (1986).

[134] A. N. Berker, J. S. Walker, *Phys. Rev. Lett.*, **47**, 1469 (1981).

[135] J. O. Indekeu, A. N. Berker, C. Chiang, C. W. Garland, *Phys. Rev. A*, **35**, 1371 (1987).

[136] N. V. Madhusudana, J. Rajan, *Liq. Cryst.*, **7**, 31 (1990).

[137] J. Prost, *Adv. Phys.*, **33**, 1 (1984).

[138] J. Prost, P. Barois, *J. Chim. Phys.*, **80**, 65 (1983).

[139] P. S. Person, J. Prost, *J. Phys. Lett. (Paris)*, **40**, L-27 (1979).

[140] P. J. Flory, R. Ronca, *Mol. Cryst. Liq. Cryst.*, **54**, 311 (1979); F. Dowell, *Phys. Rev. A*, **28**, 1003 (1983); F. Dowell, *Phys. Rev. A*, **31**, 2464 (1985).

[141] F. Dowell, *Phys. Rev.A*, **28**, 3520 (1983); C. Rosenblatt, D. Ronis, *Phys. Rev. A*, **23**, 305 (1981); D. Ronis, C. Rosenblatt, *Phys. Rev. A*, **21**, 1687 (1980).

[142] F. Dowell, *Phys. Rev. A*, **36**, 5046 (1987), *ibid*, **38** , 382 (1988).

[143] J. Katriel, G. F. Kventsel, *Phys. Rev. A*, **28**, 3037 (1983).

[144] J. Katriel, G. F. Kventsel, *Mol. Cryst. Liq. Cryst.*, **124**, 179 (1985).

[145] P. E. Cladis, R. K. Begardus, and D. Aadsen, *Phys. Rev. A*, **18**, 2292 (1978).

[146] T. R. Bose, C. D. Mukherjee, M. K. Roy and M. Saha, *Mol. Cryst. Liq. Cryst.*, **126**, 197 (1985).

[147] T. R. Bose, D. Ghose, M. K. Roy, M. Saha and C. D. Mukherjee, *Mol. Cryst. Liq. Cryst.*, **172**, 1 (1989).

[148] B. Engelen, G. Heppke, R. Hopf and F. Schneider, *Ann. Phys.*, **3**, 403 (1978).

Chapter 2

Experimental methods and theoretical background

2.1 Introduction

In this chapter I have discussed in brief the various experimental techniques that have been used in this work. I have also describe briefly the molecular theories of liquid crystals viz. the Maier–Saupe mean field theory for nematic phase [1–4], McMillan's theory for the smectic A phase [5] and the modification of McMillan's theory by Luckhurst and Timimi [6] to explain re-entrant nematic phase behavior. A number of theories for liquid crystals have been given by different workers. However, the only reason for choosing the above three theories is that the experimental results have been compared with the theoretical values from them.

2.2 Texture studies

When liquid crystalline samples placed between a crossed polarizer and an analyzer is examined under a microscope, a wide variety of patterns are observed which originates due to the discontinuity in the director distribution. The arrangement of defects and domains result in the observed visual patterns and are known as textures. Observation of these textures and their changes with temperature is an important technique for preliminary phase identification and determination of the phase transition temperatures.

The liquid crystal samples were inserted between a glass slide and a cover slip and placed in a hot stage (Mettler Toledo FP-82 HT) the temperature of which was controlled by Mettler Toledo FP 90 central processor. The textures of the phases were observed using a polarizing optical microscope (Motic Research Microscope BA300 with polarizing attachment) and the phase transition temperatures were recorded. The phase diagrams of different binary systems were then constructed. Identification of different liquid crystalline phases by the observation of textures alone is often ambiguous, therefore other methods are required to support it. Detailed description of various textures and their photographs, has been given by Demus *et. al.* [7] and I. Dierking [8].

2.3 X-ray diffraction measurement

The structural information of the liquid crystalline compounds as well as their orientational properties can be investigated on a quantitative basis very conveniently from X-ray diffraction measurements.

Almost immediately after the discovery of X-ray diffraction by Laue *et. al.* [9], Lingen [10] and Friedel [11] made an attempt to obtain the X-ray diffraction pattern of liquid crystals. However, conclusive results were only available a few years later due to the works of K. Kast [12–16] and Herremann *et. al.* [17–25] on PAA. Since then, the field of X-ray diffraction of liquid crystal has grown and matured. A number of review articles in this area are available [26–35]. Vainstein [36, 37] and Leadbetter [38, 39] have given the theoretical interpretation for the X-ray diffraction of liquid crystals. From X-ray measurements, the fourier image of the correlation density function can be determined, the reconstruction of which from the scattered data yields information both on the mutual arrangement of molecules in a liquid crystal and on the specific features of the orientational and translational order.

Generally, unaligned liquid crystal sample consists of a large number of domains, the molecules being ordered in each domain along the director $\hat{n}$. However, the different directors are randomly oriented in all possible directions. Hence, there is no single preferred direction and the sample has symmetry of revolution around the direction of the X-ray beam. This results in the X-ray diffraction pattern forming a uniform halo just like that of an isotropic liquid.

The symmetry of revolution around the direction of the X-ray beam can be broken by orienting the liquid crystalline sample along a preferred direction by applying magnetic or electric field of suitable strength or by surface alignment of the sample.

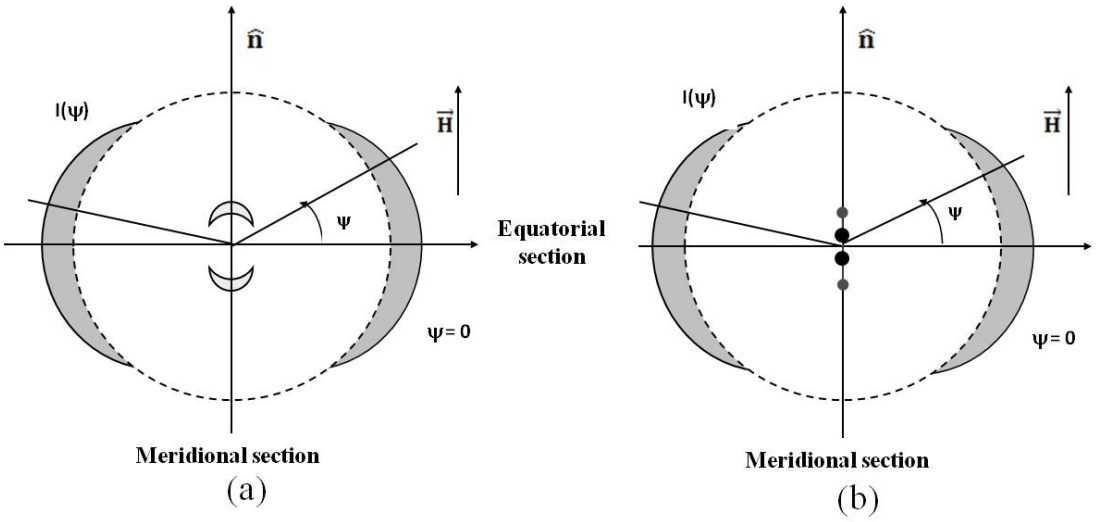

Figure 2.1: Schematic representation of X-ray diffraction pattern of an oriented (a) nematic, (b) smectic A, with X-ray beam parallel to the layer normal.

As shown in figure 2.1a, the alignment of the sample results in the splitting of the outer halo into two crescents, the intensity being maximum along the equatorial direction (perpendicular to the director). These crescents are formed mainly due to the intermolecular scattering and the corresponding Bragg angle gives the lateral intermolecular distance. In the meridional direction (parallel to the director) two crescents in the small angle region are observed whose Bragg angle gives the apparent molecular length for the nematic phase or layer thickness for the smectic phase. Sometimes, the inner diffuse crescents are replaced by spots and the corresponding phase is called “cybotactic phase” as shown in figure 2.1b. The presence of such sharp spots indicate smectic like clusters in the nematic phase, which are called “cybotactic” groups [40]. However, smectic A phase has only quasi-long range order along its layer normal [41, 42] and hence, second order Bragg reflections in the meridional direction (parallel to the director) are generally very weak and are often absent in the X-ray diffraction photographs. From X-ray diffraction photographs of aligned liquid crystal samples

the angular distribution of the X-ray intensity $I(\psi)$ can be obtained from which the orientational distribution function $f(\cos\theta)$ and hence the orientational order parameters $\langle P_2\rangle, \langle P_4\rangle$ can be determined.

The X-ray diffraction setup used in our laboratory has been designed and fabricated by Jha and Paul [43], the schematic diagram of which has been given below (figure 2.2).

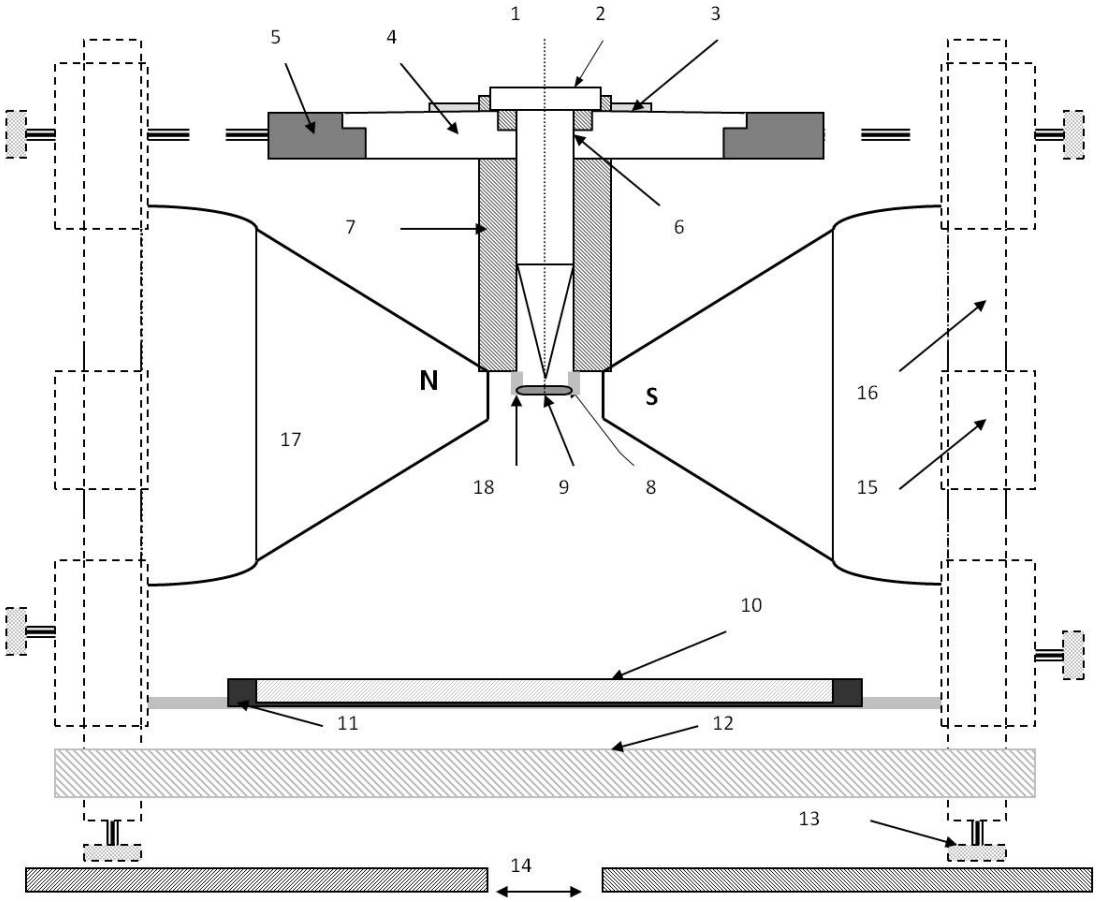

Figure 2.2: Sectional diagram of the X-ray diffraction set-up.

1. X-ray 2. Collimator 3. Brass ring 4. Ring of syndanyo board 5. Brass ring 6. Cylindrical brass chamber 7. Asbestos insulation and heater winding 8. Specimen holder and thermocouple 9. Sample position 10. Film Cassette 11. Film cassette holder 12. Base plate 13. Levelling screw 14. Brass plates over the coils of the electromagnet 15. Removable spacer 16. Supporting brass stand 17. Pole pieces 18. Asbestos insulation.

The X-ray diffraction patterns of magnetically oriented samples at various temperatures were recorded on a X-ray film in a flat plate camera in the transmission geometry, using Ni filtered Cu K_α radiation of wavelength $\lambda = 1.542$Å. The collimator of various diameters can be interchanged and the sample to film distance as well as the magnetic field strength can be varied as per requirement. A vertical X-ray beam is incident on the sample through the collimator which fits into the sample holder. The sample holder, which is made up of brass has a non magnetic heating coils which are insulated by asbestos cement and is held in place by the supporting posts. The holder is well insulated from the posts by asbestos sheets and syndanyo boards. The sample is filled in a thin walled Lindemann glass capillary of diameter 0.8 mm. The sample holder with the insulation has a thickness of about 2 cm so that the tapering pole pieces of the electromagnet can be brought close together to obtain a magnetic field of about 0.8 tesla. The four supporting posts are rigidly attached to a heavy brass plate. The film cassette is mounted on a cassette holder which is also supported by the posts. Spacers can be introduced along the posts between the clamps of the cassette holder and the heavy brass plate so that reproducible geometry can be obtained. Leveling screws can be used for adjustment and improved collimation. The temperature of the sample was regulated within $\pm 0.1\,^{\circ}C$ by a Eurotherm process controller PID 2404. The sample holder was calibrated up to $250^{\circ}C$ with a number of samples of known melting points. A Gauss meter was used to measure the magnetic field between the pole pieces. For all the photographs, Ni filter of thickness 0.009 mm was used to obtain nearly monochromatic Cu K_α radiation of wavelength $\lambda = 1.542$Å. The X-ray beam was collimated by a collimator of aperture 1.0 mm. The exact distance between the sample and the film was obtained by taking X-ray diffraction pattern of aluminium powder. For aluminium the dimension of the unit cell (F.C.C structure) is known. Hence, the Bragg angle corresponding to the reflection from the hkl plane can be determined from the following equation [44]:

$$\sin\theta' = \frac{\lambda\left(h^2+k^2+l^2\right)^{\frac{1}{2}}}{2a} \tag{2.1}$$

Thus, by measuring the diameter of the diffraction rings corresponding to (111) and (200) reflections [43] and the values of Bragg angle from equation 2.1, the

actual distance between the sample and the film can be obtained from the relation:

$$\tan\theta' = \frac{\text{Radius of the ring}}{\text{Sample to film distance}} \tag{2.2}$$

The X-ray photographs were scanned by a high resolution scanner (HP Scanjet 5590) in gray mode and at 1200 dpi resolution. The optical densities of the pixels were calculated and then converted to X-ray intensities with the help of a calibration curve following the procedure of Klug and Alexander [45]. A program was written in GNU Octave to obtain the scattered intensity profile $I(\psi)$ as a function of the azimuthal angle ψ from the X-ray diffraction photographs (figure 2.3). The intensity variation $I(q)$ as a function of the magnitude of the scattering vector, along the equatorial and the meridional direction (linear scan), was obtained similarly. All the phases exhibited by the samples under investi-

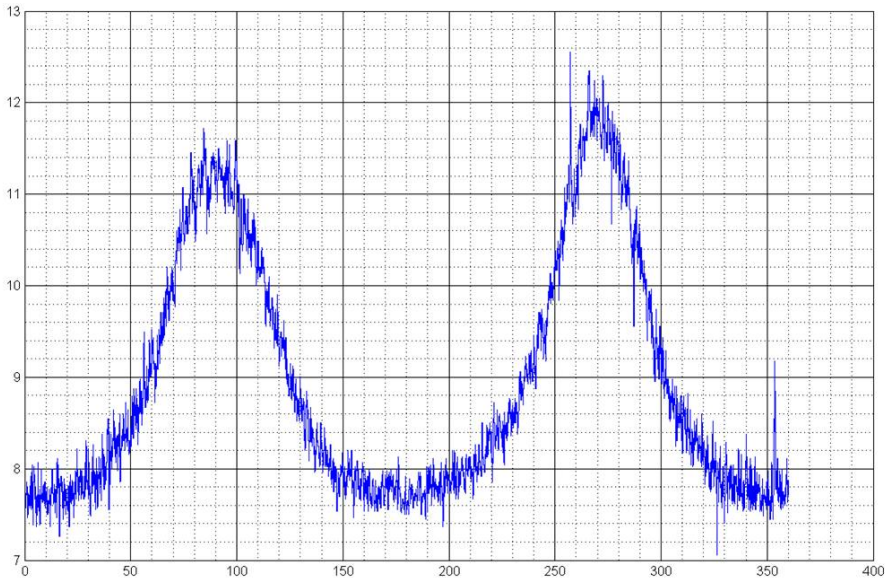

Figure 2.3: Azimuthal scan of the X-ray diffraction film in the nematic phase. Along x-axis azimuthal angle in degree, along y-axis X-ray intensity in arbitrary units.

gation are uniaxial and have a cylindrical symmetry about their long axis. The molecular long axis is oriented about director $\hat{n}$. The orientational distribution function describes the distribution of the molecular long axis about the director.

It gives the probability of finding a molecule at an angle β with respect to the director $\hat{n}$.

The scattered intensity profile $I(\psi)$ (ψ is the azimuthal angle) of the outer diffused equatorial arc is related to the orientational distribution function according to the relation given by Leadbetter and Norris [39]:

$$I(\psi) = c \int_{\beta=\psi}^{\frac{\pi}{2}} f_d(\beta) \sec^2\psi \left[\tan^2\beta - \tan^2\psi\right]^{-1/2} \sin\beta d\beta \tag{2.3}$$

where, $f_d(\beta)$ is the distribution function for the orientation β for a local cluster of molecules relative to the director $\hat{n}$ ($\beta = 0$). The above equation can be numerically inverted to give $f_d(\beta)$ which are assumed to be close to the singlet distribution function $f(\beta)$. The orientational order parameter $\langle P_2 \rangle$ and $\langle P_4 \rangle$, defined as the average orientation of the molecular long axes with respect to the director, were calculated by using the following equation:

$$\langle P_L \rangle = \frac{\int_0^1 P_L(\cos\beta) f_d(\beta) d(\cos\beta)}{\int_0^1 f_d(\beta) d(\cos\beta)} \tag{2.4}$$

where, L = 2, 4.

To calculate $f_d(\beta)$ and hence the order parameter, $I(\psi)$ values from $\psi = 0$ to $\psi = 90^\circ$ is required. We have measured the $I(\psi)$ values of four quadrants separately and the average values of $I(\psi)$ was used to calculate $f(\beta)$ and $\langle P_2 \rangle$ and $\langle P_4 \rangle$ for all the samples. The errors in the calculation of $\langle P_2 \rangle$ and $\langle P_4 \rangle$ in our experiment are estimated to be less than ± 0.015.

The average lateral distance between the neighbouring molecules (D) is related to the corresponding Bragg angle (2θ) as [40]

$$2D \sin\theta = k'\lambda \tag{2.5}$$

where, 2θ is the Bragg angle for the equatorial diffraction, λ is the X-ray wave length and k' is a constant which comes due to the cylindrical symmetry of the system. According to de Vries [40] $k' = 1.117$ for the perfectly ordered state. The dependence of the value of k' on the order parameter of the sample under consideration has been reported [46, 47]. However, since the variation of the value of k' on $\langle P_2 \rangle$ is known to be small, the value of $k' = 1.117$ has been retained

for all the calculations.

The Bragg equation $2D\sin\theta = k'\lambda$ (θ is the Bragg angle for the meridional diffraction spots) has been used to calculate the apparent molecular length (l) or layer thickness (d).

The transverse correlation length can been determined from a linear scan of the X-ray diffraction peaks. The intensity profile $I(q)$ has to be fitted to a Lorentzian form with a quadratic background, namely,

$$I(q) = \frac{a_1}{a_2 + (q - q_0)^2} + a_3 q^2 + a_4 q + a_5 \tag{2.6}$$

with q being the magnitude of the scattering vector. The transverse correlation length is defined as

$$\xi = 2\pi (a_2)^{-1/2} \tag{2.7}$$

2.4 Optical birefringence measurement

Most of the nematic liquid crystals are optically uniaxial and birefringent, and hence have two principal refractive indices viz. ordinary refractive index (n_o) and extraordinary refractive index (n_e).The birefringence is defined as: $\Delta n = n_e - n_o$.

Optical birefringence measurement has been done by two different methods. In one method, the ordinary and the extraordinary refractive indices (n_o, n_e) were measured by thin prism technique [48, 49] and from the measured values of n_o, n_e the birefringence ($\Delta n = n_e - n_o$) has been calculated. This method has been used in our laboratory to measure refractive indices of liquid crystalline samples in various phases [50–53]. In another method, the birefringence (Δn) of the samples were determined by studying the temperature variation of the intensity of the transmitted LASER beam with the sample placed between crossed polarizers. The change in intensity reflects the phase shift from which the birefringence can be evaluated [54–56].

2.4.1 Thin prism technique

The refractive indices (n_o, n_e) for wavelength $\lambda = 632.8$ nm was measured within an accuracy of ± 0.0006 by thin prism method. Hollow prism with refracting angle less than 2° was prepared using glass slides. The temperature of the prism was controlled with an accuracy of $\pm 0.1^\circ C$ using a specially constructed heater and Eurotherm PID 2404 process controller. The heater containing the liquid crystal filled prism was placed between the pole pieces of an electromagnet and a magnetic field of about 0.8T was applied. While passing through the aligned sample, light from a He-Ne LASER was split into ordinary and extraordinary beam and two spots were obtained on a screen. The images of the spots were recorded using a digital camera suitably interfaced with a computer. The high resolution digital images so obtained were further processed to obtain the center of the spots from where the ordinary (n_o) and extraordinary (n_e) refractive index could be obtained. The prisms were filled with ultrapure, degassed water and the refractive index was measured, wherefrom the angle of the prism was determined. The block diagram of the experimental set-up designed by me in our laboratory is shown in figure 2.4.

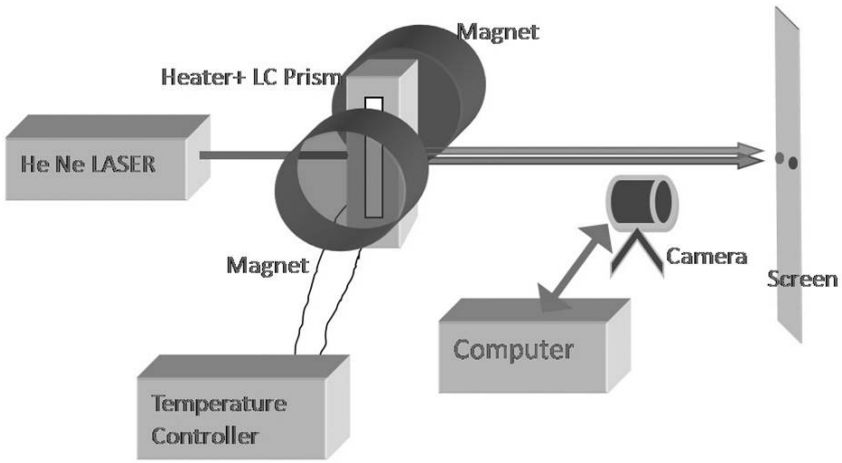

Figure 2.4: Schematic diagram of the experimental set-up for refractive index measurement.

To prepare the hollow prisms, optically flat glass slides were taken and cut so as to get the desired size of the prism. These slides were then cleaned with detergent and water and then treated in an acid mixture at $60^\circ C$ for one

hour. The slides were then washed with distilled water and then treated further in 1 molar solution of KOH at 60°C for one hour. After this, the slides were further washed thoroughly with distilled water and then with acetone. A thin glass spacer was introduced between one of the vertical edge of the prism so as to get the desired refracting angle which was kept less than 2°. The glass plates were sealed using a high temperature adhesive and after curing were baked in an oven for several hours.

2.4.2 Optical transmission method

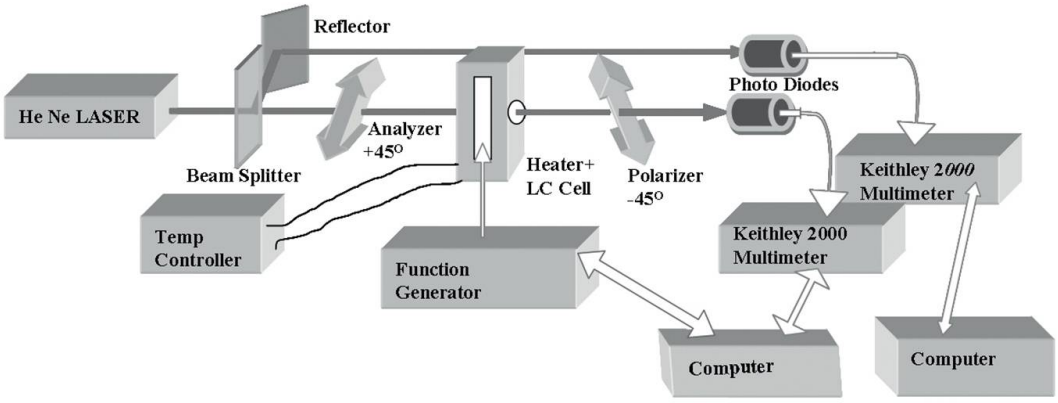

Figure 2.5: Schematic diagram of the experimental set-up for optical transmission method.

The block diagram of the experimental set-up designed by me in our laboratory is shown in figure 2.5. A He-Ne LASER (λ = 632.8nm) beam was directed onto a homogeneously aligned (planar) ITO-coated liquid crystal cell of thickness 8.9μm (purchased from AWAT Co. Ltd. Warsaw, Poland) which was placed between two crossed linear polarizers. The temperature of the cell was regulated and measured with a temperature controller (Eurotherm PID 2404) with an accuracy of ±0.1°C by placing the cell in a brass thermostat. During the experiment the temperature was varied at a rate of ±0.5°C min^{-1} and the transmitted light intensity was measured by a photodiode at an interval of 12 seconds. The stability of the LASER intensity was monitored by another identical photodiode. The photodiode outputs were measured by precession multimeter (Keithley model 2000). The entire set up was automated and controlled using a

PC. The transmitted light intensity was measured as a function of temperature in the planar aligned sample. A function generator was used to apply a 1 kHz sinusoidal voltage of magnitude much higher than the Freedericksz threshold [57, 58] voltage of the sample under investigation. Thus, for a positive dielectric anisotropy material, the application of such an electric field to the planar cell results in a homeotropic alignment of the sample. The study of the transmitted light intensity in this geometry was used as a preliminary test to rule out the existence of a tilted mesomorphic phase [54, 59]. The intensity of the transmitted LASER light can be written as [54]:

$$I_t = \frac{\sin^2\theta}{2}\left(1-\cos\Delta\phi\right) \tag{2.8}$$

where θ is the angle made by the polarizer with the optical axis and the phase difference

$$\Delta\phi = \frac{2\pi}{\lambda}\Delta n d \tag{2.9}$$

$\Delta n = n_e - n_o$, where n_e and n_o are the extraordinary and ordinary refractive indices of the liquid crystal medium and d is the sample thickness. The angle θ was set at 45° to optimize the measurements. The birefringence was calculated from the measured intensity [55, 56].

2.4.3 Determination of orientational order parameter from refractive index and optical birefringence measurements

The orientational order parameter $\langle P_2\rangle$ is related to the principal polarizabilites ($\alpha_o,\ \alpha_e$) by the following equations [60]:

$$\alpha_e = \bar{\alpha} + \frac{2}{3}\Delta\alpha\langle P_2\rangle \tag{2.10}$$

$$\alpha_o = \bar{\alpha} - \frac{1}{3}\Delta\alpha\langle P_2\rangle \tag{2.11}$$

where $\bar{\alpha} = \frac{(2\alpha_o+\alpha_e)}{3}$ is the mean polarizability and $\Delta\alpha_o = (\alpha_\parallel - \alpha_\perp)$ is the polarizability anisotropy in the crystalline state. $\alpha_\parallel$ and $\alpha_\perp$ are the principal polarizabilities parallel and perpendicular to the long axis of the molecule in the crystalline

state. Thus, from equations 2.10 and 2.11 we can write

$$\langle P_2 \rangle = \frac{\alpha_e - \alpha_o}{\alpha_\parallel - \alpha_\perp} \tag{2.12}$$

The polarizability anisotropy in the crystalline state can be obtained by the Haller's extrapolation method [61], where the temperature variation of the polarizability anisotropy ($\Delta\alpha = \alpha_e - \alpha_o$) is fitted to the following equation

$$\Delta\alpha = \Delta\alpha_0 \left(1 - \frac{T}{T^*}\right)^\beta \tag{2.13}$$

where $\Delta\alpha_0$, T^* and β are adjustable parameters, T^* is about 1-2 K higher than the clearing temperature and exponent β depends on molecular structure. This procedure enables us to extrapolate $\Delta\alpha$ to the crystalline state.

Vuks [62] suggested that the internal field is independent of the molecular interactions and the principal polarizabilities (α_o, α_e) are related to the refractive indices (n_o, n_e) as

$$\frac{n_o^2 - 1}{n^2 + 2} = \frac{4\pi N}{3}\alpha_o \tag{2.14}$$

$$\frac{n_e^2 - 1}{n^2 + 2} = \frac{4\pi N}{3}\alpha_e \tag{2.15}$$

where, $n^2 = \frac{1}{3}(2n_o^2 + n_e^2)$, n being the mean refractive index. Thus, by measuring the refractive indices and the density, the principal polarizabilities can be calculated from the above equations and hence the orientational order parameter can be determined.

Haller's extrapolation can also be applied directly to the temperature dependence of birefringence [63, 64] to obtain Δn_0 i.e. the birefringence in the crystalline state.

$$\Delta n = \Delta n_0 \left(1 - \frac{T}{T^*}\right)^\beta \tag{2.16}$$

Thus, orientational order parameter $\langle P_2 \rangle$ can be obtained directly as

$$\langle P_2 \rangle = \frac{\Delta n}{\Delta n_0} \tag{2.17}$$

Although this method of determination of order parameter ($\langle P_2 \rangle$) without consideration of the local field experienced by the liquid crystalline molecules has been used by many workers [63–76], the results differ slightly from that obtained if the local field is considered. However, this method is very useful when the density values or the individual values of the refractive indices (n_o, n_e) are not available. Moreover, from the optical transmission method (as described above) high resolution Δn values can be obtained which gives useful information regarding the nature of the phase transitions.

2.5 Density measurement

For samples with a clearing temperature below $90^{\circ}C$, the density measurements were done using an Anton Paar digital density meter DMA4500 with an accuracy of 0.01% and $\pm 0.01^{\circ}C$ accuracy in temperature measurement. However, for samples with a clearing temperature above $90^{\circ}C$, the density was measured by dilatometric technique with an accuracy of 0.1% and temperature accuracy of $\pm 0.1^{\circ}C$. The density values obtained from the two methods agree well within the limits of experimental error. The data obtained were used to calculate the molecular packing fraction using the procedure of Kitaigorodski [77].

2.6 Dipole moment measurement

Based on the Debye equation, Guggenheim [78] proposed a method of calculating the dipole moment. For this, the concentration dependence of dielectric permittivity (ϵ) and refractive index (n) of the compound dissolved in a non-polar solvent (say p-xylene) is obtained. The effective dipole moment (μ) of a solute molecule in solution of molar concentration c can be written as [78]:

$$\mu^2 = \frac{27 k_\beta T \left[\left(\epsilon_2 - n_2^2\right) - \left(\epsilon_1 - n_1^2\right) \right]}{4\pi N \left(\epsilon_1 + 2\right) \left(n_1^2 + 2\right) c} \tag{2.18}$$

where the suffixes 1 and 2 respectively refer to the solvent and solution parameters, N is the Avogadro's number, k_β the Boltzmann constant and c is the molar concentration. The concentration dependence of dipole moment can be obtained and its extrapolation to infinite dilution gives the value of the dipole moment of

the isolated molecules. Dielectric permittivities at 1 kHz were obtained by measuring the capacitance of a liquid crystal cell by using an precision LCR meter (Agilent E4980A). Refractive index of the solution was measured by thin prism method as discussed in section 2.4.1. All the measurements were carried out at $30°C$.

2.7 Static dielectric permittivity measurement

The dielectric permittivities $\epsilon_{\parallel}$ and $\epsilon_{\perp}$ along and perpendicular to the molecular long axis respectively were determined, by measuring the capacitance of suitably aligned liquid crystal filled cells. For this study, the capacitance was measured at 0.3V, 1 kHz using Agilent E4980A digital LCR-bridge with a relative accuracy of 0.05%. Planar and homeotropically aligned ITO coated liquid crystal cell of thickness $8.9\mu m$, procured from AWAT Co. Ltd., Warsaw, Poland, have been used. The measurements were done for each temperature which was maintained with an accuracy of $\pm 0.1°C$ by using an electrically powered thermostat block and a temperature controller (Eurotherm PID 2404). The stray capacitance was calculated by measuring the capacitance of spectroscopic grade pure benzene and p-xylene. If C_0 be the measured capacitance of the air filled cell, C_a the capacitance of the empty cell, excluding the stray capacitance C_s, then we can write

$$C_0 = C_a + C_s \tag{2.19}$$

Now if the cell be filled with a fluid of known dielectric permittivity ϵ then the measured capacitance can be written as:

$$C = \epsilon C_a + C_s \tag{2.20}$$

From equations 2.19 and 2.20 the value of C_s has been calculated. Knowing C_s the dielectric permittivity can be calculated as:

$$\epsilon = \frac{C - C_s}{C_0 - C_s} \tag{2.21}$$

The accuracy of the setup has been verified by measuring the dielectric constants of 5CB and 7CB, which are in close agreement with the values reported in literature [79]. Low frequency dielectric spectroscopic measurements have been done for a few mixtures, the details of which will be discussed in Chapter 8.

2.8 Elastic constant measurement

Solids and liquids differ in the way they respond to a shearing force. When a shearing force is applied on a solid restoring stress is developed and the constant of proportionality between the deformation and resorting stress is known as elastic constant. However, in liquids there is only viscous resistance to flow and no restoring stress is developed (zero static shear modulus). Deformation in a nematic liquid crystal can be described conveniently by using the concept of the vector field of the director. In a solid, the stress is caused by a change in the distance between the neighbouring points; in nematic liquid crystal the forces opposing the change of distance between the points do not exist. It is the restoring torques which is considered to oppose the curvature of the director field. Frank [80] called them as restoring stresses and assumed that the free-energy density is a quadratic function of the curvature strains in which the analogue of elastic moduli appears as coefficients.

From the theoretical point of view, the curvature of director and the dilation in layer thickness can be described in terms of continuum theory which is the analogue of the classical elastic theory of solids. The foundation of continuum theory for uniaxial nematic was laid down by Oseen [81] and Zocher [82]. Frank [80] re-examined critically Oseen's treatment and presented it as a theory of curvature elasticity. The relationship between the Frank elastic constant and the hydrostatic properties of nematic liquids have been considered by Ericksen [83, 84] and Leslie [85]. On the basis of symmetry arguments, it can be shown that in an uniaxial nematic liquid crystal there are three independent elastic constants [86–91] associated with different modes of distortion.

According to the continuum theory of liquid crystals [92], the elastic part of the internal energy density of a deformed liquid crystal is given by the equation:

$$F_{def} = \frac{1}{2}\left[K_{11}\left(\vec{\nabla}\cdot\hat{n}\right)^2 + K_{22}\left(\hat{n}\cdot\vec{\nabla}\times\hat{n}\right)^2 + K_{33}\left(\hat{n}\times\vec{\nabla}\times\hat{n}\right)^2\right] \tag{2.22}$$

where the constants K_{11}, K_{22}, K_{33} are, respectively, termed as the splay, twist, and bend elastic constants and are collectively known as the Frank elastic constants. $\hat{n}$ is the director. K_{ii} (ii=1-3) have the dimensions of energy per unit length. The splay mode is characterized by a non vanishing divergence of the vector field $\hat{n}$ ($\vec{\nabla} \cdot \hat{n} \neq 0$) . The twist and bend modes have $curl\hat{n} \neq 0$. The degree of bending is given by the component of curl $\hat{n}$ perpendicular to $\hat{n}$, whereas the amount of twist is given by the component of curl $\hat{n}$ parallel to $\hat{n}$. Since it is possible to generate deformations which are pure splay, pure twist and pure bend, each K_{ii} must be positive [88]. Several reviews on this topic are available where different aspects of experiment and theory have been discussed [87, 92–98].

The elastic constants of the liquid crystals can be determined by various methods, of which Freedericksz transition is one of the simplest and convenient method. The term Freedericksz transition refers to the deformation of a thin layer of nematic liquid crystal sample with a uniform director pattern in an external electric [57, 58, 99, 100] or magnetic field [101–107]. Freedericksz observed that when a planar surface aligned nematic liquid crystal cell is subjected to magnetic field normal to the director then the cell undergoes an abrupt change in its optical properties if the strength of the external field exceeds the threshold value, known as the critical field. If the nematic liquid crystals have positive diamagnetic/dielectric anisotropy, then as the field exceeds the critical value, the director starts to align along the external field. Depending on the geometry of the arrangement, we can determine, splay, twist or bend elastic constants (figure 2.6) from Freedericksz transition in the magnetic field.

In this work, I have used electric field induced Freedericksz transition to measure the elastic constants. The liquid crystal samples were filled in the liquid crystal measuring cell consisting of two flat indium–tin–oxide (ITO) coated glass plates with a cell gap of $8.9\mu m$. Due to the rubbed polyimide treatment of the electrode surfaces, the nematic molecules were oriented parallel to the electrodes. The cells were examined under a polarizing microscope to check the uniformity of the alignment before using in the experiment. The cells were placed in a brass thermostat with glass windows, the temperature of which was kept constant within $\pm 0.1^{\circ}C$ during the experiment using a temperature controller Eurotherm, PID 2404. A sinusoidal voltage from an Agilent E4980A digital LCR-bridge upto 20V rms, at 1kHz, was applied and the cell capacitance as a function

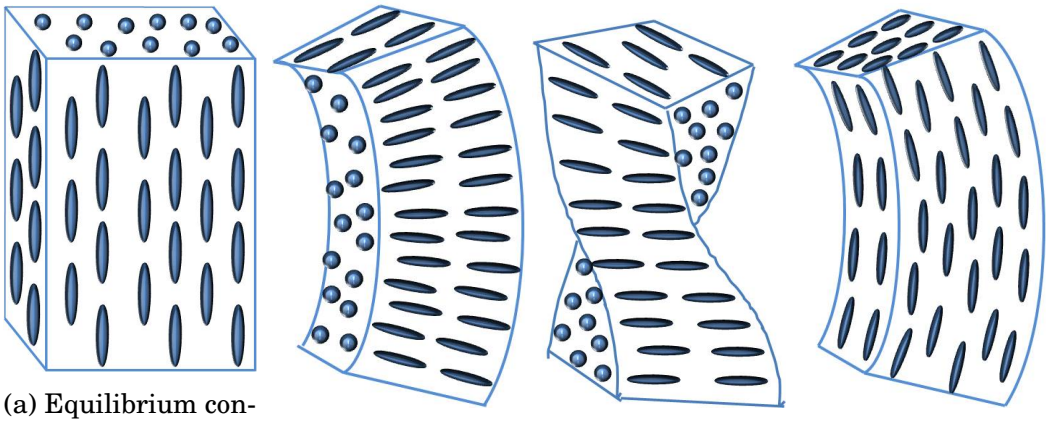

(a) Equilibrium configuration (b) Splay (c) Twist (d) Bend

Figure 2.6: An ordered liquid crystal in equilibrium configuration and different types of deformation.

of the applied voltage was recorded. The voltage increment was 20mV in the vicinity of the Freedericksz transition and 200 mV for higher voltage. The critical electric field for Freedericksz transition could be observed quite accurately (within ±0.5%) from the sudden change in the capacitance value. The relevant elastic constant was calculated from the well known equation:

$$K_{11} = \frac{\epsilon_0 \Delta\epsilon V_{th}^2}{\pi^2} \tag{2.23}$$

where ϵ_0 is the permittivity of free space and V_{th} is the critical field in r.m.s.

Gruler *et. al.* [57] obtained the relation for the voltage dependence of capacitance using which the bend elastic constant K_{33} could be obtained by multi parameter fitting of the experimental C(V) values. Uchida *et. al.* [108] developed a method in which the multi parameter fit was not needed. The voltage dependence of capacitance can be written as [108]

$$\frac{C(V)-C_\perp}{C_\perp} = \gamma - \frac{2\gamma}{\pi}\frac{V_{th}}{V}\sqrt{1+\gamma\sin^2\phi_m} \quad \times \\ \int_0^{\phi_m}\left[\frac{\left(1+\chi\sin^2\phi\right)\left(1-\sin^2\phi\right)}{\left(1+\gamma\sin^2\phi\right)\left(\sin^2\phi_m-\sin^2\phi\right)}\right]^{1/2}\cos\phi d\phi \tag{2.24}$$

where, $\chi = K_{33}/K_{11} - 1$, $\gamma = \epsilon_\parallel/\epsilon_\perp - 1$, ϕ is the tilt angle between the director $\hat{n}$ and the cell wall and ϕ_m is the tilt angle at the centre of the cell and $C_\perp$ is

the capacitance of the cell when the liquid crystal molecules are homogeneously aligned.

If the applied voltage be greater than the threshold value then the director at the centre of the cell becomes perpendicular to the cell walls and $\phi_m = \pi/2$. Then equation 2.24 reduces to

$$\frac{C(V)-C_\perp}{C_\perp} = \gamma - \frac{2\gamma}{\pi}\frac{V_{th}}{V}\sqrt{1+\gamma}\int_0^{\pi/2}\left[\frac{\left(1+\chi\sin^2\phi\right)}{\left(1+\gamma\sin^2\phi\right)}\right]^{1/2}\cos\phi d\phi \tag{2.25}$$

From equation 2.25 for $V \gg V_{th}$, $\frac{C(V)-C_\perp}{C_\perp}$ vs. 1/V curve should be linear with a slope

$$\alpha = \frac{2\gamma V_{th}}{\pi}\sqrt{1+\gamma}\int_0^{\pi/2}\left[\frac{\left(1+\chi\sin^2\phi\right)}{\left(1+\gamma\sin^2\phi\right)}\right]^{1/2}\cos\phi d\phi \tag{2.26}$$

and intercept on the $\frac{C(V)-C_\perp}{C_\perp}$ axis as $\gamma = \frac{\Delta\epsilon}{\epsilon_\perp}$

The expression for α in equation 2.26 contains only one unknown quantity, $\chi = K_{33}/K_{11} - 1$ and hence, the K_{33} values can easily be determined since K_{11} is known from equation 2.23.

2.9 Rotational viscosity measurement

A relaxation method was used to determine the rotational viscosity, where a small voltage was applied to a homogeneously aligned liquid crystal (LC) cell to deform the nematic directors by a small angle [109–114]. At time t = 0, when this voltage is removed, the molecules relax to the equilibrium state with relaxation time τ_0. For a nematic liquid crystal inserted into a homogeneously aligned cell of thickness d, τ_0 is related to the following material parameters

$$\gamma_1 = \frac{\tau_0 K_{11}\pi^2}{d^2} \tag{2.27}$$

where K_{11} is the splay elastic constant coefficient and γ_1 is the rotational viscosity of the liquid crystal.

By measuring the transmitted light intensity through a homogeneously

aligned LC cell, the optical phase was obtained as a function of time. Assuming that the LC directors are deformed on the application of voltage by a small angle, the decay time is approximated by the following equation [109]:

$$\delta(t) \approx \delta_0 \exp(-2t/\tau_0) \tag{2.28}$$

where δ_0 is the total phase change of the LC cell under a bias voltage V_B. A plot of $\ln[\delta_0/\delta(t)]$ versus time is linear, with a slope equal to $2/\tau_0$, which yields the relaxation time. In the case, where $2/\tau_0$ is close to $N\pi$ (N=integer), the expression for $\delta(t)$ (equation 2.28) becomes $\delta_0 \exp(-4t/\tau_0)$ [110]. The accuracy of the relaxation time measurement is estimated to be ±5ms.

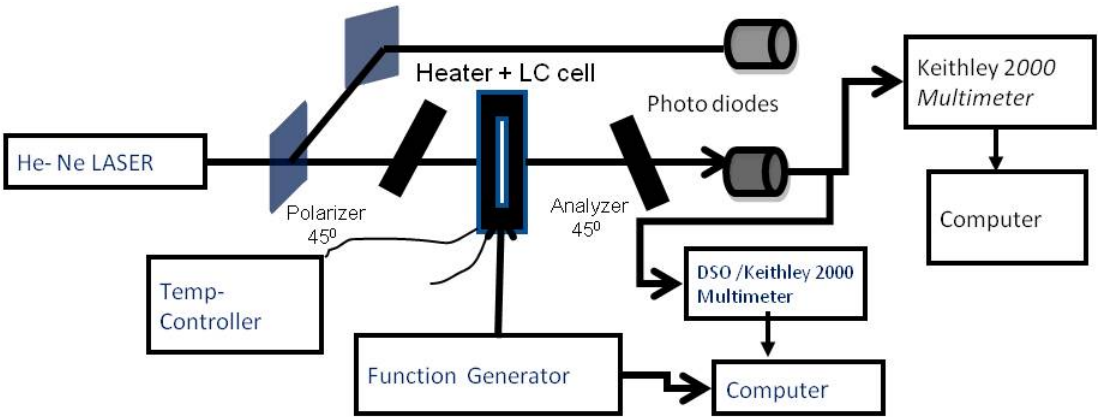

Figure 2.7: Schematic diagram of the experimental set-up for rotational viscosity measurement.

The schematic representation of the experimental set-up designed by me in our laboratory for the measurement of rotational viscosity is shown in figure 2.7. A He-Ne laser ($\lambda = 632.8nm$) was allowed to pass through a homogeneously aligned ITO coated LC cell (AWAT CO., Poland) placed between two crossed polarizers oriented at 45° to the director. The temperature of the cell was regulated and measured by a temperature controller (Eurotherm PID 2404) with an accuracy of $\pm 0.1°C$ by placing the cell in a brass thermostat with glass windows. A voltage was applied to the cell and the transmitted light intensity was measured as a function of voltage, using a photodiode. The transmitted light intensity showed maxima and minima with the applied voltage (figure 2.8). A voltage corresponding to the first maximum or minimum in the transmitted intensity was

then applied to the LC cell. The corresponding photodiode output was recorded by a digital storage oscilloscope (Agilent 54622A DSO).

When the voltage V_B was removed at t = 0, the optical transmission decreases (figure 2.9) during the relaxation process and the phase change $\delta(t)$ could be calculated from the time-dependent intensity, I(t), according to the following equation

$$I(t) = I_0 \sin^2\{(\Delta_{tot} - \delta(t))/2\} \tag{2.29}$$

where I_0 is the maximum intensity change and $\Delta_{tot} = \frac{2\pi d \Delta n}{\lambda}$ is the total optical phase retardation, which was calculated from the precession birefringence measurement. Once $\delta(t)$ was determined the relaxation time was ascertained from the slope of the $\ln[\delta_0/\delta(t)]$ versus time plot. Thus by measuring the relaxation time τ_0, and from the knowledge of the splay elastic constant K_{11} and the cell gap d, the rotational viscosity γ_1 was determined.

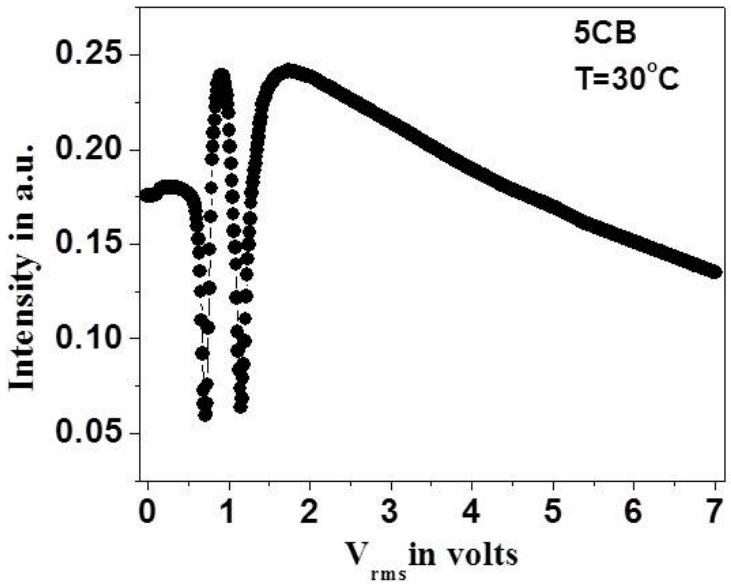

Figure 2.8: Voltage dependent transmittance of 4-n-pentyl-4′cyanobiphenyl (5CB) placed inside a 8.9 μm thick homogeneously aligned liquid crystal cell at 30°C.

In order to check the accuracy of our measurement, the rotational viscosity

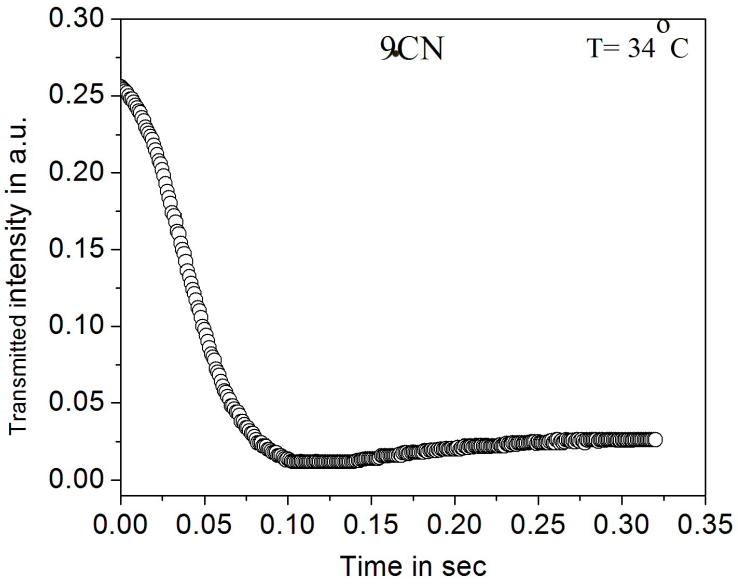

Figure 2.9: Time dependent intensity of 9.CN at 34°C, when bias voltage is removed instantaneously.

of 4-n-pentyl-4′cyanobiphenyl (5CB) were measured. These values were compared with those obtained by other workers [110] and were found to be in good agreement with our measurements.

2.10 Theoretical background

2.10.1 Maier-Saupe theory

A statistical molecular theory (analogous to the Weiss molecular field theory for ferromagnets) was proposed by Maier and Saupe in a series of papers [1–4]. Maier-Saupe theory is based on molecular mean field approximation. That is the molecules are assumed to be under the influence of the same average field due to all other particles in the system. The magnetic interactions can be neglected as they are very small and the molecules on the whole are uncharged so there can be no coulomb attraction. A large number of nematics have no permanent dipole, so no permanent dipole-dipole interactions should be required to

explain the nematic phase. Maier and Saupe suggested that anisotropic molecular force of induced dipole-induced dipole type is responsible for the stabilisation of the nematic phase.

The symmetry of the nematic phase demands that only one order parameter is needed to describe the phase and that $\hat{n} \equiv -\hat{n}$, where $\hat{n}$ is the direction of the average orientation of the molecules (director). Thus,

$$\langle P_2 \rangle = \frac{1}{2}\langle \left(3\cos^2\theta - 1\right)\rangle \tag{2.30}$$

is the required order parameter. θ being the angle between the molecular long axis and the director.

The Maier-Saupe potential is given by $V(\cos\theta) = -vP_2(\cos\theta)\langle P_2\rangle$, where v is a factor for intermolecular strength and varies from one substance to another. $V(\cos\theta)$ is the mean field approximation to the orientational potential energy function of a single molecule (single particle potential). From classical statistical mechanics the orientational distribution function $\rho(\cos\theta)$ can be written as

$$\rho(\cos\theta) = \frac{\exp(-\beta V(\cos\theta))}{Z} \tag{2.31}$$

where $\beta = \frac{1}{kT}$ and $z = \int_0^1 \exp(-\beta V(\cos\theta))d(\cos\theta)$

$$\langle P_2 \rangle = \int_0^1 P_2(\cos\theta)\,\rho(\cos\theta)\,d(\cos\theta) \tag{2.32}$$

or explicitly

$$\langle P_2 \rangle = \frac{\int_0^1 P_2(\cos\theta)\exp\left(\beta v P_2(\cos\theta)\langle P_2\rangle\right)d(\cos\theta)}{\int_0^1 \exp\left(\beta v P_2(\cos\theta)\langle P_2\rangle\right)d(\cos\theta)} \tag{2.33}$$

Now $\langle P_2\rangle$ appears on both side, thus, this self consistent equation can be solved iteratively to obtain a temperature variation of $\langle P_2\rangle$. The solution of the above equation can be plotted as shown in figure 2.10. $\langle P_2\rangle$ = 0 is a solution at all temperatures this gives the isotropic phase. For T< $0.22284v/k$ two other solutions appears. The upper branch tends to 1 and the lower branch tends to -0.5 as T→ 0 K. The correct (stable) solution can be decided upon by evaluation the free energy.

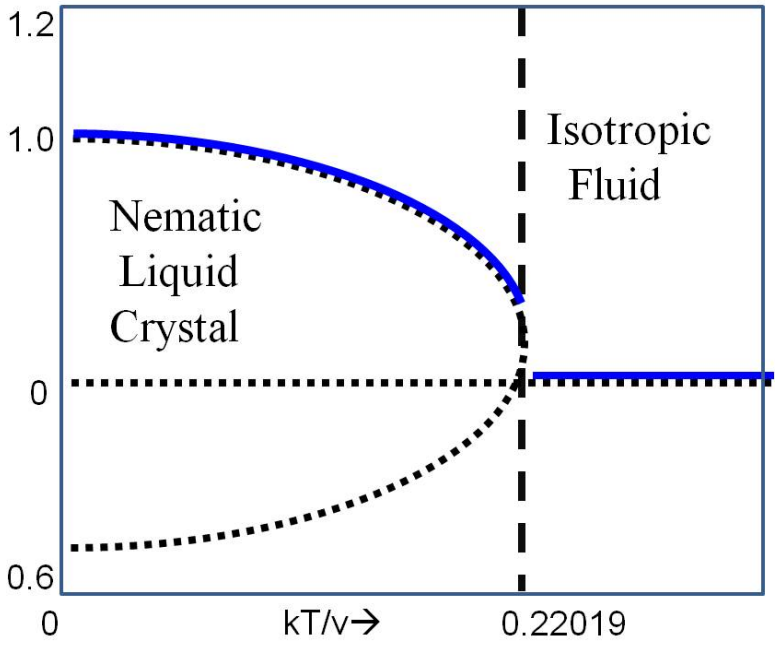

Figure 2.10: Orientational order parameter as obtained from Maier-Saupe mean field theory.

The free energy (F) can be written as

$$\frac{F}{NkT} = -\ln Z + \frac{1}{2T^*}\langle P_2\rangle^2 \tag{2.34}$$

where $T^* = kT/v$

The free energy for $\langle P_2\rangle$ = 0 branch is constant with temperature and is equal to zero. The free energy of the negative branch is negative but small in magnitude. For the positive $\langle P_2\rangle$ branch the free energy is negative (with magnitude larger than that for the negative $\langle P_2\rangle$ branch) up to $T = 0.22019v/k$. the remaining of the positive branch has a positive value of the free energy. Thus for T = 0 to $T = 0.22019v/k$ we get stable nematic phase for temperature above this isotropic phase is stable.

The order parameter $\langle P_2\rangle$ decreases from unity to a minimum value of 0.4289 at $T^* = 0.22019$. The nematic – isotropic phase transition takes place at $T^* = 0.22019$ and it is of first order, as a discontinuous change of order parameter $\langle P_2\rangle$ from 0.4289 to 0 occurs. However, the energy associated with N-I phase transition is about 0.83 cal/mole-K, which is much smaller than that of

usual solid-liquid transition, which is of the order 25 cal/mole-K.

In spite of a number of approximations and justifiable criticism from theoreticians, the Maier-Saupe theory is surprisingly successful [115] and is widely referred to by chemists and experimental physicist.

2.10.2 McMillan's theory for smectic A phase

In addition to the orientational distribution of the molecular axes, the smectic A phase also possesses a layered structure which can be described by a periodic density variation along the layer normal (say, z-axis). McMillan extended the Maier-Saupe theory to describe the nematic–Smectic A phase transition [5]. Apart from the usual orientational order parameter, another order parameter related to the amplitude of the density wave of the smectic phase was introduced in the mean field potential energy function. The normalized distribution function can be written as

$$f(\cos\theta, z) = \sum_{L-even} \sum_{n} A_{L,n} P_L(\cos\theta) \cos\left(\frac{2\pi n z}{d}\right) \tag{2.35}$$

with

$$\int_{-1}^{1} \int_{0}^{d} f(\cos\theta, z)\, dz\, d(\cos\theta) = 1 \tag{2.36}$$

as normalizing condition, where d is the layer thickness.

McMillan [5] following Kobayashi [116, 117] expressed the pair potential as

$$V_M(\cos\theta, z) = -v\left[\delta\alpha\tau\cos\left(\frac{2\pi z}{d}\right) + \left\{\eta + \alpha\sigma\cos\left(\frac{2\pi z}{d}\right)\right\} P_2(\cos\theta)\right] \tag{2.37}$$

where α and δ are the two parameters of the potential. $\eta = \langle P_2(\cos\theta)\rangle$, $\tau = \langle\cos(2\pi z/d\rangle$ and $\sigma = \langle P_2(\cos\theta)\cos(2\pi z/d\rangle$ are the orientational, translational and mixed order parameters respectively and $\langle\cdots\rangle$ denotes the statistical average of the quantities inside.

The distribution function can thus be written as

$$f_M(\cos\theta, z) = Z^{-1} \exp(-V_M(\cos\theta, z)/kT) \tag{2.38}$$

where Z is the single molecule partition function given by

$$Z = \int_0^1 \int_0^d \exp(-V_M(\cos\theta, z)/kT)\, d(\cos\theta)\, dz \tag{2.39}$$

The three self consistent equations containing η, τ and σ can be written as

$$\eta = \int_0^1 \int_0^d P_2(\cos\theta) f_M(\cos\theta, z) d(\cos\theta) dz \tag{2.40}$$

$$\tau = \int_0^1 \int_0^d \cos\left(\frac{2\pi z}{d}\right) f_M(\cos\theta, z) d(\cos\theta) dz \tag{2.41}$$

$$\sigma = \int_0^1 \int_0^d P_2(\cos\theta) \cos\left(\frac{2\pi z}{d}\right) f_M(\cos\theta, z) d(\cos\theta) dz \tag{2.42}$$

Depending on the values of the different parameters, we obtain the following three possible solutions: i) $\eta = \tau = \sigma = 0$, this describes the isotropic liquid or disordered phase; ii) $\eta \neq 0$, $\tau = \sigma = 0$, orientational order characteristic of the nematic phase in accordance with the Maier–Saupe theory; iii) $\eta \neq 0$, $\tau \neq 0$, $\sigma \neq 0$, orientational and translational order characteristic of the smectic A phase.

The parameter v is obtained from the nematic-isotropic transition temperature, assuming the simple mean field theory result. ($kT_{NI}/v = 0.22019$). The temperature dependence of the values of η, τ and σ can be calculated using the self consistent equations for various values of α and δ. The parameter δ is the ratio of the translational to the orientational part of the potential whereas the parameter α depends on the molecular length.

For $\alpha > 0.98$, the smectic A phase transforms directly into the isotropic phase, while for $\alpha < 0.98$ there is a $SmA - N$ transition followed by a nematic-isotropic transition at higher temperature. Although nematic-isotropic transition temperature is always first order according to McMillan theory, the smectic A-nematic transition can be either first order or second order. For $T_{SN}/T_{NI} < 0.87$, the $SmA - N$ transition is second order while for $T_{SN}/T_{NI} > 0.87$, the smectic A – nematic transition is first order. T_{SN} and T_{NI} are the smectic A – nematic and nematic – isotropic transition temperatures respectively.

2.10.3 McMillan's model for smectic A phase modified by Luckhurst and Timimi

Luckhurst and Timimi [6] developed a molecular theory for the re-entrant nematic and smectic A mesophases by extending McMillan's treatment of the smectic A phase [5]. According to McMillan's theory, the single particle potential is given by

$$V_M(\cos\theta, z) = -v\left[\delta\alpha\tau\cos\left(\frac{2\pi z}{d}\right) + \left\{\eta + \alpha\sigma\cos\left(\frac{2\pi z}{d}\right)\right\}P_2(\cos\theta)\right] \tag{2.43}$$

where α and δ are two adjustable parameters, z is the displacement along the layer normal, d is the layer thickness, $\eta = \langle P_2(\cos\theta)\rangle$, the orientational order parameter, while $\tau = \langle\cos(2\pi z/d\rangle$ is the translational order parameter and $\sigma = \langle P_2(\cos\theta)\cos(2\pi z/d\rangle$ is the mixed translational and orientational order parameter. The parameter v is obtained from the nematic/isotropic transition temperature, assuming the simple mean field theory result ($kT_{NI}/v = 0.22019$). The values of η, τ and σ are calculated using the self-consistent relationships (equations 2.40, 2.41 and 2.42) as a function of temperature for various values of the parameters α and δ. The stability of the smectic A_d phase is controlled by the two adjustable parameters α and δ, with α being the primary variable. In McMillan's theory the molecules are assumed to be rigid and the parameters α and δ are taken to be independent of temperature. However Luckhurst and Timimi argued that empirically it has been found that the parameter α depends on the molecular length, which varies with the chain length of the mesogenic molecules. Thus, α cannot be independent of temperature. Further, in polar systems partial dimers are formed, whose structure may change with temperature. Based on these arguments Luckhurst and Timimi identified the particles in McMillan's theory as dimers and suggested that α will have weak temperature dependence. The parameter δ, being the ratio of the translational to the orientational part of the potential, was assumed to be independent of composition and temperature. According to Luckhurst and Timimi [6], the orientational order parameter increases with decreasing temperature in a manner almost independent of the $SmA-N$ transition. If α decreases with temperature then the $SmA-N$ transition temperature will be reduced. An appropriate choice of the temperature

dependence of α parameter gives rise to a situation where lowering the temperature still produces the usual $SmA - N$ transition. Further decrease in temperature reduces α to such an extent that the SmA phase becomes unstable and reverts to a nematic phase; in other words a re-entrant nematic phase is formed.

References

[1] W. Maier, A. Saupe, *Z. Naturforsch.*, **A13**, 451 (1958).

[2] W. Maier, A. Saupe, *Z. Naturforsch.*, **A13**, 564 (1958).

[3] W. Maier, A. Saupe, *Z. Naturforsch.*, **A14**, 882 (1959).

[4] W. Maier, A. Saupe, *Z. Naturforsch.*, **A15**, 287 (1960).

[5] W. L. McMillan, *Phys. Rev. A*, **4**, 1238 (1971). *ibid*, **6**, 936 (1972).

[6] G. R. Luckhurst and B. A. Timimi, *Mol. Cryst. Liq. Cryst.*, **260**, 253 (1981).

[7] D. Demus and L. Richter, *Textures of Liquid Crystals*, Verlag Chemie, New York (1978).

[8] I. Dierking, *Textures of Liquid Crystals*, Wiley-VCH Verlag GmbH & Co., Weinheim (2003).

[9] M. Eckert, *Ann. Phys. (Berlin)*, **524** (5), A83 (2012).

[10] J. S. V. D. Lingen, *Ber. Dt. Chem. Ges.*, **15**, 913 (1913).

[11] G. Friedel, *Ann. Phys.*, **18**, 237 (1922).

[12] W. Kast, *Ann. Phys*, **83**, 418 (1927).

[13] W. Kast, *Z. Physik*, **71**, 39 (1931).

[14] W. Kast, *Z. Physik*, **76**, 19 (1932).

[15] W. Kast, *Naturwissenschaften*, **21**, 737 (1933).

[16] W. Kast, *Ann. Phys.*, **19**, 571 (1934).

[17] E. Alexander and K. Herrmann, *Z. Krist.*, **69**, 285 (1928).

[18] P. W. Glamann, K. Herrmann and A. H. Krummacher, *Z. Krist.*, **74**, 73 (1930).

[19] K. Herrmann and A. H. Krummacher, *Z. Krist.*, **79**, 134 (1931).

[20] K. Herrmann and A. H. Krummacher, *Z. Physik*, **70**, 758 (1931).

[21] K. Herrmann , A. H. Krummacher and K. May, *Z. Physik*, **73**, 419 (1931).

[22] K. Herrmann, *Ergebn. Techno. Rontgenkunde*, **2**, 23 (1931).

[23] K. Herrmann and A. H. Krummacher, *Z. Krist.*, **81**, 317 (1932).

[24] K. Herrmann, *Trans. Faraday Soc.*, **29**, 972 (1933).

[25] K. Herrmann, *Z. Krist.*, **92** (1935).

[26] J. Falguerettes and P. Delord, *Liquid Crystals and Plastic Crystals*, Eds. G. W. Gray and P. A. Winsor, E. Horwood, **Vol.2**, Ch. 3 (1974).

[27] H. Kelker and R. Hatz, *Handbook of liquid crystals*, Verlag Chemie, **Ch. 5** (1980).

[28] G. H. Brown and W. G. Shaw, *Chem. Rev.*, **57**, 1049 (1957).

[29] G. W. Gray, *Molecular Structure and the properties of liquid crystals*, Academic Press, London and N. York (1962).

[30] I. G. Chistyakov, *Sov. Phys. Vsp.*, **9**, 551 (1967).

[31] L. A. Azaroff, *Mol. Cryst. Liq. Cryst.*, **60**, 73 (1980).

[32] P. Davidson, *Structure and Bonding Liquid Crystals II*, **Vol. 95**, Eds. D. M. P. Mingos, Springer Verlag Berlin Heidelberg N. York, Ch1, 1-39 (1999).

[33] R. H. Templer, *Handbook of liquid crystals*, **Vol. 1**, Eds. D. Demus, J. Goodby, G. W. Gray, H. -W. Spiess, V. Vill, Wiley-VCH, Ch. 8, 619-634 (1998).

[34] J. M. Seddon, *Handbook of liquid crystals*, **Vol. 1**, Eds. D. Demus, J. Goodby, G. W. Gray, H. -W. Spiess, V. Vill, Wiley-VCH, Ch. 8, 635-679 (1998).

[35] L. M. Blinov, *Structure and Properties of Liquid Crystals*, Springer, Ch. 5, 75-110 (2011).

[36] B. K. Vainstein and I. G. Chistyakov, *Problem of Modern Crystallography*, Nauka, Moscow (1975).

[37] B. K. Vainstein, *Diffraction of X-rays by chain Molecules*, Elsevier (1966).

[38] A. J. Leadbetter, *The Molecular Physics of Liquid Crystals*, Eds. G. R. Luckhurst & G. W. Gray, Chap. 13, Academic Press (1979).

[39] A. J. Leadbetter and E. K. Norris, *Mol. Phys.*, **38**, 669 (1979).

[40] A. de Vries, *Mol. Cryst. Liq. Cryst.*, **10**, 219 (1970).

[41] G. Vertogen and W. H. de Jue, *Thermotropic Liquid Crystals: Fundamentals*, Springer-Verlag (1988).

[42] H. Kohli *et. al.*, *Z. Physik*, **B24**, 147 (1976).

[43] B. Jha and R. Paul, *Proc. Nucl. Phys. Solid State Phys. Symp.*, India, **19c**, 491 (1970).

[44] C. Kittel, *Introduction to Solid State Physics*, Wiley Eastern, Chap. 2 (1976).

[45] H. P. Klug and L. E. Alexander, *X-ray diffraction procedures*, John Wiley and Sons, N. York, p. 114 and 473 (1974).

[46] R. Paul and G. Chaudhuri, *Abstract in the 14th International Liquid Crystal Conference*, Pisa, Abs. no. H-P23 (1992).

[47] R. Bruinsma and D. R. Nelson, *Phys. Rev. B*, **23**, 1, 402 (1981).

[48] A. K. Zeminder, S. Paul and R. Paul, *Mol. Cryst. Liq. Cryst.*, **61**, 4191 (1980).

[49] A. Prasad and M. K. Das, *Phase Transitions*, **83**, 1072 (2010).

[50] P. D. Roy, M. K. Das and R. Paul, *Mol. Cryst. Liq. Cryst.*, **365**, 607 (2001).

[51] P. D. Roy, M. K. Das, S. Paul, R. Paul and B. Das, *Mol. Cryst. Liq. Cryst.*, **457**, 43 (2006).

[52] M. K. Das and R. Paul, *Phase Transitions*, **46**, 185 (1994).

[53] B. Adhikari and R. Paul, *Phase Transitions*, **53**, 165 (1996).

[54] A. Saipa and F. Giesselmann, *Liq. Cryst.*, **29**, 347 (2002).

[55] T. Scharf, *Polarized Light in Liquid Crystals and Polymers* (Hoboken, NJ: Wiley) (2007).

[56] G. Sarkar, B. Das, M. K. Das and W. Weissflog, *Phase Transiions*, **82**, 433 (2009).

[57] H. Gruler, T. J. Schiffer and G. Meier, *Z. Natureforsh*, **27A**, 966 (1972).

[58] M. J. Bradshaw and E. P. Rayens, *Mol. Cryst. Liq. Cryst.*, **72**, 35 (1980).

[59] G. Sarkar, B. Das, M. K. Das and W. Weissflog *Proc. 16th National Conf. on Liquid Crystals 2009*, p. 76, Lucknow (2009).

[60] P. G. de Gennes, *Mol. Cryst. Liq. Cryst.*, **12**, 193 (1971).

[61] I. Haller, H. A. Huggins, H. R. Lilienthal and T. R. McGuire, *J. Phys. Chem.*, **77**, 950 (1973).

[62] M. F. Vuks, *Optics and Spectroscopy*, **20**, 361 (1966).

[63] B. J. Zywucki and W. Kuczynski, *IEEE Trans. Dielectr. Electr. Insul.*, **8**, 512 (2001).

[64] W. Kuczynski, B. Zywucki, and J. Malecki, *Mol. Cryst. Liq. Cryst.*, **381**, 1 (2002).

[65] M. Geppi, A. Marini, B. Mennucci, P. Kula, A. Spadlo, W. Kuczynski and S. Urban, *Mol. Cryst. Liq. Cryst.*, **541**, 104 (2011).

[66] P. Pardhasaradhi , P. V. D. Prasad , D. M. Latha , V. G. K. M. Pisipati and G. P. Rani, *Phase Transitions*, **85**, 1031 (2012).

[67] K. D. Thingujama, P. R. Alapati, B. Choudhury and A. Bhattacharjee, *Phase Transitions*, **85**, 52 (2012).

[68] K. Fakruddin , R. J. Kumar , P. V. D. Prasad and V. G. K. M. Pisipati, *Mol. Cryst. Liq. Cryst*, **511**, 133 (2009).

[69] E. G. Hanson and Y. R. Shen, *Mol. Cryst. Liq. Cryst.*, **36**, 193 (1976).

[70] A. Kumar, *Liq. Cryst.*, **40**, 203 (2013).

[71] V. G. K. M. Pisipati and P. V. D. Prasad, *Mol. Cryst. Liq. Cryst.*, **506**, 13 (2009).

[72] M. S. Zakerhamidi and H. Rahimzadeh, *Mol. Cryst. Liq. Cryst.*, **569**, 92 (2012).

[73] S. S. Sastry , S. Kumar , T. V. Kumari , K. Mallika , B. Gowri S. Rao and H. S. Tiong, *Liq. Cryst.*, **39**, 1527 (2012).

[74] S. S. Sastry , T. V. Kumari , K. Mallika , B. G. S. Rao , S. Ha and S. Lakshminarayana, *Liq. Cryst.*, **39**, 295 (2012).

[75] M. K. Das, G. Sarkar, B. Das, R. Rai and N. Sinha, *J. Phys.: Condens. Matter*, **24**, 115101 (9pp) (2012).

[76] G. Sarkar , B. Das , M. K. Das , U. Baumeister and W. Weissflog, *Mol. Cryst. Liq. Cryst.*, **540**, 188 (2011).

[77] A. I. Kitaigorodski, *Molecular Crystals and Molecules*, Academic Press, New York and London, Chapter 1 (1973).

[78] E. A. Guggenheim, *Trans. Faraday Soc.*, **45**, 714 (1949).

[79] P. Galatola and C. Oldano, *Optics of Thermotropic Liquid Crystals*, (Chapter 3) Eds. S. Elston and R. Sambles, Tailor and Francis (1998).

[80] F. C. Frank, *Disc. Faraday Soc.*, **25**, 19 (1958).

[81] C. W. Oseen, *Trans. Faraday Soc.*, **29**, 883 (1933).

[82] H. Zoher, *Trans. Faraday Soc.*, **29**, 945 (1933).

[83] J. L. Ericksen, *Arch. Rat. Mech. Anal.*, **4**, 231 (1960).

[84] J. L. Ericksen, *Trans. Sot. Rheol.*, **5**, 23 (1961).

[85] F. M. Leslie, *Quart. J. Mech. Appl. Math.*, **19**, 357 (1966).

[86] S. Chandrasikhar, *Liquid Crystals*, Cambridge University Press, Cambridge (1977).

[87] P. G. de Gennes and J. Prost, *The Physics of Liquid Crystal*, Clarendon Press, Oxford (1993).

[88] M. Kleman, *Points, Lines and Walls*, Wiley, New York (1983).

[89] W. H. de Jeu, *Physical Properties of Liquid Crystalline Materials*, Gordon and Breach, London (1980).

[90] F. M. Leslie, *Quart. J. Mech. Appl. Math.*, **19**, 357 (1966).

[91] J. Nehring and A. Saupe, *J. Chem. Phys.*, **54**, 337 (1971) ibid **56**, 5527 (1972).

[92] S. Singh, *Physics Reports*, **277**, 283 (1996).

[93] L. M. Blinov, *Structure and Properties of Liquid Crystals*, Springer, Ch.8, 189-231 (2011).

[94] F. M. Leslie, *Handbook of liquid crystals*, **Vol.1**, Eds. D. Demus, J. Goodby, G. W. Gray, H. -W. Spiess, V. Vill, Wiley-VCH, Ch 1, 25-39 (1998).

[95] D. Dunmur and K. Toriyama, *Handbook of liquid crystals*, **Vol.1**, Eds. D. Demus, J. Goodby, G. W. Gray, H. -W. Spiess, V. Vill, Wiley-VCH, Ch 7, 253-280 (1998).

[96] R. Stannarius, *Handbook of liquid crystals*, **Vol. 2A**, Eds. D. Demus, J. Goodby, G. W. Gray, H. -W. Spiess, V. Vill, Wiley-VCH, Ch 3, 60-90 (1998).

[97] I. W. Stewart, *The static and dynamic Continuum Theory of Liquid crystals: A mathematical Introduction*, Taylor and Francis, N. York (2004).

[98] S. V. Pasechnik, V. G. Chigrinov, and D. V. Shmeliova, *Liquid Crystals: Viscous and Elastic Properties*, Willey-VCH Verlag GmbH & Co. KGaA, Ch.5, 179-281 (2009).

[99] H. Gruler and L. Cheung, *J. Appl. Phys.*, **46**, 5097 (1975).

[100] H. Deuling, *Liquid Crystals, Solid State Physics Suppl.* **No. 14**, Ed. L. Liebert, Academic Press, N. York, p. 77 (1978).

[101] V. Freedericksz and V. Tsvetkov, *Phy. Z. Soviet Union*, **6**, 490 (1934).

[102] V. Freedericksz and V. Zolina, *Trans. Faraday Soc.*, **29**, 919 (1933).

[103] P. P. Karat and N. V. Madhusudana, *Mol. Cryst. Liq. Cryst.*, **40**, 239 (1977).

[104] H. P. Schad, M. A. Osman, *J. Chem. Phys.*, **75** (2), 880 (1981).

[105] F. Leenhouts, H. J. Boeber, A. J. Dekker and J. J. Jonker, *J. Phys. (Paris) Colloque.*, **40**, C3-291 (1979).

[106] H. P. Schad, G. Bauer and G. Maier, *J. Chem. Phys.*, **67**, 3705 (1977).

[107] F. Leenhouts and A. J. Dekker, *J. Chem. Phys.*, **74**, 1956 (1981).

[108] T. Uchida, Y. Takahashi, *Mol. Cryst. Liq. Cryst.*, **72**, 133 (1981).

[109] S. T. Wu, C. S. Wu. *Phys. Rev. A*, **42**, 2219 (1990).

[110] M. L. Dark, M. H. Moore, D. K. Shenoy and R. Shashidhar, *Liq. Cryst.*, **33**, 67 (2006).

[111] M. K. Das, A. Pramanik, B. Das, L. Szczucinski and R. Dabrowski, *J. Phys. D: Appl. Phys.*, **45**, 415304 (2012).

[112] A. Pramanik, B. Das, M. K. Das, K. Garbat, S. Urban and R. Dabrowski , *Liq. Cryst.*, **40**, 149 (2013).

[113] A. Chakraborty, M. K. Das, B. Das, A. Lehmann and C. Tschierske, *Soft Matter*, **9**, 4273 (2013).

[114] P. Dasgupta, B. Das and M. K. Das, *Liq. Cryst.*, **39**, 1297 (2012).

[115] G. R. Luckhurst and C. Zannoni, *Nature*, **267**, 412 (1977).

[116] K. Kobayashi, *Mol. Cryst. Liq. Cryst.*, **13**, 137 (1971).

[117] K. Kobayashi, *J. Phys. Soc. (Japan)*, **29**, 101 (1970).

Chapter 3

Phase diagram and X-ray diffraction studies of a polar-polar binary system (7CPB+9.CN) exhibiting nematic, induced smectic A_d and re-entrant nematic phases

3.1 Introduction

This work aims at studying induced smectic A_d and re-entrant nematic phases along with the involved phase transitions in binary mixtures of polar-polar liquid crystals, for which a suitable system had to be identified. Apart from the well studied binary system of 6OCB-8OCB [1–32] a number of suitable binary systems having the desired phase sequence have been reported [33–39]. In this work I have constructed a new binary system of 4-cyanophenyl [4′ (4″-n-heptylphenyl)] (7CPB) and 4-cyanophenyl 4-nonylbenzoate (9.CN) showing induced smectic A_d – re-entrant nematic phases [40]. The mixtures were prepared from the pure components and the phase diagrams were constructed from polarizing optical microscopy and DSC measurements. The existence of the nematic–induced smectic A_d– re-entrant phase sequence was again confirmed from X-ray

diffraction measurements. An important feature of this phase diagram is the appearance of the induced smectic A_d phase in the shape of an elliptical island surrounded by a nematic sea i.e. the induced smectic and re-entrant nematic (N_{re}) phases appear simultaneously in such mixtures. Moreover, for a certain concentration range, the re-entrant nematic phase in these mixtures appears well ahead of the melting temperature. This phase diagram is interesting because the two components are purely nematogenic; i.e. they do not have an underlying smectic phase.

This chapter contains the results of polarization optical microscopy and X-ray diffraction measurements in the nematic, induced smectic A_d and re-entrant nematic phases. Orientational order parameters (OOP's) have been determined in the three phases, from X-ray diffraction measurements. The order parameters have been compared with the theoretical values from Maier and Saupe theory [41–44] for nematogens and a modified of McMillan's model [45, 46] as proposed by Luckhurst and Timimi [47] for those mixtures having induced smectic A_d and re-entrant nematic phases. The experimental variation of the layer thickness with mole fraction of 9.CN has also been explained fairly well by assuming the presence of two types of homo dimers (7CPB + 7CPB, 9.CN +9.CN) and one type of hetero dimer (7CPB + 9.CN).

3.2 Phase diagram and texture studies

The liquid crystal samples were procured from AWAT Co. Ltd., Warsaw, Poland (purity >99.9%) and were used without further purification. The structural formulae, chemical names and the transition temperatures of the pure compounds of this system are as follows:-

Component 1: 4-cyanophenyl [4′ (4″-n- heptylphenyl)] (7CPB in short)

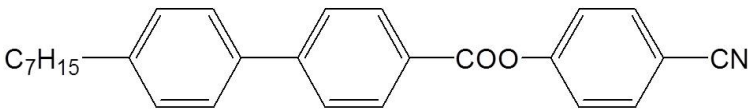

K 92°C N 206°C I

Component 2: 4-cyanophenyl 4-nonylbenzoate (9.CN in short)

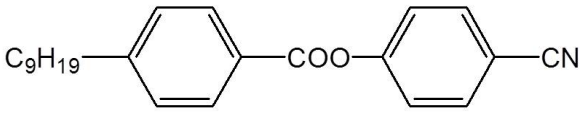

K 45°C N 53°C I

Ten mixtures were prepared for this system with mole fraction $x_{9.CN}$ = 0.176, 0.347, 0.417, 0.471, 0.559, 0.662, 0.774, 0.827, 0.865 and 0.9. The phase diagram as obtained from polarizing optical microscopy is shown in figure 3.1. The textures from polarizing optical microscopy study in the nematic, smectic A_d, re-entrant nematic phases and at the involved phase transitions for the mixture $x_{9.\ CN}$ = 0.827 are shown in the figures 3.2 (a)-(e).

In the phase diagram of this binary system of 7CPB+9.CN, the induced smectic A_d phase appears in the shape of an elliptical island surrounded by a nematic sea i.e. within the concentration range 0.4 < $x_{9.\ CN}$ < 0.87, both the induced smectic and re-entrant nematic phases are present in the mixtures. All the mixtures show a two-phase (nematic + isotropic) coexistence region, but no coexisting region is found at the nematic –smectic A_d or smectic A_d – re-entrant nematic phase boundary. In some mixtures the re-entrant nematic phase is suppressed due to solidification.

A notable feature of this new phase diagram is that above a certain concentration range (near x ≈0.8), the re-entrant nematic phase appears above the melting temperature. This is an interesting deviation from the general trends where the re-entrant nematic phase is monotropic. From polarizing microscopic studies, marbled or thread like texture were seen in the nematic and re-entrant nematic phases, while in the induced smectic phases either fan shaped or focal-conic textures were observed, both of which are typical of a smectic A phase. In figure 3.2, the optical textures of a mixture at $x_{9.\ CN}$ = 0.827 as observed on cooling from the isotropic phase is shown. Interestingly, in this case, the high temperature nematic phase, occurring between 86.5°C and 51.2°C, shows a typical schlieren texture with four-brush-disclinations (figure 3.2a) which persists throughout the phase. Furthermore, the onset of the nematic to induced smectic A_d phase is marked by the appearance of domain structure with sharp

disclination lines (figure 3.2b). This texture gradually gives way to the familiar fan shaped texture indicating the signature of the smectic A phase (figure 3.2c). If the sample is further cooled down below 40.9°C, the schlieren texture with four-brush-disclination is again reverted (figure 3.2e), accompanied by the appearance of the previously observed sharp disclination lines at the Smectic A_d - re-entrant nematic phase boundary (figure 3.2d). The change in colour of the schlieren texture with change in temperature indicates the change in birefringence. These textures studies strongly indicate that both the high temperature nematic phase and the low temperature re-entrant nematic phase are identical. Homeotropic texture studies also confirmed the presence of an orthogonal phase in the induced smectic region. DSC measurements however, show no significant peak at the Sm A_d–N and Sm A_d–N_{re} transition indicating that both the transitions are of second order (figure3.3).

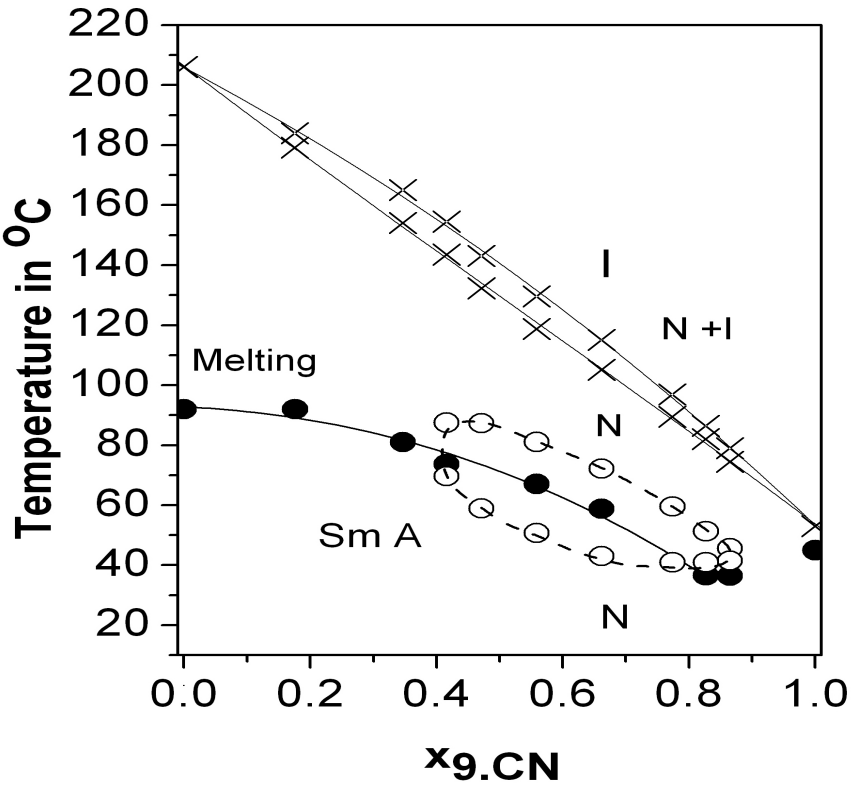

Figure 3.1: Phase diagram for the binary system of 7CPB + 9.CN. $x_{9.\,CN}$=mole fraction of 9.CN. I isotropic; (I+N) nematic–isotropic co-existing region; Sm A smectic A_d phase; N nematic phase.

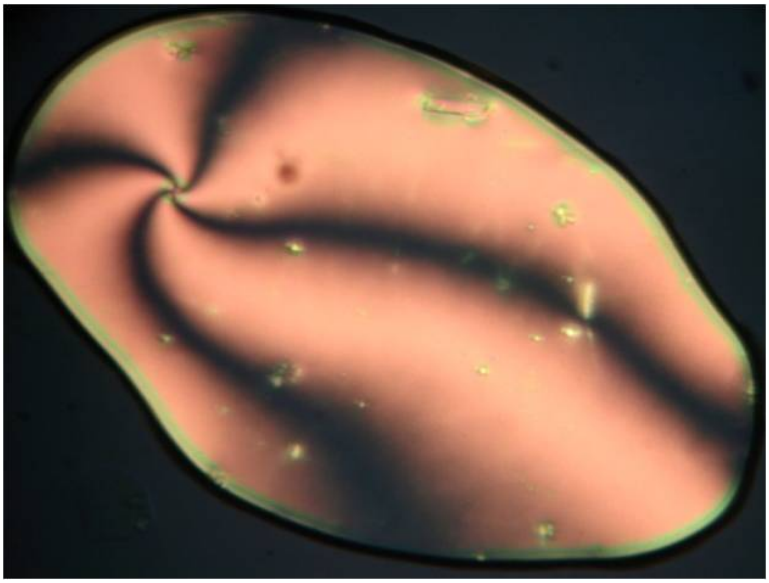

(a) Nematic phase (56.5°C)

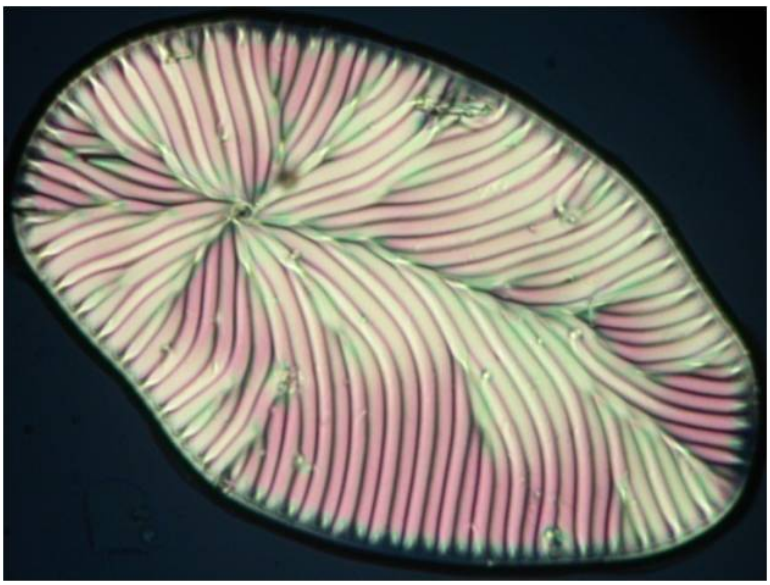

(b) N-Sm A_d phase transition (51.2°C)

Figure 3.2: Textures for mixture $x_{9.\ CN}$ = 0.827 (7CPB+9.CN) at 100X magnification during cooling.

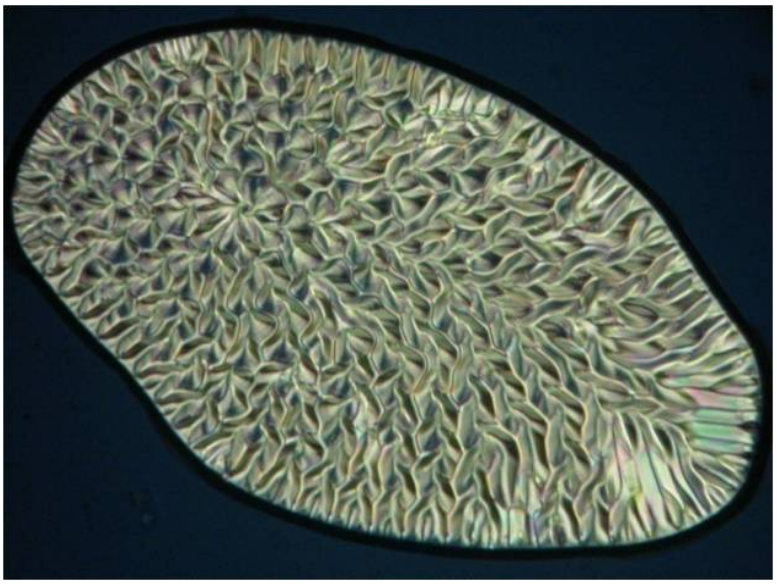

(c) Smectic A_d phase (48.0°C)

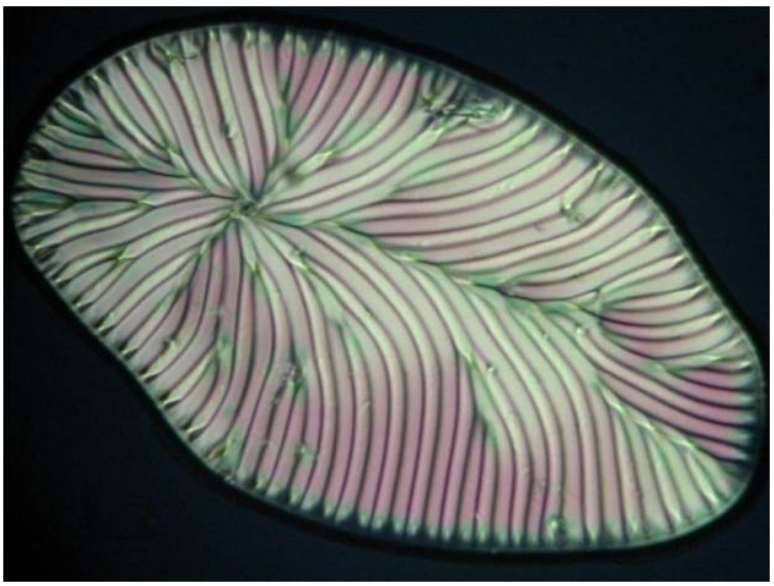

(d) Sm A_d - N_{re} phase transition (40.9°C)

Figure 3.2: (cont'd): Textures for mixture $x_{9.\,CN}$ = 0.827 (7CPB+9.CN) at 100X magnification during cooling.

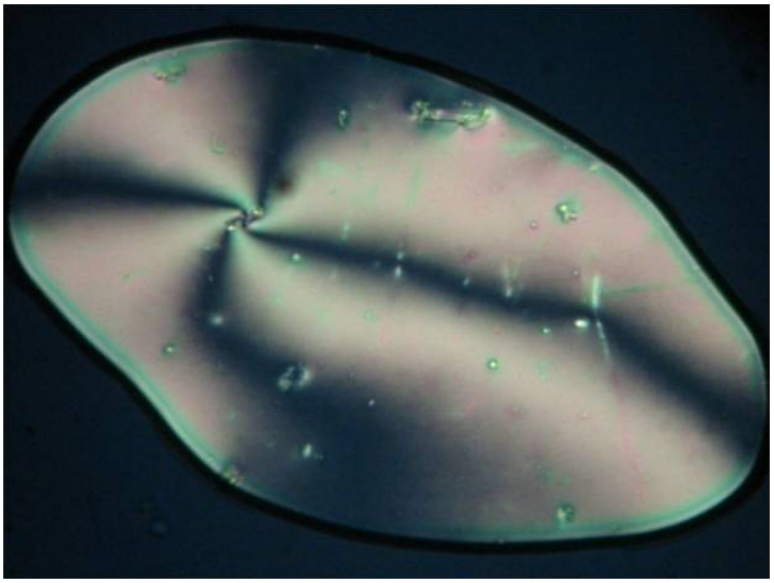

(e) Re-entrant nematic phase (38.0°C)

Figure 3.2: (cont'd): Textures for mixture $x_{9.\,CN}$ = 0.827 (7CPB+9.CN) at 100X magnification during cooling.

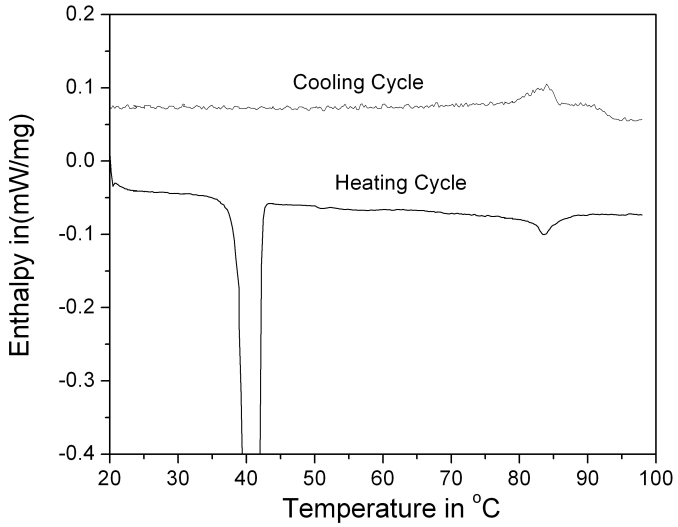

Figure 3.3: The DSC scan of mixture $x_{9.\,CN}$ = 0.827 measured during heating and cooling. No peaks in enthalpy change at the Sm A_d–N and Sm A_d–N_{re} are found, indicating the phase transitions to be of second order.

3.3 X-ray diffraction measurements

X-ray diffraction patterns were recorded throughout the mesomorphic range of all the mixtures and the pure compounds. The X-ray diffraction intensity data were analyzed to evaluate order parameters following a procedure described by Bhattacharya and Paul [48]. Structural parameters like layer thickness (d) and the apparent molecular length (l), in the smectic and nematic phases respectively were also determined from the X-ray data. The angular distribution of the X-ray intensity along the outer arc of the diffraction pattern was used to determine the orientational order parameter after necessary background correction.

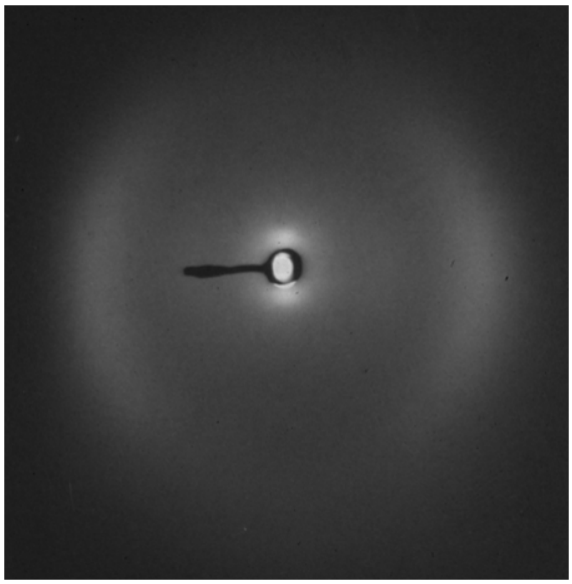

(a) Nematic phase at (78.8°C)

Figure 3.4: X-ray diffraction pattern of 7CPB+9.CN mixture with $x_{9.\,CN}$ = 0.774.

The X-ray diffraction photographs of a mixture ($x_{9.\,CN}$ = 0.774) in the nematic (74.8°C), the smectic A_d (54.5°C) and the re-entrant nematic (38.8°C) phases are shown in figure 3.4. The temperature variation of the experimentally determined orientational order parameters (OOP), $\langle P_2 \rangle$ and $\langle P_4 \rangle$, for different mixtures and pure components of this system is shown in figures 3.5a –3.5i.

The orientational order parameters, $\langle P_2 \rangle$ and $\langle P_4 \rangle$ in the nematic phases of 7CPB and mixture with $x_{9.\,CN}$ = 0.176, are in good agreement with the Maier-Saupe [44] theoretical values. However, for 9.CN, the $\langle P_2 \rangle$ values are higher than

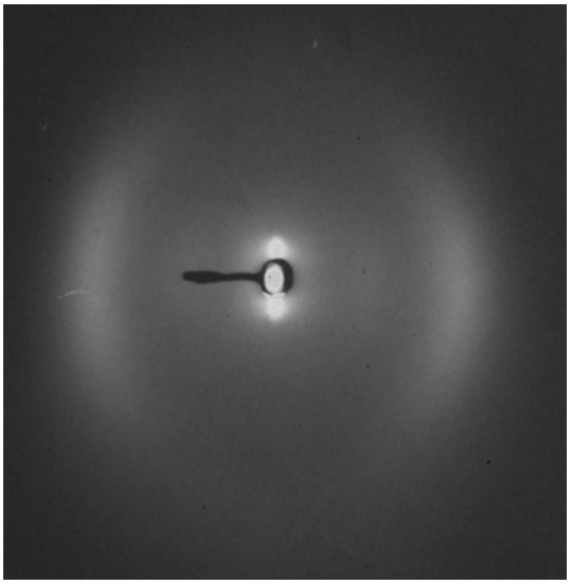

(b) Smectic A_d phase at (54.9°C)

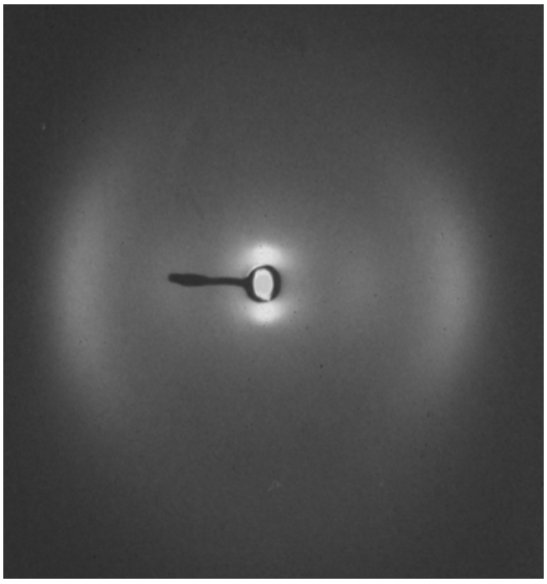

(c) Re-entrant nematic phase (38.8°C)

Figure 3.4: (cont'd): X-ray diffraction pattern of 7CPB+9.CN mixture with $x_{9.\ CN}$ = 0.774.

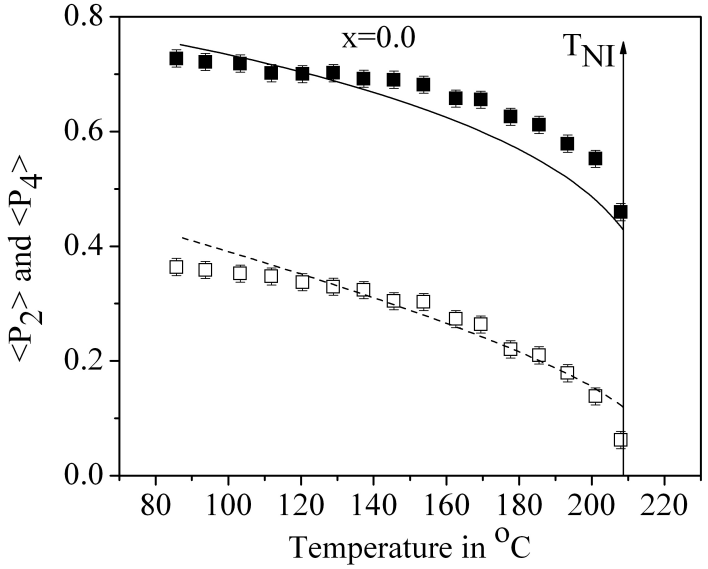

(a) Temperature variation of $\langle P_2 \rangle$ and $\langle P_4 \rangle$ for 7CPB.

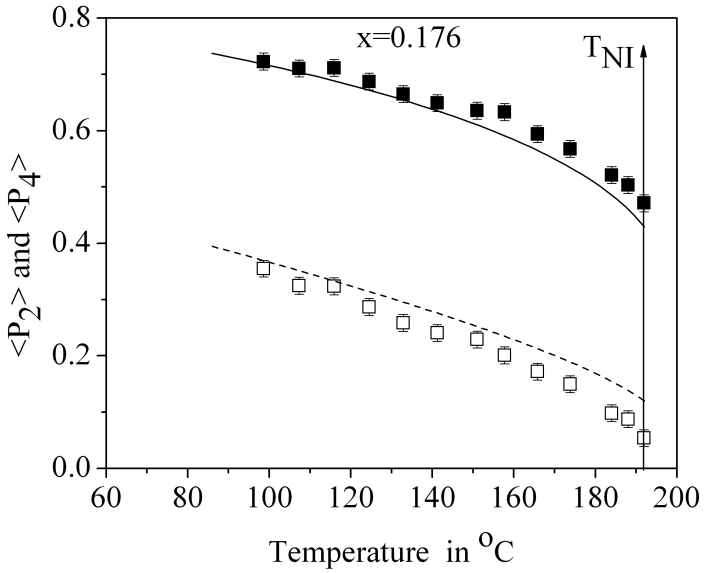

(b) Temperature variation of $\langle P_2 \rangle$ and $\langle P_4 \rangle$ for $x_{9.\,CN}$ = 0.176.

Figure 3.5: Temperature variation of $\langle P_2 \rangle$ and $\langle P_4 \rangle$ for 7CPB and $x_{9.\,CN}$ = 0.176, ■ $\langle P_2 \rangle$, □ $\langle P_4 \rangle$ from X-ray data; — $\langle P_2 \rangle$, - - - $\langle P_4 \rangle$ from Maier-Saupe theory.

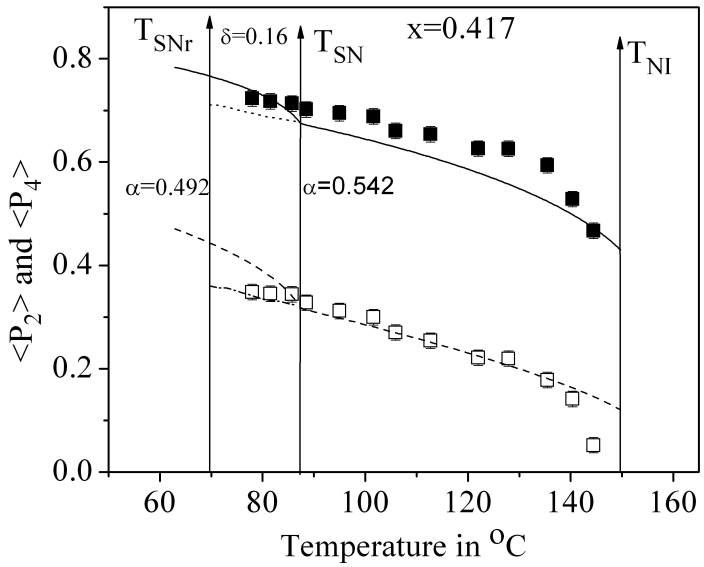

(c) Temperature variation of $\langle P_2 \rangle$ and $\langle P_4 \rangle$ for $x_{9.\,CN} = 0.417$.

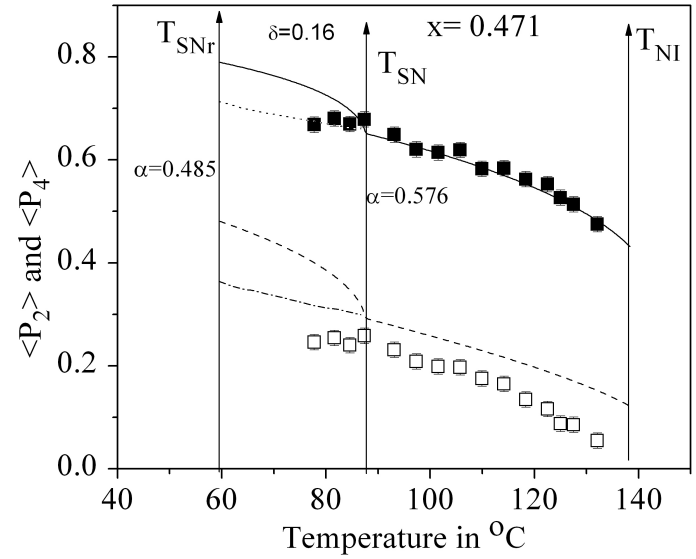

(d) Temperature variation of $\langle P_2 \rangle$ and $\langle P_4 \rangle$ for $x_{9.\,CN} = 0.471$.

Figure 3.5: (cont'd): Temperature variation of $\langle P_2 \rangle$ and $\langle P_4 \rangle$ for $x_{9.\,CN} = 0.417$ and $x_{9.\,CN} = 0.471$, ■ $\langle P_2 \rangle$, □ $\langle P_4 \rangle$ from X-ray data; — $\langle P_2 \rangle$, - - - $\langle P_4 \rangle$ from McMillan's theory. $\cdots$ $\langle P_2 \rangle$, $-\cdot-\cdot-$ $\langle P_4 \rangle$ from modified McMillan's theory by Luckhurst and Timimi.

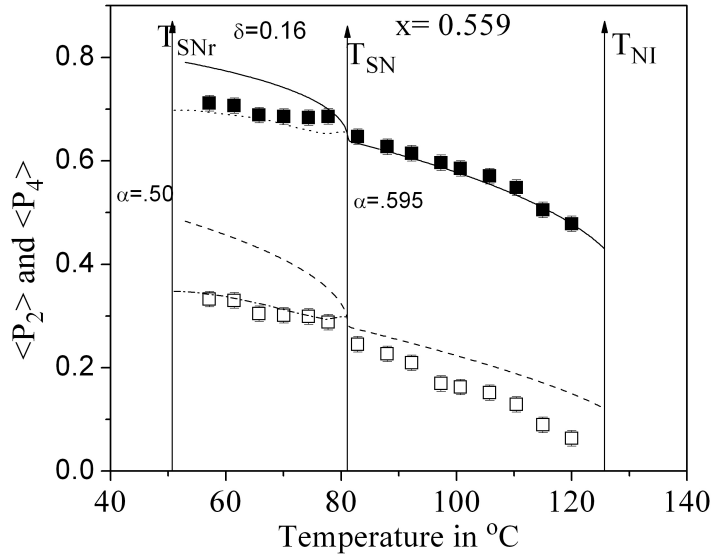

(e) Temperature variation of $\langle P_2 \rangle$ and $\langle P_4 \rangle$ for $x_{9.\,CN} = 0.559$.

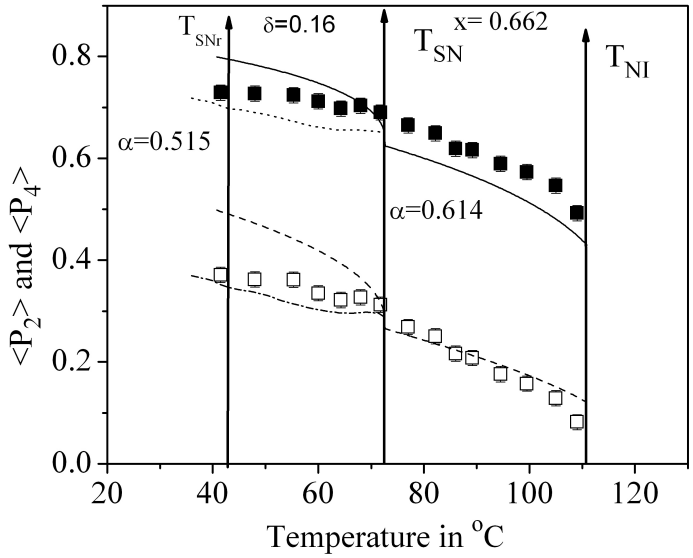

(f) Temperature variation of $\langle P_2 \rangle$ and $\langle P_4 \rangle$ for $x_{9.\,CN} = 0.662$.

Figure 3.5: (cont'd): Temperature variation of $\langle P_2 \rangle$ and $\langle P_4 \rangle$ for $x_{9.\,CN} = 0.559$ and $x_{9.\,CN} = 0.662$, ■ $\langle P_2 \rangle$, □ $\langle P_4 \rangle$ from X-ray data; — $\langle P_2 \rangle$, - - - $\langle P_4 \rangle$ from McMillan's theory. ⋯ $\langle P_2 \rangle$, $-\cdot-\cdot-$ $\langle P_4 \rangle$ from modified McMillan's theory by Luckhurst and Timimi.

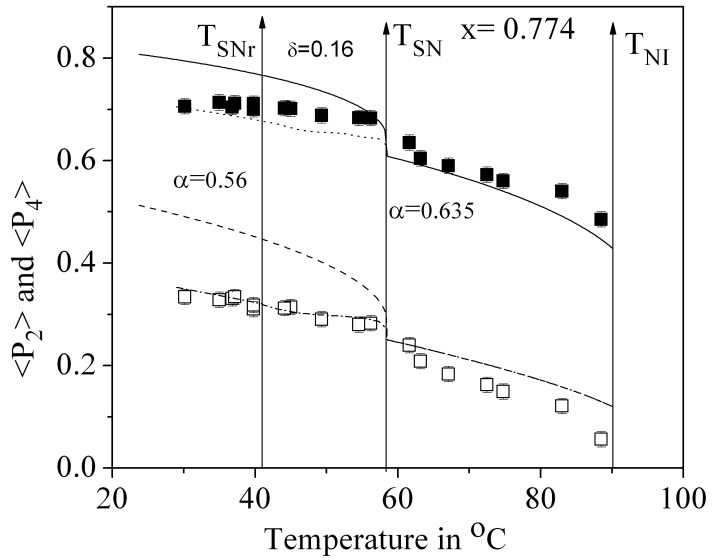

(g) Temperature variation of $\langle P_2 \rangle$ and $\langle P_4 \rangle$ for $x_{9.\,CN} = 0.774$.

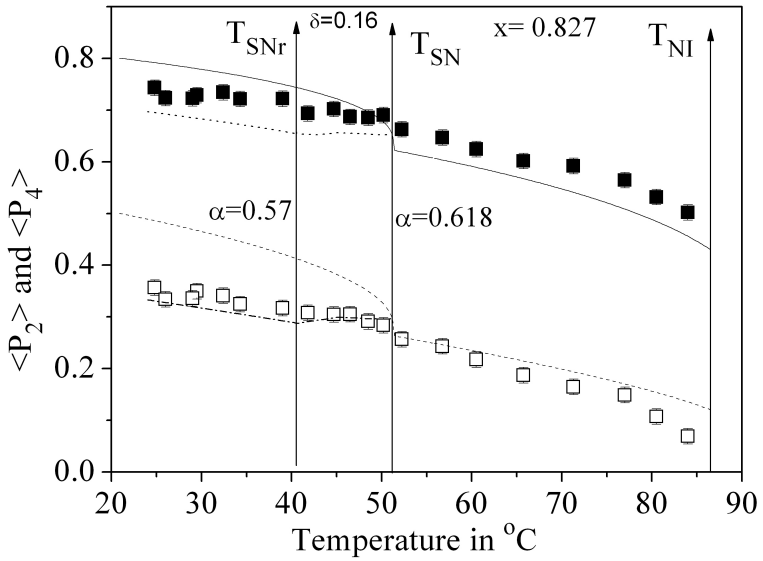

(h) Temperature variation of $\langle P_2 \rangle$ and $\langle P_4 \rangle$ for $x_{9.\,CN} = 0.827$.

Figure 3.5: (cont'd): Temperature variation of $\langle P_2 \rangle$ and $\langle P_4 \rangle$ for $x_{9.\,CN} = 0.774$ and $x_{9.\,CN} = 0.827$, ■ $\langle P_2 \rangle$, □ $\langle P_4 \rangle$ from X-ray data; — $\langle P_2 \rangle$, - - - $\langle P_4 \rangle$ from McMillan's theory. ⋯ $\langle P_2 \rangle$, – · – · – $\langle P_4 \rangle$ from modified McMillan's theory by Luckhurst and Timimi.

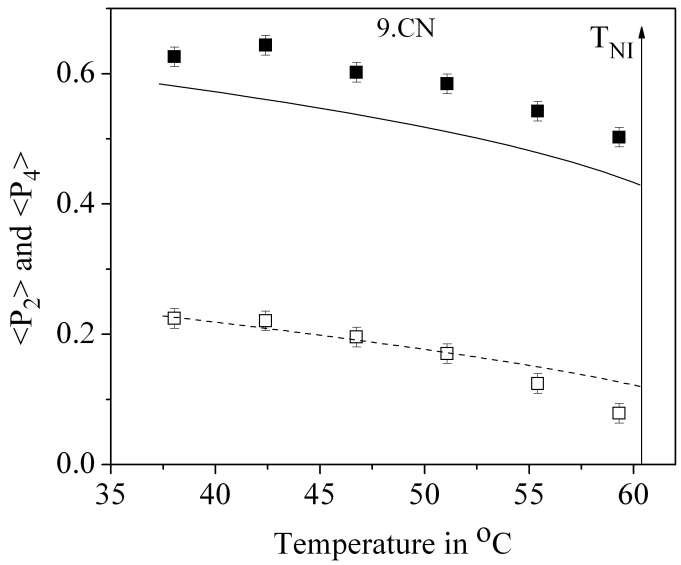

(i) Temperature variation of $\langle P_2 \rangle$ and $\langle P_4 \rangle$ for 9.CN.

Figure 3.5: (cont'd): Temperature variation of $\langle P_2 \rangle$ and $\langle P_4 \rangle$ for 9.CN, ■ $\langle P_2 \rangle$, □ $\langle P_4 \rangle$ from X-ray data; — $\langle P_2 \rangle$, - - - $\langle P_4 \rangle$ from Maier-Saupe theory.

the Maier-Saupe values but the $\langle P_4 \rangle$ values agree quite well with the theoretical values. Although from texture studies, both the induced smectic and re-entrant nematic phases was observed in the concentration range $0.4 < x_{9.\,CN} < 0.87$, but in X-ray diffraction study of the magnetically aligned bulk sample, both the induced smectic and the re-entrant nematic phases are observed only for three mixtures ($x_{9.\,CN}$ = 0.664, 0.774 and 0.827). For other mixtures showing induced smectic and re-entrant nematic phases from texture study ($x_{9.\,CN}$ = 0.417, 0.471 and 0.559), the re-entrant nematic phase and some portion of smectic A_d phase are suppressed due to the solidification. The temperature dependence of the order parameters in the N_{re} and N phases for the mixtures ($x_{9.\,CN}$ = 0.662, 0.774 and 0.827) is observed to be quite pronounced in comparison to those in the smectic A_d phase. These values are found to vary continuously across the N–Sm A_d and Sm $A_d - N_{re}$ phase transition indicating second order phase transition.

I have tried to fit the experimental data with those calculated from the theory of McMillan [45, 46] for mixtures having a smectic A_d phase using α and δ as adjustable parameters in the potential.

According to McMillan's theory, the single particle potential is given by

$$V_M(\cos\theta, z) = -v\left[\delta\alpha\tau\cos\left(\frac{2\pi z}{d}\right) + \left\{\eta + \alpha\sigma\cos\left(\frac{2\pi z}{d}\right)\right\}P_2(\cos\theta)\right] \qquad (3.1)$$

where α and δ are two adjustable parameters, z is the displacement along the layer normal, d is the layer thickness, $\eta = \langle P_2(\cos\theta)\rangle$, the orientational order parameter, while $\tau = \langle\cos(2\pi z/d\rangle$ is the translational order parameter and $\sigma = \langle P_2(\cos\theta)\cos(2\pi z/d\rangle$ is the mixed translational and orientational order parameter. The parameter v is obtained from the nematic/isotropic transition temperature, assuming the simple mean field theory result ($kT_{NI}/v = 0.22019$). The values of η, τ and σ are calculated using the self-consistent relationships as a function of temperature for various values of the parameters α and δ. The stability of the smectic A_d phase is controlled by the two adjustable parameters α and δ, with α being the primary variable. It may be mentioned that, the order parameter values have been calculated keeping δ value constant ($\delta = 0.16$) over the entire composition range. This is justified because the parameter α depends on the molecular length, which varies with the chain length, whereas the parameter δ, being the ratio of the translational to the orientational part of the potential, may be assumed to be almost constant with composition. The best fitted theoretical curve and the values of α and δ used for this calculation are shown in figures (3.5c–3.5h). The agreement between the experimental $\langle P_2\rangle$ and $\langle P_4\rangle$ values from X-ray diffraction measurements with those calculated from McMillan's theory is poor for all the mixtures, except for mixtures with $x_{9.\,CN} = 0.417$ and 0.827, where the agreement with the experimental $\langle P_2\rangle$ values are relatively good. This is not surprising, since in the Sm A_d phase the aliphatic chains of the molecules being closely packed cannot remain parallel to one another. This decreases the value of the orientational order parameter with temperature significantly and hence the temperature dependence of the orientational order parameters in the smectic phase is small in comparison to those obtained from McMillan's theory.

To account for this discrepancy, I have fitted the experimental data with those calculated from a simple extension of the McMillan's treatment of the smectic A phase. According to the calculation made by Luckhurst and Timimi [47], the orientational order parameter increases with decreasing temperature in a manner almost independent of the SmA–nematic transition. As the molecules

in McMillan's theory are assumed to be rigid, the parameter α in the pair potential is taken to be temperature independent. However, this may not be the case for the mixtures studied with polar esters forming both induced smectic and re-entrant nematic mesophases. It will be seen in the later part of this work that, in the mixtures, there exist both homo and hetero dimers and hence it is expected that their molecular length may well change with temperature. As a consequence, one may expect α to be weakly temperature dependent for such mixtures. Now, if α decreases with temperature then the SmA–N transition temperature will be reduced. An appropriate choice of the temperature dependence of α parameter gives rise to a situation where lowering the temperature still produces the usual SmA–N transition. Further decrease in temperature reduces α to such an extent that the SmA phase becomes unstable and reverts to a nematic phase; in other words a re-entrant nematic phase is formed.

I was able to obtain re-entrant nematic phase by using an essentially linear temperature variation of α . A typical dependence of α for all the mixtures studied is shown in table 3.1. Using this variation of α and setting δ equal to 0.16, the dependence of the orientational order parameters with temperature has been obtained, which are also shown in figures (3.5c–3.5h). The agreement between the experimental $\langle P_2 \rangle$ and $\langle P_4 \rangle$ values from X-ray diffraction measurements with those calculated from the modified McMillan's theory is very good for all the mixtures, particularly for those mixtures showing both induced smectic and re-entrant nematic phases. Both Sm A_d–N transitions are predicted to be second order by this model and this prediction is also in agreement with the DSC measurement, where no change in the transition enthalpies are observed at the re-entrant nematic to smectic A_d as well as smectic A_d to nematic phase transitions.

From table 3.1 it is observed that, the maximum change in α needed to obtain re-entrant nematic phase is about 0.1 and minimum is about 0.05. It has been found that in a homologous series α varies almost linearly with the length of the alkyl chain and that a change of 0.1 in α is equivalent to approximately one methylene group (1.5Å) i.e. for Sm A_d phase change in layer thickness of about 2.1 Å. So, in mixture with $x_{9.\,CN}$ = 0.827, a change of α= 0.048 is equivalent to change of 1Å length in layer thickness. Experimentally the change in layer thickness in smectic phase of the same mixture is found to be 0.8 Å, which is

Table 3.1: Change in α values required to fit experimental data for different mixtures.

$x_{9.\,CN}$	α at T_{SN}	α at $T_{SN_{re}}$	$\Delta\alpha$
0.417	0.542	0.492	0.05
0.471	0.576	0.485	0.091
0.559	0.595	0.5	0.095
0.662	0.614	0.515	0.099
0.774	0.635	0.56	0.075
0.827	0.618	0.57	0.048

very close to the expected values.

To investigate the nature of the phase transition during Sm–N, N–Iso and Sm–N_{re}, I have measured the high resolution density as a function of temperature for a mixture ($x_{9.\,CN}$ = 0.827) which is quite close to the eutectic composition in the phase diagram, and the results are presented in figure 3.6. It is immediately apparent that, the density changes smoothly at the re-entrant nematic–smectic A_d as well as smectic A_d – nematic phase transitions, consistent with the results observed in the order parameter measurements. It is also noted that the change in the density values at the N–I transition is also continuous.

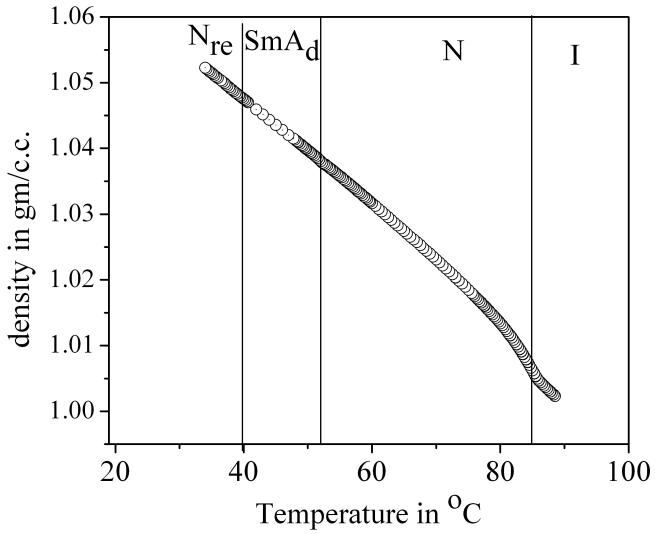

Figure 3.6: Temperature variation of the density values of 7CPB+9.CN mixture ($x_{9.\,CN}$ = 0.827).

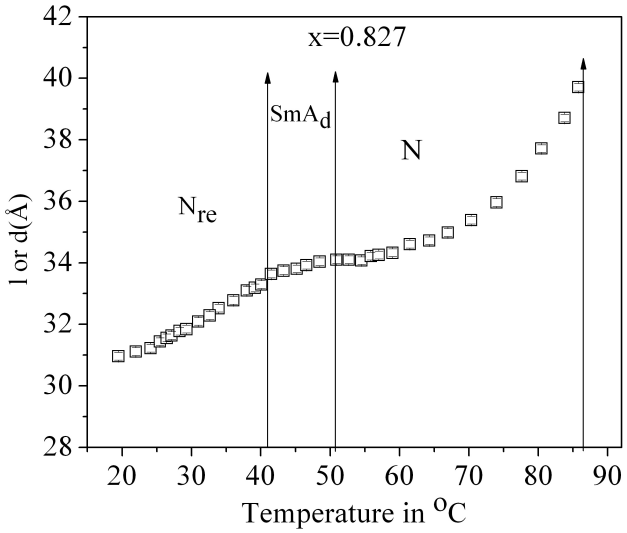

Figure 3.7: Temperature variation of apparent molecular length (l) or layer thickness of 7CPB+ 9.CN mixture ($x_{9.\,CN}$ = 0.827).

The temperature variation of the layer thickness in the smectic phase and apparent molecular length (l), i.e. density wave parallel to the director, in the nematic phase have been measured from the X-ray diffraction patterns for all the mixtures and pure compounds. It has been found that the apparent molecular lengths (l) in the nematic as well as the re-entrant nematic phases increase with increasing temperature. The layer thickness (d) values in the smectic A_d phase show a slight increase with increasing temperature (figure 3.7).

The composition variation of the layer thickness at T_{SN} - 5°C (for mixture $x_{9.\,CN}$ = 0.176 and the two pure compounds, the apparent molecular length have been taken at a temperatures where the extrapolated T - 5°C line intersect) is shown in figure 3.8. The variation shows a broad maximum of ≈35.5Å at about equimolar concentration. This is in contrast to observation of Das *et.al.* [49, 50] on some polar– non polar mixtures showing induced smectic A_d phase, where the layer thickness shows a minimum at about equimolar composition.

In order to calculate the variation of layer thickness with molar concentration it has been assumed that both the pure 9.CN molecules (molecule A) and 7CPB molecules (molecule B) form association in the nematic phase. The

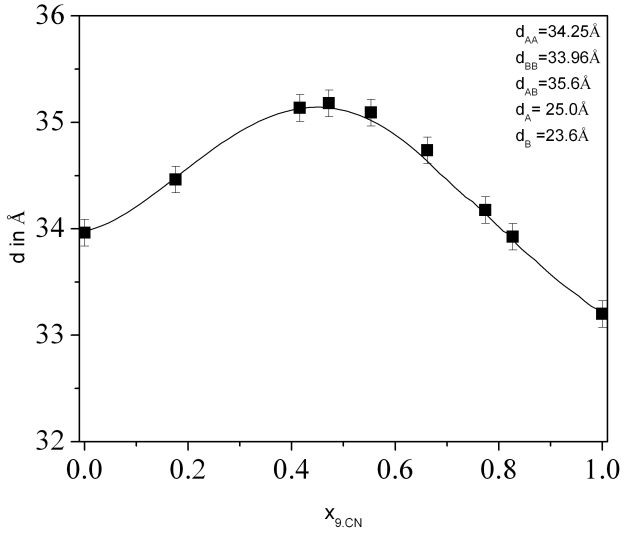

Figure 3.8: Variation of layer spacing at a temperature T=T_{SN}-5°C with mole fraction of 9.CN. ■ experimental data, full line is from theoretical calculation. The experimental values at $x_{9.\,CN}$ = 0, $x_{9.\,CN}$ = 0.176 and $x_{9.\,CN}$ =1.0 are those of apparent molecular length in nematic phase.

apparent molecular length of 7CPB as determined from X-ray diffraction studies is 33.96Å, which is much larger than its model molecular length of 26Å. It is considered that the molecules form association and the pure state is a mixture of predominantly associated dimers and monomers, which are in dynamic equilibrium. In mixtures, it can be assumed that the terminal polar molecules form homo dimers (AA and BB) as well as hetero dimers (AB). The possibility of formation of such homo and hetero complexes was proposed earlier by others [34, 51–55].

Hence in these mixtures, it can be assumed that there exists A, B, AA, BB and AB types of molecules in equilibrium. The mole fractions of different species x_A, x_B, x_{AA}, x_{BB} and x_{AB} can be determined from the equilibrium constants K_A, K_B and K_{AB} for the associations, A + A ↔ AA, B + B ↔ BB and A + B ↔ AB, respectively. Using equilibrium constants K_A = 1000, K_B = 1000 and K_{AB} = 800, the percentage of different species, A, B, AA, BB and AB as function of mole fraction have been calculated.

The average d value may then be written as

$$d = x_A d_A + x_{AA} d_{AA} + x_{AB} d_{AB} + x_B d_B + x_{BB} d_{BB} \tag{3.2}$$

where x_A, x_B, x_{AA}, x_{BB}, x_{AB} are mole fractions of respective components in chemical equilibrium, d_A and d_B are taken to be equal to the lengths of the molecules A and B as obtained from molecular model kit. d_{AA} has been adjusted so that in pure terminal polar compound, which has both A and AA molecules, the apparent molecular length equals ($= x_A d_A + x_{AA} d_{AA}$) the experimentally observed d value. In the similar procedure the value of d_{BB} can be estimated.

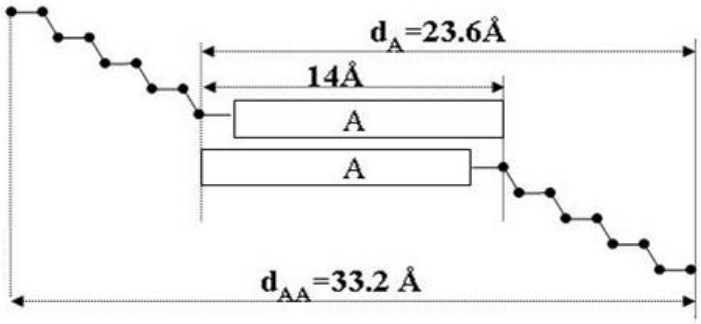

(a)

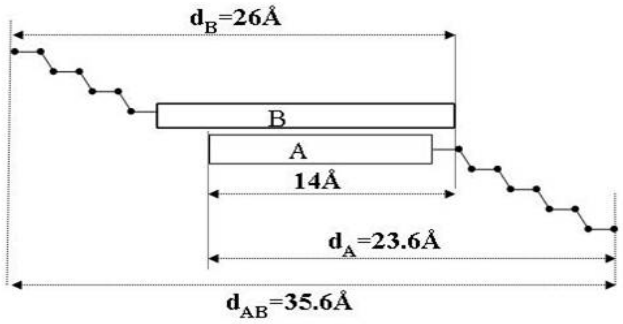

(b)

Figure 3.9: Molecular packing model of the dimers: (a) AA dimer - 9.CN + 9.CN (b) AB dimer- 9.CN + 7CPB.

To estimate the length of 7CPB + 9.CN (d_{AB}) dimers, one can proceed as follows. The length of 9.CN molecule is 23.6Å and that of its dimer is 33.2Å. If one assumes that the apparent molecular length in the nematic phase of 9.CN is

equal to its dimer length, then the overlap of the two 9.CN molecules in the dimer is about 14Å (figure 3.9a). Now, 7CPB molecule (molecular length =26Å) has a cyano terphenyl unit, which contains nearly identical segment like 9.CN. As both 7CPB and 9.CN molecules contain terminal CN group, so the dimer formation is enhanced and one can assume that in 7CPB + 9.CN dimer an identical overlap of the molecules (14Å) take place as in 9.CN + 9.CN dimer. Hence, the length of 7CPB +9.CN (d_{AB}) dimer comes out to be 26Å + 23.6Å - 14Å = 35.6Å (figure 3.9b). The values of d calculated from equation (3.2), is shown in figure 3.8. It is seen that the calculated result for layer thickness is in good agreement with the experimental values.

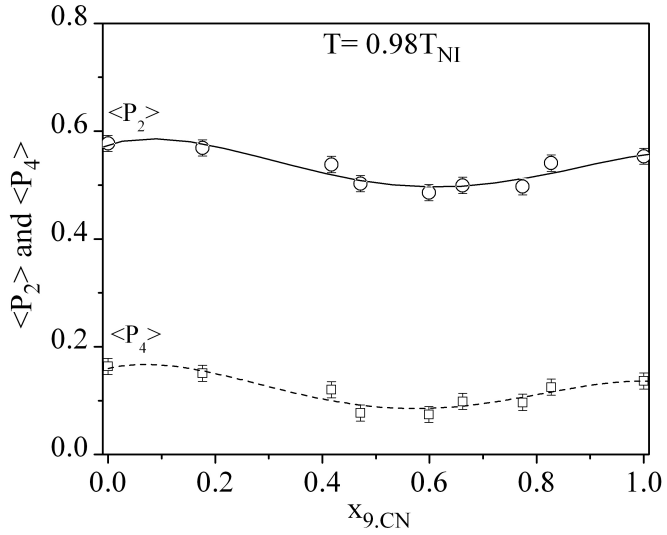

Figure 3.10: Orientational order parameters $\langle P_2 \rangle$ and $\langle P_4 \rangle$ plotted against mole fraction of 9.CN at a temperature $T = 0.98T_{NI}$.

Figure 3.10 shows the variation of $\langle P_2 \rangle$ and $\langle P_4 \rangle$ values with mole fraction of 9.CN at $T = 0.98T_{NI}$ for this system. It is seen that the OOP values decrease with increase in molar concentration of 9.CN, showing a broad minimum around $x_{9.\,CN} = 0.5$.

3.4 Conclusion

The physical properties of a polar-polar binary system comprising of two nematogenic compounds one having a biphenyl core and the other having a terphenyl core have been studied extensively by polarising optical microscopy, DSC and X-ray diffraction measurements. The phase diagram shows the presence of induced smectic and re-entrant nematic phases in the concentration range 0.4< $x_{9.\,CN}$ < 0.87. From textures studies it has been observed that both the normal and re-entrant nematic phases in this system are similar. The order of the induced smectic A_d to nematic as well as the induced smectic A_d to re-entrant nematic phase transition is continuous for all the mixtures. This observation has been supported from DSC, density and orientational order parameter values determined from X-ray diffraction measurements. Using a simple extension of McMillan's treatment of the smectic A phase, the theoretically estimated $\langle P_2 \rangle$ and $\langle P_4 \rangle$ values have been found to fit quite well with those determined from X-ray diffraction studies. Further analysis of the X-ray data has revealed a maximum in the smectic layer spacing near $x_{9.\,CN}$ = 0.5. The variation of layer thickness with molar concentration of 9.CN has been explained fairly well by assuming the presence of both homo and hetero dimers.

References

[1] D. Guillon, P. E. Cladis, J. Stamatoff, *Phys. Rev. Lett.*, **41**, 1598 (1978).

[2] N. S. Chen, S. K. Hark, J. T. Ho, *Phys. Rev. A*, **24**, 2843 (1981).

[3] F. R. Bouchet, P. E. Cladis, *Mol. Cryst. Liq. Cryst. (Lett.)*, **64**, 97 (1980).

[4] K. J. Lushington, G. B. Kasting, C. W. Garland, *Phys. Rev. B*, **22**, 2569 (1980).

[5] R. Y. Dong, *Mol. Cryst. Liq. Cryst. (Lett.)*, **64**, 205 (1981).

[6] R. Y. Dong, *J. Chem. Phys.*, **75**, 2621 (1981).

[7] R. Shashidhar. H. D. Kleinhans, G. M. Schneider, *Mol. Cryst. Liq. Cryst. (Lett.)*, **72**, 119 (1981).

[8] P. E. Cladis, *Phys. Rev. A*, **23**, 2594 (1981).

[9] A. R. Kortan, H. V. Kanel, R. J. Birgeneau, J. D. Lister, *Phys. Rev. Lett.*, **47**, 1206 (1981).

[10] A. R. Kortan, H. von Kanel, R. J. Birgenau, J. D. Litster, *J. Phys. (Paris)*, **45**, 529 (1984).

[11] A. Nayeem, J. H. Freed, *J. Phys. Chem.*, **93**, 6539 (1989).

[12] N. Hafiz, N. A. P. Vaz, Z. Yaniv, D. Affender, J. W. Doane, *Phys. Lett. A*, **91**, 41 (1982).

[13] J. W. Emsley, G. R. Luckhurst, P. J. Parson, B. A. Timimi, *Mol. Phys.*, **56**, 767 (1985).

[14] P. E. Cladis, D. Guillon, F. R. Bouchet, P. L. Finn, *Phys. Rev. A*, **23(5)**, 2594 (1981).

[15] D. D. Klug, E. Whalley, *J. Chem. Phys.*, **71**, 1874 (1979).

[16] J. M. Sorenson, G. R. Van Hecke, *J. Phys. Chem.*, **98**, 10289 (1994).

[17] K. J. Lushington, G. B. Kasting, C. W. Garland, *Phys. Rev. B*, **22(5)**, 2569 (1980).

[18] X. Shen, R. Y. Dong, *J. Chem. Phys.*, **108**, 9177 (1998).

[19] J. Bharatam, C. R. Bowers, *J. Phys. Chem. B*, **103**, 2510 (1999).

[20] R. Y. Dong, M. Cheng, *J. Chem. Phys.*, **113**, 3466 (2000).

[21] R. Nozaki, T. K. Bose, S. Yagihara, *Phys. Rev. A*, **46**, 7733 (1992).

[22] S. Urban, R. Dabrowski, B. Gestblom, A. Kocot, *Liq. Cryst.*, **27(12)**, 1675 (2000).

[23] J. Jadzyn, G. Czechowski, *Phys. Rev. E*, **64**, 052702 (2001).

[24] A. Zywocinski, *J. Phys. Chem. B*, **103**, 3087 (1999).

[25] M. K. Das, R. Paul, *Mol. Cryst. Liq. Cryst.*, **239**, 107 (1994).

[26] P. E. Cladis, *Mol. Cryst. Liq. Cryst.*, 165, 85 (1988).

[27] R. Shashidhar, S. Somasekhar, B. R. Ratna, *Mol. Cryst. Liq. Cryst.*, **133**, 19 (1986).

[28] G. Czechowski, J. Jadzyn, *Acta Physica Polonica A*, **106**, 475 (2004).

[29] J. Jadzyn, G. Czechowski, *Liq. Cryst.*, **4**, 157 (1989).

[30] D. Rodez, D. Collin, P. Martinoty, *Eur. Phys. J. E*, **14**, 43 (2004).

[31] B. R. Ratna, R. Shashidhar, M. Bock, A. Gobl-Wunsch, G. Heppke, *Mol. Cryst. Liq. Cryst.*, **99**, 285 (1983).

[32] S. Urban, R. Dabrowski, B. Gestblom, A. Kocot, *Liq. Cryst.*, **27**, 1675 (2000).

[33] M. Brodzik, R. Dabrowski, *Mol. Cryst. Liq. Cryst.*, **260**, 361 (1995).

[34] R. Dabrowski and K. Czuprynski, *Modern topics in Liquid Crystals - from Neutron Scattering to Ferroelectricity*, (Ed.) A. Buka, World Scientific, London, (1993).

[35] M. Brodzik, R. Dabrowski, *Proceeding of SPIE*, **2372**, 280 (1995).

[36] M. Tykarska, B. Wazynska, I. Ulbin, *Proceeding of SPIE*, **4147**, 55 (2000).

[37] M. Brodzik, *Ph. D. Thesis*, Wojskowa Akademia Techniczna, (1995).

[38] M. Brodzik, R. Dabrowski, *Liq. Cryst.*, **20**, 99 (1996).

[39] M. Brodzik, R. Dabrowski, J. Przedmojski, *J. Phys. II France*, **5**, 1805 (1995).

[40] A. Prasad, M. K. Das, *Phase Transitions*, **82**, 780 (2009).

[41] W. Maier, A. Saupe, *Z. Naturforsch.*, **A13**, 451 (1958).

[42] W. Maier, A. Saupe, *Z. Naturforsch.*, **A13**, 564 (1958).

[43] W. Maier, A. Saupe, *Z. Naturforsch.*, **A14**, 882 (1959).

[44] W. Maier, A. Saupe, *Z. Naturforsch.*, **A15**, 287 (1960).

[45] W. L. McMillan, *Phys. Rev. A*, **4**, 1236 (1971).

[46] W. L. McMillan, *Phys. Rev. A*, **6**, 93 (1972).

[47] G. R. Luckhurst, B. A. Timimi, *Mol. Cryst. Liq. Cryst.*, **260**, 253 (1981).

[48] B. Bhattacharjee, S. Paul, R. Paul, *Mol. Phys.*, **44**, 1391 (1981).

[49] M. K. Das, R. Paul, *Phase Transitions*, **46**, 185 (1994).

[50] M. K. Das, R. Paul, *Phase Transitions*, **48**, 255 (1994).

[51] S. Garg, T. Spears, *Mol. Cryst. Liq. Cryst.*, **409**, 335 (2004).

[52] A. C. Rauch, S. Garg, D. T. Jacobs, *J. Chem. Phys.*, **116**, 2213 (2002).

[53] T. R. Bose, C. D. Mukherjee, M. K. Roy, M. Saha, *Mol. Cryst. Liq. Cryst.*, **126**, 197 (1985).

[54] T. Kyu, H. W. Chiu, T. Kajiyama, *Phys. Rev. E*, **55**, 7105 (1997).

[55] T. Kyu, H. W. Chiu, *J. Chem. Phys.*, **103**, 7471 (1995).

Chapter 4

Study of refractive index, density and orientational order parameter of a binary system (7CPB+9.CN) exhibiting nematic, induced smectic A_d and re-entrant nematic phases

4.1 Introduction

Though it has been more than a decade since binary mixtures of nematic liquid crystals with strongly polar end groups were reported to exhibit a novel phase diagram with "induced smectic island surrounded by the nematic sea" [1–6], not much work has been done on such systems [7–9] so far. The 6OCB-8OCB binary system still remains one of the most extensively studied phase diagram showing re-entrant nematic phase [10–42], where a number of attempts have been made to study the birefringence of mixtures showing re-entrant nematic phase at normal pressure [11, 12]. Although very precise measurement on birefringence has also been reported by Chen *et. al.* [12] on the 6OCB-8OCB system, none of the reported studies have covered the entire concentration and temperature range. Again, it may be mentioned that in the 6OCB-8OCB system one of

the components, (8OCB), has an underlying smectic phase. The binary system exhibiting re-entrant nematic phase, which has purely nematic components, may behave differently and the variation of birefringence at the transitions may not be the same for all the systems and at different compositions of the mixtures.

In this chapter I have reported the temperature dependence of orientational order parameters (OOP's), which have been determined from refractive index measurements on the 7CPB + 9.CN system. As mentioned earlier in chapter 3, this system exhibits an induced smectic A_d and re-entrant nematic phase within the concentration range $0.4 < x_{9.\,CN} < 0.87$ [9]. The refractive index measurements have been done at different concentrations, throughout the mesomorphic range, using thin prism technique. The ordinary and extraordinary refractive indices as well as the density data have been used to determine the orientational order parameter ($\langle P_2 \rangle$) using the standard Vuks isotropic model [43]. The $\langle P_2 \rangle$ values determined from the refractive index data have been compared with those measured from X-ray diffraction studies. These values have also been compared with the theoretical values of Maier–Saupe [44] for the nematogens and a modification of McMillan's theory [45, 46] as proposed by Luckhurst and Timimi [47], for those mixtures having induced smectic and re-entrant nematic phases. The data obtained from the density measurements have been used to calculate the packing fraction. The nature of the phase transition at the isotropic–nematic, nematic–smectic A_d and smectic A_d – re-entrant nematic phase transitions has also been assessed.

In calculating the OOP from refractive indices data, the well known Haller's extrapolation method [48] is generally used which is rather ambiguous and the three parameter fit used to obtain the normalized polarizability anisotropy ($\Delta\alpha_0$) for the perfectly ordered crystalline state does not take into account any higher order phases which may be present below the nematic phase. I have been successful in obtaining the ordinary and extraordinary refractive indices values in the crystalline solid phase for one pure compound and for one mixture and by measuring the density values in the solid phase, the polarizability anisotropy for perfectly ordered crystal ($\Delta\alpha_0$), has been experimentally measured. These results have been compared with those obtained from extrapolation method.

Recently, some questions have been raised about the applicability of Haller's

extrapolation in the analysis of the order parameter since it gives a systematically lower value of the critical exponent β [49, 50], namely $\beta < 0.2$, as compared to those determined from other methods [49–53]. The value of β obtained from the Haller's extrapolation procedure does not match with any of the predicted theoretical values [54–63]. Hence, a modification of this procedure is required to improve the β values. A four parameter fitting procedure expressed by Chirtoc *et. al.* [49] can be suitably used. In this chapter, the polarizability anisotropy values have been fitted by this new procedure to obtain the values of the critical exponent β. The value of the critical exponent β so obtained has been compared with those obtained from the Haller's extrapolation method.

4.2 Refractive index measurements using thin prism technique

The temperature dependence of the principal refractive indices n_o and n_e and the refractive index in the isotropic phase (n_{iso}) at a wavelength $\lambda = 632.8$ nm for all the mixtures and the pure components of the 7CPB +9.CN system were measured and are shown in figures 4.1a – 4.1j. It has been found that the temperature dependence of n_o for all the mixtures is more or less identical, whereas the n_e curves show different temperature variations. For mixtures within the concentration range, $0.4 < x_{9.\,CN} < 0.87$, the extraordinary refractive index (n_e) shows a slight decrease in the Sm A_d phase during cooling but near the Sm $A_d - N_{re}$ transition n_e starts increasing again. The change in both the refractive indices and hence birefringence ($\Delta n = n_e$-n_o) is continuous at the nematic – smectic A_d as well as smectic A_d – re-entrant nematic phase transition, indicating a second order or a weakly first order phase transition. This observation is also supported from DSC and density measurements done on these mixtures [9].

Although, the birefringence changes almost continuously across the nematic – smectic A_d phase transition but in some mixtures, there is a slight increase in birefringence in going from smectic to re-entrant nematic phase. This observation is in disagreement with the observations of Chen *et. al.* [12] where they have reported an increase in the birefringence in going from nematic to smectic phase and an equal decrease in birefringence in going from smectic to re-entrant nematic phase of a system showing re-entrant nematic phase.

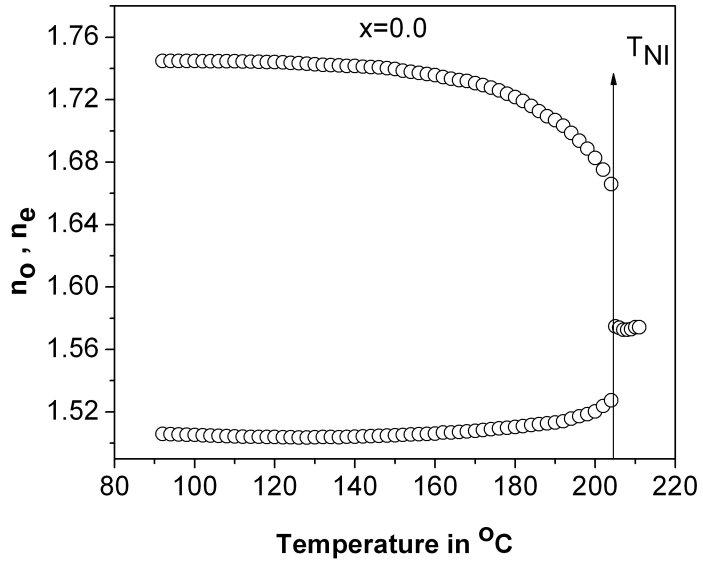

(a)

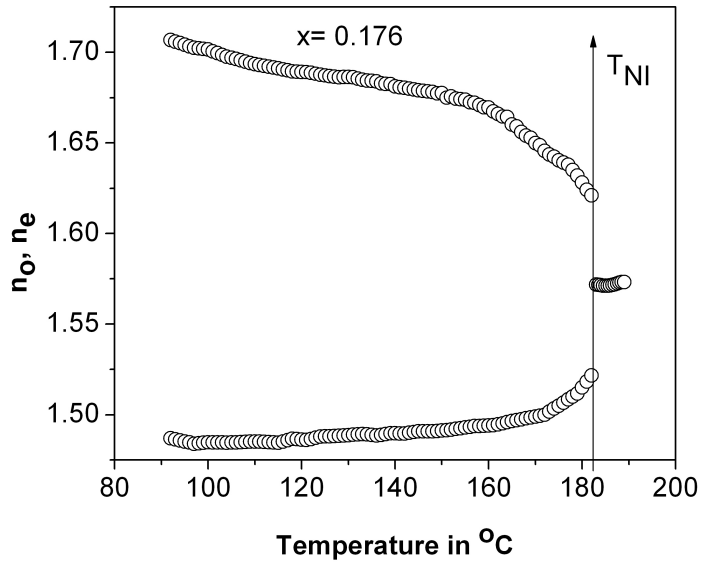

(b)

Figure 4.1: Experimental values of refractive indices n_o and n_e as a function of temperature for (a) 7CPB and (b) $x_{9.\,CN}$ = 0.176 . T_{NI} = nematic – isotropic phase transition temperature.

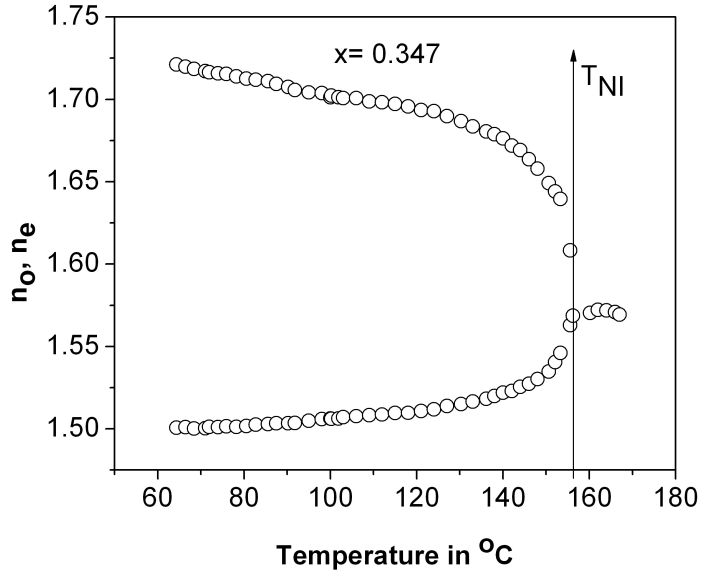

(c)

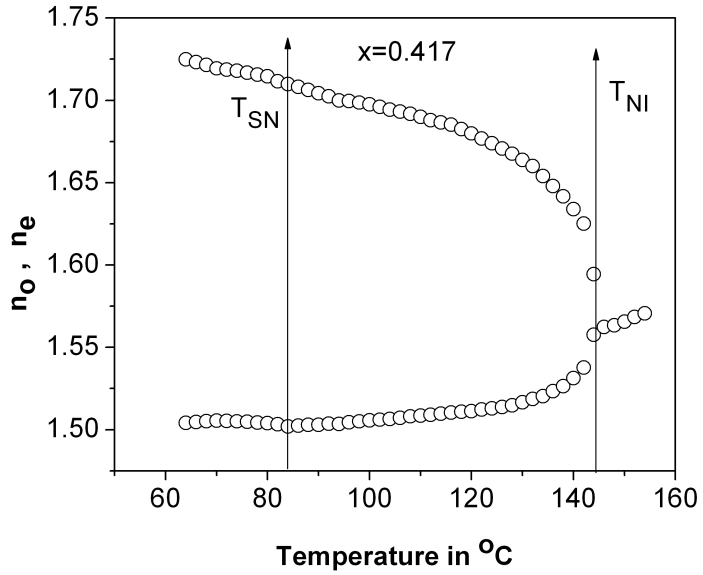

(d)

Figure 4.1:(cont'd): Experimental values of refractive indices n_o and n_e as a function of temperature for (c) $x_{9.\,CN}$ = 0.347 and (d) $x_{9.\,CN}$ = 0.417 . T_{NI} = nematic – isotropic and T_{SN} = smectic A_d – nematic phase transition temperatures.

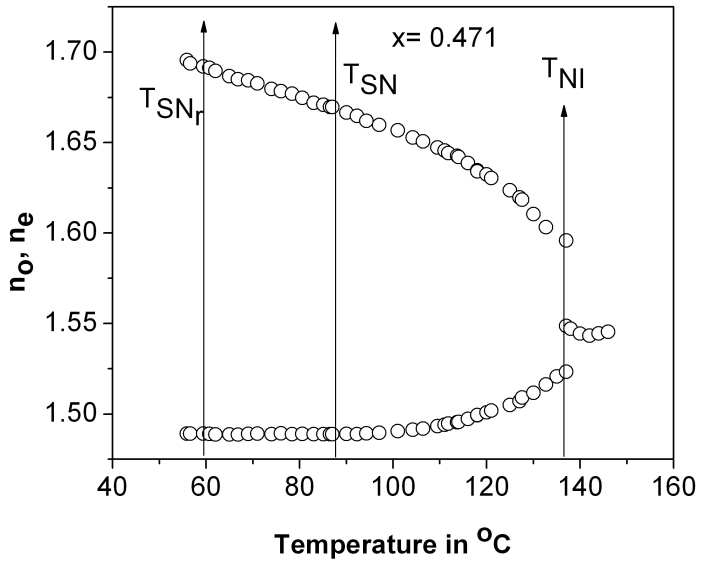

(e)

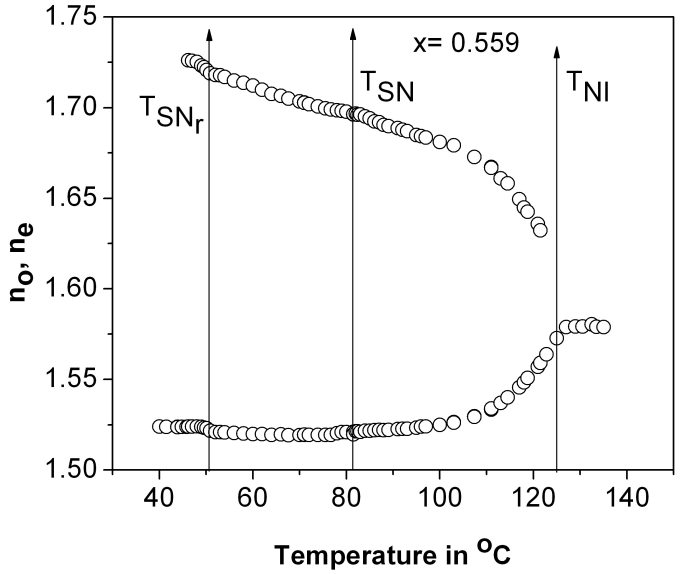

(f)

Figure 4.1: (cont'd): Experimental values of refractive indices n_o and n_e as a function of temperature for (e) $x_{9.\,CN}$ = 0.471 and (f) $x_{9.\,CN}$ = 0.559 . T_{NI} = nematic – isotropic, T_{SN} = smectic A_d – nematic and $T_{SN_{re}}$= smectic A_d – re-entrant nematic phase transition temperatures.

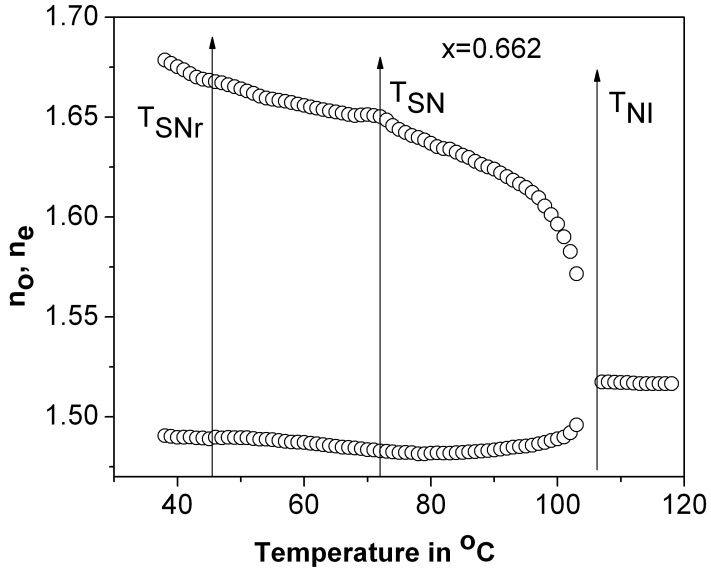

(g)

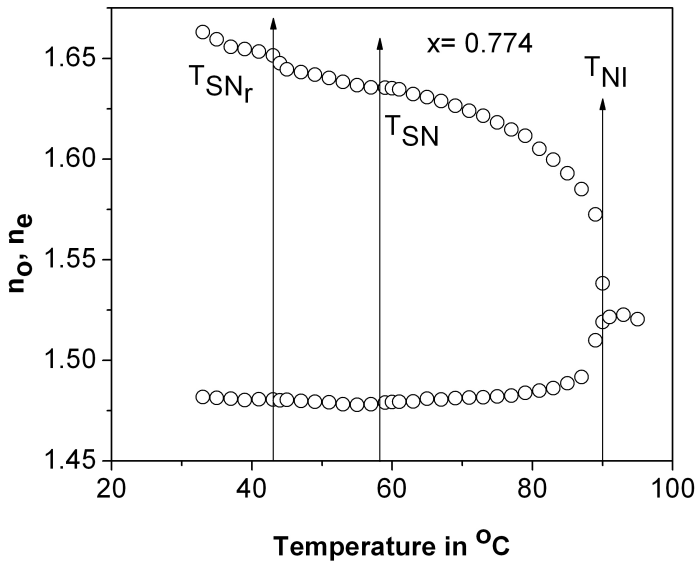

(h)

Figure 4.1: (cont'd): Experimental values of refractive indices n_o and n_e as a function of temperature for (g) $x_{9.\,CN}$ = 0.662 and (h) $x_{9.\,CN}$ = 0.774 . T_{NI} = nematic – isotropic, T_{SN} = smectic A_d – nematic and $T_{SN_{re}}$= smectic A_d – re-entrant nematic phase transition temperatures.

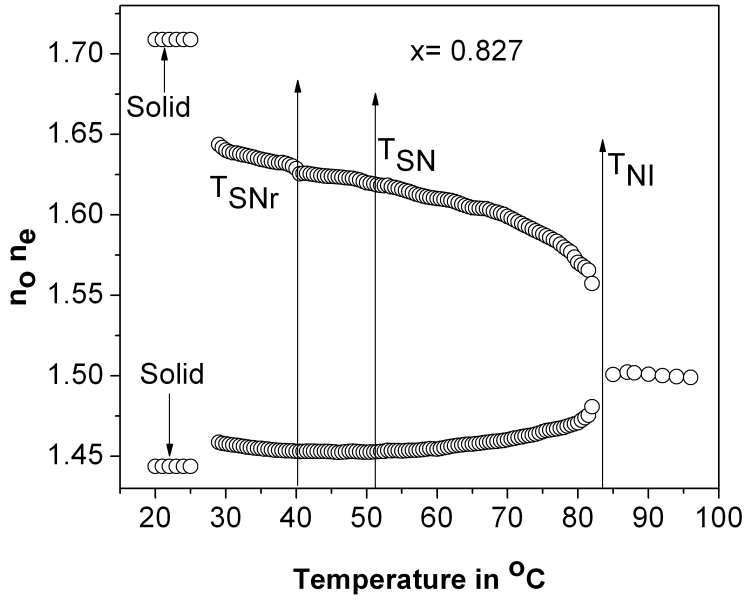

(i)

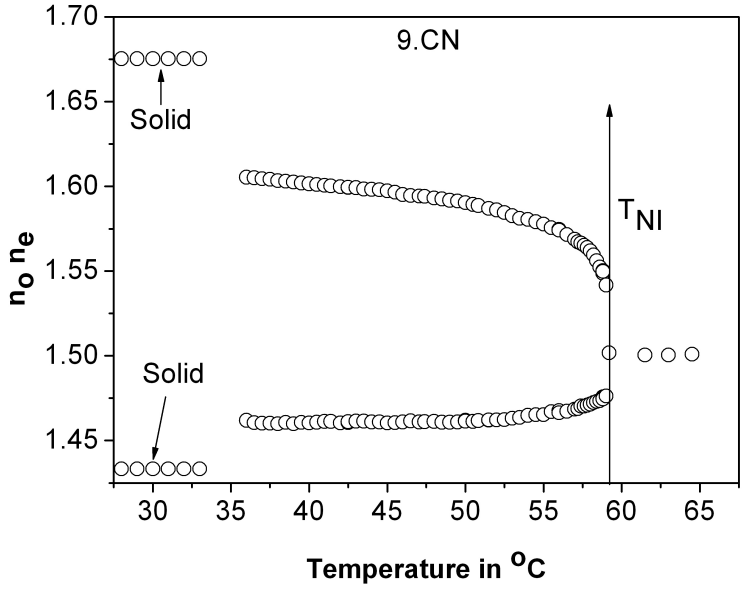

(j)

Figure 4.1:(cont'd): Experimental values of refractive indices n_o and n_e as a function of temperature for (i) $x_{9.\,CN}$ = 0.827 and (j) 9.CN . T_{NI} = nematic – isotropic, T_{SN} = smectic A_d – nematic and $T_{SN_{re}}$= smectic A_d – re-entrant nematic phase transition temperatures.

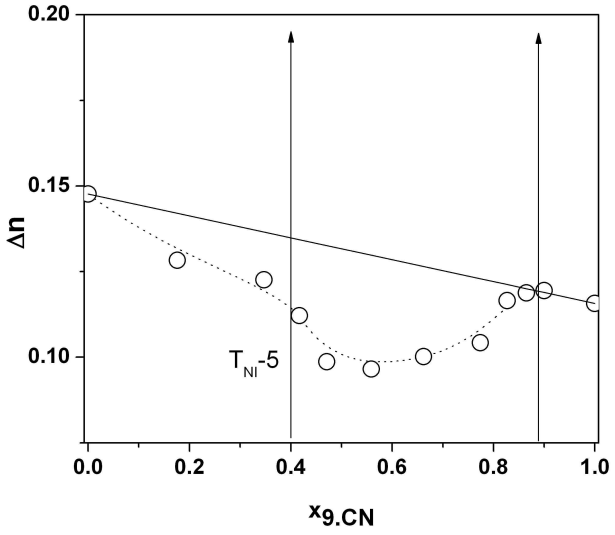

Figure 4.2: Birefringence (Δn) plotted as a function of mole fraction of 9.CN.

Figure 4.2 shows the concentration variation of birefringence at temperature T = $T_{NI}-5°C$. It is evident from the figure that for all the mixtures the birefringence is less than the weighted mean of the pure components ($x_A\Delta n_A + x_B\Delta n_B$) represented by the solid line and it has a broad minima at around $x_{9.\,CN}$ = 0.5.

4.3 Density measurements

The temperature variation of the density values for all the mixtures is shown in figures 4.3a to 4.3d. There is no discontinuity in density values at the nematic - smectic A_d and the smectic A_d – re-entrant nematic phase transition for all the mixtures.

In order to obtain a better idea about molecular organization in different liquid crystalline phases I have also calculated the molecular packing fraction. The packing fraction is defined as the ratio of the geometrical volume (van der Waals volume) of the molecule to the volume occupied per molecule in the mesophases. Following Kitaigorodski [64], I have calculated the geometrical volume of the pure components V_A and V_B, where A, B refers to 7CPB and 9.CN molecules respectively.

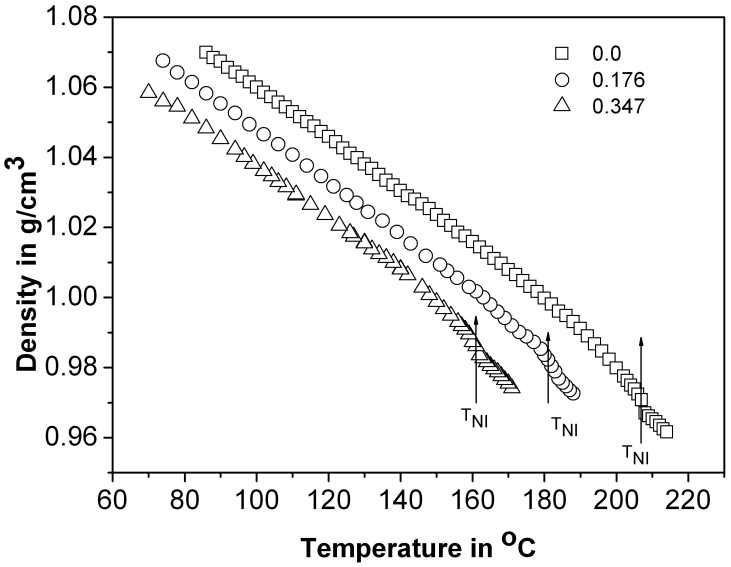

(a)

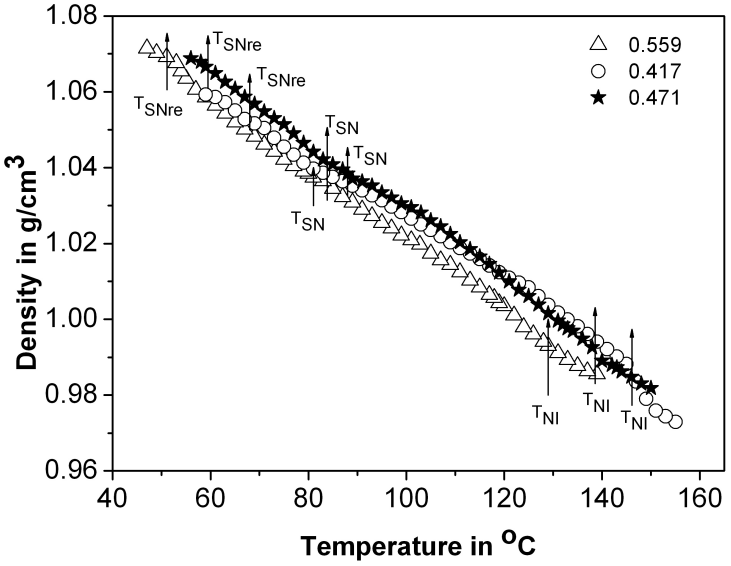

(b)

Figure 4.3: Variation of density values (ρ) as a function of temperature for (a) $x_{9.\,CN}$ = 0.0, 0.176, 0.347 and (b) $x_{9.\,CN}$ = 0.417, 0.471, 0.559.

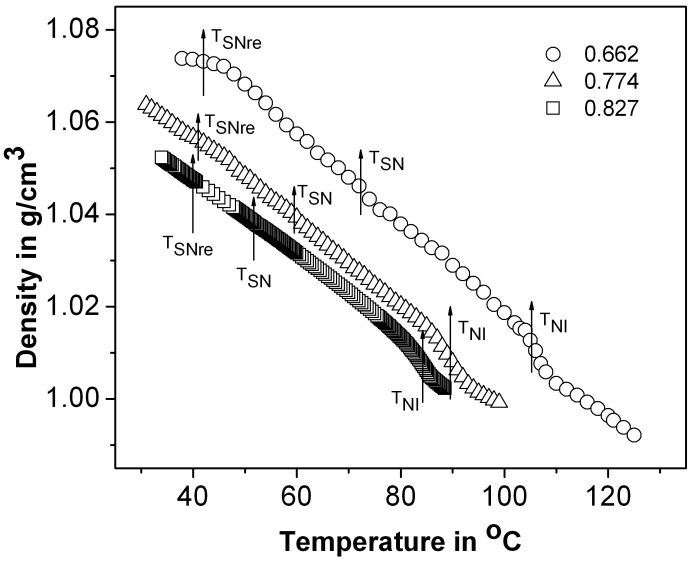

(c)

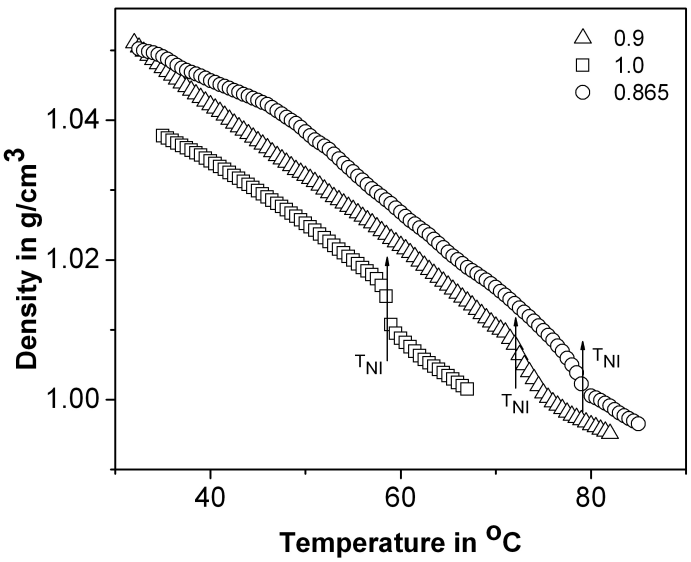

(d)

Figure 4.3: (cont'd):Variation of density values (ρ) as a function of temperature for (c) $x_{9.\,CN}$ = 0.662, 0.774, 0.827 and (d) $x_{9.\,CN}$ = 0.865, 0.9, 1.0.

For mixtures the mean molecular volume can be calculated from the expression

$$V' = x_A V_A + x_B V_B \tag{4.1}$$

where x_A, V_A, x_B, V_B are the mole fraction and the molecular volumes of the pure component. If M_A and M_B be the molecular weight of the pure components A and B, then the mean molecular weight can be written as

$$M' = x_A M_A + x_B M_B \tag{4.2}$$

For a given temperature if ρ be the density of a mixture and N_A the Avogadro's number then packing fraction

$$= \frac{\rho N_A V'}{M'} = \frac{\rho N_A (x_A V_A + x_B V_B)}{x_A M_A + x_B M_B} \tag{4.3}$$

Figure 4.5 shows the variation of packing fraction at three different temper-

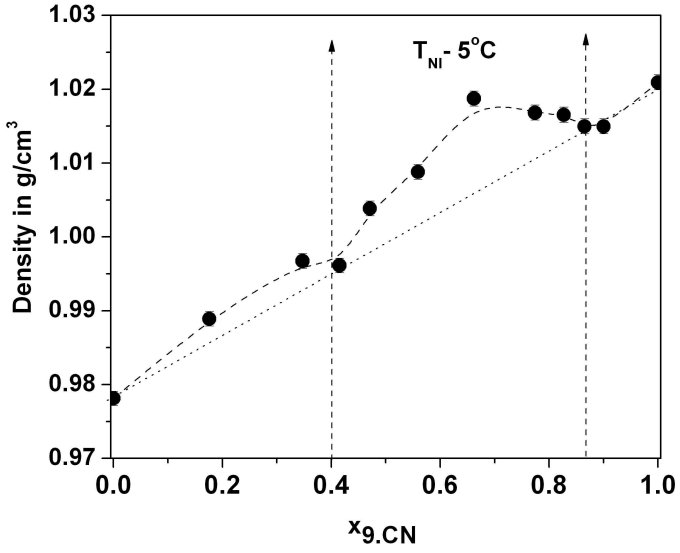

Figure 4.4: Density values plotted as a function of mole fraction of 9.CN at 5°C below the clearing temperature.

atures, T_{NI} - 5°C, T_{SN} -5°C and $T_{SN_{re}}$ - 2°C against mole fraction of 9.CN. From this figure it is clear that in the normal nematic, induced smectic A_d and re-entrant nematic phases the packing fraction values show a definite maxima

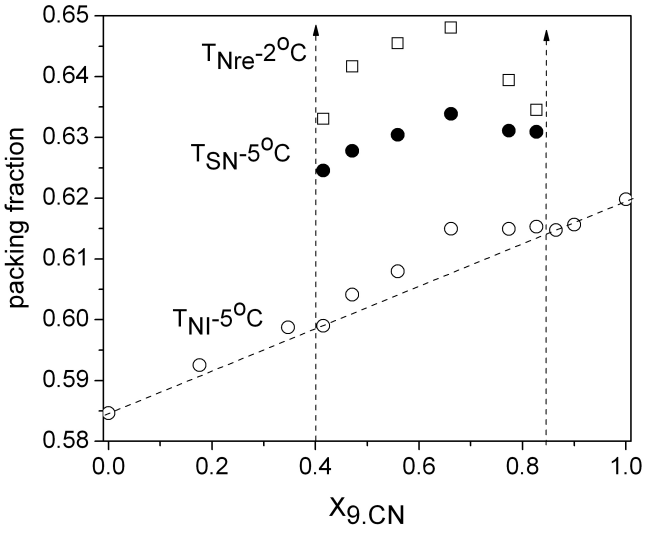

Figure 4.5: Packing fraction values plotted against mole fraction of 9.CN. ○ $5°C$ below clearing temperature, ● $5°C$ below nematic–smectic A_d phase transition temperature and □ $2°C$ below smectic A_d- re-entrant nematic phase transition temperature.

around $x_{9.\,CN}$ = 0.6. Similar maxima at around $x_{9.\,CN}$ = 0.6 is also seen in figure 4.4 where the density has been plotted against the mole fraction of 9.CN at temperature T = T_{NI}-5°C.

Using the refractive indices (n_o, n_e) and the density values the principal molecular polarizabilities (α_o, α_e) were calculated using Vuks method [43]. The orientational order parameter $\langle P_2 \rangle$ can then be calculated using the relation

$$\langle P_2 \rangle = \frac{\alpha_e - \alpha_o}{\alpha_\parallel - \alpha\perp} = \frac{\Delta\alpha}{\Delta\alpha_0} \tag{4.4}$$

where α_o and α_e are the effective polarizabilities for the extraordinary and ordinary rays respectively and $\alpha_\parallel$ and $\alpha_\perp$ are the polarizabilities parallel and perpendicular respectively to the long axis of the molecule in the solid state. The polarizability anisotropies in the perfectly ordered state ($\Delta\alpha_0$) were determined from the well known Haller's extrapolation method [48] using the following equation:

$$\Delta\alpha = \Delta\alpha_0 \left(1 - \frac{T}{T^*}\right)^\beta \tag{4.5}$$

where $\Delta\alpha_0$, T^* and β are adjustable parameters, T^* is about 1-3 K higher than the clearing temperature and exponent β depends on molecular structure and its value is close to 0.2. This procedure enables one to extrapolate $\Delta\alpha$ to absolute zero temperature ($\Delta\alpha_0$).

I was able to determine both the ordinary and extraordinary refractive indices in the solid phase of one pure compound (9.CN) and one mixture ($x_{9.\,CN}$ = 0.827). Hence, by measuring the density value in the solid phase using simple flotation technique, it was possible to measure $\Delta\alpha_0$, the polarizability anisotropies in the perfectly ordered state, and hence the orientational order parameter, $\langle P_2 \rangle$, without using any ambiguous extrapolation techniques. Thus it was possible to verify the applicability of the Haller's extrapolation method for purely nematic phase as well as for mixtures which have underlying higher ordered phases.

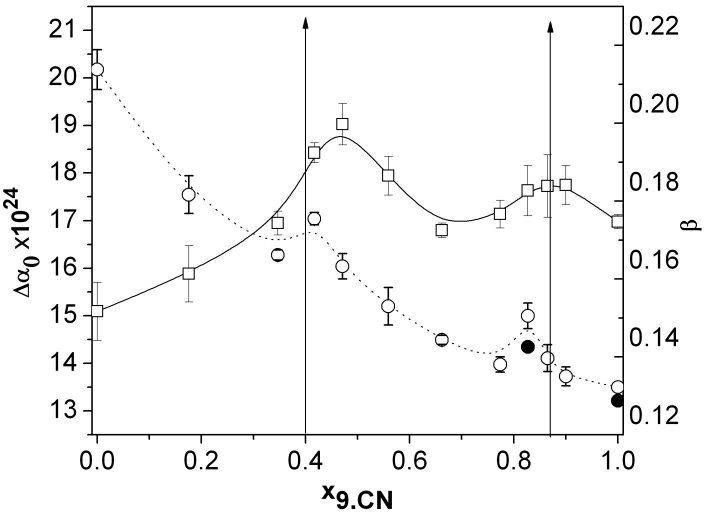

Figure 4.6: Extrapolated polarizability anisotropy ($\Delta\alpha_0$) at the absolute zero temperature (○) and exponent β (□) plotted as a function of mole fraction of 9.CN. ● polarizability anisotropy in the perfectly ordered state obtained from solid state data.

In figure 4.6, I have plotted the polarizability anisotropy $\Delta\alpha_0$=($\Delta\alpha_e - \Delta\alpha_o$) values extrapolated to absolute zero temperature $\Delta\alpha_0$ from Haller's extrapolation method and exponent β as a function of mole fraction of 9.CN. The experimentally determined $\Delta\alpha_0$ values for two samples are also plotted in this figure.

It is found that $\Delta\alpha_0$ values are greater in the lower concentration region of 9.CN and decreases gradually with the increase in mole fraction of 9.CN. However it shows two local maxima near $x_{9.\,CN}$ = 0.4 and $x_{9.\,CN}$ = 0.8. The variation of β also shows two maxima near $x_{9.\,CN}$ = 0.5 and $x_{9.\,CN}$ = 0.87. It has been found that the $\Delta\alpha_0$ values calculated from Haller's extrapolation method for 9.CN is about 2% higher compared to the experimentally determined solid state value, whereas for $x_{9.\,CN}$ = 0.827 this value is about 4% higher. This implies that the error in the measurement of $\Delta\alpha_0$ from Haller's extrapolation method is larger for mixtures having an underlying higher ordered phase; which is expected. This error is expected to be smaller in case of materials having multiple phases with a broad nematic range. As a consequence, the $\langle P_2 \rangle$ values calculated from Haller's extrapolation method are lower than those determined directly. The directly obtained values are found to be in better agreement with those calculated from X-ray diffraction measurements.

Table 4.1: Values of fitting parameters obtained from Haller's extrapolation.

$x_{9.\,CN}$	$\Delta\alpha_0 \times 10^{24}$	β	T^*
0	20.17 ± 0.42	0.15 ± 0.01	468.39 ± 0.38
0.176	17.54 ± 0.40	0.16 ±0.01	451.65 ± 0.75
0.347	16.28 ± 0.11	0.17 ± 0.003	427.20 ± 0.17
0.417	17.04 ± 0.13	0.19 ± 0.002	415.61± 0.85
0.471	16.04 ±0.27	0.20 ± 0.005	405.75 ± 0.63
0.559	14.81 ± 0.39	0.19 ± 0.01	393.59 ± 0.42
0.662	14.49 ± 0.09	0.17 ± 0.002	376.5 ± 0.95
0.774	13.98 ± 0.16	0.18 ± 0.004	361.5 ± 0.89
0.827	15.0 ±0.27	0.18 ± 0.006	355.50 ± 0.26
0.865	14.11 ± 0.28	0.18 ± 0.008	349.98 ± 0.45
0.9	13.73 ± 0.20	0.18 ± 0.005	346 ± 0.97
1	13.5 ± 0.25	0.17 ±0.002	332.81 ±0.28

The determination of orientational order parameter $\langle P_2 \rangle$ from refractive index data, using Haller's extrapolation technique is a common practice [54–63]. However, Haller's extrapolation procedure does not always agree with the weakly first order character of the nematic–isotropic phase transition. It is expected that the critical exponent β should indicate membership of one of the possible universality class of liquid crystal critical behavior [49, 51]. The critical exponent β of the order parameter $\langle P_2 \rangle$ obtained by Haller's extrapolation lies in between 0.14

and 0.2 [54–63], which does not match with any of the predicted theoretical values. Since the three parameter Haller's extrapolation leads to a systematically lower values of β (< 0.20), than those extracted from refractive index [49, 50], dielectric permittivity anisotropy [51, 52] and anisotropy in thermal conductivity data [53], a need to replace it by a four parameter power-law expression has been expressed recently [49]. This four parameter power-law expression is consistent with the mean-field theory for a critical as well as a tricritical point for a weakly first-order transition (nonzero cubic term) [51, 53, 65, 66] and can be written as [49, 67]:

$$P = A\left[B + (1-B)\left(1 - \frac{T}{T^{**}}\right)^{\beta}\right] \tag{4.6}$$

where P is the physical property under consideration and A, B, β and T^{**} are parameters to be determined from the experimental data. T^{**} denotes the temperature at which the N-I transition would occur coming from the nematic phase if it were second order and is slightly larger than the observed transition temperature T_{NI}. In equation 4.6, B = 0 leads to the Haller's extrapolation equation with $T^{**} = T^{*}$.

Table 4.2: Value of fitting parameters obtained from four parameter fit.

$x_{9.\,CN}$	A$\times 10^{24}$	B	T^{**}	β
0	21.42 ± 3.09	0.08 ± 0.68	468.40± 3.35	0.19± 0.24
0.176	17.07 ± 0.39	0.13 ± 0.06	452.34± 1.34	0.19± 0.03
0.347	17.87 ± 0.65	0.02± 0.09	428.08± 1.92	0.21± 0.04
0.417	18.21 ± 1.04	0.08 ± 0.17	416.06± 1.20	0.25± 0.09
0.471	17.81 ± 0.75	0.00 ± 0.18	409.83± 1.53	0.26± 0.08
0.559	16.02 ± 1.36	0.08 ± 0.28	394.53± 2.11	0.25± 0.14
0.662	14.83 ± 0.82	0.13 ± 0.18	376.22± 0.96	0.22± 0.08
0.774	13.96 ± 0.80	0.13 ± 0.07	362.07± 0.10	0.22± 0.05
0.827	15.00 ± 0.76	0.13 ± 0.03	355.54± 1.20	0.23± 0.03
0.865	13.44 ± 0.40	0.20 ± 0.05	348.30± 0.93	0.22± 0.03
0.9	13.40 ± 0.15	0.17 ± 0.02	344.60± 1.52	0.22± 0.01
1	12.89± 0.30	0.20± 0.02	332.03± 1.98	0.22±0.02

The values of the four parameters obtained by fitting the experimental data to equation 4.6 has been tabulated in table 4.2. The critical exponent β obtained from the four parameter fitting and Haller's extrapolation procedures has been plotted as a function of mole fraction of 9.CN in figure 4.7. It is clearly observed

that the β values obtained for the four parameter fit are higher as compared to the previous values. However, they show similar concentration variation.

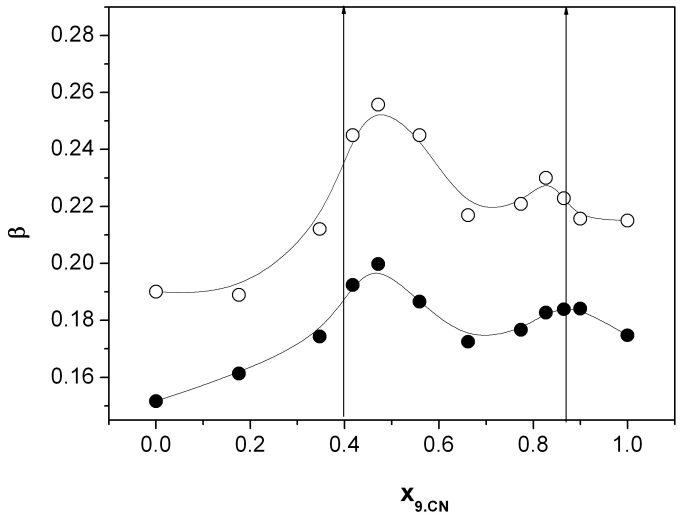

Figure 4.7: Critical exponent β plotted as a function of mole fraction of 9.CN. ● values obtained from Haller extrapolation procedure, ○ values obtained from four parameter fit.

The temperature variation of the orientational order parameter, as obtained from refractive index measurements by thin prism technique and from X-ray diffraction measurements (chapter 3), for all the mixtures and the pure compounds are shown in figures 4.8a-4.8l. It is observed that near the nematic – isotropic phase transition temperature, the order parameter values as determined from refractive index measurement decreases rapidly and is always less than the theoretically predicted values. This rapid decrease in the OOP values near the nematic isotropic transition temperature, as obtained from refractive index measurements, has been reported by others [68–70]. On the other hand, near the clearing temperature the $\langle P_2 \rangle$ values obtained from X-ray diffraction studies are higher than those obtained from refractive index measurements and are in better agreement with the theoretical values. This can be explained by the fact that in X-ray studies one is measuring the short range order which decreases slowly as the nematic–isotropic transition temperature is approached.

However, in refractive index measurements one is measuring long range order which decreases rapidly as the clearing temperature is approached.

The experimental $\langle P_2 \rangle$ values have been fitted with the theoretical value of Maier–Saupe for the nematogens and for those mixtures exhibiting induced smectic and re-entrant nematic phases, the modified McMillan's theory as proposed by Luckhurst and Timimi have been used [47] which has been discussed in detail in chapter 2 and chapter 3 of this thesis.

The agreement between the experimental $\langle P_2 \rangle$ values obtained from birefringence measurements with those calculated from McMillan's theory is poor for all the mixtures. However, the experimental orientational order parameter values determined from refractive index measurements agree quite well with the theoretical Luckhurst and Timimi values except near the nematic to isotropic transition temperature for all the mixtures. The $\langle P_2 \rangle$ values obtained from refractive index measurements, x ray diffraction measurements, McMillan's theory and from the modified McMillan's theory as proposed by Luckhurst and Timimi are shown in figures 4.8d-4.8j. Both the N - Sm A_d and Sm A_d - N_{re} phase transitions are found to be continuous from the modified McMillan's theory as proposed by Luckhurst and Timimi and this prediction is also supported from DSC measurement as mentioned earlier in chapter 3 [9]. Mixtures with $x_{9.\,CN}$ = 0.176, 0.347, 0.9 and the two pure compounds (figures 4.8b, 4.8c, 4.8k, 4.8a and 4.8l, respectively) have only a nematic phase; hence the experimental $\langle P_2 \rangle$ values have been compared with the theoretical Maier-Saupe values. In this case, agreement is not good even in the region far away of the nematic–isotropic transition temperature. The orientational order parameter values for all the cases are larger in comparison to the theoretical values. This may due to the formation of cybotactic clusters in the nematic phase. The existence of such cybotactic clusters has been confirmed from the X-ray diffraction patterns as mentioned in chapter 3.

It is to be noted that the order parameter values calculated from experimental solid state polarizability anisotropy data for mixture $x_{9.\,CN}$ = 0.827 agree quite well with the X-ray data. Again, the difference between the two sets of data, one from the Haller's extrapolation method and other from the actual solid state data is around 4.5%. However, for the pure compound 9.CN this difference is found to be only about 2%. The possible reason for the obvious large

difference in case of mixture $x_{9.\,CN}$ = 0.827 is due to the fact that the mixture shows multiple phases and fitting was done only for the upper nematic phase. For mixtures with $x_{9.\,CN}$ = 0.662 and 0.774, the $\langle P_2 \rangle$ values decreases in the Sm A_d phase but near the Sm A_d–/Nre transition it starts increasing again. On the other hand, for mixtures with $x_{9.\,CN}$ = 0.827 although the $\langle P_2 \rangle$ values increases slightly with decrease in temperature within the Sm A_d phase, but near the smectic A_d –re-entrant nematic transition a sharp increase in $\langle P_2 \rangle$ is found with decrease in temperature and with further decrease in temperature it remains almost constant. For all the mixtures showing induced smectic and re-entrant nematic phases the change in $\langle P_2 \rangle$ at the nematic - smectic A_d and the smectic A_d – re-entrant nematic phase boundary is continuous.

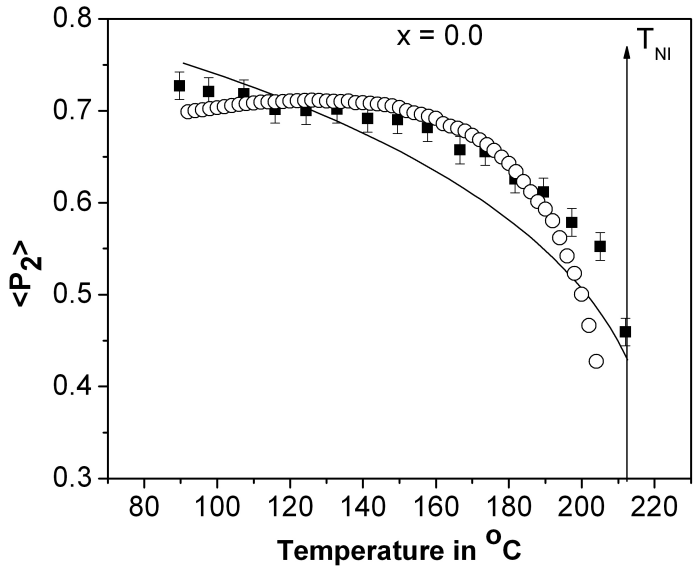

(a) Temperature variation of $\langle P_2 \rangle$ for 7CPB

Figure 4.8: Temperature variation of $\langle P_2 \rangle$ for 7CPB, ○ refractive index data, ■ X-ray data, — from Maier-Saupe theory.

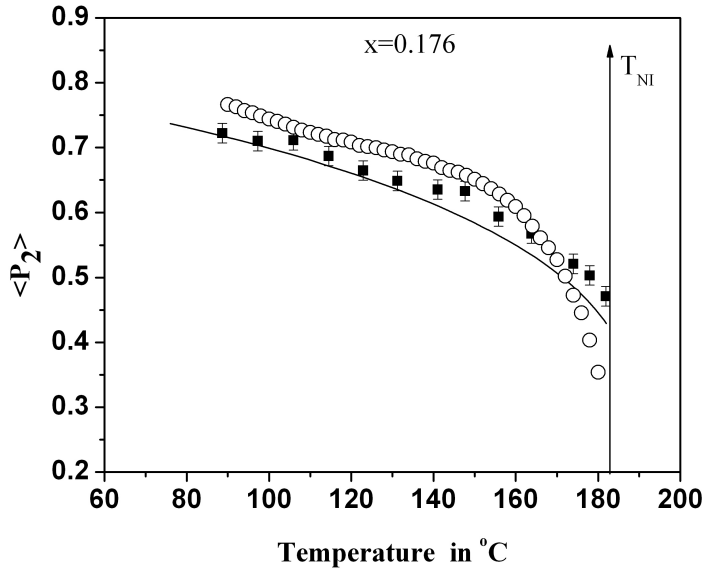

(b) Temperature variation of $\langle P_2 \rangle$ for $x_{9.\,CN}$ = 0.176

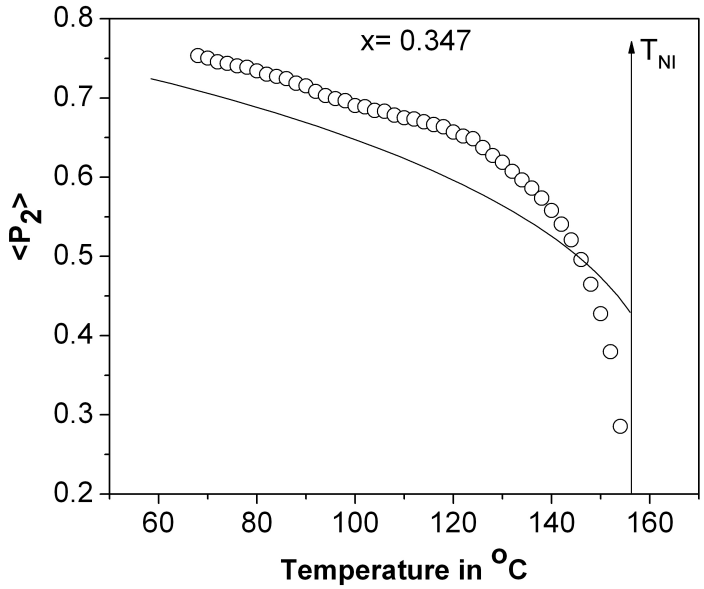

(c) Temperature variation of $\langle P_2 \rangle$ for $x_{9.\,CN}$ = 0.347

Figure 4.8: (cont'd): Temperature variation of $\langle P_2 \rangle$ for $x_{9.\,CN}$ = 0.176 and $x_{9.\,CN}$ = 0.347, ○ refractive index data, ■ X-ray data, — from Maier-Saupe theory.

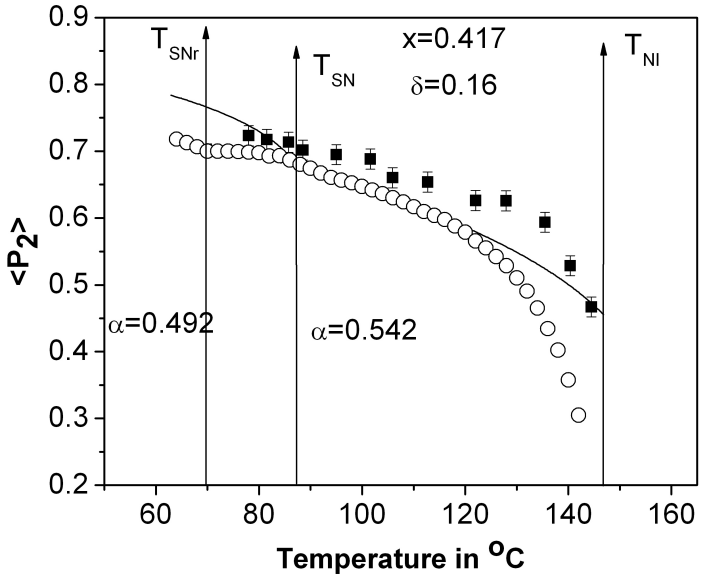

(d) Temperature variation of $\langle P_2 \rangle$ for $x_{9.\,CN} = 0.417$

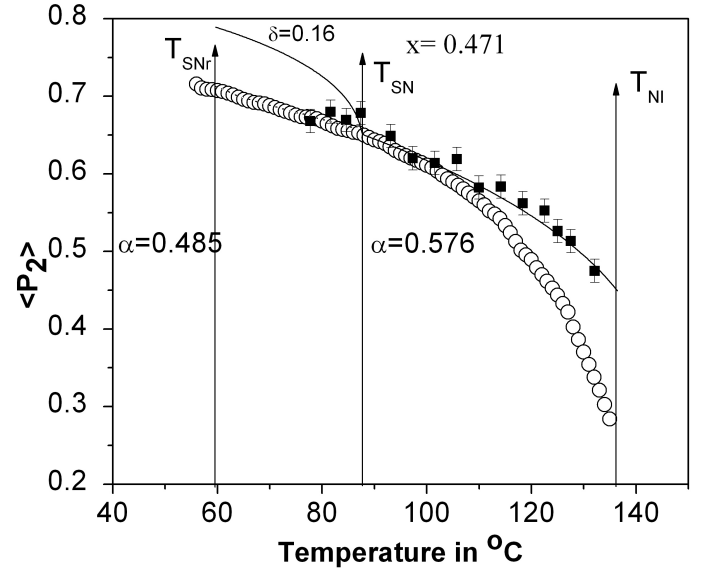

(e) Temperature variation of $\langle P_2 \rangle$ for $x_{9.\,CN} = 0.471$

Figure 4.8: (cont'd): Temperature variation of $\langle P_2 \rangle$ for $x_{9.\,CN} = 0.417$ and $x_{9.\,CN} = 0.471$, ○ refractive index data, ■ X-ray data; — $\langle P_2 \rangle$ from McMillan's theory. $\cdots$ $\langle P_2 \rangle$, from modified McMillan's theory by Luckhurst and Timimi.

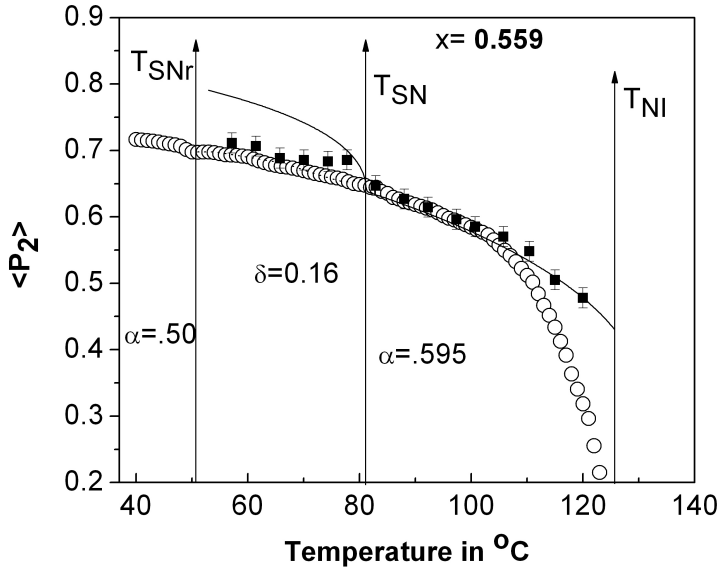

(f) Temperature variation of $\langle P_2 \rangle$ for $x_{9.\,CN} = 0.559$

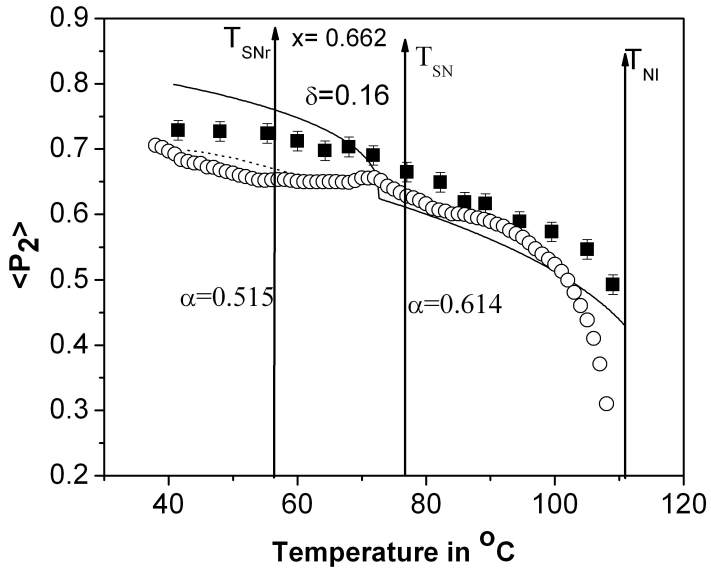

(g) Temperature variation of $\langle P_2 \rangle$ for $x_{9.\,CN} = 0.662$

Figure 4.8: (cont'd): Temperature variation of $\langle P_2 \rangle$ for $x_{9.\,CN} = 0.559$ and $x_{9.\,CN} = 0.662$, ○ refractive index data, ■ X-ray data; — $\langle P_2 \rangle$ from McMillan's theory. $\cdots$ $\langle P_2 \rangle$, from modified McMillan's theory by Luckhurst and Timimi.

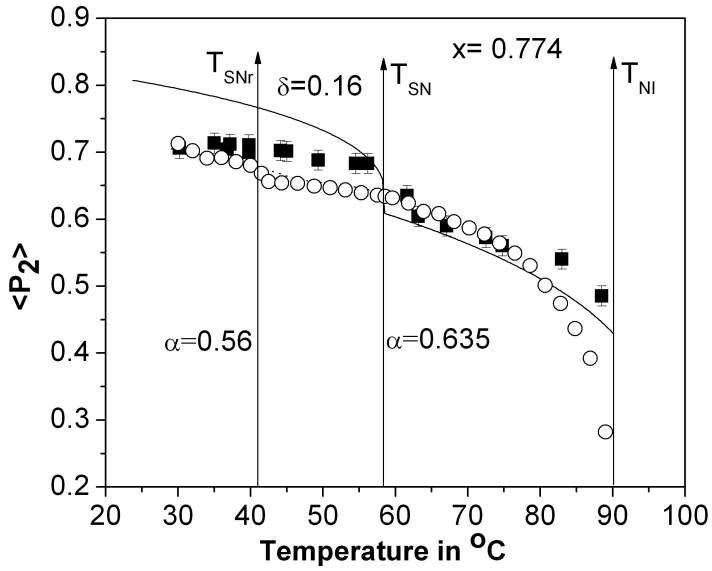

(h) Temperature variation of $\langle P_2 \rangle$ for $x_{9.\,CN} = 0.774$

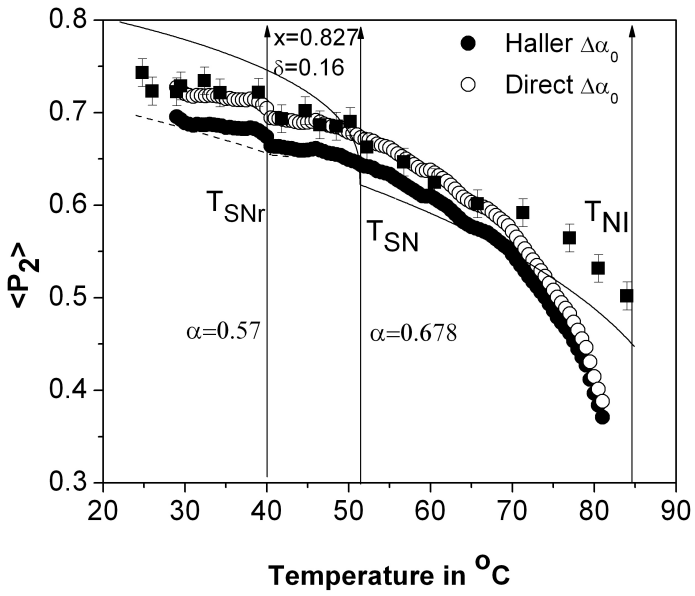

(i) Temperature variation of $\langle P_2 \rangle$ for $x_{9.\,CN} = 0.827$

Figure 4.8: (cont'd): Temperature variation of $\langle P_2 \rangle$ for $x_{9.\,CN} = 0.774$ and $x_{9.\,CN} = 0.827$, ○ refractive index data, ■ X-ray data; — $\langle P_2 \rangle$ from McMillan's theory. ⋯ $\langle P_2 \rangle$, from modified McMillan's theory by Luckhurst and Timimi.

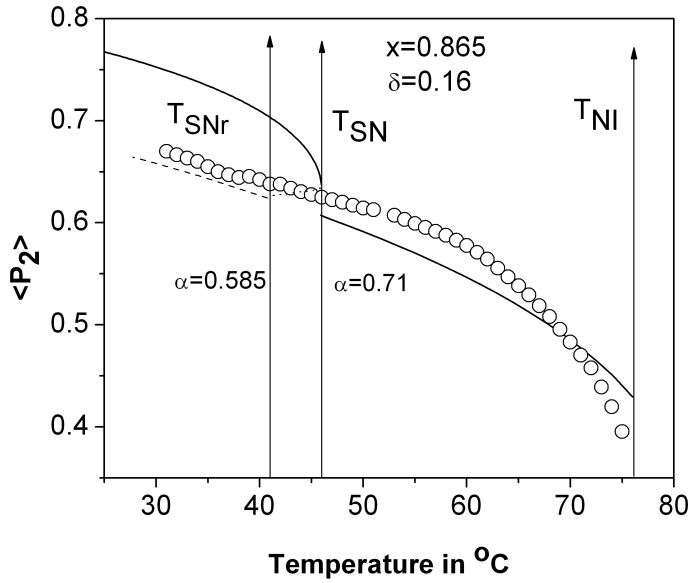

(j) Temperature variation of $\langle P_2 \rangle$ for $x_{9.\,CN}$ = 0.865

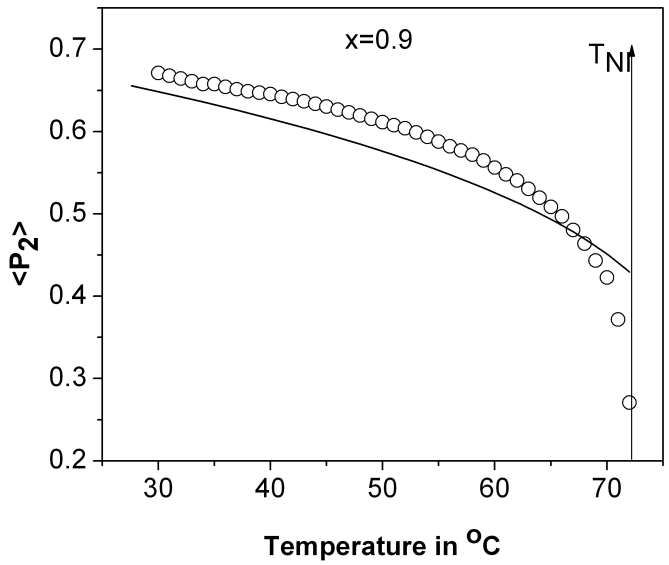

(k) Temperature variation of $\langle P_2 \rangle$ for $x_{9.\,CN}$ = 0.9

Figure 4.8: (cont'd): Temperature variation of $\langle P_2 \rangle$ for $x_{9.\,CN}$ = 0.865 and $x_{9.\,CN}$ = 0.9, ○ refractive index data, ■ X-ray data; (j) — $\langle P_2 \rangle$ from McMillan's theory. $\cdots$ $\langle P_2 \rangle$, from modified McMillan's theory by Luckhurst and Timimi, (k) — from Maier-Saupe theory.

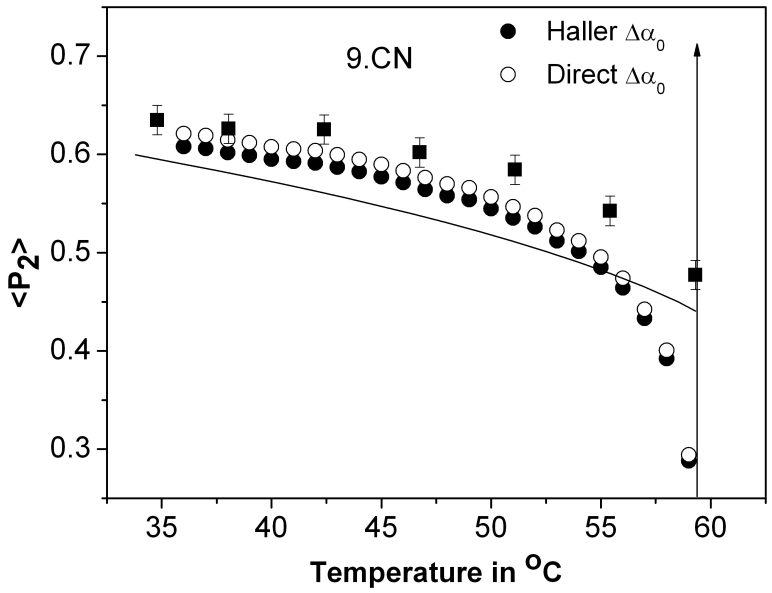

(l) Temperature variation of $\langle P_2 \rangle$ for 9.CN

Figure 4.8: (cont'd): Temperature variation of $\langle P_2 \rangle$ for 9.CN, ○ refractive index data, ■ X-ray data, — from Maier-Saupe theory.

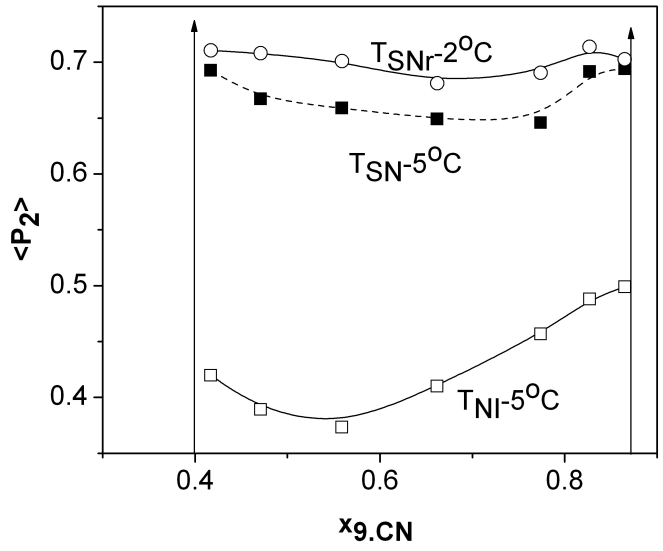

Figure 4.9: $\langle P_2 \rangle$ values plotted against mole fraction of 9.CN for □ $5°C$ below clearing temperature; ■ $5°C$ below nematic– smectic A_d transition temperature and ○ $2°C$ below smectic A_d- re-entrant nematic transition temperature.

Figure 4.9 shows the variation of $\langle P_2 \rangle$ values with mole fraction of 9.CN at three different temperatures, T_{NI} - 5°C, T_{SN} - 5°C and $T_{SN_{re}}$ - 2°C corresponding to the normal nematic, induced smectic and re-entrant nematic phases. It is observed that the OOP's in the nematic phase show a definite minimum at around $x_{9.\,CN}$ = 0.5, which corroborates the findings of the X-ray diffraction measurements done on this system which has been discussed in chapter 3 [9]. On the other hand, within the induced smectic phase the orientational order parameter values show a very broad minimum near $x_{9.\,CN}$ = 0.6. The minima in the order parameter values corresponds to that region of the phase diagram where the induced smectic A_d phase is highly stabilised. This minimum in the order parameter values is attributed to specific interactions between the molecules, which in trying to pack the different molecules within the layers of the smectic A_d phase, in effect, reduces the orientational free volume within the layers. This observation is very similar to polar–non-polar systems showing induced smectic A_d phase [51, 54, 64]. From the orientational order parameter point of view, the re-entrant nematic phase behave very similar to the induced smectic phase and shows a similar minima around the same concentration $x_{9.\,CN}$ = 0.6.

4.4 Conclusion

Refractive index and density measurements have been performed on a binary system of nematogenic compounds exhibiting induced smectic A_d and re-entrant nematic phases. The change in both the refractive indices and hence birefringence (Δn=n_e-n_o) is continuous at the nematic – smectic A_d and smectic A_d – re-entrant nematic phase transition. The density measurements also show a continuous change across the nematic – smectic A_d and the smectic A_d – re-entrant nematic phase transition. However, the variation of packing fraction with the mole fraction of 9.CN shows a definite maxima around $x_{9.\,CN}$ = 0.6 in the normal nematic, induced smectic A_d and the re-entrant nematic phases.

The Haller's extrapolation procedure was employed to obtain the value of polarizability anisotropy in the perfectly ordered stated ($\Delta\alpha_0$). On knowing the value of ($\Delta\alpha_0$) the orientational order parameter could be determined from the values of the polarizability anisotropy ($\Delta\alpha$). The orientational order parameter values ($\langle P_2 \rangle$) have been compared with those obtained from X-ray diffraction

measurements and the agreement is good except near the clearing temperature. The experimentally determined values of $\langle P_2 \rangle$ have been compared with the theoretical values of Maier–Saupe for the nematogens and McMillan's theory and its modification by Luckhurst and Timimi for mixtures having induced smectic and re-entrant nematic phases. The agreement between the experimental $\langle P_2 \rangle$ values from the refractive index measurement with those calculated from McMillan's theory have been found to be poor in the smectic A_d phase. Taking into account a slight temperature dependence of the α parameter in McMillan's theory, this discrepancy has been removed by recalculating the orientational order parameter values according to a modified McMillan's theory as proposed by Luckhurst and Timimi. Both the Sm A_d–N_{re} and N–Sm A_d phase transitions are predicted to be second order by this model and are also found to be in agreement with the temperature dependence of the refractive index, density and orientational order parameter values as well as from DSC measurements.

The measurement of density and refractive indices in the solid phase enabled me to verify the validity of Haller's extrapolation technique for those mixtures where a higher ordered phase is present below the nematic phase. The value of the critical exponent β obtained for all the mixtures and the two pure compounds from Haller's extrapolation is less than 0.2. The temperature dependence of polarisibility anisotropy has also been fitted by a four parameter fitting procedure which yields an average value of $\langle \beta \rangle$ as 0.223 ± 0.07 which is close to the tricritical hypothesis predicting $\beta = 0.25$. The values of β as obtained from the four parameter fit are higher as compared to those obtained from Haller's procedure. However, the β values obtained from both the fitting procedures show a similar concentration variation.

References

[1] M. Brodzik, R. Dabrowski, *Mol. Cryst. Liq. Cryst. (Lett.)*, **260**, 361 (1995).

[2] M. Brodzik, R. Dabrowski, *SPIE*, **2372**, 280 (1995).

[3] M. Tykarska, B. Wazynska, I. Ulbin, *Proceeding of SPIE*, **4147**, 55 (2000).

[4] M. Brodzik, *Ph. D. Thesis*, Wojskowa Akademia Techniczna (1995).

[5] M. Brodzik, R. Dabrowski, I. Ulbin, *Liquid Crystals*, **20**, 99 (1996).

[6] M. Brodzik, R. Dabrowski, J. Przedmojski, *J. Phys. II France*, **5**, 1805 (1995).

[7] S. Wrobel, M. Brodzik, R. Dabrowski, B. Gestblom, W. Haase, S. Hiller, *Mol. Cryst. Liq. Cryst.*, **302**, 223 (1997).

[8] S. K. Giri, N. K. Pradhan, R. Paul, S. Paul, P. Mandal, R. Dabrowski, M. Brodzik, K. Czuprynski, *Proceeding of SPIE*, **3319**, 149 (1998).

[9] A. Prasad, M. K. Das, *Phase Transitions*, **82**, 780 (2009).

[10] S. Singh, *Phase Transitions*, **72**, 183 (2000).

[11] M. K. Das, R. Paul, *Mol. Cryst. Liq. Cryst.*, **239**, 107 (1994).

[12] N. S. Chen, S. K. Hark, J. T. Ho, *Phys. Rev. A*, **24**, 2843 (1981).

[13] D. Guillon, P. E. Cladis, J. Stamatoff, *Phys. Rev. Lett.*, **41**, 1598 (1978).

[14] F. R. Bouchet, P. E. Cladis, *Mol. Cryst. Liq. Cryst. (Lett.)*, **64**, 97 (1980).

[15] K. J. Lushington, G. B. Kasting, C. W. Garland, *Phys. Rev. B*, **22**, 2569 (1980).

[16] R. Y. Dong, *Mol. Cryst. Liq. Cryst. (Lett.)*, **64**, 205 (1981).

[17] R. Y. Dong, *J. Chem. Phys.*, **75**, 2621 (1981).

[18] R. Shashidhar. H. D. Kleinhans, G. M. Schneider, *Mol. Cryst. Liq. Cryst. (Lett.)*, **72**, 119 (1981).

[19] P. E. Cladis, *Phys. Rev. A*, **23**, 2594 (1981).

[20] A. R. Kortan, H. V. Kanel, R. J. Birgeneau, J. D. Lister, *Phys. Rev. Lett.*, **47**, 1206 (1981).

[21] A. R. Kortan, H. von Kanel, R. J. Birgeneau, J. D. Lister, *J. Phys. (Paris)*, **45**, 529 (1984).

[22] A. Nayeem, J. H. Freed, *J. Phys. Chem.*, **93**, 6539 (1989).

[23] N. Hafiz, N. A. P. Vaz, Z. Yaniv, D. Affender, J. W. Doane, *Phys. Lett. A*, **91**, 41 (1982).

[24] J. W. Emsley, G. R. Luckhurst, P. J. Parson, B. A. Timimi, *Mol. Phys.*, **56**, 767 (1985).

[25] P. E. Cladis, D. Guillon, F. R. Bouchet, P. L. Finn, *Phys. Rev. A*, **23** (5), 2594 (1981).

[26] D. D. Klug, E. Whalley, *J. Chem. Phys.*, **71**, 1874 (1979).

[27] J. M. Sorenson, G. R. Van Hecke, *J. Phys. Chem.*, **98**, 10289 (1994).

[28] K. J. Lushington, G. B. Kasting, C. W. Garland, *Phys. Rev. B*, **22** (5), 2569 (1980).

[29] X. Shen, R. Y. Dong, *J. Chem. Phys.*, **108**, 9177 (1998).

[30] J. Bharatam, C. R. Bowers, *J. Phys. Chem. B*, **103**, 2510 (1999).

[31] R. Y. Dong, M. Cheng, *J. Chem. Phys.*, **113**, 3466 (2000).

[32] R. Nozaki, T. K. Bose, S. Yagihara, *Phys. Rev. A*, **46**, 7733 (1992).

[33] S. Urban, R. Dabrowski, B. Gestblom, A. Kocot, *Liq. Cryst.*, **27** (12), 1675 (2000).

[34] J. Jadzyn, G. Czechowski, *Phys. Rev. E*, **64**, 052702 (2001).

[35] A. Zywocinski, *J. Phys. Chem. B*, **103**, 3087 (1999).

[36] P. E. Cladis, *Mol. Cryst. Liq. Cryst.*, **165**, 85 (1988).

[37] R. Shashidhar, S. Somasekhar, B. R. Ratna, *Mol. Cryst. Liq. Cryst.*, **133**, 19 (1986).

[38] G. Czechowski, J. Jadzyn, *Acta Physica Polonica A*, **106**, 475 (2004).

[39] J. Jadzyn, G. Czechowski, *Liq. Cryst.*, **4**, 157 (1989).

[40] D. Rodez, D. Collin, P. Martinoty, *Eur. Phys. J. E*, **14**, 43 (2004).

[41] B. R. Ratna, R. Shashidhar, M. Bock, A. Gobl-Wunsch, G. Heppke, *Mol. Cryst. Liq. Cryst.*, **99**, 285 (1983).

[42] S. Urban, R. Dabrowski, B. Gestblom, A. Kocot, *Liq. Cryst.*, **27**, 1675 (2000).

[43] M. F. Vuks, *Opt. Spectros.*, **20**, 361 (1966).

[44] W. Maier and A. Saupe, *Z. Naturforsch Tail II*, **15a**, 287 (1960).

[45] W. L. McMillan, *Phys. Rev. A*, **4**, 1236 (1971).

[46] W. L. McMillan, *Phys. Rev. A*, **6**, 93 (1972).

[47] G. R. Luckhurst, B. A. Timimi, *Mol. Cryst. Liq. Cryst.*, **64**, 253 (1981).

[48] I. Haller, *Prog. Solid State Chem.*, **10**, 103 (1975).

[49] I. Chirtoc, M. Chirtoc, C. Glorieux, J. Thoen, *Liq. Cryst.*, **31**, 229 (2004).

[50] S. Yildiz, H. Ozbek, C. Glorieux, J. Thoen, *Liq. Cryst.*, **34**, 611 (2007).

[51] J. Thoen, T. Bose, *Handbook of Low and High Dielectric Constant Materials and Their Applications, edited by H. S. Nalwa*, **Vol. 1**, Academic, London, (1999).

[52] J. Thoen, G. Menu, *Mol. Cryst. Liq. Cryst.*, **97**, 163 (1983).

[53] M. Marinelli, F. Mercuri, *Phys. Rev. E*, **61**, 1616 (2000).

[54] M. S. Zakerhamidi, Z. Ebrahimi, H. Tajalli, A. Ghanadzadeh, M. Moghadam, A. Ranjkesh, *J. Mol. Liq.*, **157**, 119 (2010).

[55] A. Prasad, M. K. Das, *Phase Transitions*, **83**, 1072 (2010).

[56] J. Li, S. Gauza, S. T. Wu, *J. Appl. Phys.*, **96**, 19 (2004).

[57] P. Sathyanarayana, M. C. Varia, A. K. Prajapati, B. Kundu, V. S. S. Sastry, and S. Dhara, *Phys. Rev. E*, **82**, 050701 (2010).

[58] S. S. Sastry, T. V. Kumari, S. S. Begum, V. V. Rao, *Liq. Cryst.*, **38**, 277 (2011).

[59] S. S. Sastry, T. V. Kumari, K. Mallika, B. G. S. Rao, S. T. Ha, S. Lakshminarayana, *Liq. Cryst.*, **39**, 295 (2012).

[60] J. L. Kumari, P. V. D. Prasad, D. M. Latha, V. G. K. M. Pisipati, *Phase transitions*, **85**, 52 (2012).

[61] M. Ramakrishna, N. Rao, P. V. D. Prasad and V. G. K. M. Pisipati , *Mol. Cryst. Liq. Cryst.*, **528**, 49 (2010).

[62] V. G. K. M. Pisipati, P. V. D. Prasad, *Mol. Cryst. Liq. Cryst.*, **506**, 13 (2009).

[63] P. V. D. Prasad, V. G. K. M. Pisipati, *Mol. Cryst. Liq. Cryst.*, **511**, 102 (2009).

[64] A. I. Kitaigorodski, *Molecular Crystals and molecules*, Academic Press, New York and London, Chapter 1, (1973).

[65] M. A. Anisimov, P. E. Cladis, E. E. Gorodetskii, D. A. Huse, V. E. Podneks,V. G. Taratuta, W. van Saarloos, and V. P. Voronov, *Phys. Rev. A*, **41**, 6749 (1990).

[66] S. Singh, *Phys. Rep.*, **324**, 107 (2000).

[67] M. Simoes, D. S. Simeao, *Phys. Rev. E*, **74**, 051701 (2006).

[68] P. D. Roy, A. Prasad, M. K. Das, *J. Phys.: Condens. Matter*, **21**, 075106 (2009).

[69] M. Mitra, R. Paul, *Mol. Cryst. Liq. Cryst.*, **148**, 185 (1987).

[70] P. D. Roy, B. Das, M. K. Das, *J. Phys.: Condens. Matter*, **21**, 335108 (2009).

Chapter 5

Optical birefringence studies of a binary mixture (7CPB+9.CN) with nematic – smectic A_d– re-entrant nematic phase sequence

5.1 Introduction

In the previous chapter (chapter 4) I have reported the results of refractive indices measurements, where the refractive indices were measured using thin prism technique. The orientational order parameter was determined from the refractive indices and the density values using the Vuks method [1]. However, in this technique bulk sample is taken for the measurements and hence proper alignment of the sample, particularly smectic A or higher order smectic phases using thin prism technique may not always be possible to achieve. Moreover, even for the nematic samples the alignment is not good near the clearing temperature. On the other hand, if the sample is taken in a liquid crystal measuring cell of sufficiently low thickness then not only an uniform alignment of the sample is achieved up to the clearing point, but also at the same time the system is kept in conditions similar to what it will experience when used for display applications. Moreover, in this technique high resolution (in both temperature and birefringence) measurements can be obtained which is not possible in the thin prism technique.

Although the method of determination of order parameter ($\langle P_2 \rangle$) without consideration of the local field experienced by the liquid crystalline molecules has been used by many workers [2–14], the results differ slightly from that obtained if the local field is considered. However, this method is very useful when the density values or the individual values of the refractive indices (n_o, n_e) are not available. An optical transmission method for the determination of high resolution birefringence Δn values have been designed by me (chapter 2), which gives very useful information particularly near the phase transitions.

Thus the birefringence of the mixtures and the pure compounds were also measured using optical transmission technique, the results of which will be discussed in this chapter. The orientational order parameter $\langle P_2 \rangle$ has been calculated directly from the birefringence values using the Haller's extrapolation technique [15]. The $\langle P_2 \rangle$ values so obtained have been compared with those measured from X-ray diffraction studies (chapter 3) and the refractive indices measurements using the thin prism technique (chapter 4). These values have also been compared with the theoretical values of Maier–Saupe [16] for the nematogens and a modification of McMillan's theory [17, 18] as proposed by Luckhurst and Timimi [19] for those mixtures having induced smectic and re-entrant nematic phases.

An attempt has also been made to assess the nature of the nematic -smectic A_d and smectic A_d–re-entrant nematic phase transitions by fitting the temperature derivative of the high resolution birefringence values to a suitable expression to obtain the value of the critical exponent α' which has been shown to be similar to the specific heat critical exponent [20]

5.2 Birefringence measurements from optical transmission (OT) method

The birefringence (Δn) has been measured from the transmitted intensity of light from a cell of thickness of 8.9 μm. The experimental details and the theoretical background have been discussed in details in the second chapter of this thesis. In order to obtain an estimate of the precession of the experimental set-up, the birefringence of one pure sample (9.CN) has been compared with the values of birefringence obtained from refractive indices measurement by using

thin prism technique [21–25]. The values of Δn determined from transmission method are found to be about 4 % higher than those measured by thin prism method. Such higher value of Δn in the transmission method of thin samples has also been reported by others [26].

Figure 5.1 shows the comparison between the experimentally determined values of the birefringence, (Δn=n_e–n_o) from refractive index measurements of one of the pure components (9.CN) by optical transmission as well as thin prism technique. Also shown in the same figure is the temperature dependence of the orientational order parameter $\langle P_2 \rangle$. The values of Δn and $\langle P_2 \rangle$ in the transmission method are found to be about 4% and 1% higher respectively than those measured by thin prism method. Both the optical birefringence Δn and the orientational order parameter values $\langle P_2 \rangle$ as determined from the thin prism method are observed to decrease rapidly near the nematic-isotropic phase transition. However, Δn and $\langle P_2 \rangle$ values determined from the optical transmission method are relatively higher near the nematic-isotropic transition temperature.

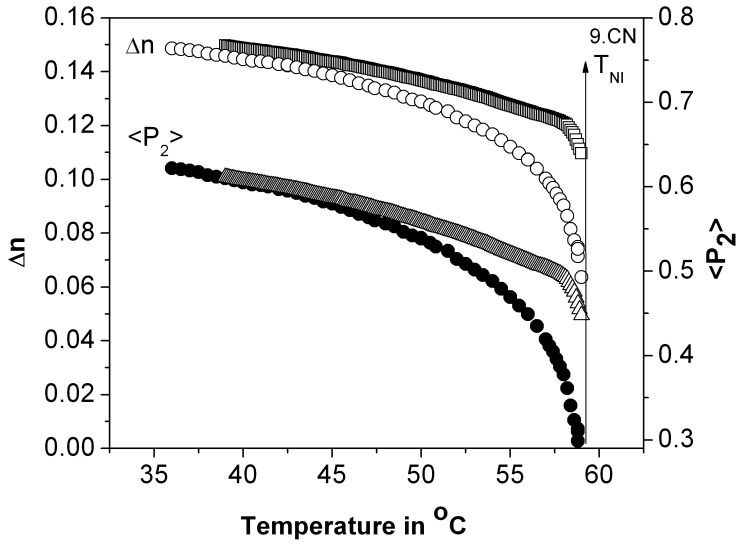

Figure 5.1: Temperature dependence of Δn and $\langle P_2 \rangle$ for pure sample 9.CN. □ data for Δn measured from optical transmission method; ○ data for Δn measured from thin prism method; △ data for $\langle P_2 \rangle$ measured from optical transmission method; ● data for $\langle P_2 \rangle$ measured from thin prism method.

The possible reason for the obvious discrepancy in the two sets of measurements near the transition is due to the fact that in thin prisms the sample thickness is very much higher (20-40 times) than in a 8.9 μm cell which is used in the transmission method. Therefore, the surface anchoring (which is much better in case of thin cells) retains the mono domain alignment right up to the nematic-isotropic transition in comparison to the bulk samples in thin prisms. It is to be noted here that the optical transmission method is an excellent system for identification of phase transition temperatures. Again, this method can also be used to identify the presence of tilted phases in the liquid crystalline system by studying the transmitted intensity for both the planar and homeotropic aligned cell [27, 28]. Figure 5.2 shows the temperature dependence of the optical intensity for the pure sample 9.CN. The DSC data for the same sample is also included for comparison. It is clearly seen that the melting and N-I transition temperatures are distinguishable from the optical transmission method.

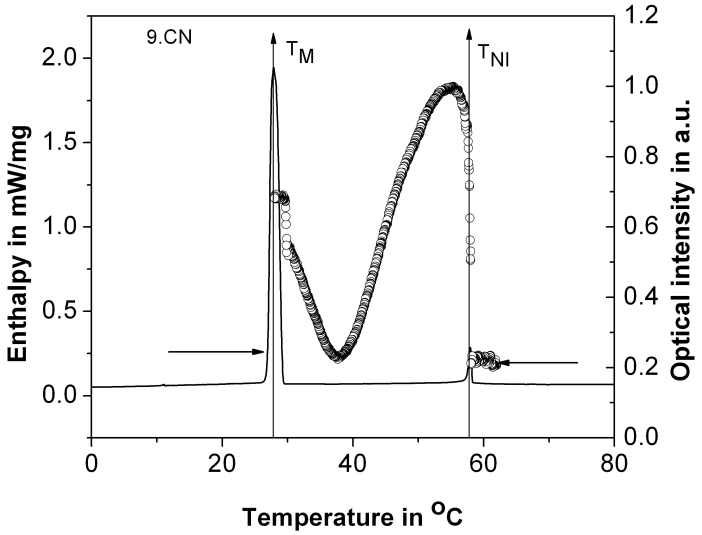

Figure 5.2: DSC thermogram (—) and transmitted intensity (○) as a function of temperature during heating of 9.CN. (DSC scan rate $2°C\ \mathrm{min}^{-1}$).

The temperature variation of the optical birefringence values for different mixtures as a function of temperature is shown in figure 5.3. The birefringence values of 7CPB are higher than those obtained from 9.CN. This is expected because 9.CN contains two phenyl rings in the rigid core whereas 7CPB molecule

contains three benzene rings in its core. As expected, the addition of one aromatic benzene ring leads to an increase in the anisotropy of 7CPB. In mixtures, the Δn values are found to decrease with increase in mole fraction of 9.CN. There is no discontinuity in the Δn values at the N_{re} – Sm A_d as well as Sm A_d – N phase transition. These observations indicate that re-entrant nematic to induced smectic A_d and induced smectic A_d to nematic phase transition for all the mixtures are of second order. High resolution DSC measurements have also been done. Since the order of transition is second order no peak was detected at the Sm A_d–N and Sm A_d–N_{re} transition [29].

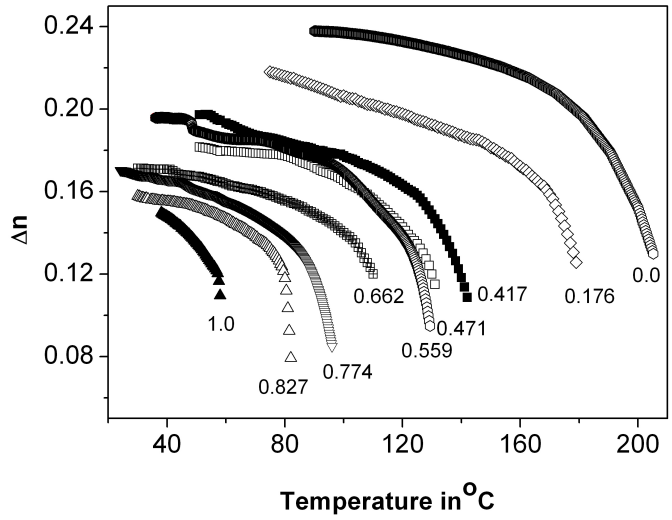

Figure 5.3: Birefringence ($\Delta n = n_e$–n_o) as a function of temperature for different mixtures and pure compounds. Mole fractions of different mixtures are indicated in the figure.

In this work, a simple procedure has been adopted for the determination of order parameters from birefringence measurement. In case of an uniaxial liquid crystalline phase, the temperature dependence of the birefringence is fitted to the following form:

$$\Delta n = \Delta n_0 \left(1 - \frac{T}{T^*}\right)^{\beta} \tag{5.1}$$

Where Δn_0, T^* and β are adjustable parameters. T^* is about 1-3 K higher than the clearing temperature and the exponent β depends on molecular structure

and its value is close to 0.2. This procedure enables one to extrapolate Δn to the absolute zero temperature (Δn_0) [15].

The temperature dependent birefringence is related to the order parameter as:

$$\langle P_2 \rangle = \frac{\Delta n}{\Delta n_0} \tag{5.2}$$

where Δn_0 is the birefringence in the completely ordered state, which was obtained from Haller's approximation for the order parameter (equation 5.1).

It is to be noted that the typical procedure for the evaluation of the long range order parameter from optical method require the measurement of both the ordinary and extraordinary refractive indices as well as the density data. In such cases, using these three measured quantities, either the standard Vuk's isotropic model [1] or the Neugebauer's relations based on the anisotropy of the internal field [30] are adopted to determine the principal polarizabilities parallel and perpendicular to the molecular long axes and hence, the anisotropy of the molecular polarizabilities ($\Delta\alpha$) can be calculated. The normalized polarizability ($\Delta\alpha_0$) for perfectly ordered crystal is determined from the well-known Haller's extrapolation procedure and the order parameter is calculated from the ratio $\frac{\Delta\alpha}{\Delta\alpha_0}$. According to de Jue [31], the variation of density (ρ) over the nematic range is usually small and the temperature dependence of Δn gives a good indication of the variation of order parameter with temperature. Kuczynski *et. al.* [32] have also shown that the order parameter determined directly from birefringence measurements are consistent with the $\langle P_2 \rangle$ values calculated from the polarizability data.

Since most of the mixtures studied in this system have two nematic phases, and one smectic phase, the temperature variation of Δn is different for different phases; therefore I have fitted equation 5.1 by taking the values of Δn only in the higher temperature nematic phase [33–36].

The experimental order parameter values calculated from equation 5.2 is shown in figure 5.4. It is observed that for all the mixtures, the temperature dependence of the order parameter in N_{re} and N phases is quite pronounced in comparison to those in the smectic A_d phase. These values are found to vary continuously across the N–Sm A_d and Sm A_d–N_{re} phase transition indicating second order phase transition

The order parameter values for both the pure compounds (figure 5.4a - 5.4b)

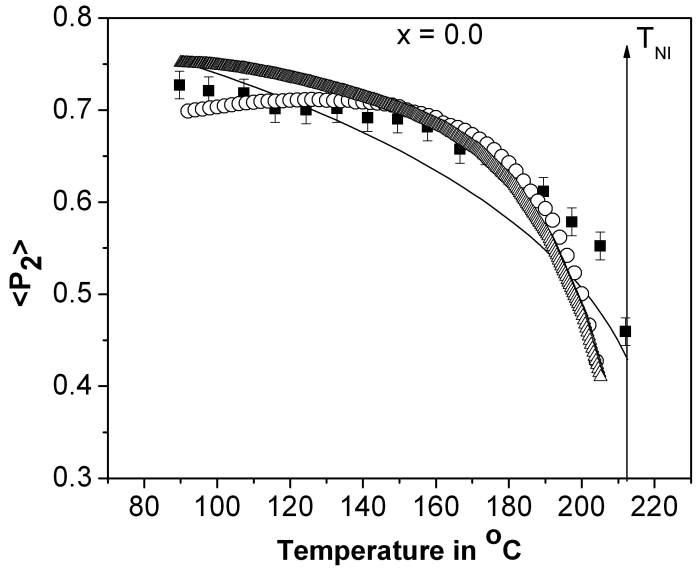

(a) Temperature variation of $\langle P_2 \rangle$ for 7CPB

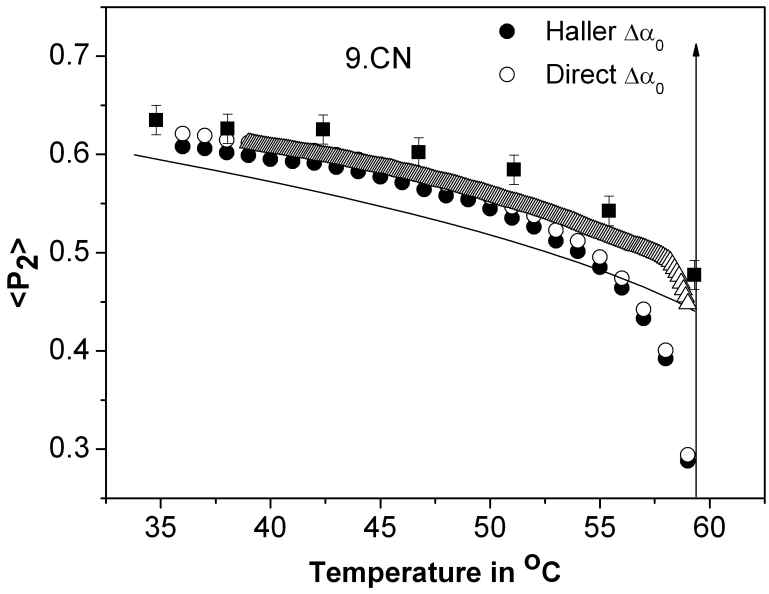

(b) Temperature variation of $\langle P_2 \rangle$ for 9.CN.

Figure 5.4: Temperature variation of $\langle P_2 \rangle$ for 7CPB and 9.CN, ○ refractive index data (thin prism method), △ birefringence (OT) data, ■ X-ray data, — $\langle P_2 \rangle$ from Maier-Saupe theory.

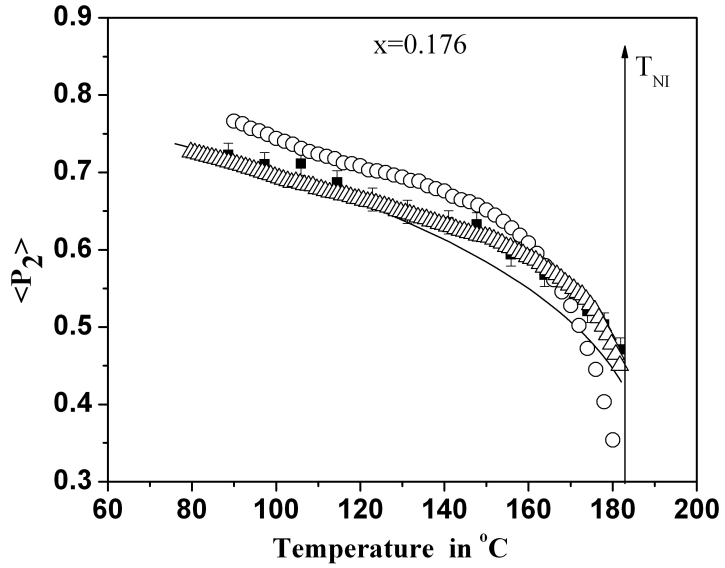

(c) Temperature variation of $\langle P_2 \rangle$ for $x_{9.\,CN}$ = 0.176.

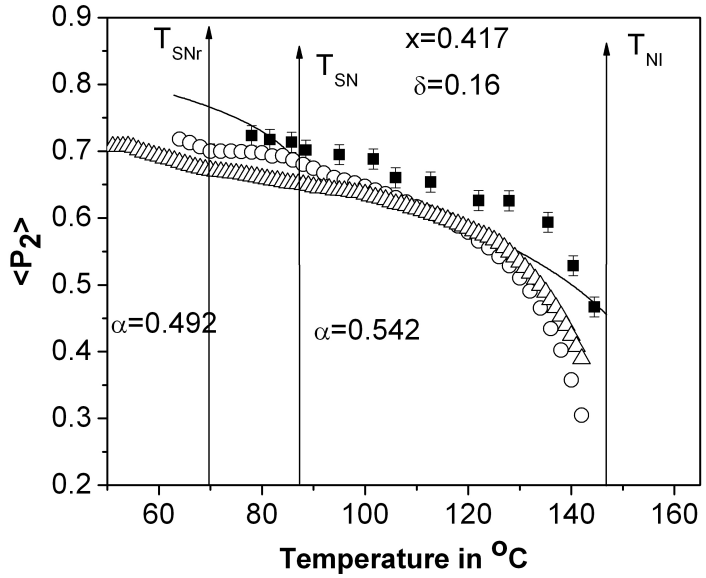

(d) Temperature variation of $\langle P_2 \rangle$ for $x_{9.\,CN}$ = 0.417.

Figure 5.4: (cont'd): Temperature variation of $\langle P_2 \rangle$ for $x_{9.\,CN}$ = 0.176 and $x_{9.\,CN}$ = 0.417, ○ refractive index data (thin prism method), △ birefringence (OT) data, ■ X-ray data, — $\langle P_2 \rangle$ from McMillan's theory, $\cdots$ $\langle P_2 \rangle$ from modified McMillan's theory by Luckhurst and Timimi.

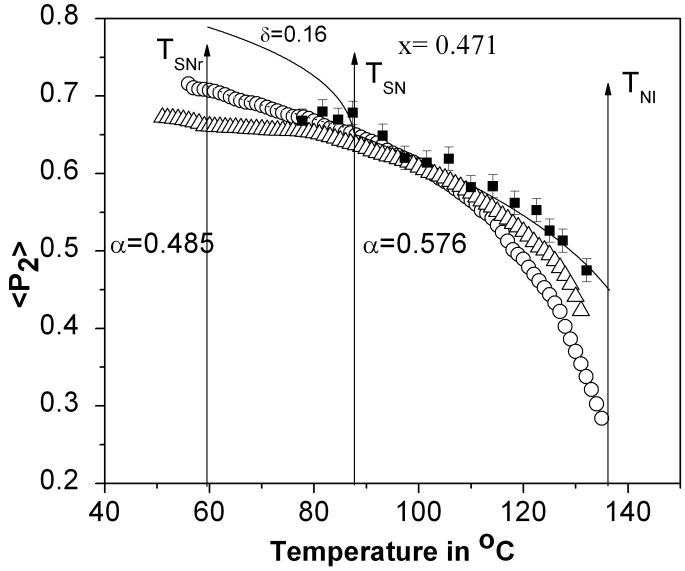

(e) Temperature variation of $\langle P_2 \rangle$ for $x_{9.\,CN} = 0.471$.

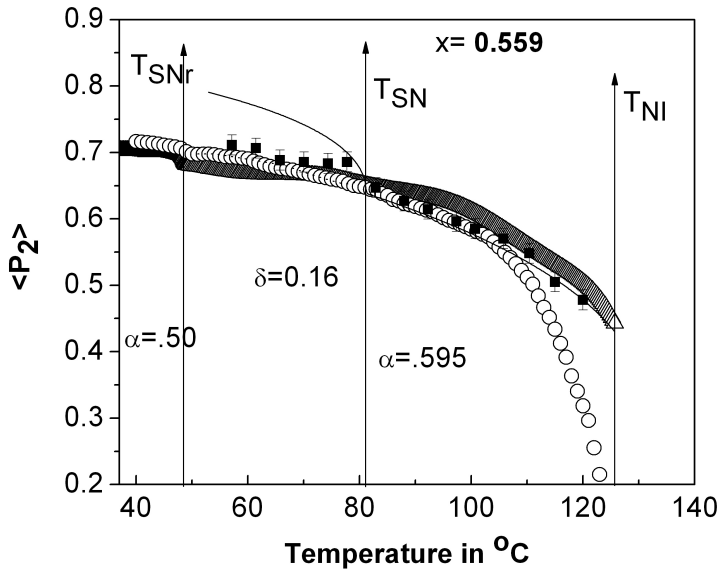

(f) Temperature variation of $\langle P_2 \rangle$ for $x_{9.\,CN} = 0.559$.

Figure 5.4: (cont'd): Temperature variation of $\langle P_2 \rangle$ for $x_{9.\,CN} = 0.471$ and $x_{9.\,CN} = 0.559$, ○ refractive index data, △ birefringence (OT) data, ■ X-ray data; — $\langle P_2 \rangle$ from McMillan's theory, $\cdots$ $\langle P_2 \rangle$ from modified McMillan's theory by Luckhurst and Timimi.

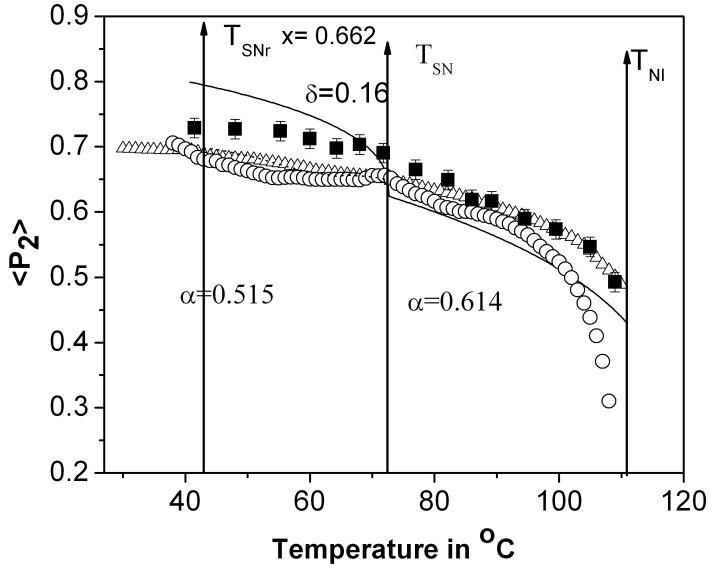

(g) Temperature variation of $\langle P_2 \rangle$ for $x_{9.\,CN} = 0.662$.

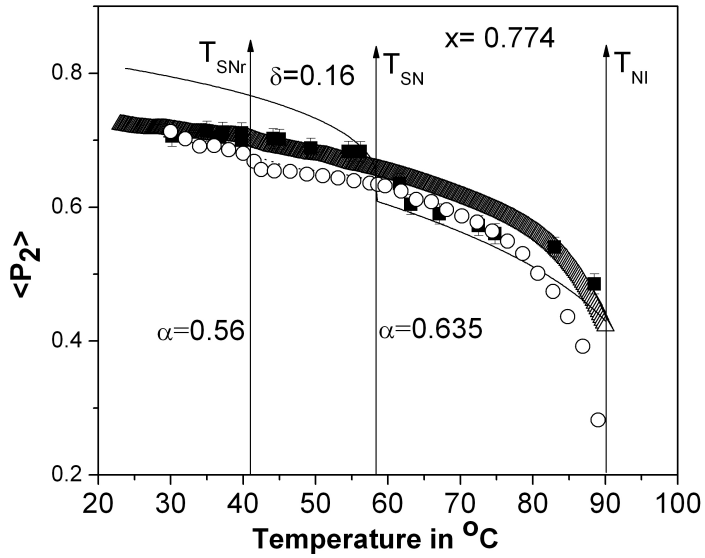

(h) Temperature variation of $\langle P_2 \rangle$ for $x_{9.\,CN} = 0.774$.

Figure 5.4: (cont'd): Temperature variation of $\langle P_2 \rangle$ for $x_{9.\,CN} = 0.662$ and $x_{9.\,CN} = 0.774$, ○ refractive index data, △ birefringence (OT) data, ■ X-ray data; — $\langle P_2 \rangle$ from McMillan's theory, $\cdots$ $\langle P_2 \rangle$ from modified McMillan's theory by Luckhurst and Timimi.

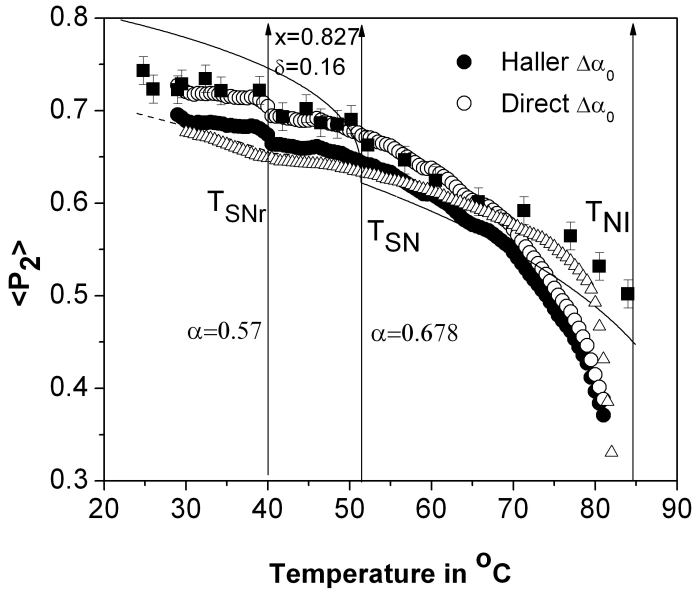

(i) Temperature variation of $\langle P_2 \rangle$ for $x_{9.\,CN}$ = 0.827.

Figure 5.4: (cont'd): Temperature variation of $\langle P_2 \rangle$ for $x_{9.\,CN}$ = 0.827 and $x_{9.\,CN}$ = 0.865, ○ refractive index data, △ birefringence (OT) data, ■ X-ray data; — $\langle P_2 \rangle$ from McMillan's theory, $\cdots$ $\langle P_2 \rangle$ from modified McMillan's theory by Luckhurst and Timimi.

do not agree well with Maier-Saupe theory [16]. However for mixture $x_{9.\,CN}$ = 0.176 (figure 5.4c), where only nematic phase exists, the agreement with the theory is quite good. The order parameters have been fitted to those calculated from McMillan's theory [17, 18]. The best fitted theoretical curve and the values of α used for this calculation are shown in figures (5.4d - 5.4i). As it was in the case for X-ray and refractive index studies, the agreement between the experimental $\langle P_2 \rangle$ values from the birefringence measurements with those calculated from McMillan's theory is poor for all the mixtures. However the agreement is better with the modified McMillan's theory as proposed by Luckhurst and Timimi [19]. The temperature dependence of the $\langle P_2 \rangle$ values is shown in figures (5.4d - 5.4i). The agreement between the experimental $\langle P_2 \rangle$ values from birefringence measurements with those calculated from modified McMillan's theory is very good for all the mixtures particularly for those mixtures showing both induced smectic and re-entrant nematic phases. Both Sm A_d – N transitions are predicted

to be second order by this model and this prediction is also in agreement with the DSC measurement [29], where no change in the transition enthalpies are observed at the re-entrant nematic to smectic A_d as well as smectic A_d to nematic phase transitions.

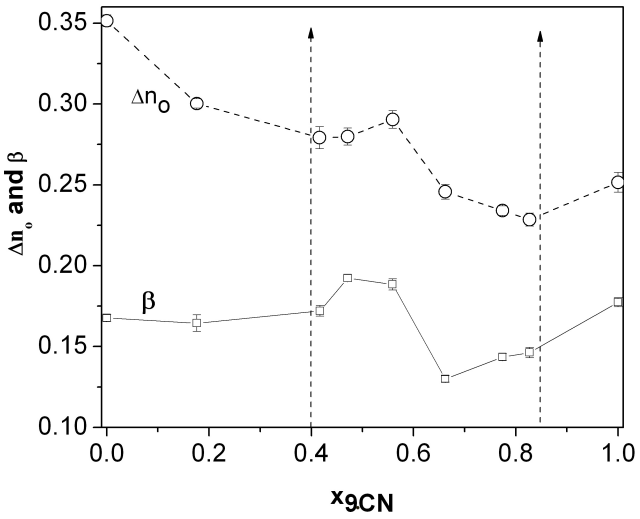

Figure 5.5: Extrapolated birefringence at the absolute zero temperature (Δn_0) and exponent β plotted as a function of mole fraction of 9.CN.

In figure 5.5, I have plotted the birefringence values extrapolated to absolute zero (Δn_0) and exponent β as a function of mole fraction of 9.CN. It is found that the Δn_0 values are greater in the lower concentration region of 9.CN and decreases gradually with the increase in mole fraction of 9.CN. However it shows local maxima near equimolar concentration. The β values of both the pure compounds are nearly the same. The variation of β also shows local maxima near equimolar concentration. It is may not be out of place to mention that the variation of layer thickness with concentration shows a maximum near the same concentration range as discussed in chapter three. As the anisotropy is almost proportional to the apparent molecular length (molecular width being constant) the X-ray result do support the local maximum of Δn_0. Figure 5.6 shows the variation of $\langle P_2 \rangle$ values with mole fraction of 9.CN at $T = T_{SN}$ - 5°C, where all the mixtures have smectic phase. It is observed that the OOP's in the smectic phase show a definite minimum at around $x_{9.\,CN}$ = 0.5, which corroborates the findings

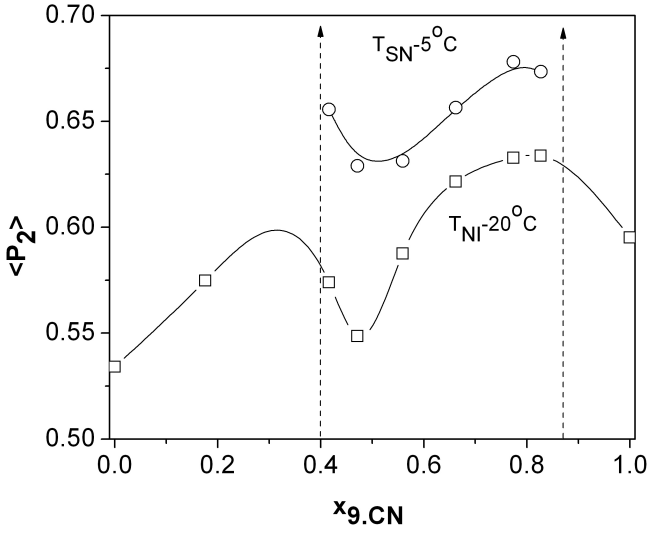

Figure 5.6: Concentration dependence of $\langle P_2 \rangle$ within the nematic phase at T_{NI}-20°C and smectic phase at T_{SN}-5°C.

of the X-ray diffraction measurements done on this system [29]. This minimum in the order parameter values is attributed to specific interactions between the molecules, which in trying to pack the different molecules within the layers of the smectic A_d phase, in effect, reduces the orientational free volume within the layers. This observation is very similar to polar-non-polar systems showing induced smectic A_d phase [21, 22, 25]. This lowering in the order parameter values has also been observed in the nematic phase of this system (figure 5.6).

The work and results discussed so far in this chapter had been reported [37] about 3 years ago. However, recently Erkan *et. al.* [20] have reported high resolution birefringence measurements on a liquid crystalline material having a nematic-smectic A_1 phase transition. They have analyzed the birefringence data to obtain a critical exponent α' similar to the specific heat capacity critical exponent α. While attempting to apply such analysis in the case of nematic–smectic A_d and smectic A_d–re-entrant nematic phase transitions, a need to improve the resolution both in the measurement of birefringence and temperature was felt. Hence the existing experimental set up was modified as described below.

To improve the thermal stability the previously described custom built heater was placed inside another hollow cylindrical heater. The temperature of

this outer heater was also controlled by using a different temperature controller (Eurotherm PID 2404) and its temperature was varied at the same rate as that of the inner heater.

Earlier the temperature of the heater was varied at a rate of $\pm 0.5^{\circ}C$ min^{-1} and the transmitted light intensity was measured by a photodiode at an interval of 12 seconds. This translates into the temperature difference of $0.1^{\circ}C$ between two readings. However, with improved temperature stability the photo diode output could be measured at an interval of 3 seconds. When the heater temperature is varied at a rate of $\pm 0.5^{\circ}C$ min^{-1}, this translates into a temperature difference of $0.025^{\circ}C$ between two readings. The experiment was repeated for selected mixtures using the modified setup and a solid state green laser (λ = 532 Å).

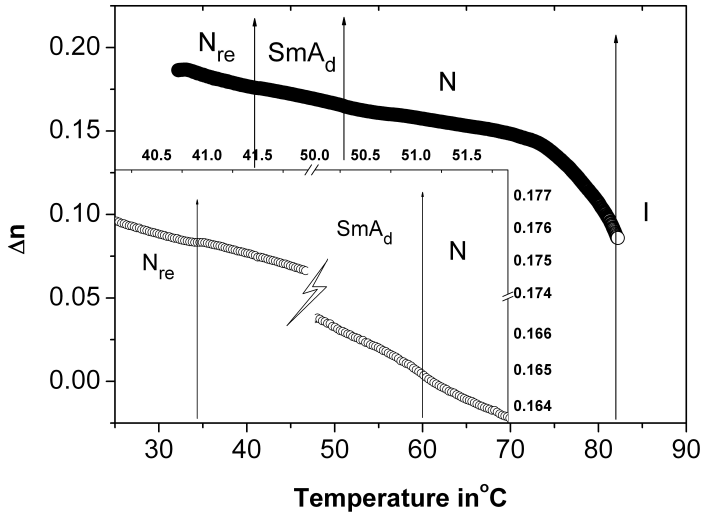

Figure 5.7: Birefringence ($\Delta n = n_e$-n_o) as a function of temperature for the mixtures $x_{9.\,CN}$ = 0.827. The inset zooms on the variation of Δn at N–Sm A_d and Sm A_d–N_{re} transitions.

The result of the high resolution (in both temperature and birefringence) measurement for the mixture $x_{9.\,CN}$ = 0.827 is shown in figure 5.7. It is observed that in going from nematic to smectic A_d there is a very small increase in the value of Δn and on entering the re-entrant nematic phase from the smectic A_d phase the value of Δn decreases by a similar amount. This change in the value

of Δn at the two transitions was so small that it could not be detected by the previous experimental setup with a temperature resolution of $0.1^{\circ}C$. The experiment was repeated again using He-Ne LASER (λ=632.8nm) and solid state red LASER (λ=630-670nm) and similar results were obtained, but the change in the value of Δn at the two transitions were less prominent. Similar changes in the value of Δn at the nematic–smectic A_d and smectic A_d–re-entrant nematic transitions were observed for the other mixtures. This observation is in agreement with the results of Chen *et. al.* [38]. However, this behaviour is different from our previous refractive index measurements by thin prism technique. The possible reason may be due to the fact that in refractive index measurements by thin prism technique the applied magnetic field strength of about 0.8 tesla may not have been sufficient to properly align the smectic A_d phase.

From the figures it is seen that there is no discontinuity in the birefringence data at the N–Sm A_d and Sm A_d–N_{re} transition, indicating second order nature of the N–Sm A_d transition. Since there is no discontinuity in the Δn value the quantity d(Δn)/dT has been used to locate the phase transition temperatures [39]. The transition temperatures so obtained are consistent with the transition temperature as obtained from the polarizing optical microscopy data (chapter 3).

Kityk *et. al.* [39] have proposed that d(Δn)/dT is related to the specific heat anomaly. Erkan *et. al.* [20] have found that though the quantity d(Δn)/dT can be computed by numerical differention of Δn(T), the result is too scattered due to the very small value of the temperature steps. In order to overcome this problem they have defined a new quotient $Q(T)$ such that

$$Q(T) = -\frac{\Delta n\,(T) - \Delta n\,(T_{NA})}{T - T_{NA}} \tag{5.3}$$

where $\Delta n(T_{NA})$ is the birefringence value at the transition temperature T_{NA} as obtained by differentiating Δn. This quotient $Q(T)$ is similar to the quantity $C(T) = (H_T - H_c)/(T - T_c)$, where $H(T)$ is the enthalpy as a function of temperature as obtained from adiabatic scanning calorimetry [20, 40, 41]. They have further argued that if d(Δn)/dT follows a power law behavior with a critical exponent α', then the limiting behavior of $Q(T)$ also follows a power law with the same critical exponent and the background term but different critical amplitude [2] and this critical exponent α' is in excellent agreement with the α value from calorimetric data for 4-butyloxyphenyl-4′-decyloxybenzoate, which is a non polar

liquid crystal.

In an attempt to study the critical behavior of $Q(T)$ at the nematic–smectic A_d and smectic A_d–re-entrant nematic phase transitions the parameter $Q(T)$ have been fitted with the equation containing four parameters as

$$Q(T) = A_{\pm} \mid t \mid^{-\alpha'} + B \tag{5.4}$$

where A_+ and A_- are the critical amplitudes above and below the Sm A_d–N transition temperature (T_{NA}), B is the background term, α' is the critical exponent and $t = \mid (T - T_{NA})/(T_{NA}) \mid$ is the reduced temperature.

Figure 5.8 and 5.9 shows the temperature variation of $Q(T)$ in the vicinity of the N–Sm A_d and Sm A_d–N_{re} transitions respectively. The values of the fitting parameters have been shown in the table 5.1.

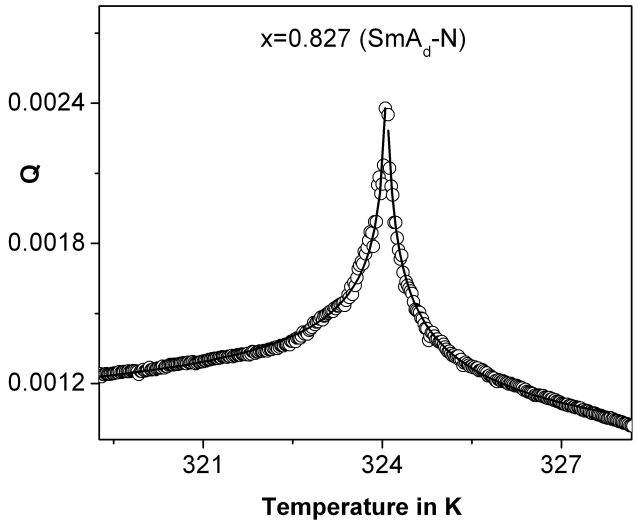

Figure 5.8: Temperature behavior of the quotient $Q(T)$ in the vicinity of the N–Sm A_d transition. The solid line is the fit to equation 5.4.

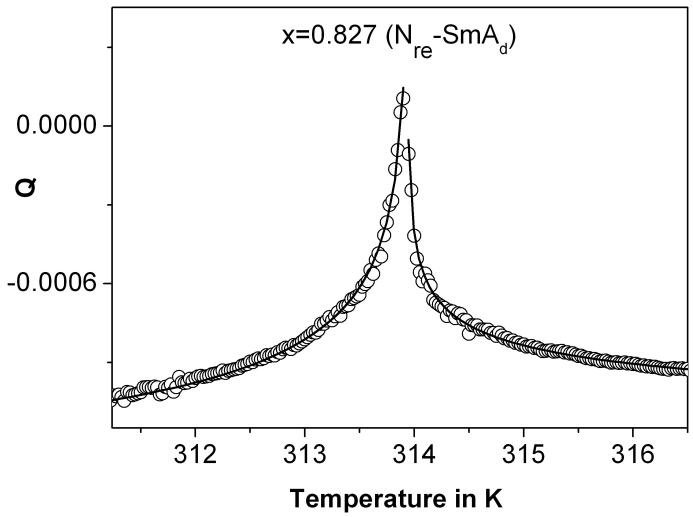

Figure 5.9: Temperature behavior of the quotient $Q(T)$ in the vicinity of the Sm A_d–N_{re} transition. The solid line is the fit to equation 5.4.

Table 5.1: Values of the fitting parameters of equation 5.4 at N–Sm A_d and Sm A_d–N_{re} phase transitions.

N–Sm A_d

Side	A	T_{NA}	α'	B
left	0.00016±0.00002	324.11±0	0.27±0.01	0.00074±0.00003
Right	0.00018±0.00002	324.02± 0	0.28±0.01	0.00044±0.00003

Sm A_d–N_{re}

Side	A	T_{NA}	α'	B
left	0.00034±0.00012	314.45±0.44	0.21±0.05	-0.00197±0.00013
Right	0.00016± 0.00004	314.43±0.01	0.21±0.02	-0.00137±0.00006

5.3 Conclusion

Optical transmission studies have been undertaken to measure the birefringence of a binary system of nematogenic compounds exhibiting induced smectic A_d and re-entrant nematic phases. A simple and precise method for the determination of the optical birefringence as a function of temperature was used in

this work. It was possible to measure the birefringence Δn with reasonably good accuracy (greater than $\pm 10^{-4}$) in all the liquid crystalline phases. No discontinuity has been observed in the Δn values at the N_{re} – Sm A_d as well as Sm A_d – N transition temperatures. These observations indicate that the re-entrant nematic to induced smectic A_d and induced smectic A_d to nematic phase transition for all the mixtures in this system is of second order. Similar to X-ray diffraction measurements, the agreement between the experimental $\langle P_2 \rangle$ values from the birefringence measurements with those calculated from McMillan's theory have been found to be poor in the smectic A_d phase. This discrepancy has been removed by recalculating the orientational order parameter values according to a modified McMillan's theory as proposed by Luckhurst and Timimi, taking into account a slight temperature dependence of the α parameter. Both N–Sm A_d and Sm A_d–N_{re} phase transitions which are predicted to be of second order by this model, are also found to be in agreement with the birefringence as well as DSC measurements.

With improved temperature resolution a very small increase in the value of Δn was observed at the N–Sm A_d transition. A decrease by a similar amount in the value of Δn was again observed at the Sm A_d–re-entrant transition. From the analysis of the optical birefringence data on both sides of the nematic-smectic A_d and smectic A_d–re-entrant transition, with the help of fitting expression (equation 5.4), the values of the critical exponent associated with the power law divergence of the quotient $Q(t)$ has been obtained. The value of this critical exponent, which is expected to be similar to the specific heat critical exponent α, is found to be 0.275 and 0.21 at the N–Sm A_d and Sm A_d–re-entrant nematic transitions respectively. These values lie between the 3D XY and tricritical values.

References

[1] M. F. Vuks, *Opt. Spectros.*, **20**, 361 (1966).

[2] B. J. Zywucki and W. Kuczynski, *IEEE Trans, Dielectr. Electr. Insul.*, **8**, 512 (2001).

[3] W. Kuczynski, B. Zywucki, and J. Malecki, *Mol. Cryst. Liq. Cryst.*, **381**, 1 (2002).

[4] M. Geppi, A. Marini, B. Mennucci, P. Kula, A. Spadlo, W. Kuczynski and S. Urban, *Mol. Cryst. Liq. Cryst.*, **541**, 104 (2011).

[5] P. Pardhasaradhi, P. V. Datta Prasad, D. M. Latha, V. G. K. M. Pisipati and G. Padmaja Rani, *Phase Transitions*, **85**, 1031 (2012).

[6] K. D. Thingujama, P. R. Alapati, B. Choudhury A. Bhattacharjee, *Phase Transitions*, **85**, 52 (2012).

[7] K. Fakruddin, R. J. Kumar, P. V. D. Prasad and V. G. K. M. Pisipati, *Mol. Cryst. Liq. Cryst.*, **511**, 133 (2009).

[8] A. Kumar, *Liq. Cryst.*, **40**, 203 (2013).

[9] V. G. K. M. Pisipati and P. V. Datta Prasad, *Mol. Cryst. Liq. Cryst.*, **506**, 13 (2009).

[10] M. S. Zakerhamidi and H. Rahimzadeh, *Mol. Cryst. Liq. Cryst.*, **569**, 92 (2012).

[11] S. S. Sastry, S. Kumar, T. V. Kumari, K. Mallika, B. G. S. Rao and H. S. Tiong, *Liq. Cryst.*, **39**, 1527 (2012).

[12] S. S. Sastry, T. V. Kumari, K. Mallika, B. G. S. Rao, Sie-Tiong Ha and S. Lakshminarayana, *Liq. Cryst.*, **39**, 295 (2012).

[13] M. K. Das, G. Sarkar, B. Das, R. Rai and N. Sinha, *J. Phys.: Condens. Matter*, **24**, 115101 (9pp) (2012).

[14] G. Sarkar, B. Das, M. K. Das, U. Baumeister and W. Weissflog, *Mol. Cryst. Liq. Cryst.*, **540**, 188 (2011).

[15] I. Haller, *Prog. Solid State Chem.*, **10**, 103 (1975).

[16] W. Maier and A. Saupe, *Z. Naturforsch Tail II*, **15a**, 287 (1960).

[17] W. L. McMillan, *Phys. Rev. A*, **4**, 1236 (1971).

[18] W. L. McMillan, *Phys. Rev. A*, **6**, 93 (1972).

[19] G. R. Luckhurst, B. A. Timimi, *Mol. Cryst. Liq. Cryst.*, **64**, 253 (1981).

[20] S. Erkan, M. Cetinkaya, S. Yildiz, and H. Ozbek, *Phys. Rev. E*, **86**, 041705 (2012).

[21] M. K. Das and R. Paul, *Phase Transitions*, **46**, 185 (1994).

[22] P. D. Roy, A. Prasad, M. K. Das, *J. Phys.: Condens. Matter*, **21**, 075106 (2009).

[23] P. D. Roy, B. Das, M. K. Das, *J. Phys.: Condens. Matter*, **21**, 335108 (2009).

[24] P. D. Roy, N. Pradhan, M. K. Das, *Mol. Cryst. Liq. Cryst.*, **365**, 593 (2001).

[25] P. D. Roy, M. K. Das, S. Paul, R. Paul and B. Das, *Mol. Cryst. Liq. Cryst.*, **457**, 43 (2006).

[26] S. Dhara and N. V. Madhusudana, *Phase Transitions*, **81**, 561 (2008).

[27] G. Sarkar, B. Das, M. K. Das and W. Weissflog, *Proc. 16th National Conference on Liquid Crystals (India)*, Lucknow, 2009, p. 76.

[28] A. Saipa, F. Giesselmann, *Liq. Cryst.*, **29**, 347 (2002).

[29] A. Prasad and M. K. Das, *Phase Transitions*, **82**, 780 (2009).

[30] H. E. Neugebauer, *Canad. J. Phys.*, **32**, 1 (1954).

[31] W. H. de Jue, *Physical Properties of Liquid Crystalline Materials*, Gordon and Breach Science Publishers, (1980).

[32] W. Kuczynski, B. Zywucki and J. Malecki, *Mol. Cryst. Liq. Cryst.*, **381**, 1 (2002).

[33] B. Adhikari and R. Paul, *Mol. Cryst. Liq. Cryst.*, **261**, 241 (1995).

[34] B. Das, S. Grande, W. Weissflog, A. Eremin, M. W. Schroeder, G. Pelzl., S. Diele and H. Kresse, *Liq. Cryst.*, **30** (5), 529 (2003).

[35] M. K. Das and R. Paul, *Mol. Cryst. Liq. Cryst.*, **239**, 107 (1994).

[36] B. Adhikari and R. Paul, *Phase transitions*, **56**, 165 (1996).

[37] A. Prasad and M. K. Das, *J. Phys.: Condens. Matter*, **22**, 195106 (2010).

[38] N. R. Chen, S. K. Hark and J. T. Ho, *Phys. Rev. A*, **24**, 2843 (1981).

[39] A. V. Kityk and P. Huber, *Appl. Phys. Lett.*, **97**, 153124 (2010).

[40] J. Thoen, *Physical Properties of Liquid Crystals*, Eds. D. Demus, J. Goodby, G. W. Gray, H. W. Spiess, and V. Vill, Wiley-VCH, Weinheim, (1999).

[41] J. Thoen, *Heat Capacities: Liquids, Solutions, and Vapours*, Eds. E. Wilhelm and T. M. Letcher, Royal Society of Chemistry, London, (2010).

Chapter 6

Static dielectric properties of two nematogenic compounds and their binary mixtures (7CPB+9.CN) showing induced smectic A_d and re-entrant nematic phases

6.1 Introduction

To meet the specific demands of electro-optic display devices, mixtures of liquid crystals are often prepared where the composition of the mixture is adjusted to attain the desired physical properties. However, the physical properties of such mixtures cannot always be interpolated from the properties of the pure components. One such example is the formation of induced smectic phase which is generally observed in binary mixtures of pure nematogenic compounds, one having terminal polar end and the other being non polar one [1–10]. Strong induction of smectic A_d (Sm A_d) is also possible in mixtures of polar nematic compounds [11–13], some of which also exhibit the re-entrant nematic (N_{re}) phase. In all the cases, dipole-dipole or dipole-induced dipole interaction play a major role in the stabilization of the induced phase. However, it has been shown that

steric effects are also important for phase stabilization [14]. In most of the theories which have been more or less successful in explaining the re-entrant nematic phase, the dipole-dipole interaction has been of prime importance. A successful theory that explains re-entrance is the frustration theory of Berker *et. al.* [15–17]. Here the re-entrance has been explained in terms of dipolar interaction. An extension of McMillan's theory [18, 19] by Luckhurst and Timimi [20] can also explain re-entrance based on a small temperature dependence of the scaled strength parameter α in the McMillan's potential which is related to the layer thickness which in turn is a result of dipole-dipole and dipole- induced dipole interaction as discussed in chapter 3.

In spite of immense importance of the dipole-dipole interaction and of dielectric anisotropy, not much of such work has been done on re-entrant systems whose components are purely nematic and not having any underlying smectic phase.

In the previous chapters (chapter 3-5) I have reported a binary system of two nematogenic compounds 7CPB and 9.CN showing an induced Sm A_d and re-entrant nematic phase in the concentration range of $0.4 < x_{9.\,CN} < 0.88$. The detailed phase diagram and X-ray diffraction measurements have been discussed. The X-ray measurements show that the layer spacing is greater than the molecular length, which has been attributed to anti-parallel association due to dipole-dipole and dipole-induced dipole interaction. The experimental variation of layer thickness with mole fraction of 9.CN was also explained fairly well by assuming the presence of two types of homo dimers and one hetero dimer. The temperature dependence of dimer length leads to a temperature dependence of α parameter in the McMillan potential. The $\langle P_2 \rangle$ variation obtained by X-ray and optical birefringence methods [21–23], in all the three phases, was successfully explained by selecting a linear dependence of α on temperature.

In this chapter, I have reported the results of static dielectric permittivity measurements carried out on binary mixtures of 7CPB and 9.CN throughout the entire composition range. Free molecular dipole moment of 7CPB and 9.CN has been determined using Guggenheim method [24]. Mesogenic molecular dipole moments μ and their inclination angles β with the molecular long axis have also been determined following Maier and Meier's extension [25] of Onsager's theory [26], where the mean effective values of the dipole moment in the parallel

and perpendicular directions to the director can be obtained from the dielectric functions, density and refractive indices values. The experimental molecular dipole values have been compared with those calculated using semi-empirical molecular orbital package, MOPAC [27, 28].

The nature of nematic-isotropic phase transition is generally said to be weakly first order because the enthalpy and the volume changes at the transitions are small as compared to those observed at the melting point. Also, a large pretransitional effect is generally seen in the vicinity of nematic-isotropic phase transition. However, such pretransitional effects are characteristic of second order phase transition. This pretransitional effect is due to the development of short range orientational order of the molecules which forms pseudonematic domains in the isotropic liquid. However, the mean field theories cannot account for these pretransitional effects. With the exception of linear dielectric properties of polar molecules, the pretransitional effects manifest themselves mainly in the nonlinear studies, when the liquid crystalline molecules are subjected to sufficiently strong external stimuli. Experimental techniques such as nonlinear dielectric effect [29, 30], light scattering [31], birefringence due to magnetic [32] or electric field [33], dynamic studies on molecular spin-lattice relaxation [34, 35], dynamic light scattering [36] and transient grating optical Kerr effect [37, 38] have been used to study the pretransitional effects in the vicinity of nematic-isotropic phase transition. Recently, a number of attempts have been made [30, 39–46] to study the pretransitional effects at the nematic-isotropic phase transitions by linear dielectric studies and similar study on the system 7CPB+9.CN is expected to yield interesting result. The dielectric permittivity values have been measured up to $T - T_{NI}$ =55°C for a mixture $x_{9.\,CN}$ = 0.827 and an attempt has been made to obtain the critical exponent α'.

6.2 Static dielectric permittivity studies

I have determined the dipole moments of 7CPB and 9.CN by measuring the concentration dependence of dielectric permittivity (ϵ) and refractive index (n) of the compounds dissolved in a non-polar solvent p-xylene using Guggenheim method [24]. The experimental details have been discussed in details in chapter 2 of this thesis. The experimental data for the dipole moment μ has

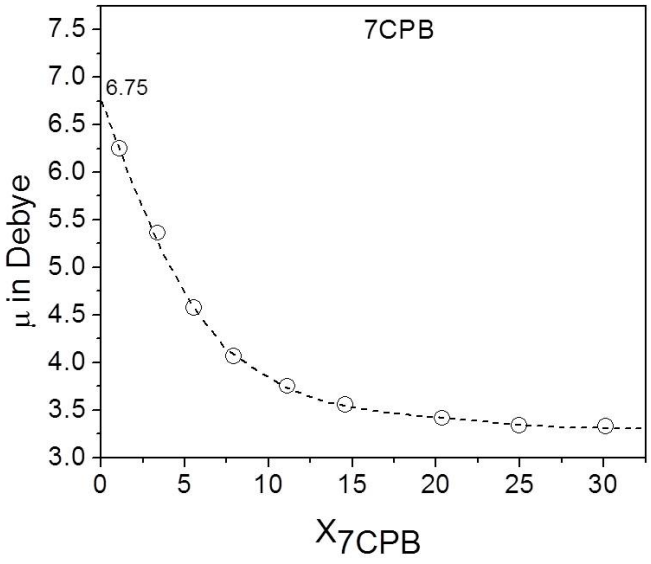

(a)

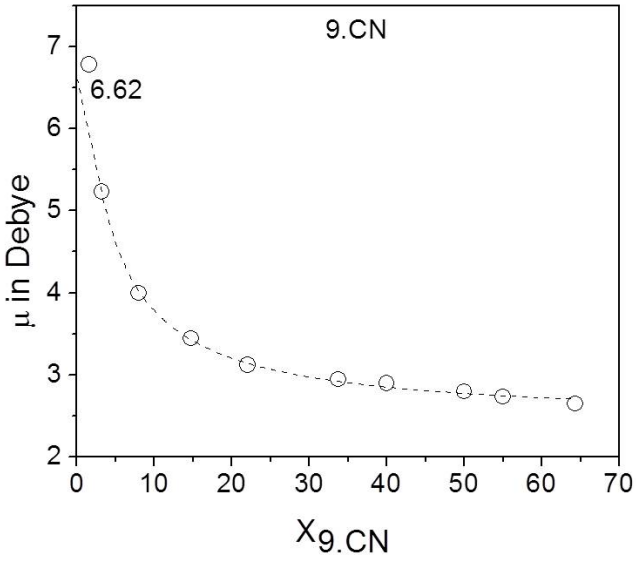

(b)

Figure 6.1: The dipole moments of (a) 7CPB and (b) 9.CN in p-xylene solution as a function of molar concentration (x).

been compared with those obtained from the semi-empirical molecular orbital package MOPAC [27] for the two pure compounds in their minimum energy configuration. Mesogenic molecular dipole moments μ and their inclination angles β with the molecular long axis have also been determined following Maier and Meier equations [25].

The concentration dependence of the dipole moments for the solution of 7CPB + p-xyline and 9.CN + p-xyline are shown in figures 6.1a-6.1b. The extrapolation of the best fitted polynomial curve to infinite dilution gives the dipole moment of the single molecule. The molecular dipole moments of 9.CN and 7CPB are found to be 6.62D and 6.75D respectively which are slightly higher than those obtained using MOPAC with the molecules in the minimum energy configuration (9.CN = 6.11 Debye and 7CPB = 6.15 Debye).

The temperature variation of the dielectric parameters [$\epsilon_{\parallel}$, $\epsilon_{\perp}$, ϵ_{iso}, $\Delta\epsilon = (\epsilon_{\parallel} - \epsilon_{\perp})$ and $\epsilon_{av} = (2\epsilon_{\perp} + \epsilon_{\parallel})/3$] for the two pure compounds and their mixtures are shown in figures 6.2a-6.2l. There is a sharp discontinuity in the measured permittivity components for pure compounds 9.CN, 7CPB at the nematic to isotropic phase transition. However, for the mixtures an almost continuous change in the permittivity components at the nematic-isotropic phase transition is observed. This is perhaps due to the presence of the co-existing nematic-isotropic phase. All the mixtures including the pure compounds exhibit a large positive dielectric anisotropy ($\Delta\epsilon > 0$) due to the presence of terminal polar CN group.

For both the pure compounds and all the mixtures, the value of the isotropic dielectric permittivity (ϵ_{iso}) extrapolated to the nematic, smectic A_d and re-entrant nematic phases is always greater than the average dielectric permittivity ϵ_{av}. This decrease in ϵ_{av} values with respect to the isotropic value (ϵ_{iso}) is due to the stronger dipole - dipole correlation in the nematic, smectic and re-entrant nematic phases as compared to the isotropic phase.

The change in static permittivity behavior in going from isotropic to (isotropic + nematic) coexistence region and from (isotropic + nematic) to nematic region is different from each other. The permittivity value changes sharply in the beginning of the two phase region, whereas on entering the nematic phase the change is smooth and the transition between the two phase region and the nematic phase cannot be determined precisely from static permittivity measurements. Such, observations have also been reported by others [42].

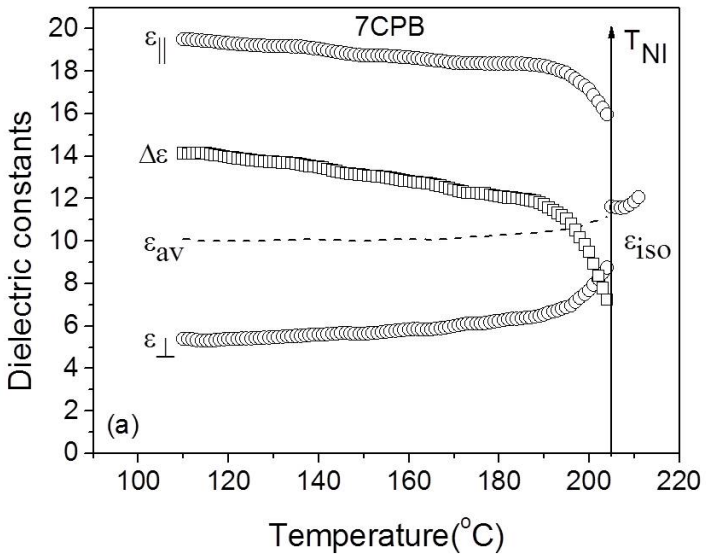

(a)

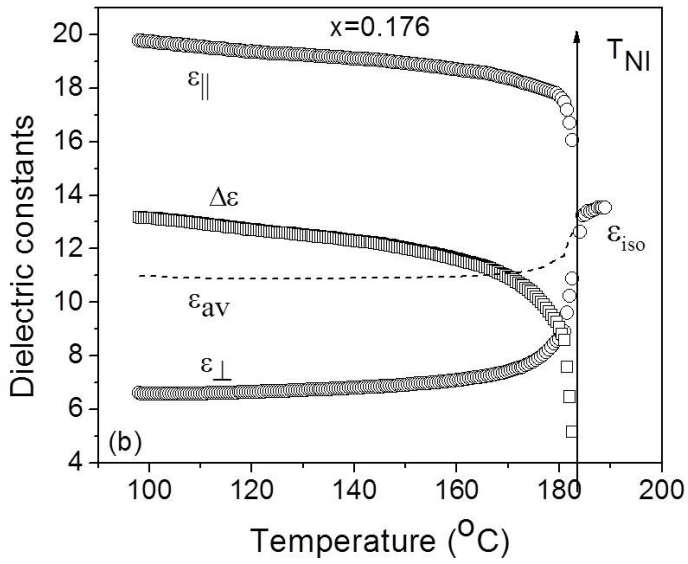

(b)

Figure 6.2: Temperature variation of dielectric parameters of 7CPB + 9.CN mixture for (a) 7CPB and (b) $x_{9.\,CN}$ = 0.176. T_{NI} = nematic – isotropic phase transition temperature.

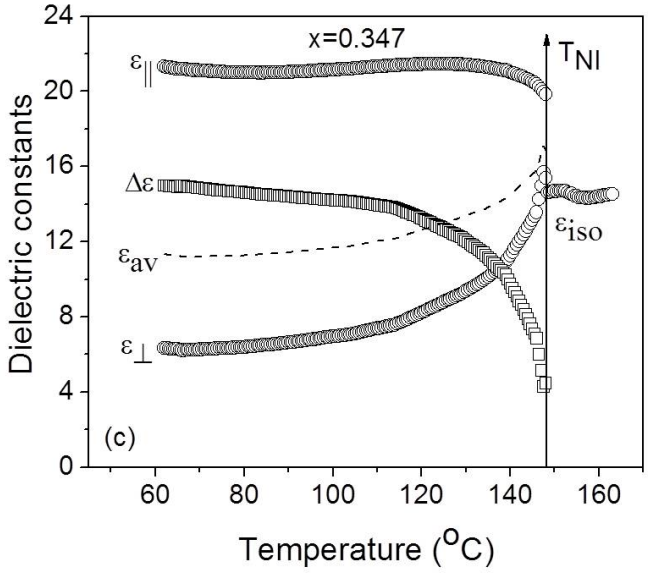

(c)

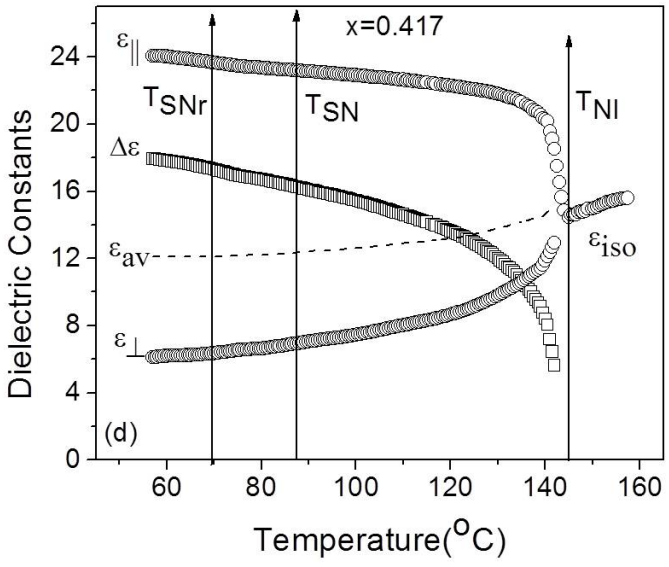

(d)

Figure 6.2: (cont'd): Temperature variation of dielectric parameters of 7CPB + 9.CN mixture for (c) $x_{9.\,CN}$ = 0.347 and (d) $x_{9.\,CN}$ = 0.417 . T_{NI} = nematic – isotropic, T_{SN} = smectic A_d – nematic and $T_{SN_{re}}$= smectic A_d – re-entrant nematic phase transition temperatures.

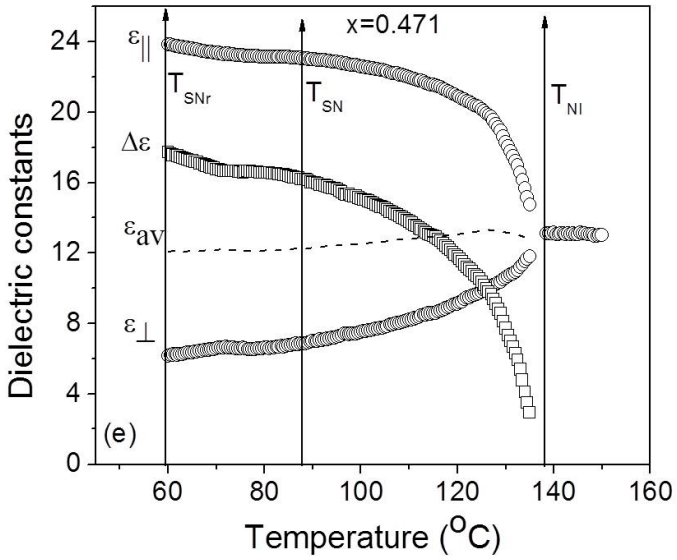

(e)

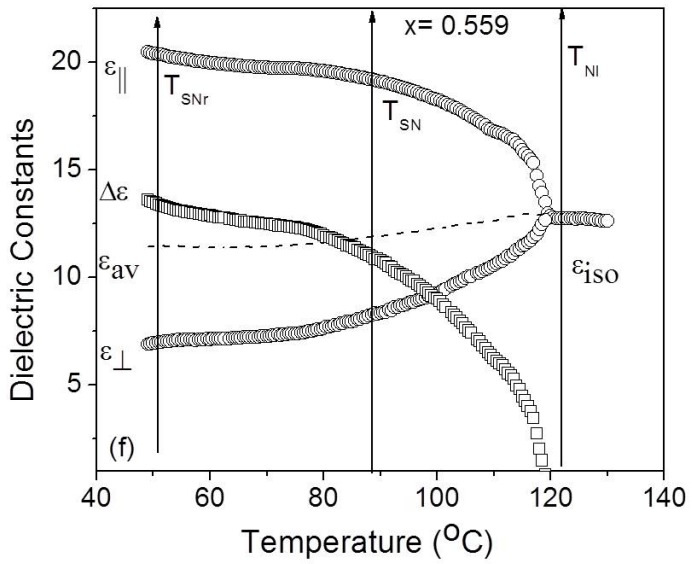

(f)

Figure 6.2: (cont'd): Temperature variation of dielectric parameters of 7CPB + 9.CN mixture for (e) $x_{9.\,CN}$ = 0.471 and (f) $x_{9.\,CN}$ = 0.559 . T_{NI} = nematic – isotropic, T_{SN} = smectic A_d – nematic and $T_{SN_{re}}$= smectic A_d – re-entrant nematic phase transition temperatures.

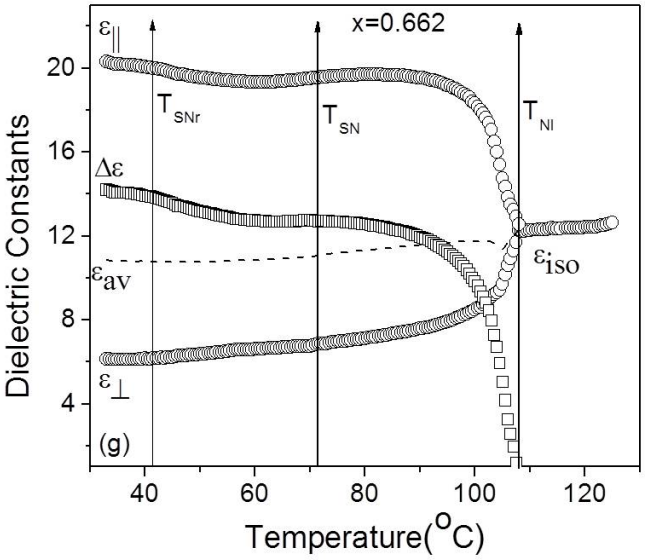

(g)

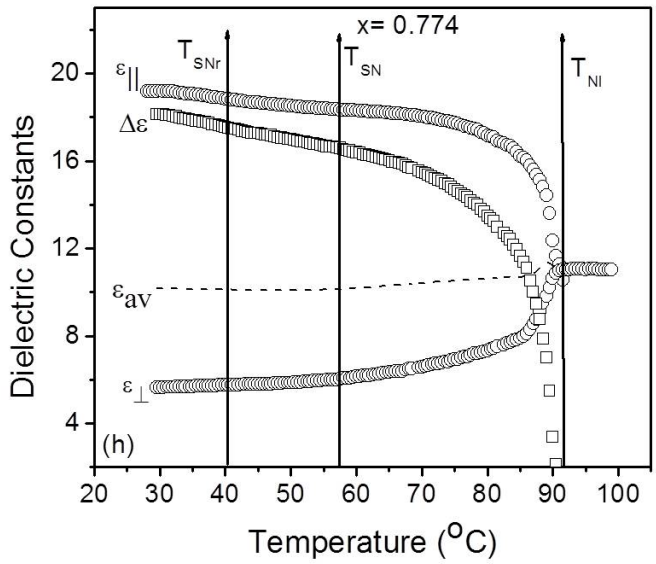

(h)

Figure 6.2: (cont'd): Temperature variation of dielectric parameters of 7CPB + 9.CN mixture for (g) $x_{9.\,CN}$ = 0.662 and (h) $x_{9.\,CN}$ = 0.774 . T_{NI} = nematic – isotropic, T_{SN} = smectic A_d – nematic and $T_{SN_{re}}$= smectic A_d – re-entrant nematic phase transition temperatures.

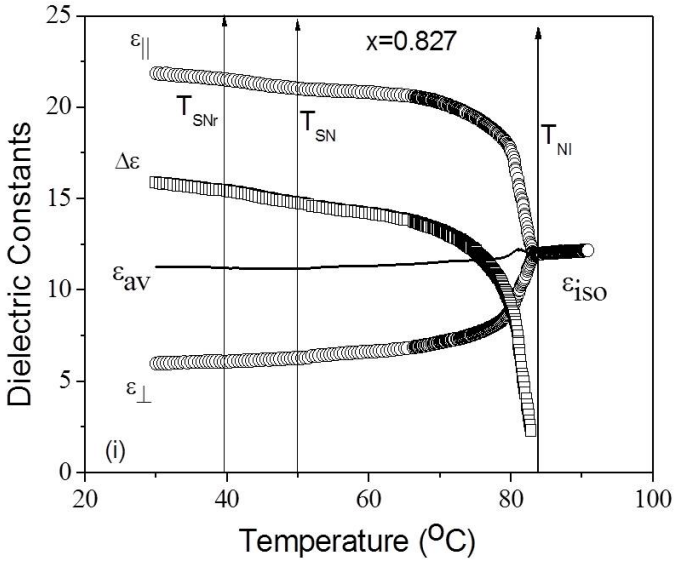

(i)

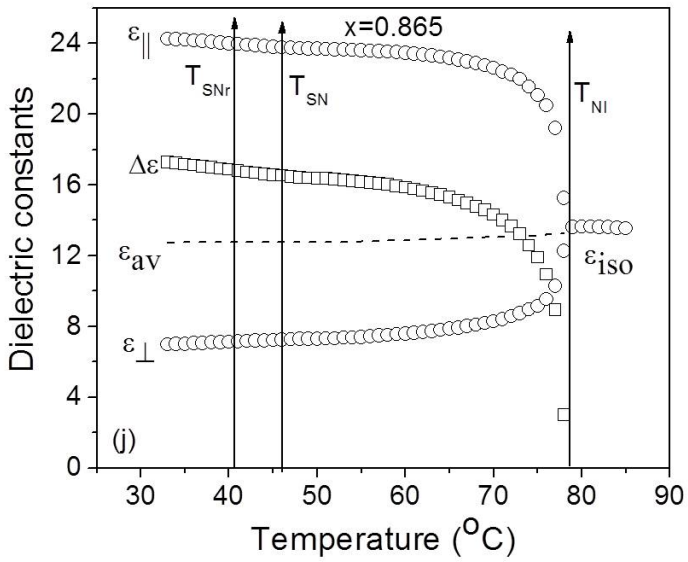

(j)

Figure 6.2: (cont'd): Temperature variation of dielectric parameters of 7CPB + 9.CN mixture for (i) $x_{9.\,CN}$ = 0.827 and $x_{9.\,CN}$ = 0.865. T_{NI} = nematic – isotropic, T_{SN} = smectic A_d – nematic and $T_{SN_{re}}$= smectic A_d – re-entrant nematic phase transition temperatures.

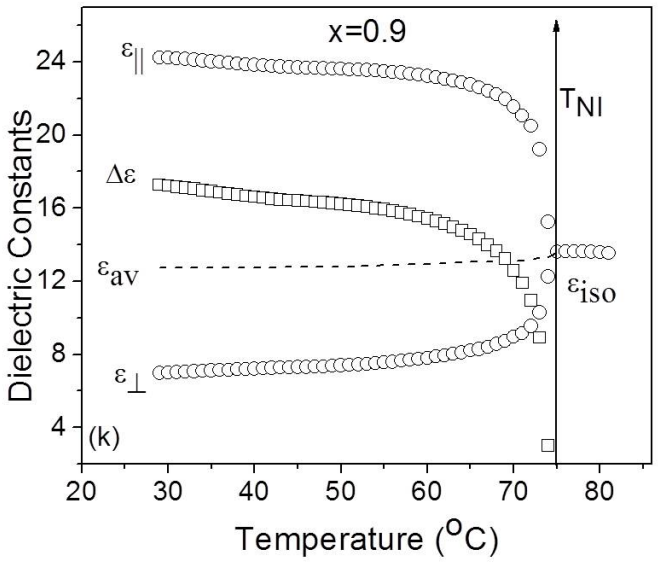

(k)

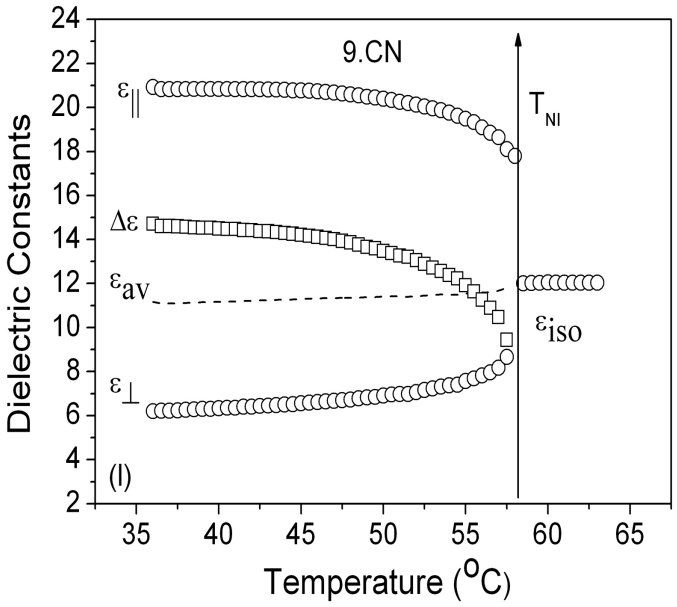

(l)

Figure 6.2: (cont'd): Temperature variation of dielectric parameters of 7CPB + 9.CN mixture for (i) $x_{9.CN}$ = 0.9 and 9.CN. T_{NI} = nematic – isotropic phase transition temperature.

All the mixtures having induced smectic and re-entrant nematic phases ($x_{9.\,CN}$ = 0.4 to 0.88) show no significant jump in the permittivity components at the smectic-nematic as well as smectic – re-entrant nematic phase transitions. The temperature dependence of $\epsilon_\perp$ is identical in nature for both the pure components as well as for the mixtures. However, the variation of $\epsilon_\parallel$ with temperature is different for those mixtures which exhibit re-entrance. The pure compounds exhibit the normal temperature variation of $\epsilon_\parallel$ i.e. on decreasing the temperature $\epsilon_\parallel$ increases. However for the mixtures belonging to the concentration range $0.4 < x_{9.\,CN} < 0.88$, $\epsilon_\parallel$ behaves normally in the upper nematic and the re-entrant nematic phase, but in the induced smectic phase $\epsilon_\parallel$ exhibits a shallow broad minima, the depth of which varies with the mole fraction of the mixture.

The maximum decrease i.e. difference between the extrapolated and the experimental $\epsilon_\parallel$ value is found to be 4% for mixture x = 0.662 and this falls off on both sides of the smectic island. This may be due to the increase in the dipole- dipole interaction in the layered interdigitated structure of the Sm A_d phase. Another interesting observation is that this shallow minimum in $\epsilon_\parallel$ is not only observed in those mixtures having induced smectic and re-entrant nematic phases but it is also found in mixtures which are purely nematic and is visible (on a reduced scale) even for mixtures with x = 0.176 and 0.9 which are far away from the smectic island. Similar observations have also been reported by others [47] in the close proximity of the smectic phase.

Since there is a continuous change in most of the parameters across the nematic – smectic A_d and smectic A_d – re-entrant neamtic phases, an attempt was made to distinguish between different mesophases from dielectric permittivity measurements by performing $\epsilon_\perp$ measurements with a homogeneously aligned cell and a bias voltage of 0.75V. The results for this measurement for two mixtures are shown in figure 6.3. It is observed that the boundary of the Sm A_d phase is clearly visible in this figure. The $\epsilon_\perp$ values for all the mixtures in the Sm A_d phase are more or less constant but increases gradually just after the phase transitions (Sm A_d–N and Sm A_d–N_{re}). The difference between the low bias (0.3V) and high bias data in both the nematic phases (figure 6.3) is due to the electric field induced Freedericksz transition when the biasing voltage exceeds the threshold value.

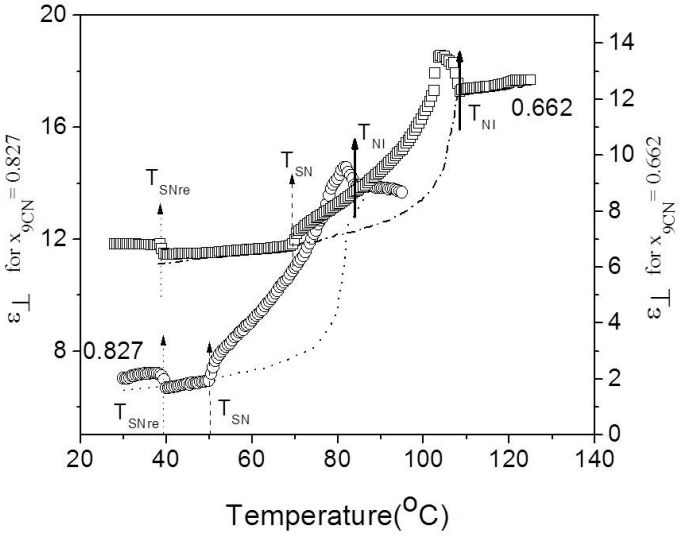

Figure 6.3: Variation of electric permittivity ($\epsilon_\perp$) as a function of temperature. ○ ($x_{9.\,CN}$ = 0.827); □ ($x_{9.\,CN}$ = 0.662) for measuring voltage 0.75V and ⋯ ($x_{9.\,CN}$ = 0.827); $-\cdot-\cdot-$ ($x_{9.\,CN}$ = 0.662) for measuring voltage 0.3V.

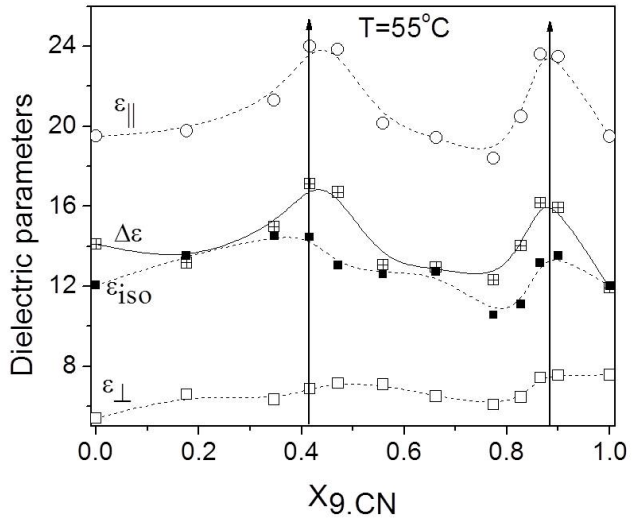

Figure 6.4: Variation of $\epsilon_\parallel$, $\epsilon_\perp$, $\Delta\epsilon$ and ϵ_{iso} at a temperature T = 55°C with molar concentration of 9.CN. ↑ represents the induced smectic A_d region.

The concentration dependence of the dielectric parameters $\epsilon_{\parallel}$, $\epsilon_{\perp}$, ϵ_{iso} and $\Delta\epsilon$ at T = 55°C is shown in figure 6.4. All the parameters show a saddle like dependence with two minima between them. $\epsilon_{\parallel}$ and $\epsilon_{\perp}$ have their minima at $x_{9.\,CN}$ = 0.7 while $\epsilon_{\perp}$ and ϵ_{iso} exhibit a minima at around $x_{9.\,CN}$ = 0.8. Interestingly, this minimum in the dielectric parameters is observed near about that region of the phase diagram where there is a strong induction of the smectic A_d phase.

Maier and Meier extended [25] the Onsager's theory [26] of dielectric polarization of isotropic liquids to explain the static dielectric behavior of liquid crystals. They showed that the dielectric permittivities $\epsilon_{\parallel}$ and $\epsilon_{\perp}$ are related to molecular polarizability ($\Delta\alpha$), dipole moment (μ) and its orientation relative to the long principal axis (β) in the molecular frame and the orientational order parameter, $\langle P_2\rangle$ by the relations

$$\epsilon_{\parallel} - 1 = 4\pi N h F \left(\overline{\alpha} + \frac{2}{3}\Delta\alpha\langle P_2\rangle + \frac{F\mu^2\left[1-\left(1-3\cos^2\beta\right)\langle P_2\rangle\right]}{3k_{\beta}T} \right) \tag{6.1}$$

$$\epsilon_{\perp} - 1 = 4\pi N h F \left(\overline{\alpha} - \frac{1}{3}\Delta\alpha\langle P_2\rangle + \frac{F\mu^2\left[1+\frac{1}{2}\left(1-3\cos^2\beta\right)\langle P_2\rangle\right]}{3k_{\beta}T} \right) \tag{6.2}$$

$$\epsilon_{iso} = 1 + 4\pi N h F \left(\alpha_{iso} + \frac{F\mu^2}{3k_{\beta}T} \right) \tag{6.3}$$

$$\bar{\epsilon} = \frac{\epsilon_{\parallel} + 2\epsilon_{\perp}}{3} = 1 + 4\pi N h F \left(\overline{\alpha} + \frac{F\mu^2}{3k_{\beta}T} \right) \tag{6.4}$$

where N is the molecular number density, $N = \rho\frac{N_A}{M}$, ρ is the mass density, N_A the Avogadro's number, M is the molecular weight, k_{β} = Boltzmann constant, $\overline{\alpha}$ is the mean polarizability and $\Delta\alpha$ is the polarizability anisotropy.

The reaction field factor $F = \frac{1}{1-\overline{\alpha}f}$ with $f = \frac{4\pi}{3}N\frac{2\bar{\epsilon}-2}{2\bar{\epsilon}+1}$ is the Onsager factor and cavity field factor $h = \frac{3\bar{\epsilon}}{2\bar{\epsilon}+1}$.

Using the experimentally observed $\epsilon_{\parallel}$ and $\epsilon_{\perp}$ data, the values of the effective molecular dipole moments in the mesomorphic phases as well as their inclination angles (β) with the molecular long axes of all the mixtures, have been calculated using equations 6.1 and 6.2. The order parameter $\langle P_2\rangle$, average molecular polarizability ($\bar{\alpha}$) and polarizability anisotropy ($\Delta\alpha$), calculated from the measured values of the refractive indices and densities (from chapter 4, 5) were used in this calculation. It has been found that the free molecular dipole

moments (μ_m) for the pure compounds are greater than the effective dipole moments (μ_{eff}) calculated from equations 2.9 and 2.10 (chapter 2). For 9CN, μ_m and μ_{eff} values at 30°C are 6.62D and 5.28D respectively whereas for 7CPB these values are 6.75D and 5.38D (extrapolated value) respectively. For all the mixtures and pure compounds, the μ_{eff} values increases with increase in temperature. This may be due to the fact that with increase in temperature, the number of homo and hetero dimers (in mixtures) decreases thereby affecting a rise in the effective dipole moment of the binary system.

A typical temperature dependence of the effective molecular dipole moment of a mixture ($x_{9.\,CN}$ = 0.827) is shown in figure 6.5. The μ_{eff} values are found to increase from 5.54D at 30°C to 6.44D at 82°C. Moreover, μ_{eff} in the smectic A_d phase are seen to be slightly smaller than those obtained by extrapolation from either the nematic or re-entrant nematic phases. However, the maximum deviation (≈0.5 %) is found near the middle of the Sm A_d phase. The lower effective dipole moment in the smectic A_d phase implies the development of additional anti-parallel ordering of the molecular dipoles in the induced smectic phase. However hetero dimers may also form which may also influence the lowering of the dipole moment in the smectic phase. Therefore, it is obvious to assume that the dimer type associations on the molecular level are responsible for both the induced smectic and re-entrant nematic phases.

According to Cladis [3], the re-entrant phenomenon in cyano compounds is due to the sensitive balance between dipolar and steric forces. When dipolar forces dominate, re-entrance from frustration is obtained, but when steric forces dominate, other types of re-entrant phenomena occur. The former mechanism is dominant in terminal cyano compounds. As the molecules form dimers, they are assumed to become somewhat bulgy in the middle due to the presence of rigid aromatic core. Once the Sm A_d phase is formed, the bulgy parts line up in a plane while the alkyl chains cannot fill the rest of the space. As the temperature decreases, the dimer population increases and additionally due to the stiffening of the terminal alkyl chains, the packing becomes unfavourable so that the Sm A_d phase becomes unstable and re-entrant nematic phase appears. The results obtained from dielectric measurements in this work also seem to support this model. Figure 6.6 shows μ_{eff} as a function of mole fraction of 9.CN at T=55°C, a temperature at which the mixtures $x_{9.\,CN}$ = 0.559, 0.662, 0.774, 0.827 have

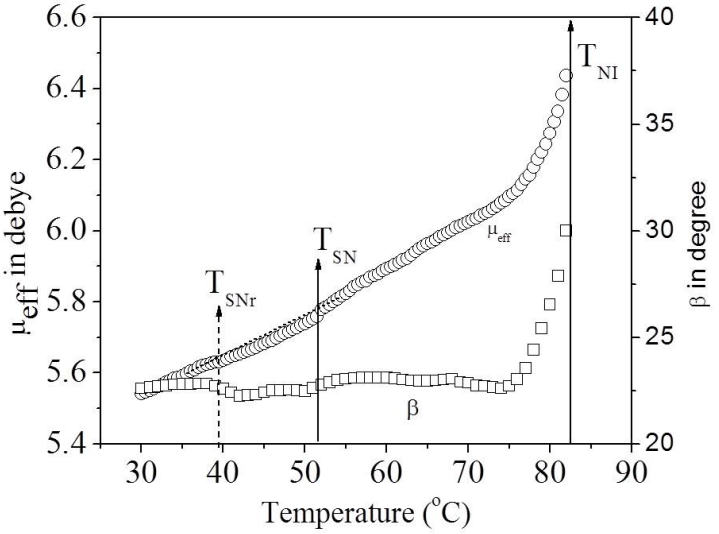

Figure 6.5: Temperature dependence of effective molecular dipole moment (μ_{eff}) and the effective angle of inclination β of a mixture $x_{9.\,CN}$ = 0.827.

smectic phase. In the concentration range $x_{9.\,CN} > 0.4$ to $x_{9.\,CN} < 0.88$, μ_{eff} exhibits a broad minima near x = 0.7. From x = 0 to x = 0.4 the μ_{eff} values are more or less constant. However, for $x_{9.\,CN} > 0.88$ this value decrease with molar concentration.

Figure 6.7 shows the concentration variation of the effective angle of inclination β at T = 55°C. In 7CPB and 9.CN the molecular dipoles on the average were found to be inclined to the molecular long axis at an angle (β) of about 30° and 24° respectively. In mixtures, the calculated β values are found to decrease on increasing the molar concentration of 9.CN and shows almost linear concentration dependence in the range $0.2 < x_{9.\,CN} < 0.827$.

Another interesting feature of this system is the existence of the nematic isotropic co-existing region, in the vicinity of which pretransitional effects are clearly visible. However, the mean field approach adopted in this chapter cannot account for these pretransitional effects. Recently a number of attempts have been made [30, 39–46] to study the pretransitional effects at the nematic-isotropic phase transitions and similar study is expected to yield interesting result.

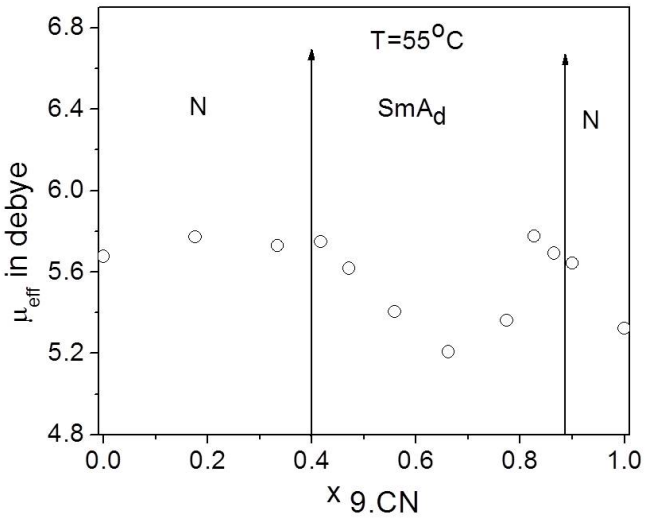

Figure 6.6: The effective dipole moment (μ_{eff}) plotted against mole fraction (x) at a temperature T=55°C.

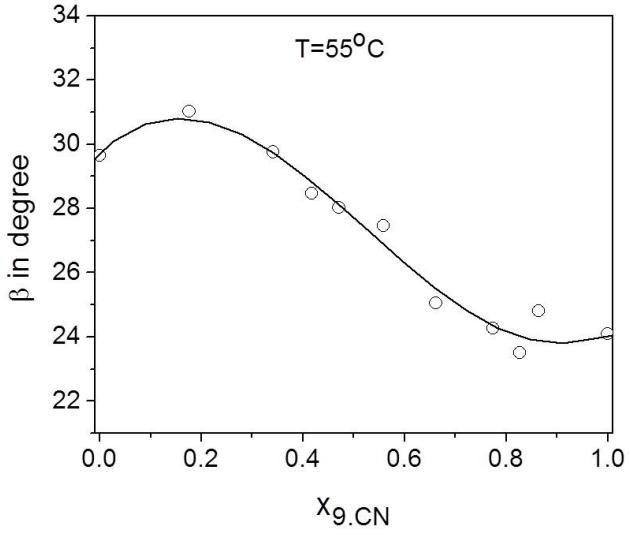

Figure 6.7: Variation of the effective angle of inclination β with mole fraction of 9.CN at a temperature T=55°C.

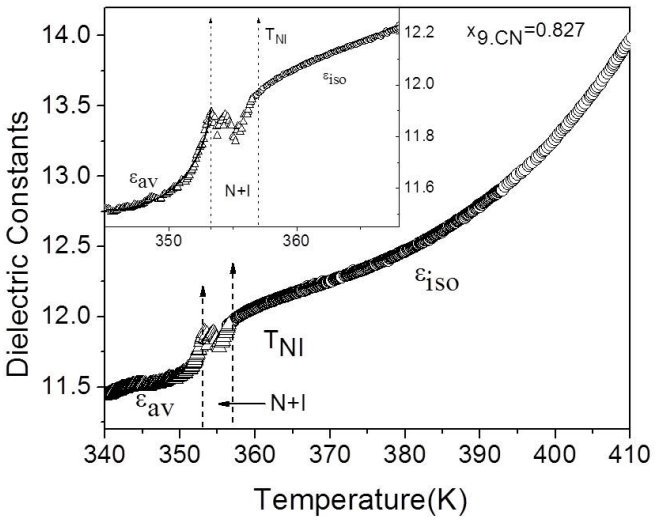

Figure 6.8: Temperature variation of ϵ_{iso} and ϵ_{av} for the mixture $x_{9.\,CN}$ = 0.827. The solid line in the inset represents ϵ_{av} value in the nematic phase fitted by equation (6.5).

For calamatic molecules having a permanent dipole moment approximately parallel to its long axis [48], the pretransitional effect can be described by:

$$\epsilon_{av} = \epsilon^{**} + a_T^- \left(T^{**} - T\right) + A_T^- \left(T^{**} - T\right)^{1-\alpha'} \tag{6.5}$$

for $T < T_{NI} = T^{**} - \Delta T$

$$\epsilon_{iso} = \epsilon^{*} + a_T^+ \left(T - T^{*}\right) + A_T^+ \left(T - T^{*}\right)^{1-\alpha'} \tag{6.6}$$

for $T > T_{NI} = T^{**} + \Delta T$

where T^{**} denotes the temperature at which the N–I transition would occur coming from the nematic phase if it were second order and T^* has the same meaning when temperature decreases from the isotropic phase. ϵ_{iso} is the value of the permittivity in the isotropic phase and ϵ_{av} is the mean value of the permittivity below the isotropic–nematic transition. ϵ^{**} and ϵ^* are the values of ϵ_{av} and ϵ_{iso} at temperatures T^{**} and T^* respectively [45]. ΔT is about 1 degree, a_T and A_T are amplitudes and α' is the critical exponent (similar to specific heat critical exponent, which is normally represented as α in the literature. However, in

order to avoid the confusion between the parameter α in the McMillan potential and the critical exponent, the latter has been written as α' in this dissertation.).

For the mixture $x_{9.\,CN}$ = 0.827, the dielectric permittivity value was measured up to $T - T_{NI}$ =55°C, the result of which is shown in figure 6.8. It is clearly visible that as one approaches the clearing temperature from the isotropic phase, the value of ϵ_{iso} decreases gradually and near the transition ϵ_{iso} varies almost linearly. This behavior differs from the reported data of 6OCB, 7OCB [39], HCCP, 8CB, 5CB, mixture 5CB+MBBA [30, 40] and 9CB [43]. However, it is to be noted that these reported values of ϵ_{iso} were measured at a frequency of 10 kHz or more. An attempt was made to fit the ϵ_{av} values to equation 6.5 and ϵ_{iso} to equation 6.6.

Table 6.1: Results of the fitting for the N-I transition of the mixture $x_{9.\,CN}$ = 0.827 for 10kHz.

Parameter	Value±error
ϵ^{**}	12.01±0.02
$a_T^-(K^{-1})$	0.075±0.015
$A_T^-(K^{-1})$	-0.34±0.01
T^{**}	353.4 ± 0.3
α'	0.45 ±0.05

Parameter	Value±error
ϵ^{*}	11.23±0.02
$a_T^+(K^{-1})$	-0.053±0.003
$A_T^+(K^{-1})$	0.23±0.01
T^{*}	355.5± 0.002
α'	0.505 ± 0.03

From figure 6.8 one observes that the average dielectric permittivity in the nematic phase could be described by equation 6.5 with $\epsilon^{**} = 12.01 \pm 0.02$, $a_T^-(K^{-1}) = 0.075 \pm 0.015$, $A_T^-(K^{-1}) = -0.34 \pm 0.01$, $T^{**} = 353.4 \pm 0.3K$ and $\alpha' = 0.45 \pm 0.05$ (table 6.1). The values of ϵ_{iso} for the mixture $x_{9.\,CN}$ = 0.827 obtained at a frequency of 1 kHz and 10 kHz are shown in figure 6.9. For frequency 1 kHz, ϵ_{iso} could not be described by equation 6.5 except for the unjustifiable value of $\alpha' = -2.70$. However, for measurements at 10 kHz, the experimental data for ϵ_{iso} fitted well with the following values of the parameters $\epsilon^* = 11.23 \pm 0.02$, $a_T^+ = -0.053 \pm 0.003$, $A_T^+ = 0.23 \pm 0.01$, $T^* = 355.5 \pm 0.002$K and $\alpha' = 0.505 \pm 0.03$, as indicated in table 6.1.

Also, one finds that the ϵ_{iso} values at 10 kHz presented here are in good agreement with those reported in the literature [30, 39, 40, 43]. In both the cases (ϵ_{iso},ϵ_{av}), within the limits of experimental errors, nearly same value of the exponent $\alpha' \approx 0.5$ have been obtained. The value of the critical exponent α' obtained

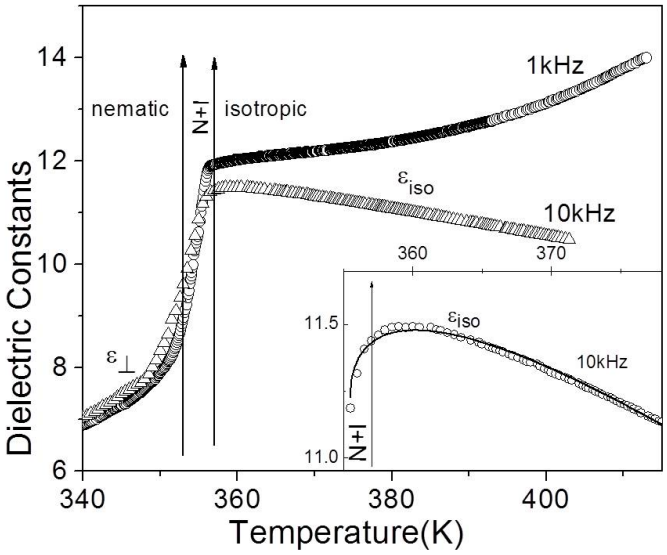

Figure 6.9: Temperature variation of dielectric constant ($x_{9.\,CN}$ = 0.827) at 1 kHz and 10 kHz. The solid line in the inset represents ϵ_{iso} values in the isotropic phase fitted by equation 6.6.

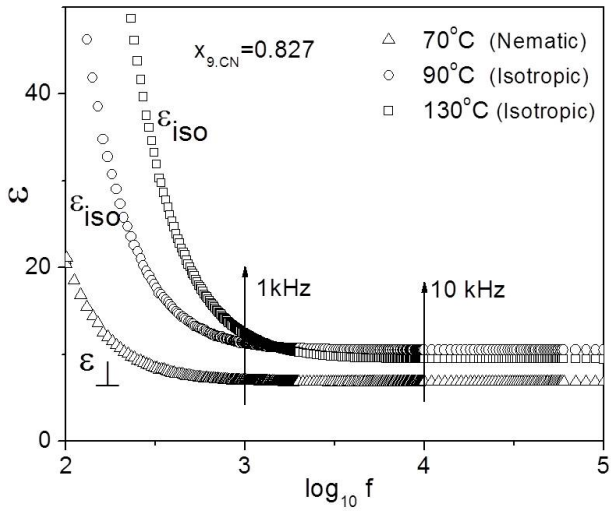

Figure 6.10: Frequency variation of dielectric permittivity $\epsilon_{\perp}$ and ϵ_{iso} in the nematic and isotropic phases respectively of $x_{9.\,CN}$ = 0.827.

corresponds to the tricritical hypothesis of the I–N transition. However, the difference between the temperature variations of ϵ_{iso} obtained at two different frequencies could possibly be due to the ionic effects whose contribution increases in the isotropic phase with increase in temperature at 1 kHz. However, at the same frequency, the ionic effects are negligibly small in the mesogenic phases as visible from figure 6.10 and the measured values of dielectric constants agree for both the frequencies.

6.3 Conclusion

The static dielectric permittivity of two nematogenic compounds and their binary mixtures at ten different compositions have been determined throughout their mesomorphic range. The temperature variation of the dielectric permittivity at the nematic – smectic A_d and smectic A_d – re-entrant nematic transition for all the mixtures has been found to be continuous. In the case of mixture with $x_{9.\,CN}$ = 0.662, the parallel component of the dielectric permittivity shows a pronounced decrease in the Sm A_d phase due to dipole-dipole correlation. This behaviour is also observed in other mixtures, including the purely nematic ones, but on a reduced scale. The maximum decrease is found for mixtures situated near the middle of the Sm A_d island. The effective values of the dipole moments in the mixtures are found to be less than the values observed in the pure compounds. The effective molecular dipole moments are found to increase with increase in temperature. Moreover, μ_{eff} in the smectic A_d phase is found to be slightly smaller than those obtained by extrapolation from either the nematic or re-entrant nematic phases. The lower effective dipole moment in the smectic A_d phase implies the development of additional anti-parallel ordering of the molecular dipoles in the induced smectic phase, in conformity with the model proposed by Cladis. For the average value of the nematic permittivity, ϵ_{av}, as well as the isotropic permittivity ϵ_{iso}, the value of the critical exponent α' is nearly the same (≈ 0.5) which corresponds to the tricritical behaviour of the I–N transition.

References

[1] C. S. Oh, *Mol. Cryst. Liq. Cryst.*, **42**, 1 (1977).

[2] D. A. Dunmur, R. G. Walker and P. Palffy-Muhoray, *Mol. Cryst. Liq. Cryst.*, **122**, 321 (1985).

[3] P. E. Cladis, *Mol. Cryst. Liq. Cryst.*, **67**, 177 (1981).

[4] M. K. Das and R. Paul, *Phase Transitions*, **46**, 185 (1994).

[5] M. K. Das, R. Paul and D. A. Dunmur, *Mol. Cryst. Liq. Cryst.*, **285**, 239 (1995).

[6] M. Brodzik and R. Dabrowski, *Mol. Cryst. Liq. Cryst.*, **260**, 361 (1995).

[7] S. Garg and T. Spears, *Mol. Cryst. Liq. Cryst.*, **409**, 335 (2004).

[8] R. Dabrowski and K. Czuprynski, *Modern Topics in Liquid Crystal, from Neutron Scattering to Ferroelecricity*, Ed. Agnes Buka, London: World Scientific (1993).

[9] P. D. Roy, S. Paul and M. K. Das, *Phase Transitions* **79**, 323 (2006).

[10] P. D. Roy, A. Prasad and M. K. Das, *J. Phys.: Condens. Matter*, **21**, 075106 (2009).

[11] M. Brodzik and R. Dabrowski, *Liq. Cryst.*, **18**, 61 (1995).

[12] M. Tykarska, B. Wazynska and I. Ulbin, *Proc. of SPIE*, Vol. **4147** p 55 (2000).

[13] S. Wrobel, M. Brodzik, R. Dabrowski, B. Gestblom, H. Hasse and S. Hiller, *Mol. Cryst. Liq. Cryst.* **302**, 223 (1997).

[14] G. Pelzl, I. Latif, S. Diele, M. Novak, D. Demus and H. Sackmann, *Mol. Cryst. Liq. Cryst.*, **139**, 333 (1986).

[15] A. N. Berker and J. S. Walker, *Phys. Rev. Lett.*, **47** (20), 1469 (1981).

[16] J. O. Indekeu and A. N. Berker, *Phys. Rev. A*, **33** (2), 1158 (1986).

[17] J. F. Marko, J. O. Indekeu and A. N. Berker, *Phys. Rev. A*, **39** (8), 4201 (1989).

[18] W. L. McMillan, *Phys. Rev. A*, **4**, 1238 (1971).

[19] W. L. McMillan, *Phys. Rev. A*, **6**, 936 (1972).

[20] G. R. Luckhurst and B. A. Timimi, *Mol. Cryst. Liq. Cryst.*, **64**, 253 (1981).

[21] A. Prasad and M. K. Das, *Phase Transitions*, **82**, 780 (2009).

[22] A. Prasad and M. K. Das, *Phase Transitions*, **83**, 1072 (2010).

[23] A. Prasad and M. K. Das, *J. Phys.: Condens. Matter*, **22**, 195106 (2010).

[24] E. A. Guggenheim, *Trans. Faraday Soc.*, **45**, 714 (1949).

[25] W. Maier and G. Meier, *Z. Naturforsch.*, **16a**, 262 (1961).

[26] L. Onsager, *Chem. J. Am. Soc.*, **58**, 1486 (1936).

[27] J. J. P. Stewart, *MOPAC 2009*, Stewart Computational Chemistry, Colorado Springs, Co, USA. **http://OpenMOPAC.net** (2008).

[28] H. Ma, R. Z. Sun, Z. X. Li, *Chin. Phys. B*, **15**, 1009 (2006).

[29] J. Malecki and J. Ziolo, *Chem. Phys.*, **35**, 187 (1987).

[30] A. Drozd-Rzoska, S. J. Rzoska, and J. Ziolo, *Phys. Rev. E*, **54**, 6452 (1996).

[31] T. D. Gierke and W. H. Flygare, *J. Chem. Phys.*, **61**, 2231 (1974).

[32] J. D. Litster and T. W. Stinson III, *J. Appl. Phys.*, **41**, 996 (1970).

[33] J. C. Filippini and Y. Poggi, *Phys. Lett. A*, **65**, 30 (1978).

[34] B. Cabane and G. Clarke, *Phys. Rev. Lett.*, **25**, 91 (1970).

[35] S. Gosh, E. Tettamanti, and E. Indovina, *Phys. Rev. Lett.*, **29**, 638 (1973).

[36] T. W. Stinson III and J. D. Litster, *Phys. Rev. Lett.*, **25**, 503 (1970).

[37] F. W. Deeg, S. R. Greenfield, J. J. Stankus, V. J. Newell, and M. D. Fayer, *J. Chem. Phys.*, **93**, 3503 (1990).

[38] J. J. Stankus, R. Torre, C. D. Marshal, S. R. Greenfield, A. Sengupta, and M. D. Fayer, *Chem. Phys. Lett.*, **194**, 213 (1992).

[39] S. J. Rzoska, J. Ziolo, W. Sulkoski, J. Jadzyn and G. Czechowski, *Phys. Rev. E.*, **64**, 052701 (2001).

[40] A. Drozd- Rzoska, S. J. Rzoska, *Pretransitional behavior near the isotropic–nematic phase transition: Phase Transition. Application to liquid crystal, Organic Electronics and Optoelectronics*, Ed. Vlad Popa-Nita, Research Signpost, Kerala, (2006).

[41] M. Ginovska, H. Kresse, D. Bauman, G. Czechowski and J. Jadzyn, *Phys. Rev. E*, **69**, 022701 (2004).

[42] J. Jadzyn, G. Czechowski and M. Ginovska, *Phys. Rev. E*, **71**, 052702 (2005).

[43] J. Jadzyn, G. Czechowski and J. -L. Dejardin, *J. Phys.: Condens. Matter*, **18**, 1839 (2006).

[44] J. Jadzyn, G. Czechowski, C. Legrand and R. Douali, *Phys. Rev. E*, **67**, 041705 (2003).

[45] P. Cusmin, M. R. de la Fuente, J. Salud, M. A. Perez-Jubindo, S. Diez-Berart and D. O. Lopez, *J. Phys. Chem. B*, **111**, 8974 (2007).

[46] B. Van Roie, J. leys, K. Denoif, C. Glorieux, G. Pitsi and J. Thoen, *Phys. Rev. E*, **72**, 041702 (2005).

[47] B. R. Ratna, R. Shashidhar, M. Bock, A. Gobl-Wunsch and G. Heppke, *Mol. Cryst. Liq. Cryst.*, **99**, 285 (1983).

[48] S. J. Rzoska, P. K. Mukherjee and M. Rutkowska, *J. Phys.: Condens. Matter*, **24**, 375101 (2006).

Chapter 7

Determination of elastic constants and rotational viscosity of a binary system (7CPB+9.CN) showing nematic, induced smectic A_d and re-entrant nematic phases

7.1 Introduction

The most important application of liquid crystals is in the field of display devices. The usefulness of these materials in display devices depends, among other things, on its elastic and viscous properties. These properties are related to the switching behaviour of the liquid crystal molecules in presence of an external field and they control parameters like steepness of the transmission-voltage curve, response time, controlling voltage, etc. [1].

The elastic constants of a liquid crystalline medium are basically related to restoring torques and Frank [2] has shown that an arbitrary deformation state can be described by three elastic coefficients: splay (K_{11}), twist (K_{22}) and bend (K_{33}), which are collectively known as the Frank elastic constants. A brief introduction about the elastic constants of liquid crystals has been given in chapter 2 of this thesis.

Depending upon the relative orientation of the director and the flow direction, five anisotropic viscosity coefficients may result, of which three are shear viscosities (Miesowicz viscosities η_i, i =1 - 3). The other two account for the director rotation (γ_1) and coupling between the director and flow pattern (η_{12}) [3].

These properties are also important from a fundamental science point of view as they offer valuable insight into the molecular interactions and phase transitions. One of the first studies ever done on a re-entrant system was the measurement of the bend elastic constant of a binary mixture of HBAB (p-[(p-hexyloxybenzylidene)-amino]) and CBOOA (n-p-cyanobenzylidene-p-n-octyloxyaniline) by P. E. Cladis [4]. However, studies of the visco-elastic properties for systems in which the induced smectic and re-entrant nematic phases occur seem to be scanty [4–9]. Moreover, I am not aware of any rotational viscosity (γ_1) measurement in binary systems where the induced smectic and re-entrant nematic phases are simultaneously present. Again, activation energy measurements in the high temperature normal nematic phase and in the low temperature re-entrant nematic phase as determined from dielectric and NMR measurements have been found to give contradictory results [10, 11]. Therefore, the viscosity data on this system (7CPB+9.CN) may be utilized to comment on this discrepancy.

Determination of rotational viscosity requires measurement of the splay elastic constant (K_{11}) and relaxation time (τ_0) of the liquid crystalline material. The relaxation time has been measured by optical phase-decay-time measurement method [12–17]. Splay elastic constant has been determined from electric field induced Freedericksz transition [18–21]. For the analysis of splay elastic constant, dielectric anisotropy data of this system as reported in chapter 6 has been used. Moreover, for the determination of relaxation time by optical method, the optical phase retardation of the sample filled cell is required which has been obtained from optical birefringence measurements as reported in chapter 5.

In this chapter, I report the temperature variation of the splay and bend elastic constants, measured by electric field induced Freedericksz transition method. The results of the rotational viscosity measurements determined from relaxation method have also been presented.

7.2 Measurement of splay and bend elastic constants.

The splay elastic constant was determined from electric field induced Freedericksz transition using the well known equation

$$K_{11} = \frac{\epsilon_0 \Delta\epsilon V_{th}^2}{\pi^2} \tag{7.1}$$

where ϵ_0 is the permittivity of free space and V_{th} is the critical voltage in r.m.s. To determine the critical voltage (V_{th}) and the bend elastic constant, capacitance method was used, where the voltage (V) dependence of the capacitance (C) of a planar ITO coated liquid crystal cell filled with the sample under investigation was determined. The experimental details have been discussed in chapter 2. Gruler *et. al.* [18] have reported the relation between applied voltage and capacitance, using which the bend elastic constant K_{33} could be obtained by multi parameter fitting of the experimental C(V) values. Uchida *et. al.* [22] developed a method in which the multi parameter fit was not required. The voltage dependence of capacitance can be expressed as [9, 22–24]

$$\frac{C(V)-C_\perp}{C_\perp} = \gamma - \frac{2\gamma}{\pi}\frac{V_{th}}{V}\sqrt{1+\gamma\sin^2\phi_m} \quad \times \int_0^{\phi_m}\left[\frac{\left(1+\chi\sin^2\phi\right)\left(1-\sin^2\phi\right)}{\left(1+\gamma\sin^2\phi\right)\left(\sin^2\phi_m-\sin^2\phi\right)}\right]^{1/2}\cos\phi d\phi \tag{7.2}$$

where, $\chi = K_{33}/K_{11} - 1$, $\gamma = \epsilon_\parallel/\epsilon_\perp - 1$, ϕ is the tilt angle between the director $\hat{n}$ and the cell wall and ϕ_m is the tilt angle at the centre of the cell and $C_\perp$ is the capacitance of the cell when the liquid crystal molecules are homogeneously aligned.

If the applied voltage is greater than the threshold value then the director at the centre of the cell becomes perpendicular to the cell walls and $\phi_m = \pi/2$. Equation 7.2 then reduces to

$$\frac{C(V)-C_\perp}{C_\perp} = \gamma - \frac{2\gamma}{\pi}\frac{V_{th}}{V}\sqrt{1+\gamma}\int_0^{\pi/2}\left[\frac{\left(1+\chi\sin^2\phi\right)}{\left(1+\gamma\sin^2\phi\right)}\right]^{1/2}\cos\phi d\phi \tag{7.3}$$

For $V \gg V_{th}$, $\frac{C(V)-C_\perp}{C_\perp}$ vs. 1/V curve should be linear with a slope

$$\alpha = \frac{2\gamma V_{th}}{\pi}\sqrt{1+\gamma}\int_0^{\pi/2}\left[\frac{(1+\chi\sin^2\phi)}{(1+\gamma\sin^2\phi)}\right]^{1/2}\cos\phi d\phi \tag{7.4}$$

and intercept on the $\frac{C(V)-C_\perp}{C_\perp}$ axis is $\gamma = \frac{\Delta\epsilon}{\epsilon_\perp}$

The expression for α in equation 7.4 contains only one unknown quantity, $\chi = K_{33}/K_{11} - 1$ and hence, the K_{33} can be determined if K_{11} is known.

Freedericksz transition is generally not observed in the smectic A phase [9]. However in the binary mixtures of 7CPB+9.CN, Freedericksz transition could be induced by the application of an electric field of appropriate strength. Hence, the splay elastic constant K_{11} could be measured throughout the temperature and concentration range.

The variation of capacitance with voltage for different temperatures, for

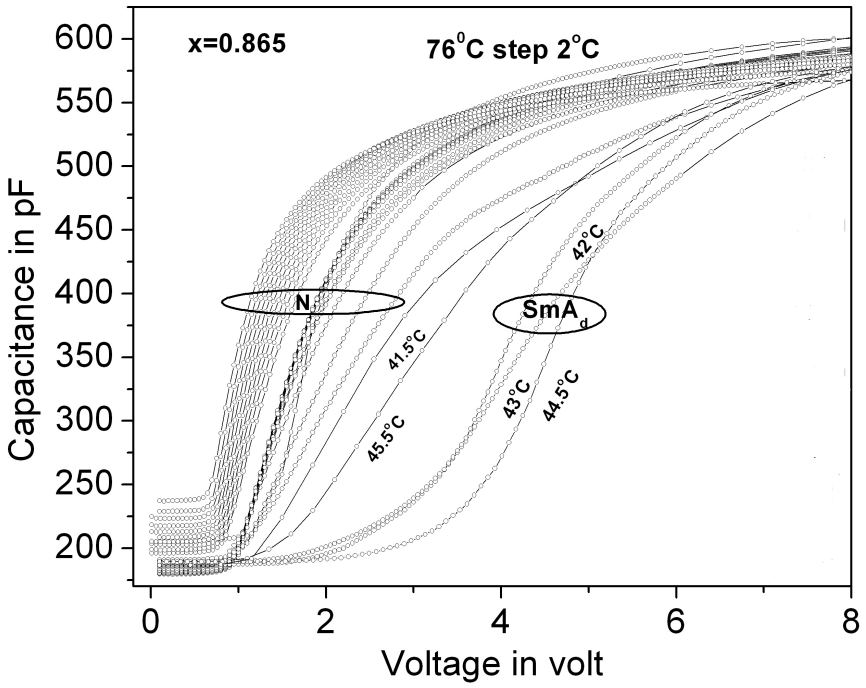

Figure 7.1: Voltage dependence of the capacitance of the planar cell at different temperatures for $x_{9.\,CN}$ = 0.865.

mixture $x_{9.\,CN}$ = 0.865 are presented in figure 7.1. From figure 7.1, it is observed that the Freedericksz transition in the nematic as well as re-entrant nematic phases are observed at a threshold voltage V_{th} of about 1V, and the threshold value depends only slightly on temperature up to the smectic phase. In smectic A_d phase, the Freedericksz transition appears for much higher voltage and the threshold voltage depends strongly on temperature.

In figure 7.2a the temperature dependence of the ratio of the bend and splay elastic constant (K_{33}/K_{11}) for the pure compound 9.CN has been plotted. Figure 7.2b shows the values of the splay and bend elastic constants for the same compound. The splay and bend elastic constants and their ratio (K_{33}/K_{11}) shows a normal temperature dependence for the pure compound 9.CN. Both the splay and the bend elastic constant increases with the decrease in temperature and their values vary from about 4-9 pN and 6-19 pN respectively, the K_{33} value being more than the value of K_{11}.

The nematic phase is the only liquid crystalline phase exhibited by the mixture $x_{9.\,CN}$ = 0.9 and it lies very close to the induced smectic A_d island in the phase diagram. The temperature variation of the ratio K_{33}/K_{11} and the individual values of the two elastic constants for this mixture have been shown in figures 7.3a and 7.3b respectively. The K_{33}/K_{11} values increase with decrease of temperature, as expected, but around $40°C$ this value drops down and decreases quite rapidly with change of temperature. The reason for this deviation from the normal behavior is the formation of smectic like clusters in the mixture, which are not sufficiently strong enough to induce the smectic phase but their presence is reflected in the temperature dependence of the bend elastic constant.

The mixtures $x_{9.\,CN}$ = 0.347 and $x_{9.\,CN}$ = 0.176 also do not show induced smectic phase and their behavior is similar to that exhibited by $x_{9.\,CN}$ = 0.9. However, these mixtures are further away from the smectic island in the phase diagram and hence the effect is less prominent. The temperature variation of the ratio of the bend and splay elastic constants K_{33}/K_{11} for mixtures $x_{9.\,CN}$ = 0.347 and 0.176 are shown in figures 7.10a and 7.11a respectively. The individual values of the elastic constants K_{11} and K_{33} have been shown in figures 7.10b and 7.11b.

The mixtures $x_{9.\,CN}$ = 0.865, 0.827, 0.774, 0.662, 0.559 and 0.471 exhibit

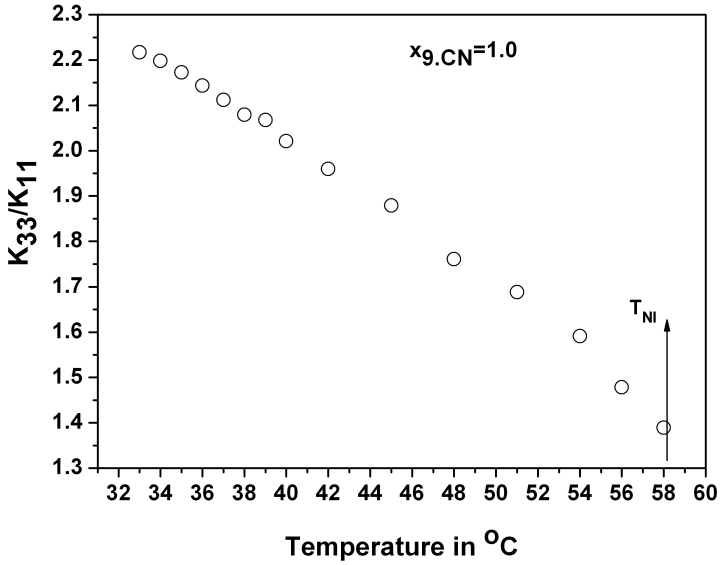

(a)

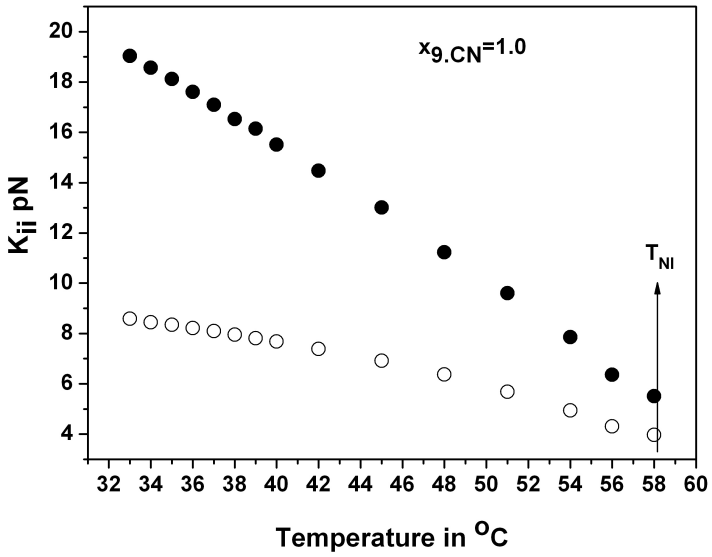

(b)

Figure 7.2: (a) Ratio of the bend (K_{33}) and splay (K_{11}) elastic constant. (b) ○ splay (K_{11}) and ● bend (K_{33}) elastic constant for the compound 9.CN.

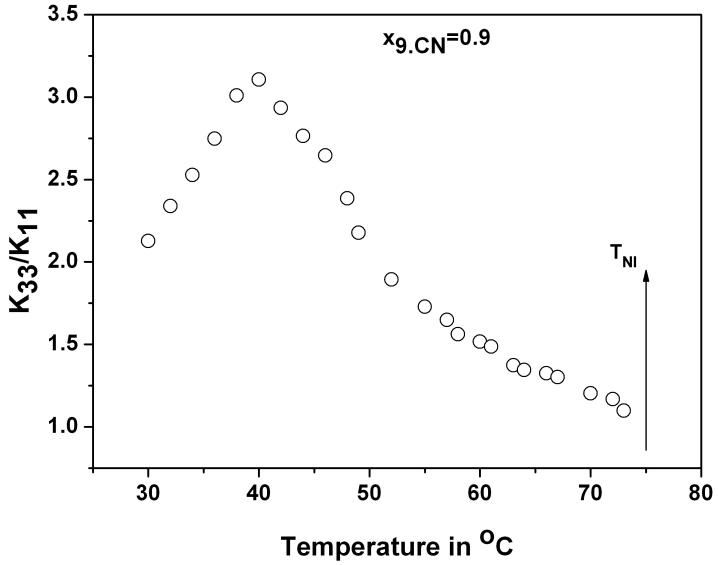

(a)

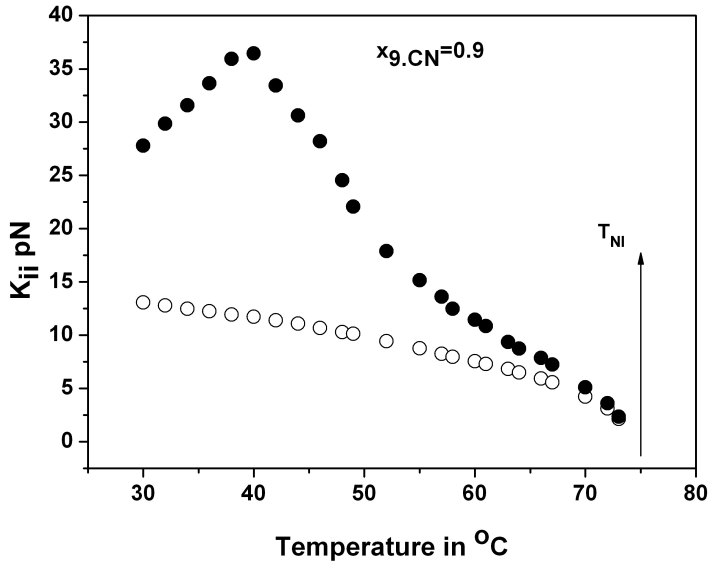

(b)

Figure 7.3: (a) Ratio of the bend (K_{33}) and splay (K_{11}) elastic constant. (b) ○ splay (K_{11}) and ● bend (K_{33}) elastic constant for mixture $x_{9.\,CN}$ = 0.9.

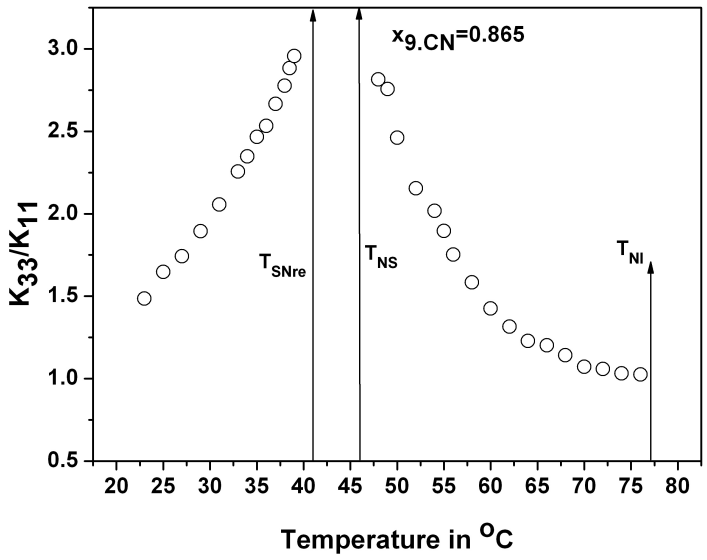

(a)

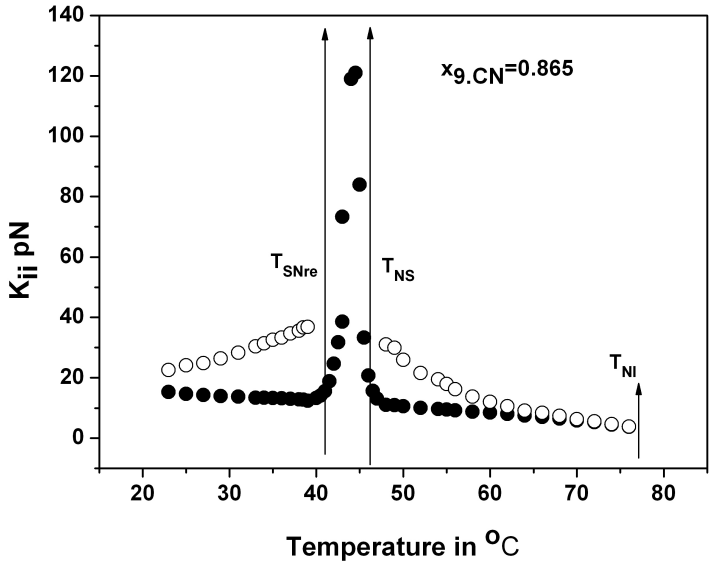

(b)

Figure 7.4: (a) Ratio of the bend (K_{33}) and splay (K_{11}) elastic constant. (b) ○ splay (K_{11}) and ● bend (K_{33}) elastic constant for mixture $x_{9.\,CN}$ = 0.865.

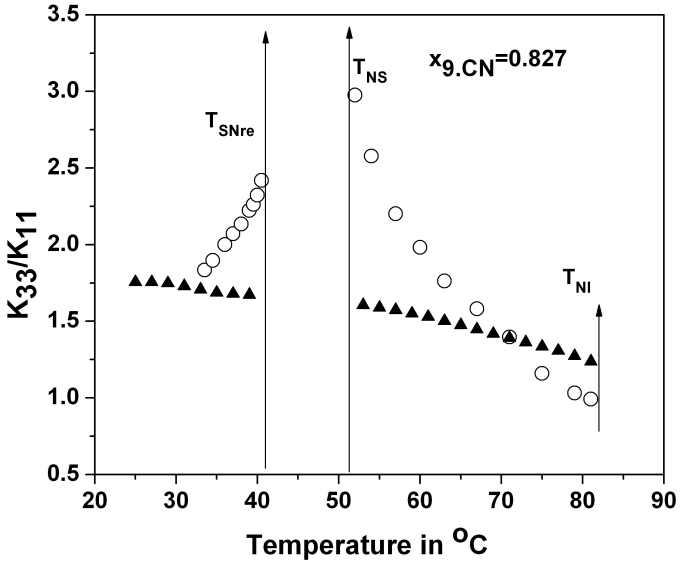

(a)

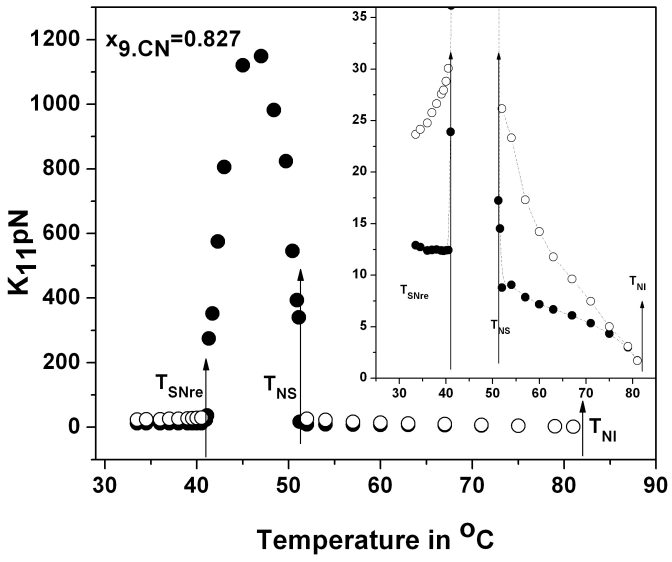

(b)

Figure 7.5: (a) Ratio of the bend (K_{33}) and splay (K_{11}) elastic constant, ▲ from Priest theory. (b) ○ splay (K_{11}) and ● bend (K_{33}) elastic constant for mixture $x_{9.\,CN}$ = 0.827.

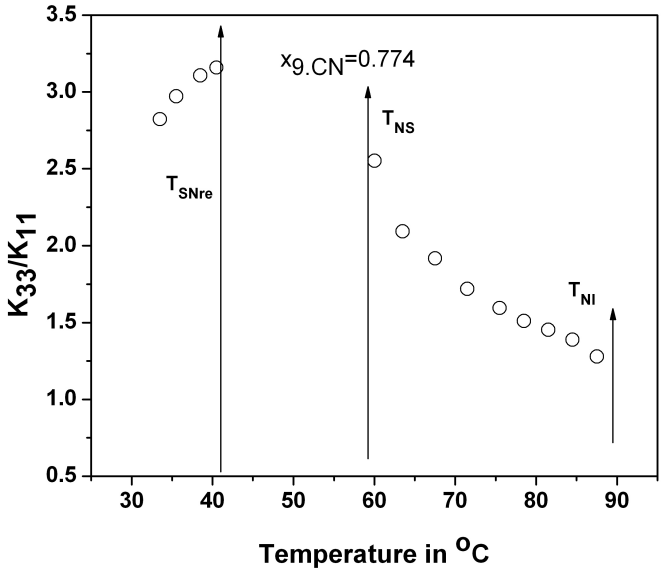

(a)

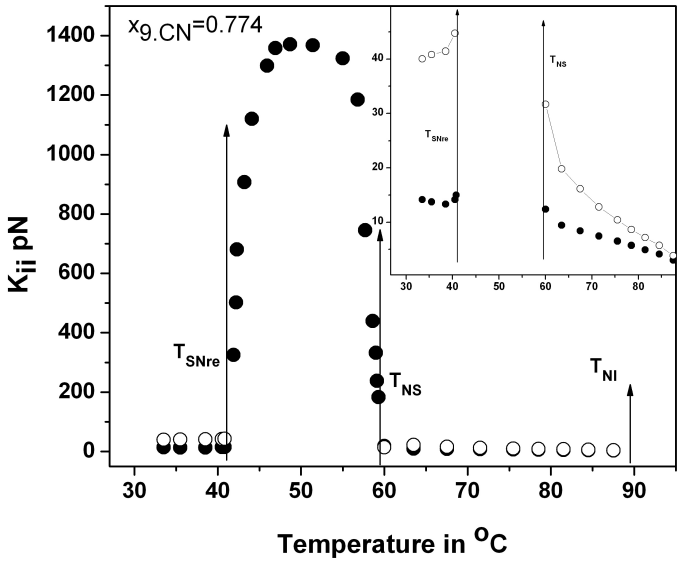

(b)

Figure 7.6: (a) Ratio of the bend (K_{33}) and splay (K_{11}) elastic constant. (b) ○ splay (K_{11}) and ● bend (K_{33}) elastic constant for mixture $x_{9.\,CN}$ = 0.774.

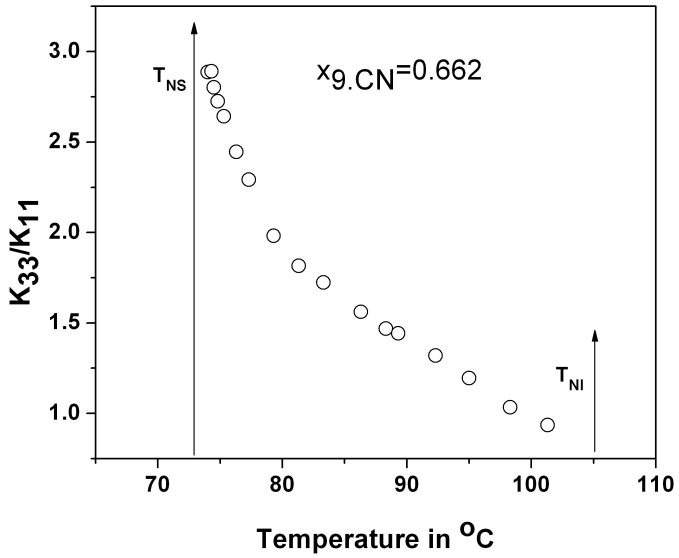

(a)

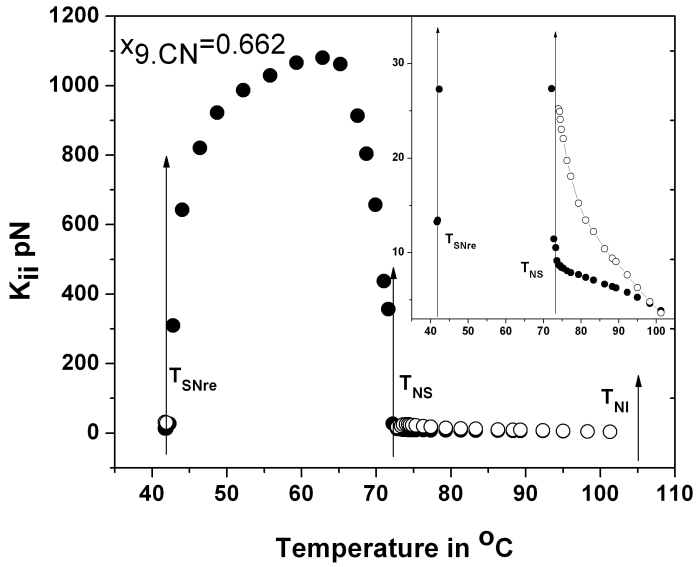

(b)

Figure 7.7: (a) Ratio of the bend (K_{33}) and splay (K_{11}) elastic constant. (b) ○ splay (K_{11}) and ● bend (K_{33}) elastic constant for mixture $x_{9.\,CN}$ = 0.662.

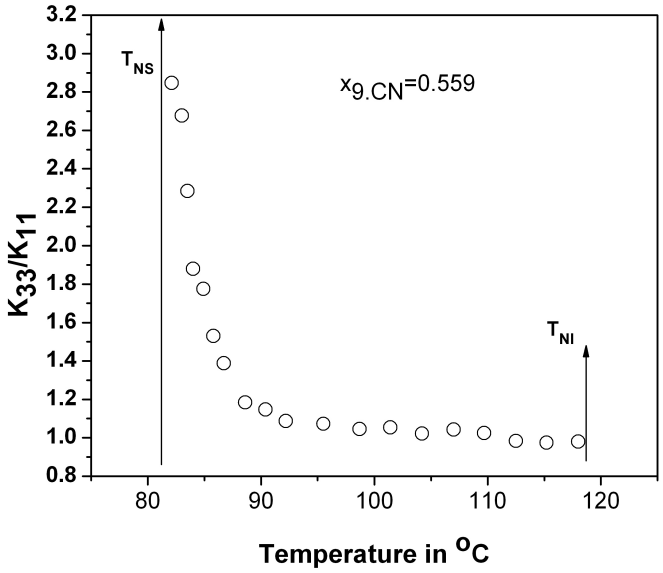

(a)

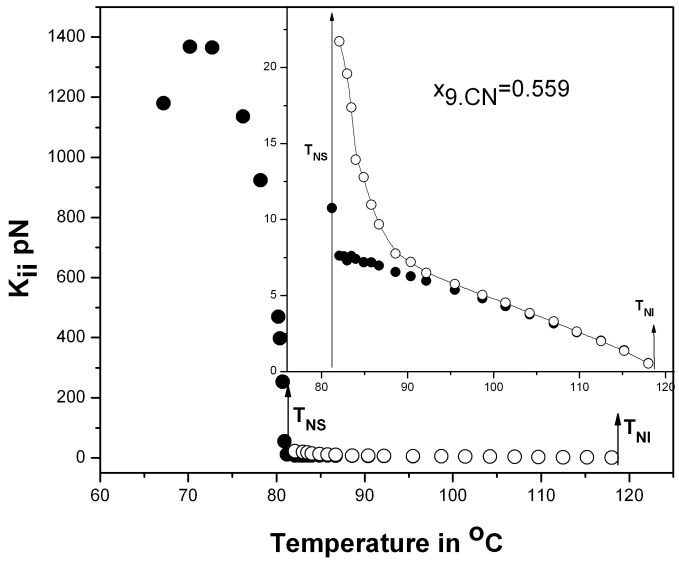

(b)

Figure 7.8: (a) Ratio of the bend (K_{33}) and splay (K_{11}) elastic constant. (b) ○ splay (K_{11}) and ● bend (K_{33}) elastic constant for mixture $x_{9.\,CN}$ = 0.559.

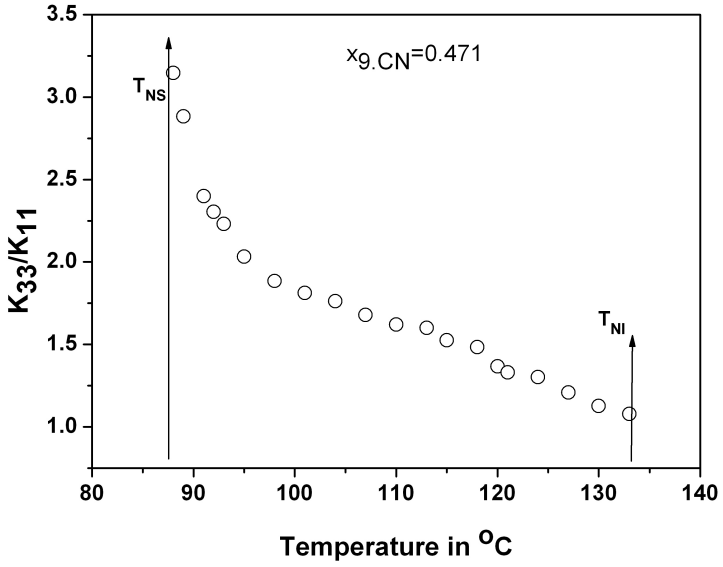

(a)

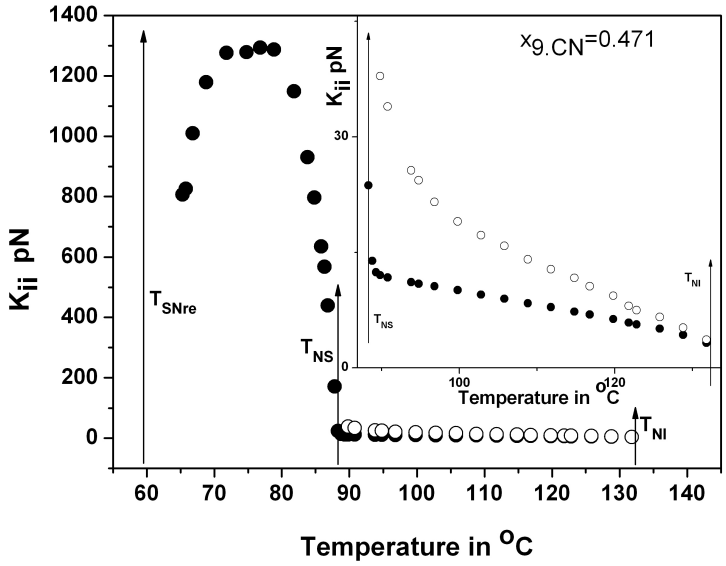

(b)

Figure 7.9: (a) Ratio of the bend (K_{33}) and splay (K_{11}) elastic constant. (b) ○ splay (K_{11}) and ● bend (K_{33}) elastic constant for mixture $x_{9.\,CN}$ = 0.471.

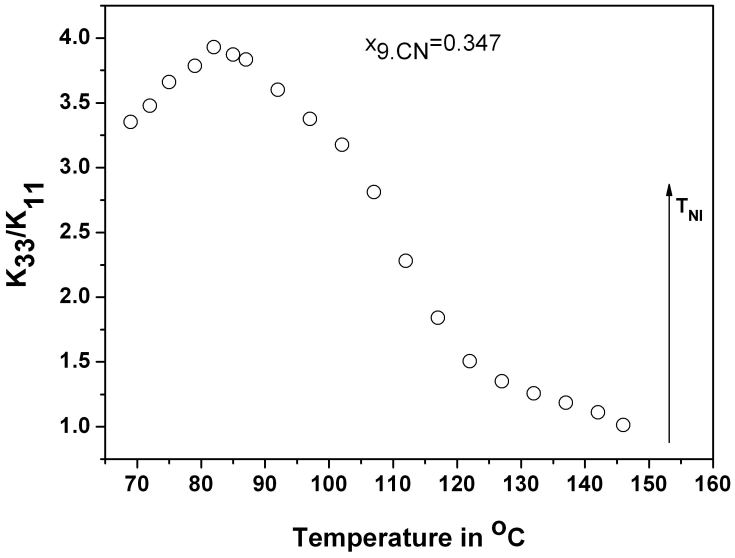

(a)

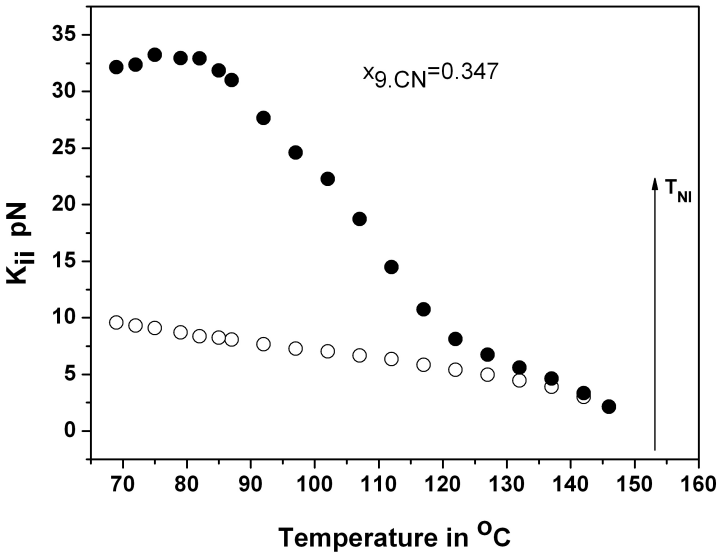

(b)

Figure 7.10: (a) Ratio of the bend (K_{33}) and splay (K_{11}) elastic constant. (b) ○ splay (K_{11}) and ● bend (K_{33}) elastic constant for mixture $x_{9.\,CN}$ = 0.347.

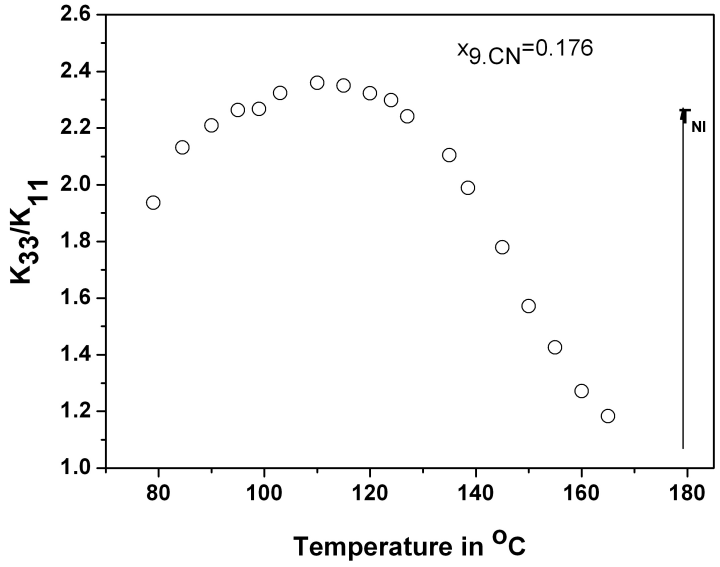

(a)

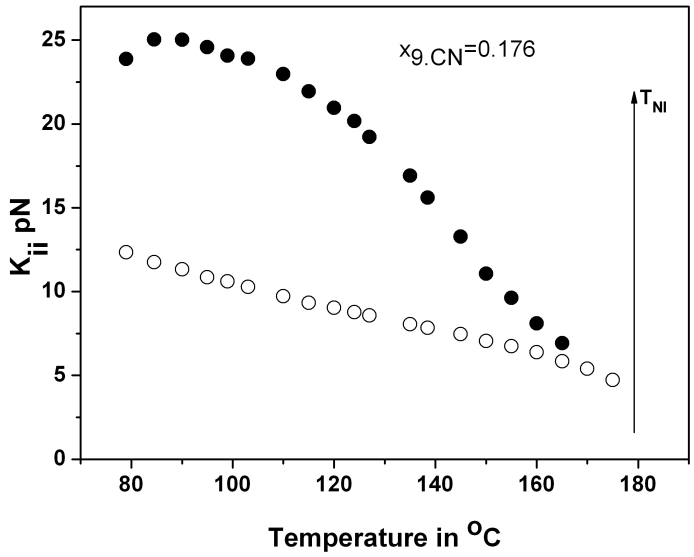

(b)

Figure 7.11: (a) Ratio of the bend (K_{33}) and splay (K_{11}) elastic constant. (b) ○ splay (K_{11}) and ● bend (K_{33}) elastic constant for mixture $x_{9.\,CN}$ = 0.176.

isotropic–nematic–induced smectic A_d –re-entrant phase sequence. The temperature variation of the splay elastic constants for these mixtures have been shown in figures 7.4b - 7.9b. For these mixtures it is observed that the splay elastic constant (K_{11}) increases with decrease in temperature, not only in the ordinary nematic phase but also in the re-entrant nematic phase. In both the nematic and re-entrant nematic phases, K_{11} has the same order of magnitude. However, in the induced smectic A_d phase the value of the splay elastic constant is found to be about one to two order higher than that in the nematic or re-entrant nematic phases. Within the smectic phase, the K_{11} value shows a broad maximum on varying the temperature. No pre-smectic effects are seen in the temperature variation of the splay elastic constant in the nematic phase as well as in the re-entrant nematic phase. This behavior is expected, as splay deformation is permitted in the smectic phase [25].

According to the continuum theory, bend elastic constant is not permitted in the smectic phase [25–27] and the ratio K_{33}/K_{11} and hence K_{33} could be determined only for the nematic and the re-entrant nematic phases.

In figure 7.4a to 7.9a the temperature dependence of the ratio of the bend and splay elastic constant for mixtures exhibiting induced smectic A_d and re-entrant nematic phases have been plotted, whereas figures 7.4b to 7.9b show the temperature variation of the respective splay and bend elastic constants for these mixtures.

In the upper nematic phase, the ratio K_{33}/K_{11} increases as the temperature decreases and as the nematic - smectic A_d temperature is approached the ratio increases sharply and diverges near the transition temperature. In the re-entrant nematic phase the temperature variation of the ratio K_{33}/K_{11} is opposite to that in the normal nematic phase and it rises with the rise in temperature and diverges near the re-entrant nematic–smectic transition. This observation is in agreement with that of other workers [4, 9, 28–31], where they have shown that the ratio K_{33}/K_{11} diverges to infinity as the nematic smectic transition is approached. The value of K_{33} has been calculated by determining the ratio K_{33}/K_{11} and the value of K_{11}. Since the splay elastic constant does not exhibit any pre-smectic effect, the temperature variation of the bend elastic constant reflects the pre-smectic effects which has been observed in the temperature variation of the ratio K_{33}/K_{11}.

Of the several molecular theories [32–43] for the elastic constant of liquid crystals, probably the simplest one is the theory proposed by Priest [35]. In this theory the elastic constants K_1, K_2 and K_3 has been expressed in terms of the ratio of the order parameters $\langle P_2 \rangle$ to $\langle P_4 \rangle$ and of the length to width of the molecule, which have been assumed to be spherocylinders.

For the mixture $x_{9.\,CN}$ = 0.827 the ratio of K_{33}/K_{11} has also been calculated from Priest theory [35]. According to Priest theory

$$K_1 = \overline{K}\left(1+\Delta-3\Delta'\gamma\right) \tag{7.5}$$

$$K_2 = \overline{K}\left(1-2\Delta-\Delta'\gamma\right) \tag{7.6}$$

$$K_3 = \overline{K}\left(1+\Delta+4\Delta'\gamma\right) \tag{7.7}$$

where

$$\overline{K} = \frac{(K_1+K_2+K_3)}{3} \qquad \Delta = \frac{\left(2R^2-2\right)}{\left(7R^2+20\right)}$$

$$\gamma = \frac{\langle P_4 \rangle}{\langle P_2 \rangle} \qquad \Delta' = \frac{9\left(3R^2-8\right)}{16\left(7R^2+20\right)}$$

$$R = (L-D)/D$$

From equations 7.5 and 7.7 we can write

$$\frac{K_3}{K_1} = \frac{\left(1+\Delta+4\Delta'\gamma\right)}{\left(1+\Delta-3\Delta'\gamma\right)} \tag{7.8}$$

L and D are the overall length and diameter of the spherocylinder respectively. The apparent molecular length as obtained from x- ray is taken as L. Assuming a simple tetragonal lattice, with L as the longest axis and using the value of density and other parameters from the previous x ray measurements (chapter 3) the value of D has been calculated. Both L and D are expected to be functions of temperature, however, as their variations over the mesomorphic temperature range is very small Δ and Δ' are assumed to be constant. Using the orientational order parameters $\langle P_2 \rangle$ and $\langle P_4 \rangle$ values from X-ray diffraction measurements (chapter 3), K_{33}/K_{11} could be calculated from equation 7.8.

Figure 7.5a shows the temperature variation of K_{33}/K_{11} of the mixture $x_{9.\,CN}$ = 0.827 as obtained from Priest theory as well as from experiment. It is

observed that the order or magnitude of the K_{33}/K_{11} ratio in the nematic phase is similar in both the cases, but Priest theory fails to account for the divergence of this ratio on either of the smectic–nematic phase transition. This was expected because of the drastic assumptions of the theory. In the limit $\langle P_4 \rangle \ll \langle P_2 \rangle$ Priest theory predicts $K_{33} = K_{11}$ and departure from this equality is related in a simple way to the ratio $\langle P_4 \rangle / \langle P_2 \rangle$ [35]. Thus the temperature variation of the value of K_{33}/K_{11} obtained from the theory strongly reflects the temperature dependence of $\langle P_4 \rangle / \langle P_2 \rangle$. In chapter 3 it has been reported that the variation of $\langle P_2 \rangle$ and $\langle P_4 \rangle$ is continuous across the nematic smectic and smectic re-entrant nematic transition and that no appreciable difference was seen in the values of the $\langle P_2 \rangle$ and $\langle P_4 \rangle$ in the three different phases. Due to this fact the Priest theory has given an almost linear variation of K_{33}/K_{11} as one approaches the nematic-smectic A_d transition and also the re-entrant nematic – smectic A_d transition.

7.3 Rotational viscosity measurements

A relaxation method was used to determine the rotational viscosity [12–17], the experimental details of which has been discussed in chapter 2. A small voltage was applied to a homogeneously aligned liquid crystal (LC) cell to deform the nematic directors by a small angle. At time t = 0, when this voltage is removed, the molecules relax to the equilibrium state with relaxation time τ_0. For a LC inserted into a homogeneously aligned cell of thickness d, τ_0 is related to the following material parameters:

$$\gamma_1 = \frac{\tau_0 K_{11} \pi^2}{d^2} \tag{7.9}$$

where K_{11} is the splay elastic constant coefficient and γ_1 is the rotational viscosity of the liquid crystal. Knowing the values of the splay elastic constants and by measuring the relaxation time τ_0, the rotational viscosity can be determined.

The experimentally determined relaxation times in the nematic and re-entrant nematic phases for mixtures having $x_{9.\,CN}$ = 0.176, 0.347, 0.471, 0.559, 0.774, 0.827 are shown in figure 7.12 as a function of temperature. The temperature dependence of τ_0 for the mixture $x_{9.\,CN}$ = 0.827 and 0.774 are shown separately in figure 7.13. The relaxation times in both the N and N_{re} phases are

found to be of the same order of magnitude. However, as expected, these values are always higher in N_{re} phase compared to the normal nematic phase. The relaxation time for mixtures having higher concentration of 9.CN is smaller with respect to those mixtures belonging to the lower concentration side of the phase diagram. It has been found that the temperature dependence of relaxation time for mixture $x_{9.\,CN}$ = 0.347 show unusual behavior. On reducing the temperature, at about 90°C, the τ_0 curve shows a steep rise up to 74°C followed by an almost equal steep fall. This may be due to the fact that the mixture at $x_{9.\,CN}$ = 0.347 is just outside the induced Sm A_d island and strong smectic fluctuations are still present in this mixture which leads to higher values of the relaxation time within a certain temperature range.

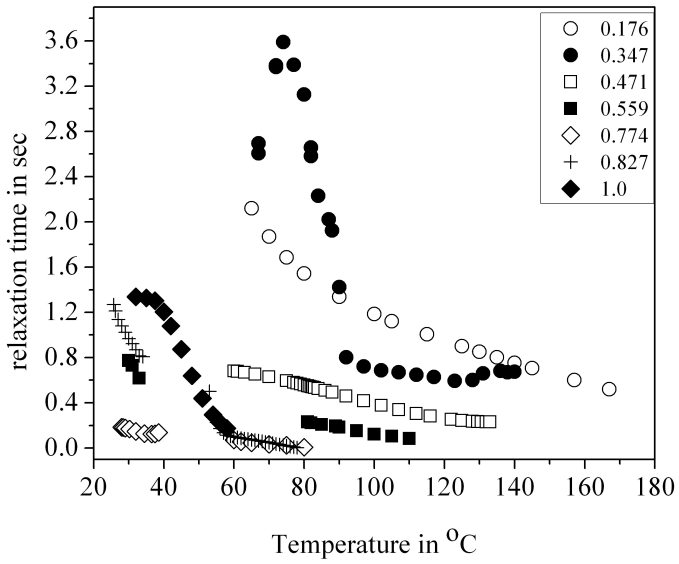

Figure 7.12: Temperature dependence of the relaxation time (τ_0) in the nematic and re-entrant nematic phases for mixtures: ○ 0.176, ● 0.347, □ 0.471, ■ 0.559, ◊ 0.774, + 0.827 and ♦ 9.CN.

The temperature dependence of rotational viscosity of a few mixtures ($x_{9.\,CN}$ = 0.176, 0.559, 0.774, 0.827, 1.0) in the nematic and re-entrant nematic phases is shown in figure 7.14. The rotational viscosity coefficient (γ_1) increases with decrease in temperature, not only in the ordinary nematic phase but also in the re-entrant nematic phases. The rotational viscosity γ_1 in both the nematic and

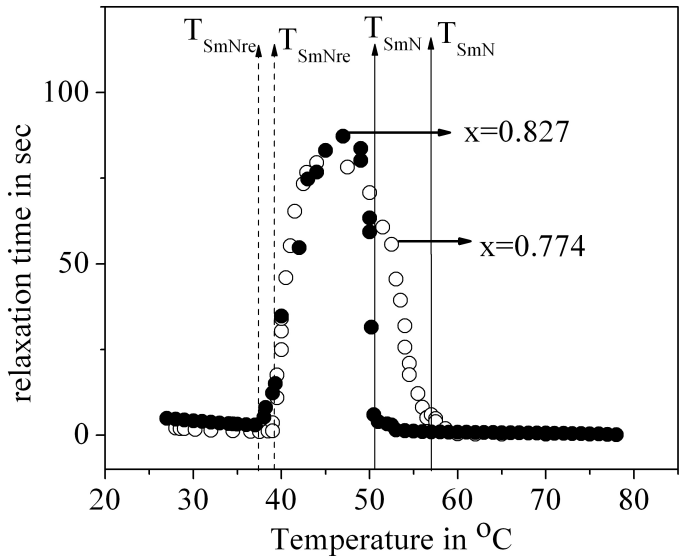

Figure 7.13: Temperature dependence of the relaxation time (τ_0) in the nematic, smectc A_d and re-entrant nematic phases for mixtures ○ $x_{9.\,CN}$= 0.774 and ● 0.827.

re-entrant nematic phases are in the range of 0.5 Pa s to a few Pa s with small temperature dependence. However, in the Sm A_d phase, the γ_1 values initially increase with decrease in temperature, attain a maximum value (1000 Pa s) and then decreases with decrease in temperature and to attain a value comparable to the nematic phase values at the Sm A_d–N_{re} transition temperature. Moreover, γ_1 changes continuously at the Sm A_d and Sm A_d – N_{re} transition. This behaviour is found to be consistent with the results obtained from the birefringence, density and order parameter measurements as discussed in chapters 3–5.

The temperature dependence of γ_1 is fitted with the following expression using the values of the orientational order parameter (S) from birefringence measurement:

$$\gamma_1 = \gamma_0 S \exp\left(\frac{E_a}{k_\beta T}\right) \tag{7.10}$$

where k_β is the Boltzmann constant and E_a is the associated activation energy. The variation of $\ln(\gamma_1/S)$ with 1/T for $x_{9.\,CN}$ = 0.827 is shown in figure 7.15. From

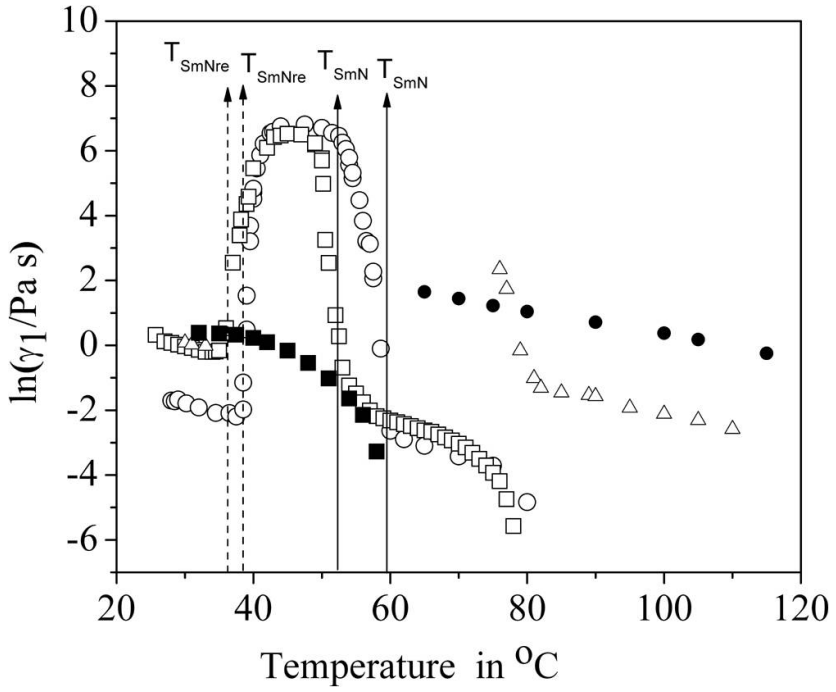

Figure 7.14: Temperature dependence of the rotational viscosity for mixtures ● $x_{9.\,CN}$ = 0.176, Δ 0.559, ○ 0.774, □ 0.827 and ■ 9.CN.

the slope of the curve the activation energy E_a can be evaluated. The variation of activation energy (E_a) associated with ln(γ_1/S) as a function of mole fraction of 9.CN is shown in figure 7.16.

It may be mentioned that the activation energies associated with ln(γ_1/S) for the nematic phase are distinctly higher than those obtained for the re-entrant nematic phase. This result contradicts the results of activation energy calculated from dielectric method [10]. However, the results of this work do agree well with the rotational viscosity measurements of Sailaja *et. al.* [11] on 6OCB+8OCB binary system. There seems to be a systematic variation of E_a with concentration. E_a increases with the increase in the concentration of 9.CN in nematic phase but in the N_{re} phase the activation energy show a local minimum around $x_{9.\,CN}$ = 0.6 i.e. at the centre of the smectic island. It should be mentioned that in the system under study the re-entrant nematic range is very narrow and close to the the crystallisation point. Hence pretransitional effect due to the approaching solidification could have influenced the observed behaviour. Further studies are necessary to come to a conclusive answer.

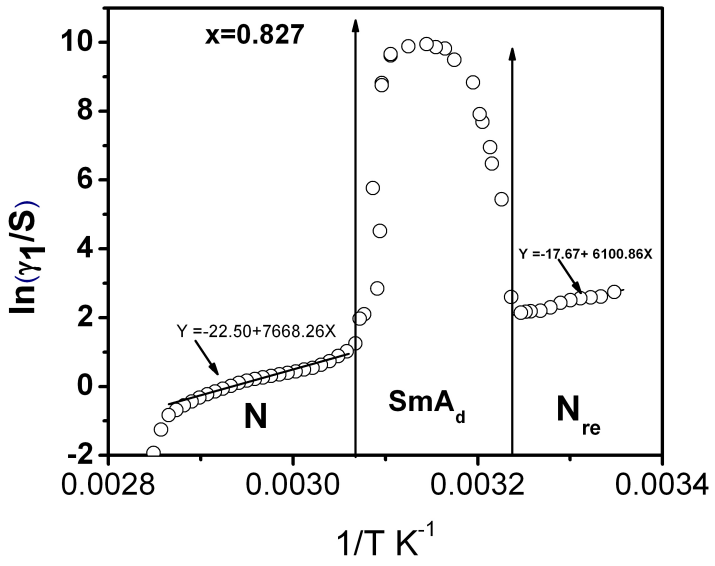

Figure 7.15: Variation of ln(γ_1/S) with 1/T for binary mixture, $x_{9.\,CN}$ = 0.827.

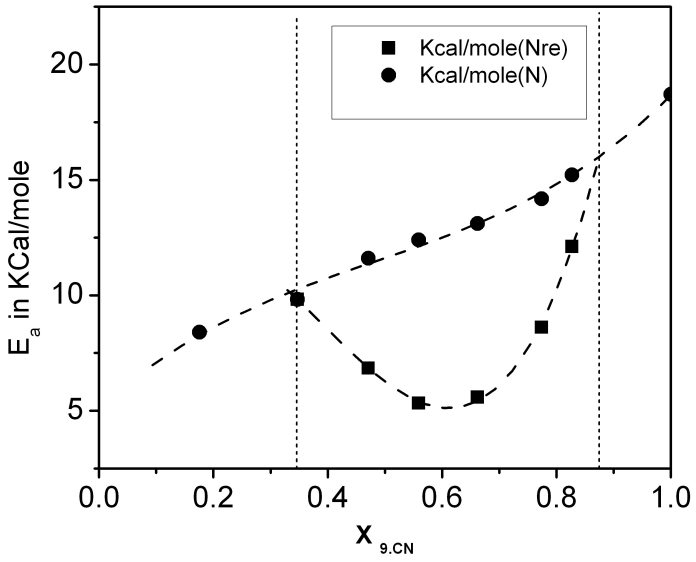

Figure 7.16: Variation of activation energy (E_a) associated with ln(γ_1/S) as a function of mole fraction of 9.CN.

7.4 Conclusion

The splay elastic constant (K_{11}) for the system of binary mixture 7CPB + 9.CN has been measured throughout the concentration and temperature range by electric field induced Freedericksz transition. As bend deformation is not permitted in the smectic A phase, bend elastic constant (K_{33}) could only be determined in the nematic and re-entrant nematic phases from the voltage dependence of the capacitance. In both the ordinary nematic phase and also in the re-entrant nematic phases the splay elastic constant increases with decrease in temperature and has the same order of magnitude. However, in the induced smectic A_d phase the value of K_{11} is found to be about one to two order higher than that in the nematic or re-entrant nematic phase. The splay elastic constant for all the mixtures under study did not show any pre transitional effect.

The bend elastic constant shows a strong pre transitional effect near the nematic–smectic and smectic–re-entrant nematic transitions. The influence of the presence of the induced smectic phase is observed even in those mixtures which have no induced smectic phases. The reason for this being the formation of smectic clusters which are not sufficiently strong enough to induce the smectic phase but their presence is reflected in the temperature dependence of the bend elastic constant.

In the upper nematic phase, the ratio K_{33}/K_{11} increases as the temperature decreases and as the nematic - smectic A_d temperature is approached the ratio increases sharply and diverges to infinity. In the re-entrant nematic phase the temperature variation of the ratio K_{33}/K_{11} is opposite to that in the normal nematic phase and it rises with rise in temperature and diverges to infinity near the re-entrant nematic-smectic transition.

A simple electro-optical method was used to determine the relaxation time and hence the rotational viscosities (γ_1) of a system of binary mixture (7CPB + 9.CN) possessing nematic –Smectic A_d – re-entrant nematic phase sequence. Upon cooling, the γ_1 values not only increase in the normal nematic phase but also in the N_{re} phase and have same order of magnitudes about 0.5 to a few Pa s. Rotational viscosity values are about two to three order of magnitude higher in the Sm A_d phase than those measured in the nematic phase. The activation energies for the N_{re} phase have been found to be smaller than those for the normal nematic phase. The difference $[(E_a)_N - (E_a)_{N_{re}}]$ is maximum near the

centre of the phase diagram. This result indicates that the interaction between monomer molecules or that between dimer aggregates is weaker in the N_{re} phase than in the normal nematic phase. For normal nematic phase, the activation energy increases with an increase in mole fraction of 9.CN, while that for N_{re} phase it shows a local minimum near $x_{9.\,CN}$ = 0.6, i.e. at centre of the phase diagram.

References

[1] S. V. Pasechnik, V. G. Chigrinov and D. V. Shmeliova, *Liquid Crystals: Viscous and Elastic Properties*, Willey-VCH Verlag GmbH & Co. KGaA, Ch.2, 7 (2009).

[2] F. C. Frank, *Disc. Faraday Soc.*, **25**, 19 (1958).

[3] B. Bahadur, *Liquid Crystals, Applications and Uses*, Ed., World Scientific, **Vol. 1** (1990).

[4] P. E. Cladis, *Phys. Rev. Lett.*, **35**, 48 (1975).

[5] A. Kubono, K. Yoshino, T. Ninomiya, R. Akiyama and K. Tanaka, *Liq. Cryst.*, **29**, 1089 (2002).

[6] A. P. Filippov and Lindau, *J Polymer Sci. A* **42**, 743 (2000).

[7] S. A. Ivanov, V. V. Belaiev, R. A. Zeinalov and B. I. Ostrovskij, *Zh. Exp. Theor. Fiz.*, **91**, 560 (1986).

[8] S. Bhattacharya and S. V. Letcher, *Phys. Rev. Lett.*, **44**, 414 (1980).

[9] G. Czechowski and J. Jadzyn, *Act. Phys. Pol. A* , **106**, 475 (2004).

[10] B. R. Ratna, R. Shashidhar, M. Bock, A. Gobl-Wunsch and G. Heppke, *Mol. Cryst. Liq. Cryst.*, **99**, 285 (1983).

[11] A. S. Sailaja, K. Venu, V. V. S. Sastry, *Mol. Cryst. Liq. Cryst.* **250**, 177 (1994).

[12] S. T. Wu, C. S. Wu. *Phys. Rev. A*, **42**, 2219 (1990).

[13] M. L. Dark, M. H. Moore, D. K. Shenoy and R. Shashidhar, *Liq. Cryst.*, **33**, 67 (2006).

[14] M. K. Das, A. Pramanik, B. Das, L. Szczucinski and R. Dabrowski, *J. Phys. D: Appl. Phys.*, **45**, 415304 (2012).

[15] A. Pramanik, B. Das, M. K. Das, K. Garbat, S. Urban and R. Dabrowski, *Liq. Cryst.*, **40**, 149 (2013).

[16] A. Chakraborty, M. K. Das, B. Das, A. Lehmann and C. Tschierske, *Soft Matter*, **9**, 4273 (2013).

[17] P. Dasgupta, B. Das and M. K. Das, *Mol. Cryst. Liq. Cryst.* **39**, 1297 (2012).

[18] H. Gruler, T. J. Schiffer and G. Meier, *Z. Natureforsh*, **27a**, 966 (1972).

[19] M. J. Bradshaw and E. P. Rayens, *Mol. Cryst. Liq. Cryst.*, **72**, 35 (1980).

[20] H. Gruler and L. Cheung, *J. Appl. Phys.*, **46**, 5097 (1975).

[21] H. Deuling, *Liquid Crystals, Solid State Physics Suppl. no. 14*, Ed. L. Liebert, Academic Press, NY, p. 77 (1978).

[22] T. Uchida, Y. Takahashi, *Mol. Cryst. Liq. Cryst.*, **72**, 133 (1981).

[23] P. Chattopadhyay and S. K. Roy, *Mol. Cryst. Liq. Cryst.*, **257**, 89 (1994).

[24] Y. Zhou and S. Sato, *Jpn. J. Appl. Phys.*, **37**, 4397 (1997).

[25] S. Singh, *Physics Reports*, **277**, 283 (1996).

[26] L. M. Blinov, *Handbook of liquid crystals*, **Vol.1**, Eds. D. Demus, J. Goodby, G. W. Gray, H. -W. Spiess, V. Vill, Wiley-VCH, Ch 7, 477-534 (1998).

[27] J. A. Geurst and W. J. A. Goossens, *Phys. Lett. A*, **41** (4), 369 (1972).

[28] M. R. Dodge, R. G. Petschek, C. Rosenblatt, M. E. Neubert and M. E. Walsh, *Phys. Rev. E*, **68**, 031703 (2003).

[29] J. Huang and J. T. Ho, *Phys. Rev. Lett.*, **58** (21), 2239 (1987).

[30] L. Cheung, R. B. Meyer and H. Gruler, *Phys. Rev. Lett.*, **31** (6), 349 (1973).

[31] S. Dasgupta, P. Chattopadhyay and S. K. Roy, *Phys. Rev. E*, **63**, 041703 (2001).

[32] J. Nehring and A. Saupe, *J. Chem. Phys.*, **54**, 337 (1971).

[33] J. Nehring and A. Saupe, *J. Chem. Phys.*, **56**, 5527 (1972).

[34] R. G. Priest, *Mol. Cryst. Liq. Cryst.*, **17**, 129 (1972).

[35] R. G. Priest, *Phys. Rev. A*, **7**, 720 (1973).

[36] Y. Singh and K. Singh, *Phys. Rev. A*, **33**, 3481 (1986).

[37] J. P. Straley, *Phys. Rev. A*, **8**, 2181 (1973).

[38] A. Poniewierski and J. Stecki, *Mol. Phys.*, **38**, 1931 (1979).

[39] T. Faber, *Proc. R. Sot. Lond. A*, **353**, 261 (1977).

[40] S. D. Lee, *Phys. Rev. A*, **39**, 3631 (1989).

[41] A. M. Somoza and P. Takazona, *Phys. Rev. A*, **40**, 6069 (1989).

[42] A. M. Somoza and P. Takazona, *Mol. Phys.*, **72**, 911 (1991).

[43] S. D. Lee and R. B. Meyer, *J. Chem. Phys.*, **84**, 3443 (1986).

Chapter 8

X-ray diffraction and dielectric studies of a binary system (7BCB+9.CN) exhibiting nematic – induced smectic A_d – re-entrant nematic phase sequence

8.1 Introduction

In the previous chapters (3 to 7) I have discussed the results of various measurements in the nematic, induced smectic A_d and re-entrant nematic phases of the binary mixtures of 7CPB+9.CN. In this chapter another binary system which is similar to the previous one has been discussed. Brodzik *et. al.* [1] have reported this phase diagram which is very similar to the one reported by me in chapter 3. In this system the component 4-cyanobiphenyl-4′ 4-heptylbenzoate (7BCB) differs from the structure of 4-cyanophenyl [4′ (4″-n- heptylphenyl)] benzoate (7CPB) only by the position of the ester group. However, due to this small change in structure, a marked change in the size of the induced smectic region is observed [1, 2].

In this chapter, I report the results of polarizing optical microscopy, X-ray diffraction and dielectric measurements in the nematic, induced smectic A_d and re-entrant nematic phases of a few mixtures belonging to the binary system

of 7BCB+9.CN. Transition temperatures determined from texture studies have been compared with those reported by Brodzik *et. al.* and are found to be in good agreement. From X-ray diffraction measurements, the orientational order parameters (OOP's) have been determined in the nematic, induced smectic A_d and re-entrant nematic phases. The obtained OOP values have been compared with the theoretical results of Maier-Saupe theory [3–6] for nematogens. The order parameters of those mixtures which have an induced smectic A_d and re-entrant nematic phases has been compared with McMillan's theory [7, 8] and modified McMillan's theory as proposed by Luckhurst and Timimi [9]. Static dielectric measurements have been done at six different mole fractions of 9.CN. In order to explain certain anomalies in the values of $\epsilon_\parallel$ in the re-entrant nematic and at low temperature region of the induced smectic phase, low frequency dielectric spectroscopy have been performed on selected mixtures.

8.2 Experimental

By examining the sample under a polarizing microscope and a Mettler FP80/82 thermo-system, the transition temperatures of the samples were determined. All the transition temperatures agreed well with the phase diagram previously reported by Brodzik *et. al.* [1] and is shown in figure 8.1.

X-ray diffraction photographs of magnetically oriented samples were recorded on a flat plate camera in the transmission geometry using Cu K_α radiation. X-ray diffraction patterns of the monodomain samples were scanned by a high resolution scanner. A program was developed using GNU Octave software to obtain the scattered intensity profile as a function of the azimuthal angle for determination of the orientational order parameter (OOP). The transverse ($\xi_\perp$) correlation lengths for a particular mixture in the N, induced Sm A_d as well as N_{re} phases has been measured. A detailed discussion about the experimental method has been given in chapter 2 of this thesis.

The static dielectric permittivities $\epsilon_\parallel$ and $\epsilon_\perp$ along and perpendicular to the molecular long axis respectively were determined by measuring the capacitance of a suitably aligned liquid crystal filled cell. For this study the capacitance was measured at 0.3V, 10 kHz using Agilent E4980A digital LCR-bridge with a

relative accuracy of 0.05%. The details of this measurement have been discussed in chapter 2 of this thesis.

Low frequency dielectric spectra of selected mixtures have been measured in the frequency range 20Hz to 2MHz using Agilent E4980A digital LCR-bridge. Planar and homeotropically aligned ITO coated liquid crystal cell of thickness $8.9\mu m$, procured from AWAT Co. Ltd., Warsaw, Poland, have been used for both types of dielectric measurements.

In the case of dispersive material the measured dielectric spectrum can be described with the help of generalized Cole-Cole equation [10–12].

$$\epsilon^* = \epsilon' - j\epsilon'' = \epsilon'(\infty) + \sum_i \frac{\delta\epsilon'_i}{1 + (j2\pi f\tau_i)^{(1-h_i)}} \tag{8.1}$$

here $\delta\epsilon'$ is the dielectric strength of relaxation and $\epsilon'(\infty)$ is the high frequency limiting values of dielectric permittivity corresponding to a particular mode of relaxation. τ is the relaxation time and h_i is the symmetric distribution parameter ($0 \leq h_i \leq 1$). Subscript i denotes mode of relaxation. Real and imaginary parts of equation 8.1 are

$$\epsilon' = \epsilon'(\infty) + \sum_i \frac{\delta\epsilon\left[1 + (2\pi f\tau_i)^{(1-h_i)}\sin(h_i\pi/2)\right]}{1 + (2\pi f\tau_i)^{2(1-h_i)} + (2\pi f\tau_i)^{(1-h_i)}\sin(h_i\pi/2)} \tag{8.2}$$

$$\epsilon'' = \sum_i \frac{\delta\epsilon\left[(2\pi f\tau_i)^{(1-h_i)}\cos(h_i\pi/2)\right]}{1 + (2\pi f\tau_i)^{2(1-h_i)} + (2\pi f\tau_i)^{(1-h_i)}\sin(h_i\pi/2)} \tag{8.3}$$

Due to the presence of electrode polarization capacitance and ionic conductance $\epsilon'(dc)f^n$ and $\frac{\sigma(dc)}{\epsilon_0 2\pi f^k}$ terms are added in equations 8.2 and 8.3 respectively. $\sigma(dc)$ is the ionic conductance and ϵ_0 ($= 8.85pF/m$) is the free space permittivity. With small values of h_i and in the presence of electrode polarization capacitance and ionic conductance, equations 8.2 and 8.3 changes to

$$\epsilon' = \epsilon'(dc)f^n + \epsilon'(\infty) + \sum_i \frac{\delta\epsilon\left[1 + (2\pi f\tau_i)^{(1-h_i)}\sin(h_i\pi/2)\right]}{1 + (2\pi f\tau_i)^{2(1-h_i)} + (2\pi f\tau_i)^{(1-h_i)}\sin(h_i\pi/2)} \tag{8.4}$$

$$\epsilon'' = \frac{\sigma(dc)}{\epsilon_0 2\pi f^k} + \sum_i \frac{\delta\epsilon\left[(2\pi f\tau_i)^{(1-h_i)}\cos(h_i\pi/2)\right]}{1 + (2\pi f\tau_i)^{2(1-h_i)} + (2\pi f\tau_i)^{(1-h_i)}\sin(h_i\pi/2)} + Af^n \tag{8.5}$$

The capacitance of the empty measuring cell (C_0), capacitance (C) and conductance (G) of liquid crystal filled cell and calculated stray capacitance (C_s) values have been used to calculate $\epsilon'\left(=\frac{C-C_s}{C_0-C_s}\right)$ and $\epsilon''\left(=\frac{G}{2\pi f C_0}\right)$ as a function of frequency at different temperatures. In order to correct the dielectric spectrum at high and low frequencies and to obtain the optimum value of the parameters, equation 8.5 was fitted to the dielectric loss ϵ'' vs frequency curve.

8.3 Phase diagram and texture studies

The liquid crystal samples were procured from AWAT Co. Ltd., Warsaw, Poland (purity >99.9%) and were used without further purification. The structural formulae, chemical names and the transition temperature of the pure compounds of this system are as follows:

Component 1: 4-cyanophenyl [4′ (4- heptylbenzoate)] (7BCB in short)

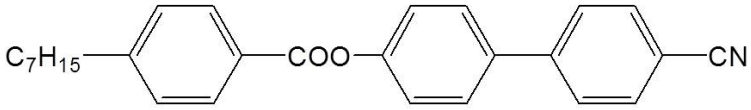

K 89.3°C N 222°C I

Component 2: 4-cyanophenyl 4-nonylbenzoate (9. CN in short)

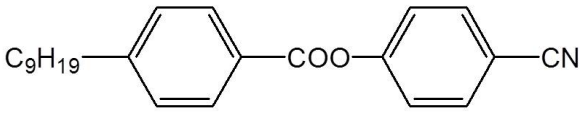

K 45.3°C N 60°C I

The phase diagram [1] as obtained from polarizing optical microscopy is shown in figure 8.1. Nine mixtures were prepared for this system with mole fraction $x_{9.\,CN}$ = 0.1, 0.2, 0.3, 0.4, 0.5, 0.6, 0.7, 0.8 and 0.9.

In this system, the induced smectic phase appears in the concentration range 0.1< $x_{9.\,CN}$ < 0.9 and occupiers a dominant area of the phase diagram. All the mixtures show a two-phase (nematic + isotropic) coexistence region, but no co-existing region is found at the nematic / smectic A_d or smectic A_d / re-entrant nematic phase transitions. In some cases, the re-entrant nematic phase is suppressed due to solidification. The re-entrant nematic phase of all the mixtures in this 7BCB+9.CN system is monotropic. The texture of 7BCB, 9.CN and their

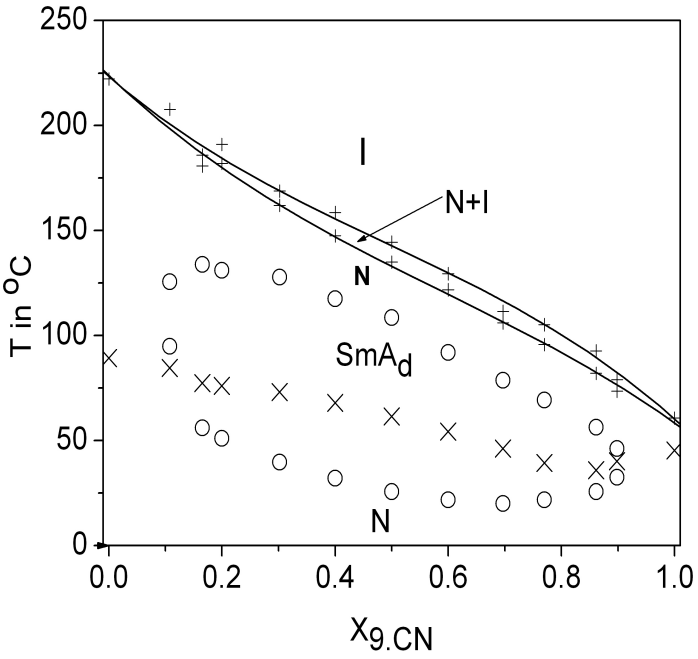

Figure 8.1: Phase diagram for the binary system of 7BCB + 9.CN. $x_{9.\,CN}$ = mole fraction of 9.CN. I isotropic; (I+N) nematic-isotropic co-existing region; Sm A smectic A_d phase; N nematic phase.

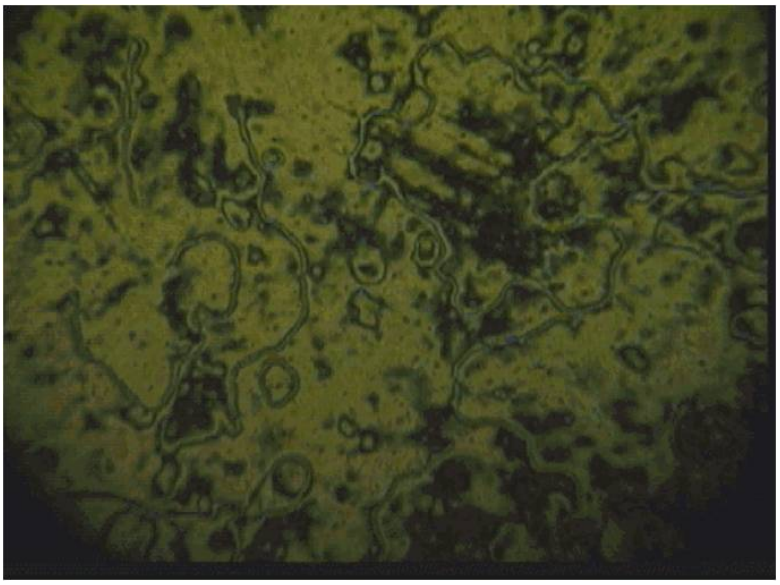

(a) Nematic phase ($157.7°C$)

Figure 8.2: Texture for mixture $x_{9.\,CN}$ = 0.4 (7BCB+9.CN) at 100X magnification during cooling.

(b) Smectic A_d phase (98.2°C)

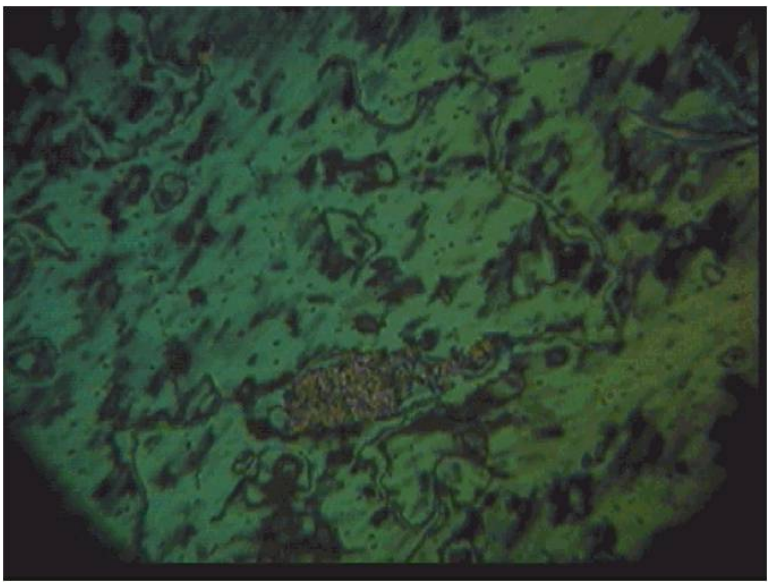

(c) Re-entrant nematic phase (24.4°C)

Figure 8.2: (cont'd): Textures for mixture $x_{9.\,CN}$ = 0.4 (7BCB+9.CN) at 100X magnification during cooling.

mixtures in the nematic and re-entrant nematic phase was found to be marbled or thread like. However in the smectic phase fan shaped texture typical of the Sm A phase was obtained. Photographs of these textures are shown in figures 8.2a–8.2c. The only difference between 7BCB and 7CPB is the position of the ester group (-COO). It is interesting to observe that a change in the position of the ester group leads to a stronger induction of the smectic A_d phase with the area of the induced smectic island being increased considerably in the phase diagram.

8.4 X-ray diffraction measurements

From X-ray diffraction measurements, orientational order parameters (OOP's) have been determined in the normal nematic, induced smectic A_d and re-entrant nematic phases. The experimental order parameter values have been fitted to those calculated from Maier-Saupe theory [3–6] for nematogens. The order parameters of those mixtures which have an induced smectic and re-entrant nematic phase has been compared with McMillan's theory [7, 8] and modified McMillan's theory as proposed by Luckhurst and Timimi [9].

The temperature variation of the orientational order parameter, as obtained from X-ray diffraction measurements, for all the mixtures and the pure compounds are shown in figures 8.3a-8.3h. It is observed that for all the mixtures the temperature dependence of the order parameter in N_{re} and N phases is quite pronounced in comparison to those in the smectic A_d phase. These values are found to vary continuously across the N-Sm A_d and Sm A_d - N_{re} phase transition indicating second order phase transition.

The continuous curves correspond to the Maier-Saupe mean field theory [3–6] in case of the two pure compounds possessing nematic phase only (figure 8.3a and 8.3h). For other mixtures, the continuous curve corresponds to McMillan's theory [7, 8] (figure 8.3a and 8.3h). The experimental order parameter values for 7BCB agree quite well with the Maier-Saupe theory, however the experimental OOP values for 9.CN are higher than the theoretical values. The order parameters have been fitted to those calculated from a modified McMillan's theory as proposed by Luckhurst and Timimi [9] as discussed in details in the chapter 2 and 3 of this thesis. In the calculation using McMillan's model, the parameter

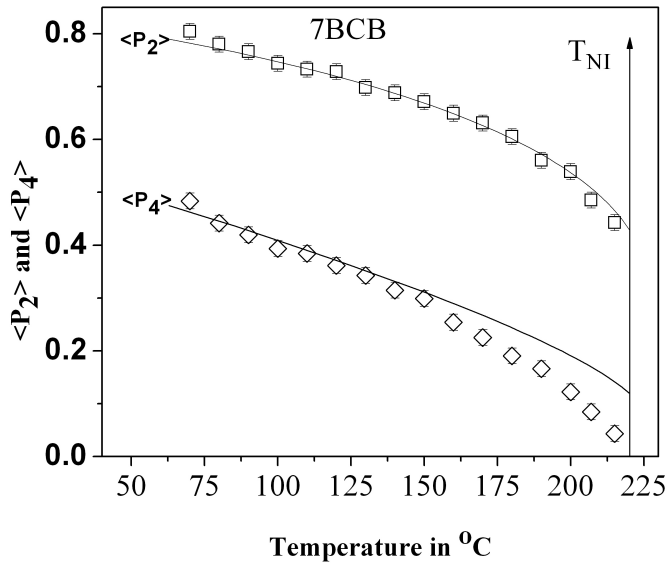

(a) Temperature variation of $\langle P_2 \rangle$ and $\langle P_4 \rangle$ for 7BCB.

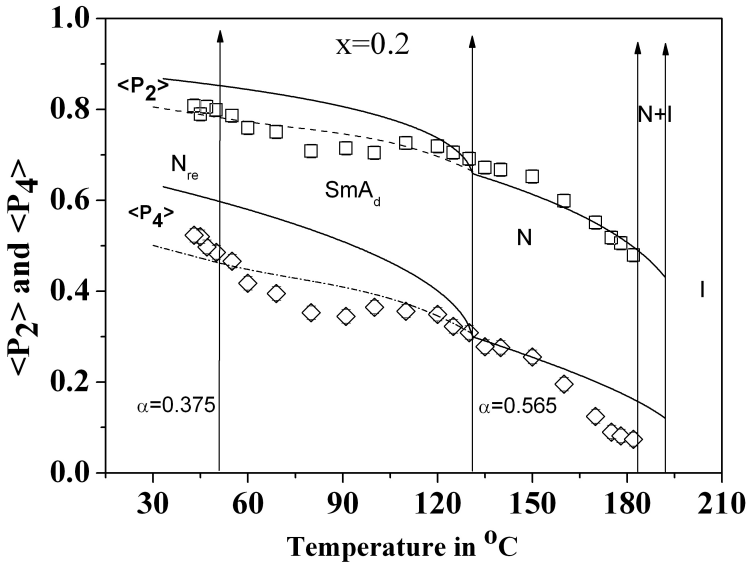

(b) Temperature variation of $\langle P_2 \rangle$ and $\langle P_4 \rangle$ for $x_{9.\,CN}$ = 0.2.

Figure 8.3: Temperature variation of $\langle P_2 \rangle$ and $\langle P_4 \rangle$ for 7CPB and $x_{9.\,CN}$ = 0.2, □ $\langle P_2 \rangle$, ◇ $\langle P_4 \rangle$ from X-ray data; — from Maier-Saupe theory (for a), from McMillan's theory (for b) . − − − $\langle P_2 \rangle$, − · − · − $\langle P_4 \rangle$ from modified McMillan's theory by Luckhurst and Timimi.

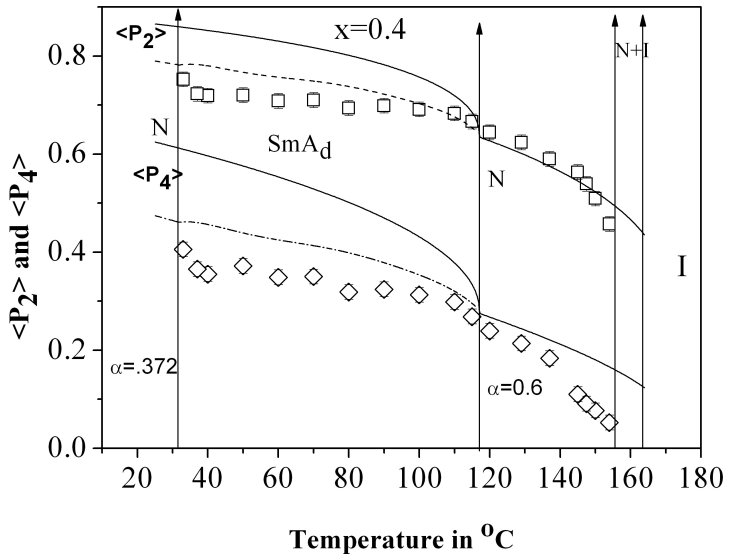

(c) Temperature variation of $\langle P_2 \rangle$ and $\langle P_4 \rangle$ for $x_{9.\,CN}$ = 0.4.

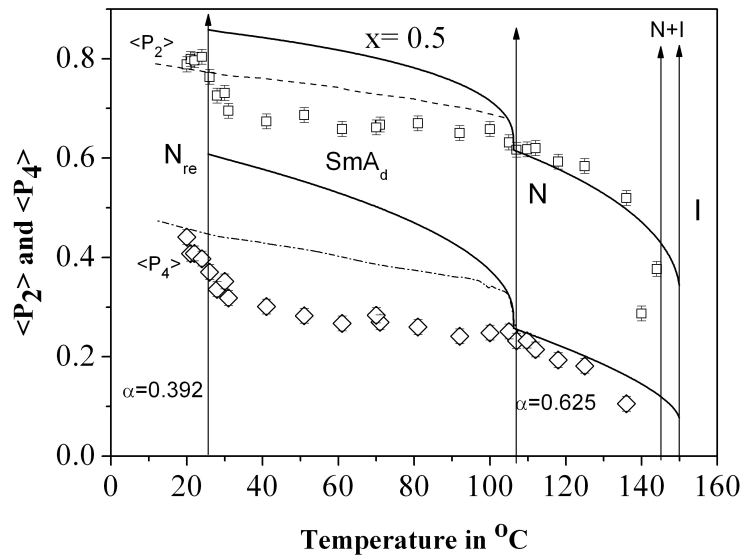

(d) Temperature variation of $\langle P_2 \rangle$ and $\langle P_4 \rangle$ for $x_{9.\,CN}$ = 0.5.

Figure 8.3: (cont'd): Temperature variation of $\langle P_2 \rangle$ and $\langle P_4 \rangle$ for $x_{9.\,CN}$ = 0.4 and $x_{9.\,CN}$ = 0.5, □ $\langle P_2 \rangle$, ◇ $\langle P_4 \rangle$ from X-ray data; — from McMillan's theory. − − − $\langle P_2 \rangle$, − · − · − $\langle P_4 \rangle$ from modified McMillan's theory by Luckhurst and Timimi.

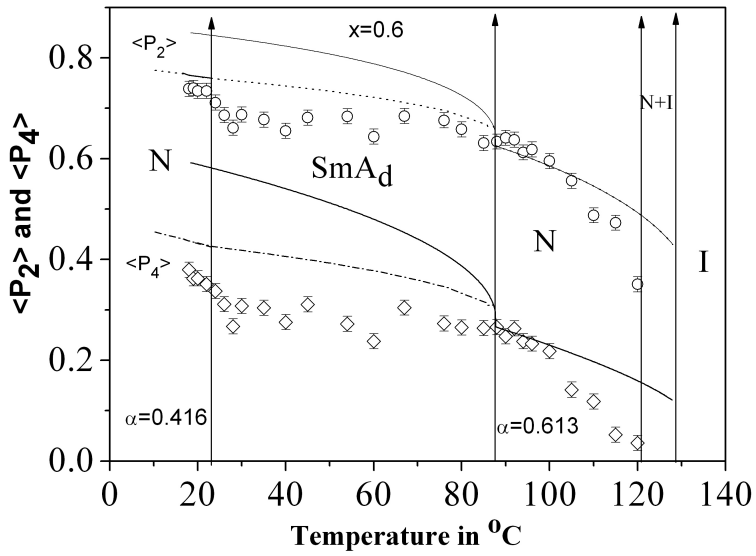

(e) Temperature variation of $\langle P_2 \rangle$ and $\langle P_4 \rangle$ for $x_{9.\,CN}$ = 0.6.

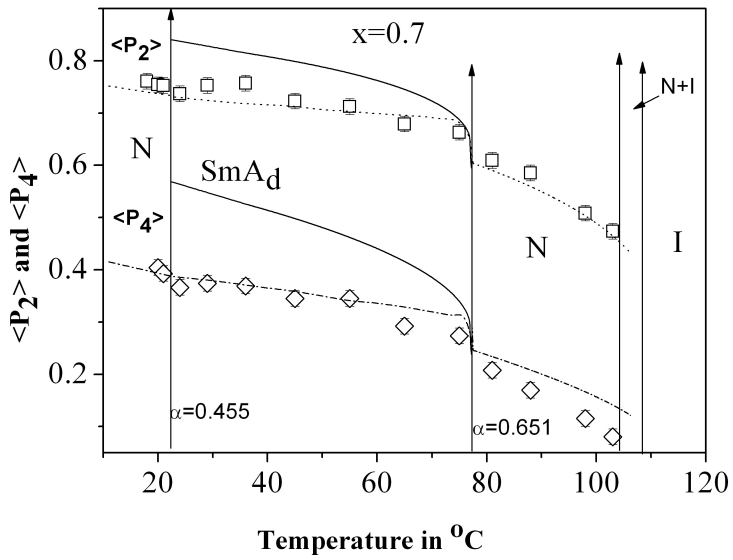

(f) Temperature variation of $\langle P_2 \rangle$ and $\langle P_4 \rangle$ for $x_{9.\,CN}$ = 0.7.

Figure 8.3: (cont'd): Temperature variation of $\langle P_2 \rangle$ and $\langle P_4 \rangle$ for $x_{9.\,CN}$ = 0.6 and $x_{9.\,CN}$ = 0.7, □ $\langle P_2 \rangle$, ◇ $\langle P_4 \rangle$ from X-ray data; — from McMillan's theory. – – – $\langle P_2 \rangle$, – · – · – $\langle P_4 \rangle$ from modified McMillan's theory by Luckhurst and Timimi.

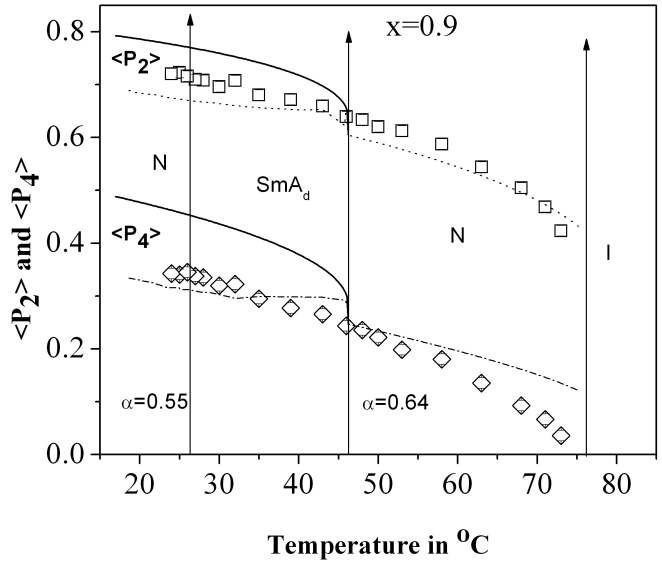

(g) Temperature variation of $\langle P_2 \rangle$ and $\langle P_4 \rangle$ for $x_{9.\,CN}$= 0.9.

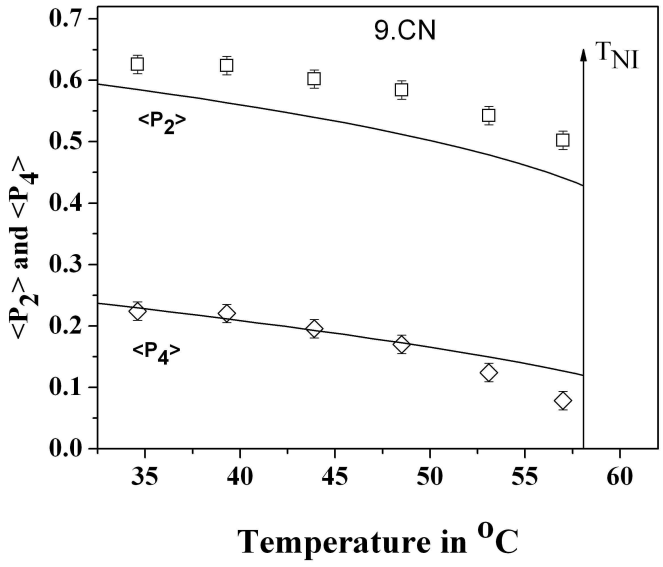

(h) Temperature variation of $\langle P_2 \rangle$ and $\langle P_4 \rangle$ for 9.CN.

Figure 8.3: (cont'd): Temperature variation of $\langle P_2 \rangle$ and $\langle P_4 \rangle$ for $x_{9.\,CN}$= 0.9 and 9.CN, — from Maier-Saupe theory (for h), from McMillan's theory (for g) . – – – $\langle P_2 \rangle$, – · – · – $\langle P_4 \rangle$ from modified McMillan's theory by Luckhurst and Timimi.

Table 8.1: Change in α values required to fit experimental data for different mixtures.

$x_{9.\,CN}$	α at T_{SN}	α at $T_{SN_{re}}$	δ
0.2	0.565	0.375	0.0.16
0.4	0.6	0.372	0.0.16
0.5	0.625	0.5	0.0.16
0.6	0.613	0.416	0.0.16
0.7	0.651	0.455	0.0.16
0.9	0.64	0.55	0.0.16

α has been varied keeping the parameter δ fixed (δ = 0.16). The best fitted theoretical curve and the values of α used for this calculation are shown in figures (8.3c-8.3g). Table 8.1 lists the change in α values required to fit the experimental data for different mixtures of the 7BCB+9.CN binary system. The agreement between the experimental $\langle P_2 \rangle$ values from X-ray diffraction measurements with those calculated from McMillan's theory is poor for all the mixtures. However the agreement between the experimental $\langle P_2 \rangle$ values obtained from X-ray diffraction measurements and those calculated from modified McMillan's theory shows marked improvement for all the mixtures. Both N–Sm A_d and Sm A_d–N_{re} transitions are predicted to be second order by this model and the experimentally obtained $\langle P_2 \rangle$ values are also in agreement with this prediction.

The transverse correlation length in the N, Sm A_d as well as in the re-entrant nematic phase of mixture $x_{9.\,CN}$ = 0.6 has been determined from a linear scan of the X-ray diffraction peaks. The intensity profile $I(q)$ was fitted to a Lorentzian form with a quadratic background, namely,

$$I(q) = \frac{a_1}{a_2 + (q - q_0)^2} + a_3 q^2 + a_4 q + a_5 \tag{8.6}$$

with q being the magnitude of the scattering vector. The transverse correlation length is defined as

$$\xi = 2\pi (a_2)^{-1/2} \tag{8.7}$$

The in-plane transverse resolution Δq for this instrument is about 1.5 $\times 10^{-3}$. The values of the correlation lengths obtained varies from 23Å to 30Å in the nematic phase and is more or less constant in the Sm A_d phase (around 26Å) and it varies from 26Å to 31Å in the re-entrant nematic phase, for this mixture

($x_{9.\,CN}$ = 0.6). For all the phases, the correlation lengths are expected to be much longer. One reason for this discrepancy may be due to the use of Ni-filtered Cu K_α radiation, which contains a white background radiation in addition to the Cu K_α peak. No correction for this white radiation, which broadens the diffraction peaks considerably, is made here. Hence, the experimental values of the correlation lengths as obtained are much shorter than the theoretically expected values. Figure 8.4 shows the temperature dependence of the transverse correlation length over the entire mesomorphic range region for the mixture $x_{9.\,CN}$ = 0.6. These values are found to diverge as the Sm A_d–N as well as Sm A_d–N_{re} transition is approached from either side, indicating a second-order phase transition. This has been supported from OOP measurements.

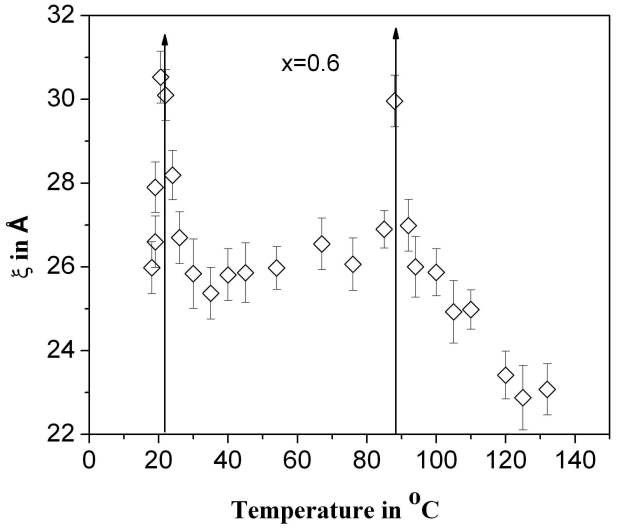

Figure 8.4: Temperature dependence of the transverse correlation length for mixture $x_{9.\,CN}$ = 0.6.

8.5 Dielectric measurements

Static dielectric permittivity measurements have been carried out on binary mixtures of 7BCB and 9.CN throughout the entire composition range. The temperature variation of the dielectric parameters [$\epsilon_\parallel$, $\epsilon_\perp$, ϵ_{iso}, $\Delta\epsilon = (\epsilon_\parallel - \epsilon_\perp)$] for the pure compound 9.CN and the mixtures of 7BCB+9.CN are shown in figures

8.5a-8.5g. All the mixtures exhibit a large positive dielectric anisotropy ($\Delta\epsilon > 0$) due to the presence of terminal polar CN group. The mixtures having induced smectic and re-entrant nematic phases ($x_{9.\,CN}$ = 0.1 to 0.9) show no significant jump in the permittivity components at the smectic-nematic as well as smectic-re-entrant nematic phase transitions.

The temperature dependence of $\epsilon_\parallel$ for the mixtures belonging to the concentration range $0.1 < x_{9.\,CN} < 0.9$ behaves normally in the upper nematic phase, however it exhibits a shallow broad minima in the induced smectic phase. This shallow minimum in $\epsilon_\parallel$ may be due to the increase in the dipole-dipole interaction in the layered interdigitated structure of the Sm A_d phase and has been also observed in the previous system of 7CPB+9.CN also. Such shallow minima have been reported by others [13]. The temperature variation of $\epsilon_\parallel$ in the low temperature region (covering the reentrant nematic phase and part of smectic A_d phase) shows a drop in the $\epsilon_\parallel$ values with decrease in temperature. However, this drop has not been observed by us in our previous 7CPB+9.CN binary system. This decrease in the value of $\epsilon_\parallel$ becomes more prominent with the increase in the proportion of 7BCB in the mixtures. The possibility of loss of alignment and hence decrease in the value of $\epsilon_\parallel$ was ruled out by using cells of different thickness ($5\mu m$ and 8.9 μm) and observing the cell under a polarizing microscope. Such a drop in $\epsilon_\parallel$ values has also been reported by others [14–16]. The decrease in $\epsilon_\parallel$ has been reported by Wrobel *et. al.* [14] in a system very similar to the one under investigation. Legrand *et. al.* [15] and Nagabhushan *et. al.* [16, 17] have also reported such a drop near the re-entrant nematic–smectic A_1 phase transition in mixture and pure compounds exhibiting multiple re-entrance and has interpreted it as due to strong increase in antiparallel correlation in the smectic A_1 phase. However, this does not seem be the case here as the fall is being observed on entering the re-entrant nematic from smectic A_d phase. Moreover, in the reports of Legrand *et. al.* [15] and Nagabhushan *et. al.* [16, 17] there was a corresponding rise of $\epsilon_\perp$ which is absent in the present case.

In order to proceed further on the behavior of $\epsilon_\parallel$ in the re-entrant nematic phase and low temperature region of the induced smectic A_d phase, dielectric spectroscopic measurements has been done on a few mixtures. In figure 8.6, the dielectric spectrum for empty cell (air filled at room temperature ($25°C$)) showing the effect of ITO resistance and lead inductance at high frequency has been

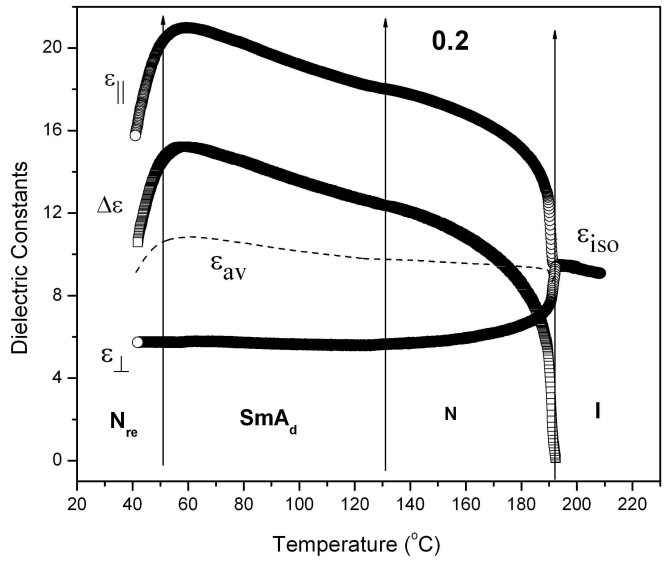

(a)

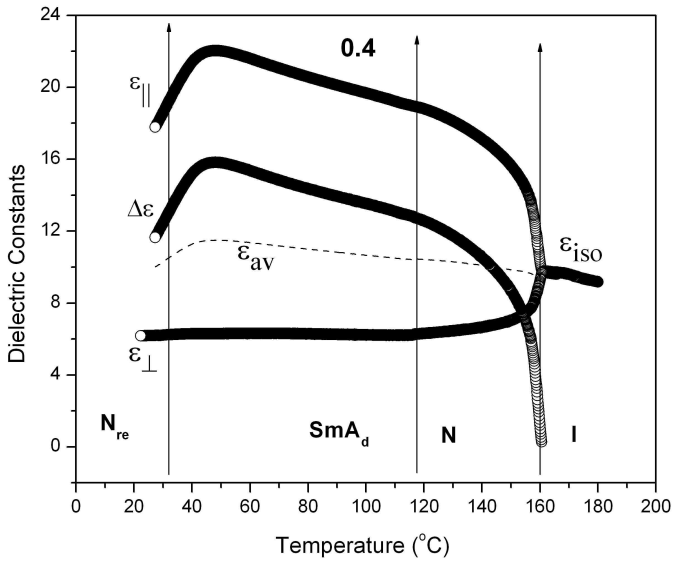

(b)

Figure 8.5: Temperature variation of dielectric parameters of 7BCB + 9.CN mixture for (a) $x_{9.\,CN}$ = 0.2 and (b) $x_{9.\,CN}$= 0.4.

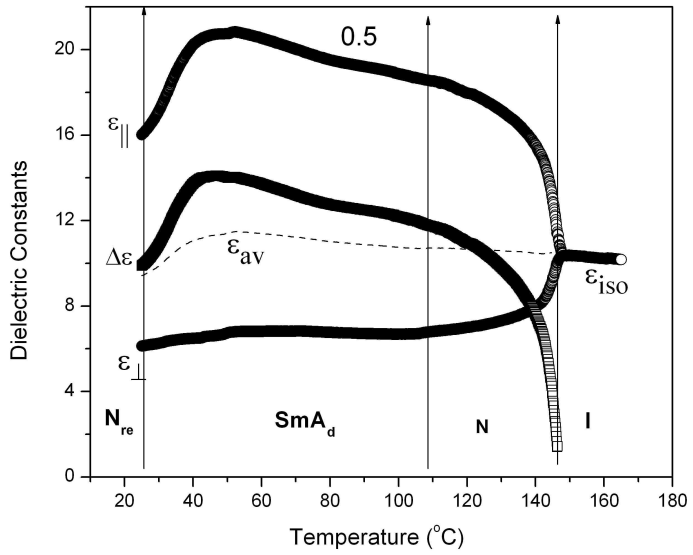

(c)

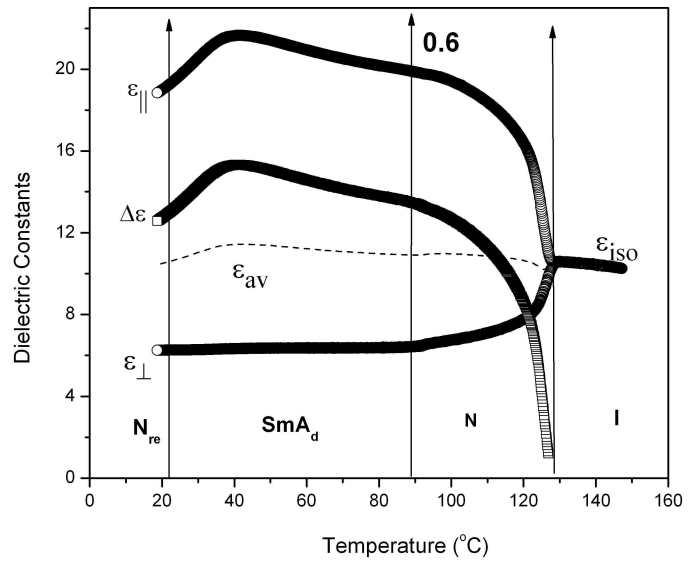

(d)

Figure 8.5: (cont'd): Temperature variation of dielectric parameters of 7BCB + 9.CN mixture for (c) $x_{9.\,CN}$ = 0.5 and (d) $x_{9.\,CN}$= 0.6.

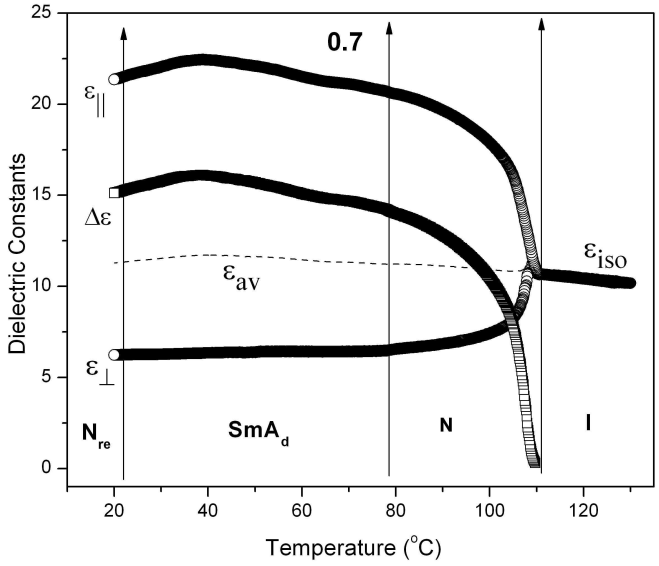

(e)

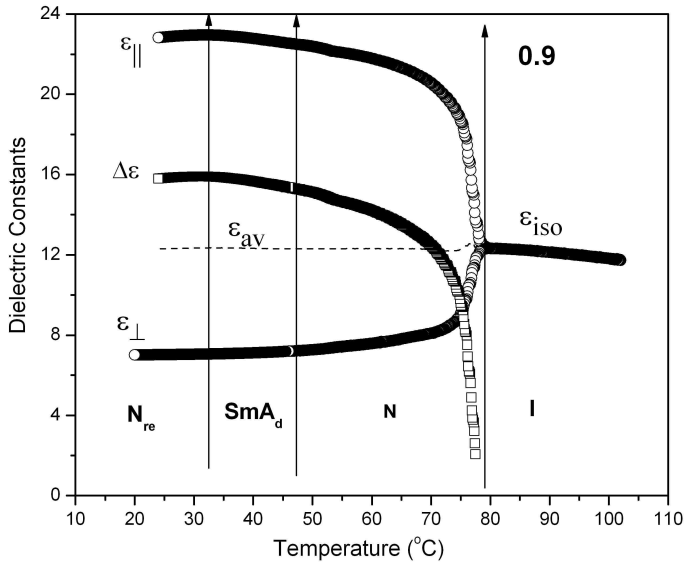

(f)

Figure 8.5: (cont'd): Temperature variation of dielectric parameters of 7BCB + 9.CN mixture for (e) $x_{9.\,CN}$ = 0.7 and (f) $x_{9.\,CN}$= 0.9.

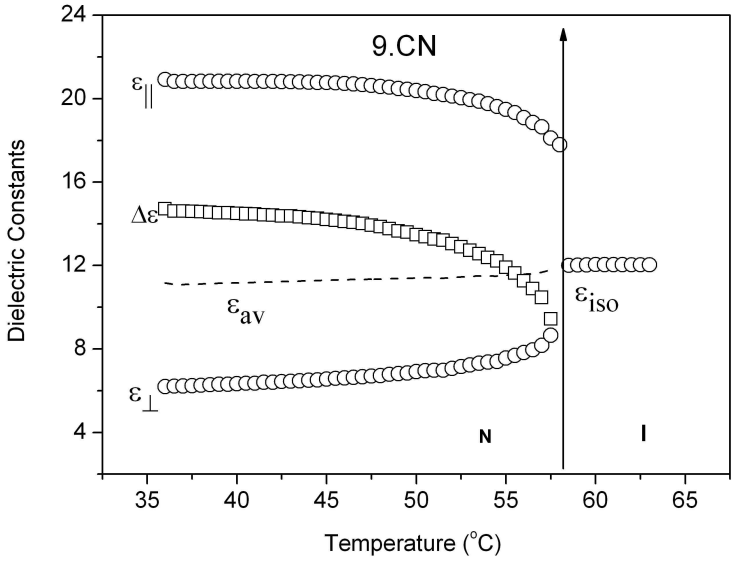

(g)

Figure 8.5: (cont'd): Temperature variation of dielectric parameters for 9.CN.

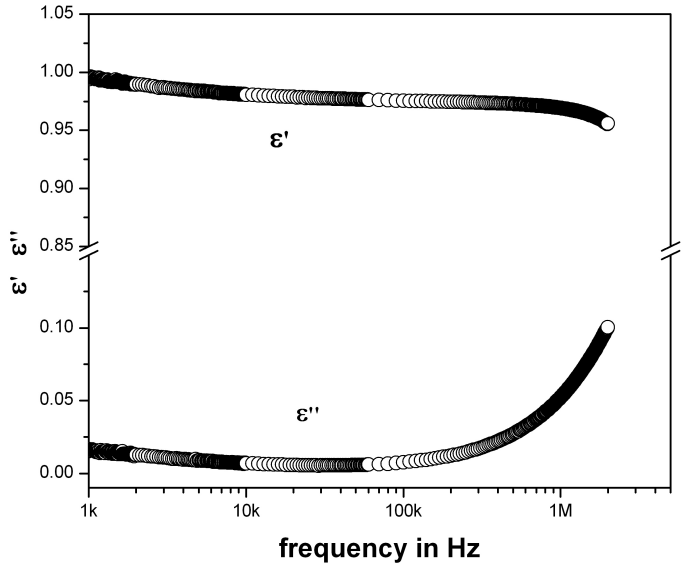

Figure 8.6: Dielectric spectrum for empty cell (air filled at room temperature ($25°C$)) showing the effect of ITO resistance and lead inductance at high frequency.

presented. Apart from the contribution of ionic effect and electrode polarization at low frequency (< 1 kHz) and ITO resistance at high frequency (> 200 kHz) the dielectric permittivity perpendicular to the molecular long axis $\epsilon_\perp$ does not show any change with change in frequency in range 20Hz to 2MHz indicating that the rotation of the molecules along their long axis does not occur in this frequency range.

When the dielectric permittivity is measured parallel to the molecular long axis (homeotropic configuration) strong effect of ionic conductance is observed in the low frequency region (< 1 kHz) where as in the high frequency region the effect of ITO resistance is seen (> 200 kHz) in figure 8.6 the dielectric spectrum for empty cell (air filled at room temperature ($25^\circ C$)) showing the effect of ITO resistance and lead inductance at high frequency is shown. The ionic conductivity $\sigma(dc)$ is small ($10^{-8}\ S-m^{-1}$) and almost constant in the re-entrant nematic phase and the data only below about 100 Hz are affected. However, as shown in figure 8.7, $\sigma(dc)$ increase almost exponentially to about 2 orders of magnitude ($10^{-6} S-m^{-1}$) with increase in temperature and data up to about 10kHz are affected in the upper nematic phase as visible from figures 8.8-8.9.

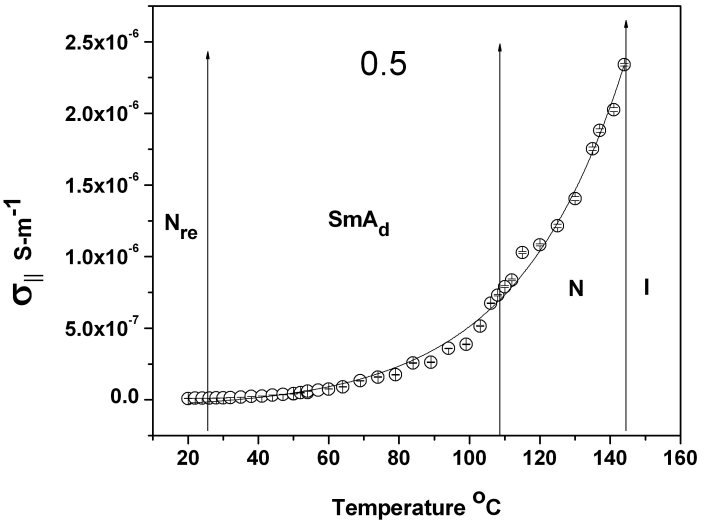

Figure 8.7: Temperature variation of ionic conductivity $\sigma(dc)$ for mixture $x_{9.\,CN}$ = 0.5.

The low frequency dielectric spectrum obtained for the re-entrant nematic

phase of the mixture $x_{9.\,CN}$ = 0.5 is given in figure 8.10. It consists of two well separated dispersion region at surprisingly low frequencies. The splitting of the two processes is quite good in the re-entrant nematic phase and low temperature range of the smectic A_d phase. However, as the temperature increases both relaxation process overlap making unique decomposition difficult. In the nematic phase only one relaxation process is observed in the frequency range upto which measurements have been possible in the existing setup. Similar result has been reported by others [14]. The value of the symmetric distribution parameter h_i for all the cases has been found to be smaller than 0.002 indicating Debye-like processes.

In case of homeotropic alignment the molecules flip-flop about their short axis. Thus absorption peaks shown in figure 8.10 represent relaxation frequencies corresponding to the rotation of the molecules about their short axis. It seems that the low frequency process corresponds to 7BCB and high frequency one to 9.CN component. This indicate that both relaxation processes are non-collective in their nature.

The decrease in the value of $\epsilon_\parallel$ with decrease in temperature during static dielectric measurements is perhaps due to dielectric loss. As observed from figures 8.8 and 8.9 the relaxation process occurs even in the vicinity of 1kHz at low temperature and this is responsible for the decrease in the value of $\epsilon_\parallel$. The experiment could not have been performed at lower frequency because in the high temperature region ionic effects are prominent even at 10kHz.

The relaxation times computed for both molecular processes are presented in the Arrhenius plots for the mixtures $x_{9.\,CN}$ = 0.4, 0.5 and 0.6 in figures 8.11, 8.12 and 8.13 respectively. It is clearly observed that the plot of ln(τ) vs 1/T is linear in the re-entrant nematic phase. However, in the smectic A_d phase the plot is non linear and the slope changes continuously as the re-entrant nematic phase is approached. This makes the determination of a unique value of the activation energy in the smectic A_d phase difficult. From the three mixtures studied, it is seen that the deviation from linearity decreases with the decrease of the width of the smectic region. Similar results has been reported by Nagabhushan *et. al.* [16, 17], who argued that if the change of slope was due to pretransitional effects, then such an effect would have been less prominent for a larger range of smectic A_d phase. Since the opposite is seen to happen experimentally the

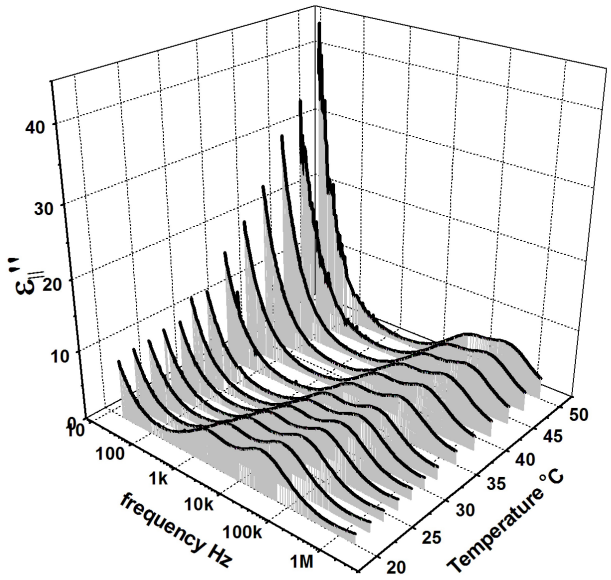

Figure 8.8: Frequency variation of dielectric loss ($\epsilon''_{\parallel}$) for homeotropic aligned sample ($x_{9.\,CN}$ = 0.5).

deviation from linearity cannot be due to pretransitional effects. They have proposed a possible explanation based on the fact that the reentrant nematic phase is generally known to have A_1 and A_d like competing smectic fluctuation, the A_d like fluctuation being more prominent at higher temperatures, while the A_1 like fluctuation is stronger at lower temperatures. The dielectric fluctuations being strongly influenced by these competing short range effects lead to the non linearity of the ln(τ) vs 1/T plot.

Table 8.2: Average activation energies in kJ/mole for mixtures $x_{9.\,CN}$ = 0.4, 0.5 and 0.6 (* indicates estimated value by taking weighed average of E_a).

$x_{9.\,CN}$	Molecule	Re-entrant nematic	Smectic A_d	Nematic
0.0	3Ph	–	–	61.4
0.4	3Ph	109.9	72.8	64.6*
	2Ph	89.1	51.7	
0.5	3Ph	114.4	73.2	65.4*
	2Ph	90.1	52.4	
0.6	3Ph	99.4	74.0	66.2*
	2Ph	83.5	51.3	
1.0	2Ph	–	–	69.4

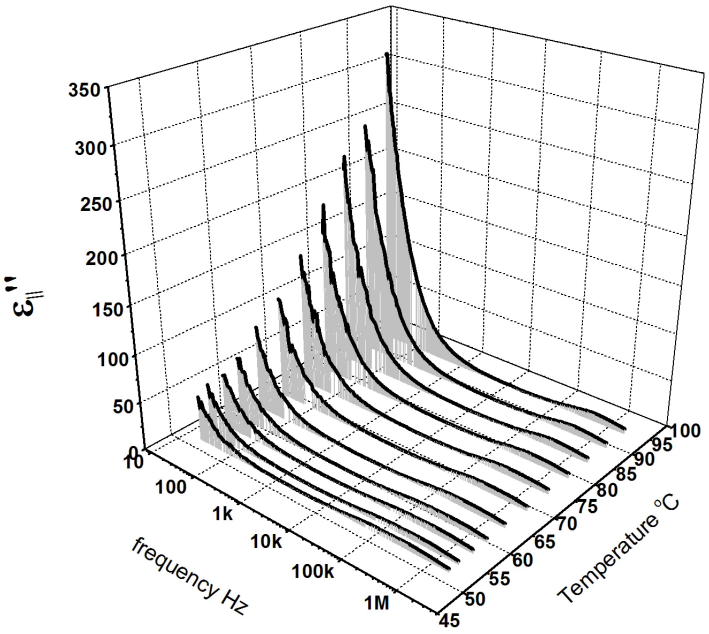

(a)

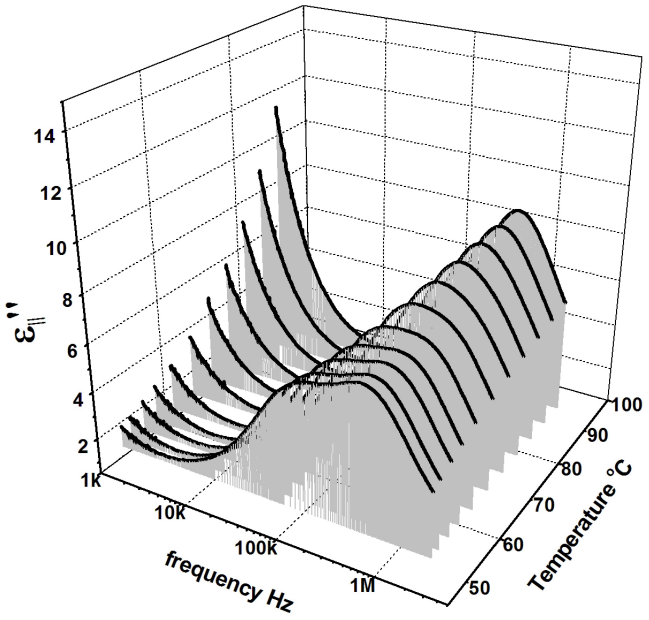

(b)

Figure 8.9: Variation of dielectric loss ($\epsilon''_{\parallel}$) for homeotropic aligned sample ($x_{9.\ CN}$ = 0.5)((a) highlights the low frequency ionic effect, (b) highlights the absorption peaks.

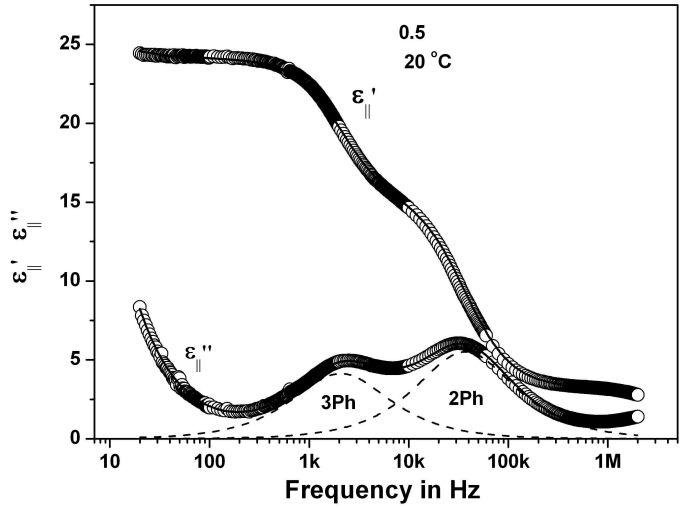

Figure 8.10: Dielectric spectrum for the re-entrant nematic phase of mixture $x_{9.\,CN}$ = 0.5 at 20°C. Solid lines represent a least square fit of equations 8.4 and 8.5 to the experimental points. Dashed lines represent the two main contributions to the spectrum.

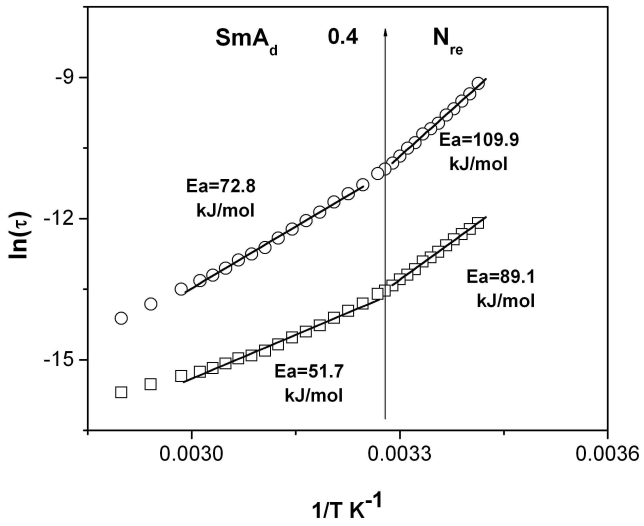

Figure 8.11: Arrhenius plots of molecular relaxation times for mixture $x_{9.\,CN}$ = 0.4.

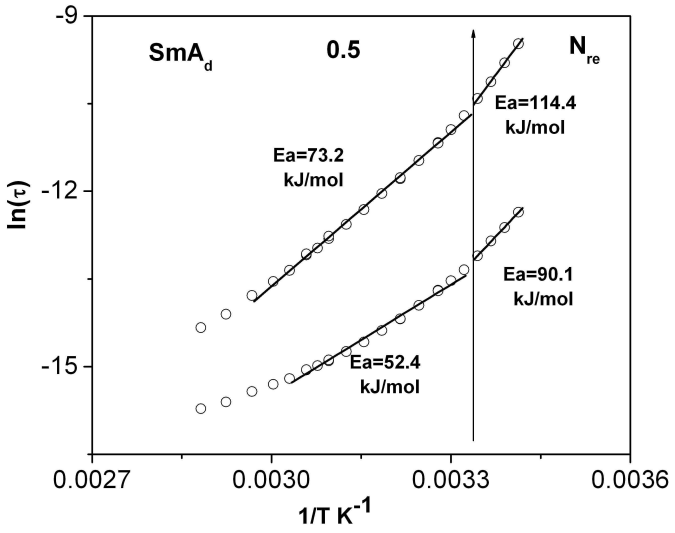

Figure 8.12: Arrhenius plots of molecular relaxation times for mixture $x_{9.\,CN}$ = 0.5.

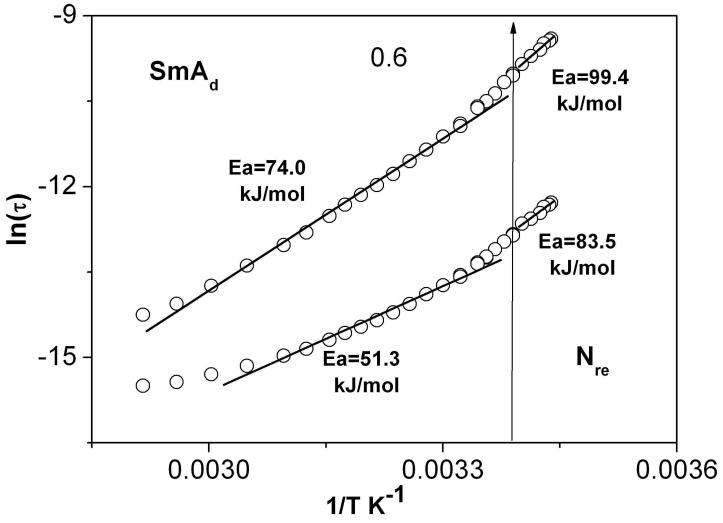

Figure 8.13: Arrhenius plots of molecular relaxation times for mixture $x_{9.\,CN}$ = 0.6.

From the table 8.2 it is observed that for both the relaxation processes the activation energy is higher in the re-entrant nematic phase compared to the induced smectic phase, the values being similar for all the three mixtures. This observation is in agreement with that reported by other workers [14, 16, 17]. However, it is totally different from the activation energy obtained for the 7CPB+9.CN system from rotational viscosity measurements which has been discussed in chapter 7 of this thesis. Due to the limitation of the existing experimental setup, I have been unable to fit the relaxation data in the upper nematic phase. However, dielectric spectroscopy measurement data of the pure compounds obtained from the Institute of Physics, Jagellonian University, Cracow, Poland using Agilent 4294A spectrometer in the frequency range 1kHz to 5MHz (homeotropic orientation was achieved by 0.7 T magnetic field and sample thickness of 0.7 mm were used) shows the the activation energy for the nematic phase to be 61.4 kJ/mol for 7BCB and 69.4 kJ/mol for 9.CN. For an approximate estimation, the weighed average have been considered for comparison as indicated in table 8.2. It may be mentioned that Legrand *et. al.* have reported values of activation energy in the smectic A_d phase which is less than that in the upper nematic phase [15]. Activation energy for both the relaxation processes in the re-entrant nematic phase are greater compared to the corresponding values in the Sm A_d phase. Interestingly, for all the mixtures studied the activation energy corresponding to the high frequency relaxation process is lower in the Sm A_d phase and higher in the N_{re} phase than the weighted average of E_a in the nematic phase.

8.6 Conclusion

The physical properties of a polar- polar binary system comprising of two nematogenic polar compounds with 4-cyanobiphenyl-4′ 4-heptylbenzoate, 7BCB as one component and 4-cyanophenyl 4-nonylbenzoate, 9.CN as the second component has been studied thoroughly from X-ray diffraction and dielectric measurements. The only difference between the previous system (7CPB+9.CN) and the present system (7BCB+9.CN) is the replacement of 7CPB by 7BCB, which translates to a shift in the position of the ester group (-COO). It is observed that a change in the position of the ester group leads to a stronger induction of the

smectic A_d phase with the area of the induced smectic island being increased considerably in the phase diagram. Like the previous binary system, the order of the induced smectic A_d to nematic as well as the induced smectic A_d to re-entrant nematic phase transition is continuous for all the mixtures. In analogy to the previously studied system, the McMillan's theory of the smectic A phase was modified in conformity with the Luckhurst-Timimi model, by considering a temperature dependent term α parameter to yield theoretical values of the OOP's $\langle P_2 \rangle$ and $\langle P_4 \rangle$ which were found to fit quite well with those determined from X-ray diffraction studies. The transverse correlation length in the N, Sm A_d as well as in the re-entrant nematic phase of these mixtures are found to diverge at the Sm A_d-N as well as Sm A_d-N_{re} phase transition again indicating a second-order phase transition. The static dielectric measurements have been done throughout the mesomorphic and composition range. It is observed that the value of $\epsilon_{\parallel}$ falls with the decrease in temperature in the re-entrant nematic and low temperature region of the smectic A_d phase. This decrease in $\epsilon_{\parallel}$ value with decrease in temperature has been explained from the results of low frequency dielectric spectroscopy measurements. In the dielectric loss graph two well separated dispersion region has been obtained. Activation energy in the N_{re} and part of the Sm A_d phase for both dispersion processes has been obtained from Arrhenius plots for three mixtures. It is seen that the activation energy is higher in the re-entrant nematic phase as compared to the Sm A_d phase. However, it is different from the activation energy obtained for the 7CPB+9.CN system from rotational viscosity measurements. Further investigations are necessary to arrive at a conclusive statement regarding this discrepancy.

References

[1] M. Brodzik and R. Dabrowski, *Mol. Cryst. Liq. Cryst.*, **260**, 361 (1995).

[2] A. Prasad, M. K. Das, *Phase Transitions*, **82**, 780 (2009).

[3] W. Maier, A. Saupe, *Z. Naturforsch.*, **A13**, 451 (1958).

[4] W. Maier, A. Saupe, *Z. Naturforsch.*, **A13**, 564 (1958).

[5] W. Maier, A. Saupe, *Z. Naturforsch.*, **A14**, 882 (1959).

[6] W. Maier, A. Saupe, *Z. Naturforsch.*, **A15**, 287 (1960).

[7] W. L. McMillan, *Phys. Rev. A*, **4**, 1238 (1971).

[8] W. L. McMillan, *Phys. Rev. A*, **6**, 936 (1972).

[9] G. R. Luckhurst and B. A. Timimi, *Mol. Cryst. Liq. Cryst.*, **260**, 253 (1981).

[10] K. S. Cole and R. H. Cole, *J. Chem. Phys.*, **9** p. 341 (1941).

[11] M .B. Pandey, R. Dhar, V. K. Agrawal, R. P. Khare, and R. Dabrowski, *Phase Transitions*, **76**, p. 945 (2003).

[12] R. Dhar, M. Gupta, V. K. Agrawal and M. K. Singh, *Phase Transitions*, **81**, p. 341 (2004).

[13] B. R. Ratna, R. Shashidhar, M. Bock, A. Gobl-Wunsch and G. Heppke, *Mol. Cryst. Liq. Cryst.*, **99**, 285 (1983).

[14] S. Wrobel, M. Brodzik, R. Dabrowski, B. Gestblom, W. Haase and S. Hiller, *Mol. Cryst. Liq. Cryst.*, **302**, 223 (1997).

[15] C. Legrand, J. P. Parneix, A. Chapoton, N. H. Tinh and C. Destrade, *J. Phys. Lett.*, **45**, L-283 (1984).

[16] R. Shashidhar, B. R. Ratna, V. Surendranath, V. N. Raja, S. K. Prasad and C. Nagabhushan, *J. Phys. Lett.*, **46**, L-445 (1985).

[17] C. Nagabhushan, *PhD Thesis*, Raman Research Institute (1988).

[18] L. Benguigui, F. Hardouin, *J. Phys. Lett.*, **42**, L-111 (1981).

Chapter 9

Conclusions

The dissertation entitled *"Study of the induction of smectic A_d and re-entrant nematic phases in binary mixtures of liquid crystals"* submitted for the degree of Doctor of Philosophy (Physics) of the University of North Bengal embodies the results of experimental investigation of the physical properties of binary mixtures of nematic (N) liquid crystalline compounds comprising of polar esters, exhibiting induced Smectic A_d (Sm A_d) and re-entrant nematic (N_{re}) phases. The thesis comprises of eight chapters.

In chapter 1, I have given a brief introduction to liquid crystals, especially thermotropic liquid crystals. I have described only those phases which have been studied by me namely nematic and smectic A. A brief review, which covers all other aspects of liquid crystal research, is also given in this chapter.

In chapter 2, I have described the experimental techniques in details to study the physical properties of liquid crystals and the theoretical background. The experimental techniques adopted are – phase identification by texture studies, X-ray diffraction studies, the interpretation of the X-ray results, density, refractive index, static dielectric permittivity , elastic constants and rotational viscosity measurements. Methods for the calculation of orientational order parameters, apparent molecular length, intermolecular distance, refractive indices, molecular polarizabilities etc. have been outlined.

In the present work, suitable binary systems of liquid crystal mixtures exhibiting both induced smectic A_d and re-entrant nematic (N_{re}) phases have been selected. Two binary systems consisting of polar - polar compounds were identified for this purpose. Polarizing optical microscopy and DSC measurements were

undertaken for the construction of the phase diagram and determination of the transition enthalpy. The study of the physical properties of these binary mixtures were undertaken from X-ray diffraction, refractive index, density, dipole moment, dielectric permittivity, rotational viscosity, splay and bend elastic constants measurements.

System 1: Binary mixture of 7CPB and 9.CN:

1. The phase diagram shows the presence of induced smectic and re-entrant nematic phases in the concentration range $0.4 < x_{9.\,CN} < 0.87$. From textures studies it is observed that both the normal and re-entrant nematic phases in this system are similar.

2. The order of the induced smectic A_d to nematic as well as the induced smectic A_d to re-entrant nematic phase transition is continuous for all the mixtures. This observation has been supported from DSC, density and orientational order parameter values determined from X-ray diffraction measurements.

3. Using a simple extension of the McMillan's treatment of the smectic A phase, the theoretically estimated $\langle P_2 \rangle$ and $\langle P_4 \rangle$ values have been found to fit quite well with those determined from X-ray diffraction studies.

4. Further analysis of the X-ray data has revealed a maximum in the smectic layer spacing near $x_{9.\,CN} = 0.5$. The variation of layer thickness with molar concentration of 9.CN has been explained fairly well by assuming the presence of both homo and hetero dimers.

5. Optical transmission studies made on this system revealed no discontinuity in the Δn values at the N_{re}–Sm A_d as well as Sm A_d–N transition temperatures indicating second order phase transition. The agreement between the experimental $\langle P_2 \rangle$ values from the birefringence measurements with those calculated from McMillan's theory have been found to be poor in the smectic A_d phase. Similar to the orientational order parameter (OOP) values as obtained from X-ray diffraction measurements, this discrepancy has again been removed by recalculating the orientational order parameter values according to a modified McMillan's theory as proposed by Luckhurst

and Timimi. Both N–Sm A_d and Sm A_d–N_{re} phase transitions which are predicted to be of second order by this model, are also found to be in agreement with the birefringence as well as DSC measurements.

6. The static dielectric permittivity of the mixtures of the 7CPB + 9.CN system has been determined throughout their mesomorphic range. The temperature variation of the dielectric permittivity at the nematic–smectic A_d and smectic A_d–re-entrant nematic transition for all the mixtures has been found to be continuous.

7. In the case of mixture with $x_{9.\,CN}$ = 0.662, the parallel component of the dielectric permittivity shows a pronounced decrease in the Sm A_d phase due to dipole-dipole correlation. This behaviour is also observed in other mixtures, including the purely nematic ones, but on a reduced scale. The maximum decrease is found for mixtures situated near the middle of the Sm A_d island.

8. The effective values of the dipole moments in the mixtures are found to be less than the values observed in the pure compounds. The effective molecular dipole moments are found to increase with increase in temperature. Moreover, μ_{eff} in the smectic A_d phase is found to be slightly smaller than those obtained by extrapolation from either the nematic or re-entrant nematic phases. The lower effective dipole moment in the smectic A_d phase implies the development of additional anti-parallel ordering of the molecular dipoles in the induced smectic phase, in conformity with the model proposed by Cladis.

9. For the average value of the nematic permittivity, ϵ_{av}, as well as the isotropic permittivity ϵ_{iso} , the value of the critical exponent α' is nearly the same ($\approx$ 0.5) which corresponds to the tricritical behaviour of the I–N transition.

10. A simple electro-optical method was used to determine the relaxation time and hence the rotational viscosity (γ_1) of this binary system. Upon cooling, the γ_1 values not only increase in the normal N phase but also in the N_{re} phase and have same order of magnitudes about 0.5 to a few Pa s.

11. Rotational viscosity values are about two to three order of magnitude higher in the Sm A_d phase than those measured in the N phase.

12. The splay elastic constant also shows similar behavior and its magnitude is of the same order in the normal nematic and re-entrant nematic phase. However the magnitude of splay elastic constant in the induced smectic A_d phase is about two to three order of magnitude higher.

13. The activation energies in the N_{re} phase are smaller than those in the normal nematic phase. The difference $[(E_a)_N - (E_a)_{N_{re}}]$ is maximum near the centre of the phase diagram. This result indicates that the interaction between monomer molecules or that between dimer aggregates is weaker in the N_{re} phase than in the normal nematic phase.

14. For normal nematic phase, the activation energy increases with an increase in mole fraction of 9.CN, while that for N_{re} phase it shows a local minimum near $x_{9.\,CN}$ = 0.6, i.e. at centre of the phase diagram.

System 2: Binary mixture of 7BCB and 9.CN:

1. The physical properties of another polar - polar binary system comprising of two nematogenic polar compounds has been studied thoroughly from optical birefringence, X-ray diffraction and dielectric spectroscopy measurements.

2. The only difference between the previous system (system 1) and the present system (system 2) is the replacement of 7CPB by 7BCB, which translates to a shift in the position of the ester group (–COO). It is observed that a change in the position of the ester group leads to a stronger induction of the smectic A_d phase with the area of the induced smectic island being increased considerably in the phase diagram.

3. The order of the induced smectic $A_d$to nematic as well as the induced smectic A_d to re-entrant nematic phase transition is continuous for all the mixtures. This observation has been supported from DSC, birefringence and orientational order parameter values determined from X-ray diffraction measurements.

4. The transverse correlation lengths are found to diverge at the Sm A_d–N as well as Sm A_d–N_{re} phase region is approached from either side, again indicating a second-order phase transition.

5. The McMillan's theory of the smectic A phase was modified in conformity with the Luckhurst-Timimi model, by considering a temperature dependent term α parameter to yield theoretical values of the OOP's $\langle P_2 \rangle$ and $\langle P_4 \rangle$ which were found to fit quite well with those determined from X-ray diffraction studies.

6. It is observed that the value of $\epsilon_{\parallel}$ falls with the decrease in temperature in the re-entrant nematic and in the low temperature region of the smectic A_d phase. An attempt has been made to explain this decrease in $\epsilon_{\parallel}$ value with decrease in temperature from the results of low frequency dielectric spectroscopy measurements. In the dielectric loss graph, two well separated dispersion region has been obtained. It is observed that the activation energy is higher in the re-entrant nematic phase as compared to the Sm A_d phase. However, for all the mixtures studied the activation energy corresponding to the high frequency relaxation process is lower in the Sm A_d phase and higher in the N_{re} phase than the weighted average of E_a in the nematic phase.

List of publication

Referred Journals

1. Akhileshwar Prasad and Malay Kumar Das, *Orientational order parameters of a binary mixture showing both induced smectic and re-entrant nematic phases.* Phase Transitions, **82**, 780-792, (2009).

2. P. D. Roy, A. Prasad and M. K. Das, *Study of the physical properties of a mesogenic mixture showing induced smectic A_d phase by refractive index, density and x-ray diffraction measurements.* Journal of Physics: Condensed Matter, **21**, 075106 (8pp), (2009).

3. Akhileshwar Prasad and Malay Kumar Das, *Optical birefringence studies of a binary mixture with the nematic-smectic A_d– re-entrant nematic phase sequence.* Journal of Physics: Condensed Matter, **22**, 195106 (7pp), (2010).

4. Akhileshwar Prasad and Malay Kumar Das, *Refractive index and orientational order parameter of a polar-polar binary system showing induced smectic A_d and re-entrant nematic phases.* Phase Transitions, **83**, 1072-1084, (2010).

5. Malay Kumar Das and Akhileshwar Prasad, *Rotational viscosity measurement of a binary mixture showing both induced smectic and re-entrant nematic phases.* Mol. Cryst. Liq. Cryst., **540**, p. 162-168, (2011).

6. Akhileshwar Prasad and Malay Kumar Das, *Static dielectric properties of two nematogenic compounds and their binary mixtures showing induced smectic A_d and re-entrant nematic phases.* Physics Scripta, **84**, 015603 (9pp), (2011).

Paper Presented in Conferences

1. A. Prasad, M. K. Das, M. Tykarska, R. Dabrowski, *Induction of smectic A_d and re-entrant nematic phases in binary mixtures of polar esters*, abstract of papers, 14^{th} National Conference on Liquid Crystals, p. 24, Siliguri, (2007).

2. Akhileshwar Prasad and Malay Kumar Das, *Occurrence of induced smectic and re-entrant nematic phases in a new binary system of polar esters*, Solid State Physics (India), **53**, p. 221-222, (2008)(Proceedings of the DAE Solid State Physics Symposium.)

3. A. Prasad, M. K. Das, *On the appearance of induced smectic and re-entrant nematic phases in a new binary system of polar esters.* Book of Abstract, 15^{th} National Conference on Liquid Crystals, p. 82, Banglore, (2008).

4. Akhileshwar Prasad and Malay Kumar Das, *Phase transition studies of a polar-polar binary liquid crystalline system showing nematic-smectic A_d and re-entrant nematic phase sequence.* Abstract of Papers, 16^{th} National Conference on Liquid Crystals, p. 75, Lucknow, (2009).**

5. Akhileshwar Prasad and Malay Kumar Das, *Visco-elastic properties of a binary mixture showing both induced smectic and re-entrant nematic phases.* Abstract of Papers, 16^{th} National Conference on Liquid Crystals, p. 18, Lucknow, (2009).

6. B. Das, A. Prasad, M. K. Das and R Dabrowski, *Specific heat capacity measurements of a binary system showing induced smectic and re-entrant nematic phases.* Abstract of Papers, 17^{th} National Conference on Liquid Crystals p. 110, Surat, (2010).

** Adjudged the best poster paper presentation in physics section and awarded Dewan Jawahar Lal Nayar Memorial Prize for the year 2009 by the Indian Liquid Crystal Society.